Investigating the role of suppressed hydrolases during *Pseudomonas syringae* infection



Alice Godson

Keble College

Department of Biology

University of Oxford

Supervised by Professor Renier A. L. van der Hoorn

Thesis submitted for the degree of Doctor of Philosophy

Trinity 2023

Abstract

The apoplast, the extracellular space outside the plasma membrane of plant cells, is an important battleground for plant-pathogen interactions. Plants secrete hydrolytic enzymes into this space which are targeted by pathogen inhibitors. Previous work used activity-based protein profiling coupled to mass-spectrometry (ABPP-MS) to monitor hydrolase dynamics in the apoplast of *Nicotiana benthamiana* upon infection with virulent *Pseudomonas syringae* pv. *tomato* DC3000. This work detected 171 hydrolase activities, including 60 that were suppressed upon bacterial infection. We hypothesised that suppression by a bacterial inhibitor may have evolved in response to a role in immunity for some of these hydrolases.

This thesis aimed to uncover novel immune hydrolases by testing six of the suppressed hydrolases for their role in plant immunity using 'agromonas' assays. We identified *Nb*PR3, a glycosyl hydrolase with a role in bacterial immunity despite its annotation as an endochitinase. We identified a *Nicotiana*-specific substitution in the catalytic general base of *Nb*PR3 that is essential for this resistance function. A hypothesis-driven approach to identify the substrate of *Nb*PR3 uncovered a potential role in release of a bacterial elicitor to trigger the oxidative burst.

We also identified *Nb*RD21, a papain-like cysteine protease whose function in bacterial resistance appears to be dependent on effector-triggered immunity. We used transient *NbRD21* expression combined with *rd21* knockout by CRISPR-Cas9 to test potential mechanisms of *Nb*RD21 function. Proteomics data uncovered a role for *Nb*RD21 in processing of receptor-like kinases.

Finally, we developed a high-throughput assay for monitoring *Nb*RD21 activity and used it to confirm that *Nb*RD21 is inhibited during *P. syringae* infection. We presented evidence

that the inhibitor is novel, likely proteinaceous, and produced by multiple bacterial species. Overall, this work has identified two novel and distinct plant immune hydrolases, demonstrating the potential of ABPP-MS to uncover molecular plant-pathogen interactions in the apoplast.

Acknowledgements

Firstly, I would like to thank my supervisor, Renier van der Hoorn. Your encouragement, constructive feedback and support have been so valuable in making me into a (hopefully good!) scientist. Thank you also for the laughs and friendly chats at dinners, spring walks and on retreats. Thank you to Daniela Sueldo for providing the foundations for my project and for the fruitful chats about science. Also thank you to Pierre Buscaill, for guiding me at the start of my PhD.

Thank you to everyone in the van der Hoorn and Preston labs for your feedback and support and so many productive scientific discussions that helped develop my project. Thank you also for the fun times. Thank you to Urszula, Sarah and Caroline for all the technical support and help with tissue culture. To Issy, your friendship helped make the research and write-up bearable (and at times even enjoyable!). Thanks for sharing both the amazing and stressful times with me. Special thanks also to Mariana, Tee, Laura, Maria and Brian for your infinite wisdom but more importantly your friendship. Thanks to Lauren for being the best Msc student I could wish for. Finally, thank you to Konstantina, Felix, Jie, Chidam, Philippe and Rawit for the fun and laughter along the way.

Thank you to my parents Ruth and John, for always believing in me. Thank you to Clare and David for your constant support. Finally, and most importantly, thank you to my fiancé and best friend, Ollie. Without you, everything would be a million times harder.

This work was supported by funding from the Biotechnology and Biological Sciences Research Council (BBSRC).

Table of Contents

Chapter 1: Introduction……9

1.1 Introduction to plant immunity……9

1.2 The apoplastic battlefield……10

1.3 Hydrolases in plant immunity……11

1.4 *Nicotiana benthamiana* and *Pseudomonas syringae*……14

1.5 Thesis structure……17

Chapter 2: Review of apoplastic immune proteases……19

2.1 Abstract……19

2.2 Introduction……20

2.3 Overview of the catalytic classes of plant proteases……22

2.4 Meta-analysis of apoplastic immune proteases……24

2.4.1 Criterium A (Apoplast)……27

2.4.2 Criterium B (Biological role)……29

2.4.3 Criterium C (Catalytic activity)……33

2.5 Six functions of secreted immune proteases……35

2.5.1 Apoplastic proteaases display direct antimicrobial activity……35

2.5.2 Apoplastic proteases activating immune hydrolases……36

2.5.3 Apoplastic proteases mediating DAMP release……37

2.5.4 Apoplastic proteases perceive pathogen effectors……38

2.5.5 Apoplastic proteases required for the HR……39

2.5.6 Apoplastic proteases mediate SAR and priming……40

2.6 Discussion……42

2.7 Contributions……44

Chapter 3: Screen of a selection of suppressed hydrolases……45

3.1 Abstract……45

3.2 Introduction……46

3.3 Results……52

3.3.1 Silencing candidate genes by VIGS……52

3.3.2 Creation of selected overexpressed hydrolases……52

3.3.3 Agromonas screen of suppressed hydrolases……53

3.3.4 *Nb*PR3 confers resistance to multiple *P. syringae* strains……56

3.3.5 ETI-dependent role for *Nb*RD21 in plant immunity……57

3.3.6 Testing the ETI-dependence of *Nb*RD21 immune function……58

3.4 Discussion……60

3.5 Conclusion……67

3.6 Contributions……68

3.7 Supplementary Figures……68

3.8 Methods……68

Chapter 4: Analysis of the role of *Nb*PR3 in immunity……74

4.1 Abstract……74

4.2 Introduction……75

4.3 Results……78

4.3.1 *Nb*PR3 accumulates in the apoplast upon infection……78

4.3.2 Catalytic activity is required for the immune function of *Nb*PR3……79

4.3.3 *Nb*PR3 does not have endochitinase activity……82

4.3.4 Identifying residues important for the lack of chitinase activity……83

4.3.5 A *Nicotiana*-specific mutation at the catalytic general base……84

4.3.6 *Nicotiana*-specific glutamine is required for antibacterial resistance……85

4.3.7 Q112E is insufficient to restore endochitinase activity……87

4.3.8 Biochemical approaches to identify the substrate of *Nb*PR3.....88

4.3.9 Hypothesis-driven approaches to identify the substrate of *Nb*PR3.....93

4.4 Discussion.....103

4.5 Conclusion.....109

4.6 Contributions.....109

4.7 Supplementary Figures.....109

4.8 Methods.....112

Chapter 5: Analysis of the role of *Nb*RD21 in immunity.....118

5.1 Abstract.....118

5.2 Introduction.....119

5.3 Results.....124

5.3.1 Preparing tools for studying *Nb*RD21 function.....124

5.3.2 Generation of *Nbrd21* knockouts.....129

5.3.3 Hypothesis-driven approaches to identify the substrate of *Nb*RD21.....134

5.3.4 Proteomic approach to substrate identification.....138

5.3.5 No detected difference in VPE activity in *rd21* mutants.....141

5.3.6 *Nb*RD21 is involved in RLK regulation.....142

5.4 Discussion.....147

5.5 Conclusion.....156

5.6 Contributions.....156

5.7 Supplementary Figures.....157

5.8 Methods.....162

Chapter 6: Characterisation of *Nb*RD21 inhibition.....169

6.1 Abstract.....169

6.2 Introduction.....170

6.3 Results....173
6.3.1 *Nb*RD21 inhibition can be detected by convolution ABPP....173
6.3.2 Establishing a fluorescent activity assay to monitor *Nb*RD21 inhibition....175
6.3.3 *In vitro* production of *Nb*RD21 inhibitor....179
6.3.4 Optimising the protocol for detecting *Nb*RD21 inhibition....182
6.3.5 Characterisation of the inhibitor....184
6.3.6 *Nb*RD21 inhibitor is not Cip1....186
6.3.7 Determining the breadth of *Nb*RD21 inhibition....188
6.3.8 *Nb*RD21 inhibition by multiple species of bacteria....192
6.4 Discussion....194
6.5 Conclusion....201
6.6 Contributions....202
6.7 Supplementary Figures....202
6.8 Methods....205

Chapter 7: General discussion....210
7.1 A novel method to detect plant immune hydrolases....210
7.2 The challenges of identifying biological substrates....212
7.3 The importance of hydrolase localisation and regulation....215
7.3.1 Pathogen-derived regulators....215
7.3.2 Plant-derived regulators....216
7.4 Overall conclusions and future perspectives....218

Bibliography....220

Chapter 1: Introduction

1.1 Introduction to plant immunity

The interaction between plants and pathogens is both multi-layered and complex. Upon pathogen entry, pathogen-associated molecular patterns (PAMPs) such as chitin and flagellin are recognised by receptor-like proteins/kinases (RLPs/RLKs) known as pattern recognition receptors (PRRs; Saijo et al., 2018) leading to PAMP-triggered immunity (PTI) (Jones and Dangl, 2006). Adapted pathogens respond by producing effector proteins to perturb PTI, which resistant plants recognise through proteins encoded by *R*esistance (*R*) genes, resulting in effector-triggered immunity (ETI; Zipfel, 2014). Most effectors are perceived either by RLPs/RLKs at the cell surface, or nucleotide-binding leucine-rich repeat-containing receptors (NLRs) inside the cell (Kourelis and van der Hoorn, 2018). Both PTI and ETI trigger similar downstream responses, including the release of reactive oxygen species (ROS), activation of mitogen-activated protein kinases (MAPKs) and the induction of pathogenesis-related (PR) proteins such as chitinases, glucanases and proteases (Dodds and Rathjen, 2010). Local defence responses often trigger systemic acquired resistance (SAR), underpinned by the signalling hormone salicylic acid (SA). Whilst SA is generally associated with resistance to biotrophic pathogens, the hormones jasmonic acid and ethylene mediate resistance to necrotrophs (Buscaill and Rivas, 2014). ETI often culminates in a form of programmed cell death (PCD) known as the hypersensitive response (HR) at the site of infection, limiting the spread of the pathogen (Morel and Dangl, 1997).

1.2 The apoplastic battlefield

Whilst much of the plant immune response comprises intracellular events such as MAPK signalling and transcriptional reprogramming, many plant-pathogen interactions occur in the extracellular space outside the plasma membrane known as the apoplast. This is the first destination for pathogens that have entered the plant through wounds, stomata and hydathodes, and is an important site for pathogen proliferation (Jones and Dangl, 2006). The apoplast can be thought of as an ancient 'battlefield' that must be fiercely defended by the host (Doehlemann and Hemetsberger, 2013; Jashni et al., 2015b).

Plants defend the apoplast by the secretion of antimicrobial compounds. This includes enzymes that modify and reinforce the cell wall (Bacete et al., 2018), peroxidases that induce the oxidative burst (Camejo et al., 2016), antimicrobial peptides (Breen et al., 2015), phytoalexins (Ahuja et al., 2012) and hydrolytic enzymes such as proteases, lipases and glycosyl hydrolases (Grosse-Holz et al., 2018; Martínez-González et al., 2018). Many hydrolases are classed as pathogenesis-related (PR) proteins. PR proteins are induced upon pathogen invasion and are grouped into 17 families on the basis of sequence homology (van Loon et al., 2006). Proteases are found in PR families -7 and -17 whilst glycosyl hydrolases are found in PR families -2, -3, -4, -8 and -11 (Ali et al., 2018). PR proteins are crucial components of the plant defence response, with many displaying antimicrobial activity (van Loon et al., 2006; Ali et al., 2018). Constitutively-expressed hydrolases, whilst not classified as PR proteins, may also be involved in immunity (Coffeen and Wolpert, 2004).

Pathogens ensure successful replication in the apoplast by secreting effectors that manipulate plant physiology. These include cell wall-degrading enzymes (CWDEs) that damage the host cell during infection; for instance, *Magnaporthe grisea* and *Fusarium*

graminearum encode over 100 CWDEs each (Kämper et al., 2006). The secretion of effectors that interfere with pathogen perception is another common strategy. The fungus *Cladosporium fulvum* secretes the effectors Avr4 and Ecp6 into the apoplast of tomato, where they bind to long- and short-chain fungal chitin oligosaccharides, respectively (Jonge et al., 2010; van Esse et al., 2007). Avr4 protects fungal hyphae from hydrolysis by plant chitinases, whilst Ecp6 sequesters released chitin oligosaccharides, preventing their detection by PRRs (Jonge et al., 2010; van Esse et al., 2007). Additionally, pathogen effectors may inhibit the action of host immune hydrolases (Wang and Wang, 2017). For example, the tomato papain-like cysteine protease Rcr3 is inhibited by the small, cysteine-rich inhibitor Avr2 (Rooney et al., 2005), cystatin-like inhibitors EPIC1 & EPIC2B (Song et al., 2009), the venom allergen-like protein Gr-VAP1 (Lozano-Torres et al., 2012) and the small secreted lipoprotein Cip1 (Shindo et al., 2016).

1.3 Hydrolases in plant immunity

Hydrolases are biological catalysts that cleave chemical bonds using water. Hydrolytic enzymes are prominent in the plant apoplast and many are implicated in the immune response (Grosse-Holz et al., 2018). The most important classes of hydrolase in apoplastic plant immunity are lipases/esterases, glycosyl hydrolases and proteases.

1.3.1 Lipases and esterases

Esterases are enzymes that hydrolyse ester bonds. Lipases are a subset of esterases that release long-chain fatty acids from water-insoluble esters, whilst nonlipolytic esterases prefer cleavage of short-chain, soluble fatty acids (Fojan et al., 2000). However, these two enzyme classes are not always easily distinguished (Ali et al., 2012; Fojan et al., 2000). Lipases are divided into two subfamilies depending on the presence of a conserved domain

type: Gly-x-Ser-x-Gly (GXSXG) or Gly-Asp-Ser-Leu (GDSL) (Ding et al., 2019). GDSL lipases are the most extensively studied, with 105 GDSL esterases and lipases identified in *Arabidopsis thaliana* (Arabidopsis; Shen et al., 2022), and the majority contain a signal peptide for secretion (Ding et al., 2019).

Expression of lipases and esterases is induced by bacterial infection (Grosse-Holz et al., 2018) and several defence roles have been described (Lee and Park, 2019). For instance, phospholipases release lipid products that initiate MAPK cascades, activate calcium signalling and regulate PR gene transcription (Lee and Park, 2019). Furthermore, the Arabidopsis GDSL lipases *At*GLIP1 and *At*GLIP2 mediate resistance through regulating ethylene and auxin signalling, respectively (Kim et al., 2014; Lee et al., 2009). Finally, expression of apoplastic pectin methylesterases (PMEs), which catalyse the demethylesterification of homogalacturonans in the cell wall, is induced by pathogen invasion and they are important for the plant immune response (Bethke et al., 2014; Körner et al., 2009; Lionetti et al., 2007). Importantly, Arabidopsis *pme* mutants are more susceptible to both *Pseudomonas syringae* and *Botrytis cinerea* (Bethke et al., 2014; Del Corpo et al., 2020). Presumably, lipases and esterases are targeted by pathogen inhibitors that remain to be identified.

1.3.2 Glycosyl hydrolases

Glycosyl hydrolases (GHs) catalyse the hydrolysis of glycosidic bonds. Carbohydrates are very diverse and so many GHs with different substrate specificities exist, such as chitinases, glucosidases and galactosidases (Chandrasekar et al., 2014). According to the Carbohydrate-Active enZymes (CAZy) database, GHs are grouped into 167 families based on sequence similarity and bond cleavage mechanism (Cantarel et al., 2009). The Arabidopsis genome encodes for 379 GHs, divided amongst 29 families, with the majority

located in the cell wall and plasma membrane (Minic, 2007). Despite being such a large and diverse group, GHs are relatively uncharacterised.

Chitinases are amongst the most abundant hydrolases in the apoplast (Grosse-Holz et al., 2018). Chitinases hydrolyse chitin, a polymer of β-1,4-*N*-acetyl-D-glucosamine linkages, and are found in GH families 18 and 19 (Minic, 2007). They have been implicated in defence against fungi by degrading chitin in their cell wall (Collinge et al., 1993). Some chitinases display additional lysozyme activity by hydrolysing the linkages between *N*-acetyl-D-glucosamine and *N*-acetylmuramic acid in peptidoglycan, a major component of the cell walls of gram-positive bacteria (Scheltinga et al., 1994; Subroto et al., 1999).

Pathogen invasion induces the accumulation of many apoplastic GHs that modify and strengthen the cell wall, including galactosidases, xylosidases and arabinofuranosidases (Delaunois et al., 2014). In addition, PR-2 β-1,3-endoglucanases mediate the release of β-1,3-glucan elicitors from fungal hyphae to trigger the oxidative burst (Perrot et al., 2022), the *Nicotiana benthamiana* β-galactosidase BGAL1 promotes the release of immunogenic peptides from bacterial flagellin (Buscaill et al., 2019), and the Arabidopsis α-glucosidase AGLU1 has antifungal activity (Husaini et al., 2018).

Due to their role in immunity, apoplastic GHs are vulnerable to inhibition by plant pathogens. For instance, BGAL1 is inhibited by the *P. syringae* inhibitor galactosyrin (Buscaill et al., 2019), maize β-1,3-glucanases are inhibited by fumonisin toxins secreted by the fungus *Fusarium verticillioides* (Sánchez-Rangel et al., 2012), and bacteria secrete inhibitors of plant chitinases (Hodge et al., 1996). Furthermore, *Phytophthora sojae*. secretes glucanase inhibitor proteins (GIPs) to inhibit the soybean β-1,3-endoglucanase EGaseA from releasing glucan elicitors from the oomycete cell wall, thereby preventing elicitor perception (Rose et al., 2002). Interestingly, both class I chitinases and EGaseA enzymes are under positive

selection, which is likely imposed by microbial inhibitors (Bishop et al., 2005, 2000). Aside from inhibition, several apoplastic GHs are manipulated and degraded by pathogens. For example, the fungus *Verticillium dahliae* secretes the protease *Vd*SSEP1 to degrade the cotton chitinase Chi28 (Han et al., 2019), and the fungus *Bipolaris zeicola* secretes the chitinase modifying protein Bz-cmp to impair the ability of maize chitinase ChitA to bind chitin (Naumann et al., 2009).

1.3.3 Proteases

An in-depth analysis of the role of apoplastic proteases in plant immunity is covered in **Chapter 2**, which is a published review ("The front line of defence: a meta-analysis of apoplastic proteases in plant immunity"; Godson and van der Hoorn, 2021).

1.4 *Nicotiana benthamiana* and *Pseudomonas syringae*

Nicotiana benthamiana is a solanaceous relative of tobacco that is widely used to study plant-pathogen interactions. It is both easy to genetically manipulate and easily infected with a wide range of plant pathogens (Goodin et al., 2008). The apoplastic proteome of *N. benthamiana* is abundant with hydrolytic enzymes, including proteases and glycosyl hydrolases (Grosse-Holz et al., 2018, Sueldo et al., 2023).

Pseudomonas syringae is a gram-negative bacterial pathogen belonging to the *Pseudomonas* genus which also contains the opportunistic human pathogen *Pseudomonas aeruginosa* (Silby et al., 2011). *P. syringae* colonises almost all agriculturally important plants, from tomato and beans to horse-chestnut and kiwifruit (Arnold and Preston, 2019). The economic impact of *P. syringae* infection can be devastating (Vanneste, 2017). Symptoms of infection include water-soaked lesions, dark leaf spots, chlorosis and stunting

(Preston, 2000). There are over 60 pathovars, including pv. *tomato* (*Pto*) which causes bacterial speck in tomato leaves (Xin et al., 2018).

As a hemibiotrophic pathogen, *P. syringae* must adapt to changing host conditions. The pathogen has evolved several key adaptations to ensure survival on the epiphytic surface, at risk of cold stress, osmotic shock and desiccation. For example, motile flagella allow migration across the leaf surface, the secretion of surfactants facilitates chemotaxis, and exopolysaccharide production enables freeze-thaw resistance and osmotic stress tolerance (Pfeilmeier et al., 2016). After entering the host through wounds and stomatal openings (Arnold and Preston, 2019), both natural and pathogen-induced (Garnham et al., 2011; Geng et al., 2014), *P. syringae* must adapt to the harsh conditions of the apoplast. To avoid detection by PRRs, flagellin production is tightly regulated and excess flagellin monomers are degraded (Pel et al., 2014; Pfeilmeier et al., 2016). The secretion of antioxidants and toxins enables *P. syringae* to subvert apoplastic host defence mechanisms such as the oxidative burst and stomatal closure (Yu et al., 2013). Finally, manipulation of host sugar transporters increases water and carbohydrate availability (Macho, 2016). At the late stage of infection, *P. syringae* secretes effectors and toxins to induce necrosis (DebRoy et al., 2004; Pfeilmeier et al., 2016).

Critical to the pathogenesis of *P. syringae* is the production of various virulence factors, including secreted proteins, plant hormone mimics, antimetabolite toxins and lipopeptides, that damage host cells and promote bacterial growth (Ichinose et al., 2013). For instance, the phytotoxin coronatine mimics jasmonic acid to suppress SA-mediated defence responses and mediate stomatal opening (Geng et al., 2014). Furthermore, syringolin A is a peptide phytotoxin that mediates stomatal opening and wound entry through proteasome inhibition (Misas-Villamil et al., 2013; Schellenberg et al., 2010), and the antimetabolite tabtoxin inhibits host glutamine synthetase resulting in glutamine deficiency (Ichinose et al., 2013). These small virulence factors are divided into structural classes with distinct

biosynthetic pathways, including polyketides, lipopeptides, β-lactams and non-ribosomal peptides (Bender et al., 1999). An important regulator of virulence factor production is the GacA/GacS system, which consists of a sensor kinase and a transcription response regulator (Heeb and Haas, 2001).

A key determinant of *P. syringae* pathogenesis is the type III secretion system (T3SS), a needle-like structure that delivers effector proteins into the host cell (Alfano and Collmer, 2004). The T3SS is encoded by *hrp* and *hrc* genes arranged in a pathogenicity island (Collmer et al., 2000) that are regulated by both the RhpR/RhpS system, consisting of a kinase and a response regulator, and the GacA/GacS system (Deng et al., 2014; O'Malley and Anderson, 2021). There is crosstalk between regulation of the T3SS and production of other virulence factors. For instance, the RNA polymerase sigma factor HrpL, a key regulator of components of the T3SS, also regulates the production of plant hormone mimics (Fouts et al., 2002; Sreedharan et al., 2006).

Effector proteins translocated through the T3SS are encoded by *avir*ulence (*avr*) and *H*rp-dependent *o*uter *p*rotein (*hop*) genes (Collmer et al., 2000). These proteins perform a variety of functions to promote pathogenesis (Alfano and Collmer, 2004; Büttner, 2016; Dillon et al., 2019; Khan et al., 2018). For example, HopAF1 inhibits host defence responses through manipulation of Arabidopsis methylthioadenosine nucleosidases required for ethylene production (Washington et al., 2016). Furthermore, AvrRpt2 stimulates turnover of the Arabidopsis negative regulator proteins AXR2 and AXR3 to promote auxin signalling, which is associated with pathogen susceptibility (Cui et al., 2013).

Despite their virulence functions, specific recognition of effectors by their cognate R proteins triggers the HR, limiting pathogen colonisation (Cui et al., 2015). The type III effector repertoire can vary drastically between *P. syringae* strains and is therefore a determining factor in host range (Dillon et al., 2019). The strain *P. syringae* pv. *tomato*

DC3000 (*Pto*DC3000) is a model pathogen, but does not naturally cause disease in *N. benthamiana* due to recognition of the type III effector HopQ1-1 by the R protein Roq1 (Schultink et al., 2017). Instead, infection is either symptomless or induces the HR (Wei et al., 2007). However, a mutant lacking HopQ1-1 triggers only weak cell death upon recognition of the effector HopAD1 (Wei et al., 2015), and is able to grow to high levels and cause disease in *N. benthamiana* (Wei et al., 2007). The *N. benthamiana*-*Pto*DC3000Δ*hQ* interaction is therefore used to gain insights into plant-pathogen dynamics during compatible conditions.

1.5 Thesis structure

The overall aim of this thesis is to identify novel plant immune hydrolases, increasing our understanding of plant-pathogen dynamics at the molecular level. This thesis is based on previous work (Sueldo et al., 2023) that coupled activity-based protein profiling with mass-spectrometry (ABPP-MS) to identify suppressed hydrolases in the *N. benthamiana* apoplast upon infection with *P. syringae*. We aim to determine if this suppression is a bacterial response to a role in immunity for the suppressed hydrolases. If successful, this would provide a proof of concept that ABPP-MS can be used to identify immune hydrolases through their suppression. Furthermore, by identifying and subsequently characterising novel hydrolases involved in the plant immune response, we hope this work will ultimately facilitate the development of resistant crops.

Chapter 2 contains a published review of the role of apoplastic proteases in plant immunity.

The aim of **Chapter 3** is to test a selection of suppressed hydrolases for their role in immunity and identify positive candidates to put forward for further study in subsequent chapters of the thesis. We transiently expressed six suppressed hydrolases in

N. benthamiana and tested their role in plant immunity using novel 'agromonas' assays to measure *P. syringae* growth. This screen identified *Nb*PR3, a glycosyl hydrolase that confers bacterial resistance despite its annotation as an endochitinase. We also identified *Nb*RD21, a papain-like cysteine protease whose immune function appears to be ETI-dependent.

In **Chapter 4**, we aimed to determine the mechanism by which *Nb*PR3 contributes to bacterial resistance. We utilised both a biochemical and hypothesis-driven approach to study the substrate and function of *Nb*PR3. A potential role for *Nb*PR3 in bacterial elicitor release was uncovered. We identified a *Nicotiana*-specific mutation that is essential for the bacterial resistance function of *Nb*PR3, suggesting this work could lead to the identification of similar resistance mechanisms in other *Nicotiana* species.

The aim of **Chapter 5** is to elucidate the function of *Nb*RD21. We used both transient expression and *rd21* depletion to investigate hypotheses for *Nb*RD21 function in immunity. We also used mass-spectrometry to uncover changes in the proteome of *rd21* mutants in unchallenged conditions and identified a role for *Nb*RD21 in the processing of RLKs. The reconciliation of *Nb*RD21 functions in different cellular compartments is discussed.

In **Chapter 6** we aimed to confirm that *Nb*RD21 is inhibited by *P. syringae* and characterise the inhibitor. We developed a high-throughput assay to monitor *Nb*RD21 activity and used it to confirm that *Nb*RD21 is inhibited during *P. syringae* infection. We began characterisation of both the breadth of production, and biochemical properties, of the *Nb*RD21 inhibitor.

Finally, **Chapter 7** discusses the overall themes and findings of the previous four results chapters.

Chapter 2: Review of apoplastic immune proteases

The following chapter is a published review of apoplastic immune proteases; **Godson, A., and van der Hoorn, R.A.L.** 2021. The front line of defence: a meta-analysis of apoplastic proteases in plant immunity. Journal of Experimental Botany **72**, 3381–3394. https://doi.org/10.1093/jxb/eraa602 with minor textual adaptations.

The information presented here remains largely up to date, although there have been numerous discoveries since publishing. This includes further insight into the role of subtilases in activating pectin methylesterase activity (Coculo et al., 2023) and identification of a *Phytophthora sojae* effector that inhibits apoplastic protease secretion (Wang et al., 2021). Most striking is the rapid development of machine learning-based approaches such as Alphafold to identify protein structures and binding relationships (Jumper et al., 2021).

2.1 Abstract

Secreted proteases act at the front line of defence and play pivotal roles in disease resistance. However, the criteria for apoplastic immune proteases are not always defined and followed. Here, we critically reviewed 46 apoplastic proteases that function in plant defence. We found that most apoplastic immune proteases are induced upon infection and seventeen proteases are genetically required for the immune response. Proteolytic activity has been confirmed for most of the proteases but is rarely shown to be required for biological function and the apoplastic location of proteases can be subjective and dynamic. Pathogen-derived inhibitors have only been described for cysteine and serine proteases and the selection pressure acting on immune proteases is rarely investigated. We discuss six different mechanisms by which these proteases mediate plant immunity and summarise the challenges for future research.

2.2 Introduction

Proteases are present throughout the tree of life, determining the fate of proteins by irreversibly cleaving peptide bonds. This cleavage serves not only to degrade proteins, thereby rendering them non-functional and facilitating protein turnover, but also to activate proteins through the removal of inhibitory or regulatory domains and changing their subcellular location (van der Hoorn, 2008).

Plant proteases perform critical functions during the interaction between plants and pathogens. Upon pathogen entry, pathogen-associated molecular patterns (PAMPs) such as chitin and flagellin are recognised by pattern recognition receptors (PRRs), resulting in PAMP-triggered immunity (PTI) (Jones and Dangl, 2006). Adapted pathogens use effector proteins to perturb PTI. Resistant plants can recognise some of these effectors through nucleotide-binding leucine-rich repeat (NB-LRR) proteins, resulting in effector-triggered immunity (ETI) (Zipfel, 2014). ETI often culminates in a form of programmed cell death (PCD) known as the hypersensitive response (HR) at the site of infection, limiting the spread of the pathogen (Morel and Dangl, 1997). Both PTI and ETI trigger similar downstream responses, including the release of reactive oxygen species (ROS), activation of mitogen-activated protein kinases (MAPKs) and the production of pathogenesis-related (PR) proteins such as chitinases, glucanases and proteases (Dodds and Rathjen, 2010). Local defence responses often trigger systemic acquired resistance (SAR), underpinned in part by the signalling hormone salicylic acid (SA).

Whilst much of the plant immune response comprises intracellular events such as transcriptional reprogramming and MAPK signalling, most plant-pathogen interactions occur in the extracellular space known as the apoplast. This is the first and often final destination for pathogens that have entered the plant through wounds, stomata and

hydathodes, and is an important site for pathogen proliferation (Jones and Dangl, 2006). The apoplast can be thought of as an ancient 'battlefield' that must be fiercely defended by the host (Jones and Dangl, 2006; Doehlemann and Hemetsberger, 2013; Jashni et al., 2015). Plants are armed with critical weaponry in the form of apoplastic proteases, which they secrete from their cells both constitutively and inducibly (**Figure 2.1**). Their activity at acidic pH, as well as well as the increased stability provided by structural features including disulphide bridges, are crucial for their function in the proteolytically challenging environment of the apoplast (Simões and Faro, 2004; Richau et al., 2012). The MEROPS database (Rawlings et al., 2008) provides a classification of proteases into four main groups depending on their catalytic mechanism: aspartic proteases, cysteine proteases, metalloproteases and serine proteases (van der Hoorn, 2008).

There are several reviews that discuss the role of proteases in plant immunity (Figueiredo et al., 2014; Misas-Villamil et al., 2016; Balakireva and Zamyatnin, 2018; Thomas and van der Hoorn, 2018), but a recent comprehensive overview on the role of apoplastic proteases is missing. In this review we will outline the catalytic classes of plant proteases, and then undertake a meta-analysis of the current literature on apoplastic immune proteases. We will finally discuss the various functions these proteases perform to illustrate the critical role apoplastic immune proteases play at multiple stages of the defence response.

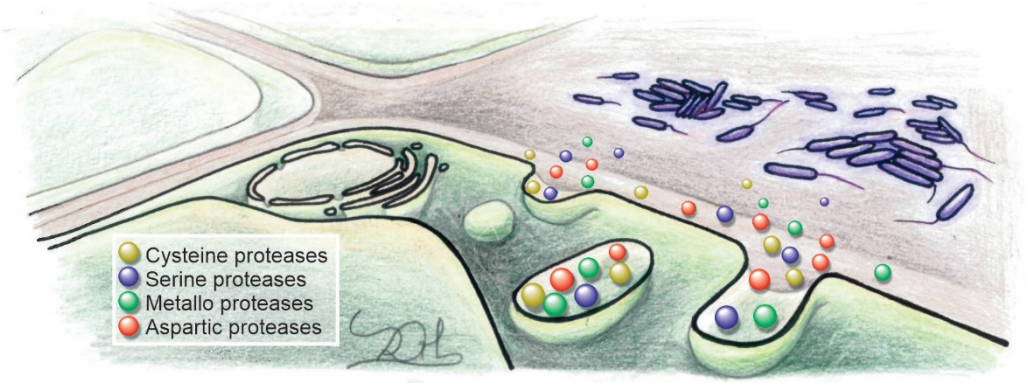


Figure 2.1: Apoplastic immune proteases at the extracellular battlefield. Proteases of the four major catalytic classes are secreted from the cell to the apoplast, an important site of pathogen proliferation. Here, they coordinate the plant immune response through six main strategies: direct antimicrobial activity, immune hydrolase activation, damage-associated molecular pattern (DAMP) release, effector perception, initiation of the hypersensitive response (HR) and the regulation of both systemic acquired resistance and priming.

2.3 Overview of the catalytic classes of plant proteases

Plants produce 500-1000 proteases, which belong to four main catalytic classes and a few additional catalytic classes (van der Hoorn, 2008).

Aspartic (Asp) proteases are characterised by the presence of two aspartic acid residues which support a molecule of water that acts as a nucleophile during proteolysis (van der Hoorn, 2008). Asp proteases are grouped into 14 different families in the MEROPS database (Rawlings et al., 2008), of which five contain plant proteases. The majority of plant Asp proteases belong to the A1 family of pepsin-like proteases (pepsins) (Simões and Faro, 2004). These pepsins may be typical, atypical, or nucellin-like, depending on their active-site motif and other sequence features such as the presence of a plant-specific insert called a swaposin (Simões and Faro, 2004). The majority of plant pepsins are intracellular, usually with a vacuolar location, but there are several plant pepsins accumulating in the apoplast (Simões and Faro, 2004).

Cysteine (Cys) proteases utilise a catalytic cysteine residue in their catalytic triad as a nucleophile during proteolysis (van der Hoorn, 2008). Plant Cys proteases are represented

in five MEROPS clans (Rawlings et al., 2008). Papain-like cysteine proteases (papains) are the only family containing extracellular Cys proteases and have long been implicated in plant immunity (Misas-Villamil et al., 2016). Papains belong to MEROPS clan CA, family C1 and are grouped into nine subfamilies (Richau et al., 2012). The general papain structure consists of a papain-like fold of an α-helix and β-sheet domain, and two papain subfamilies also carry a C-terminal granulin domain. Being very stable enzymes with multiple disulphide bridges, papains are often found in proteolytically harsh environments, such as the apoplast and vacuole (Richau et al., 2012). Their apoplastic location puts papains in direct contact with pathogens and their associated proteins, making them prime candidates for involvement in the plant immune response.

Metalloproteases utilise a catalytic metal cofactor to activate water that acts as a nucleophile during proteolysis (van der Hoorn, 2008). There are over 50 families of metalloproteases in the MEROPS database (Rawlings et al., 2008). Plants have representatives that belong to 19 families, which are grouped into eleven evolutionarily unrelated clans (van der Hoorn, 2008). The matrix metalloproteases (MMPs) of family M10 are the only plant metalloprotease family with apoplastic proteases. MMPs are zinc-dependent endopeptidases that share a conserved catalytic domain containing a zinc-binding sequence and a conserved methionine residue that forms a 'Met-turn' (Marino and Funk, 2012). All plant MMPs contain a signal peptide and are either secreted into the plant apoplast or anchored to the plasma membrane (Flinn, 2008; Marino and Funk, 2012).

Serine (Ser) proteases are the largest class of proteases in plants and are unified by the use of serine in the active site as a nucleophile (van der Hoorn, 2008). Plants contain 14 Ser protease families which are grouped into nine evolutionarily unrelated clans. Subtilisin-like proteases (subtilases) of subfamily S8A are often secreted and the most extensively studied (Schaller et al., 2018). Serine carboxypeptidase-like proteins (SCPLs) are found in MEROPS subfamily S10 and comprise another abundant serine hydrolase subfamily (van

der Hoorn et al., 2011). Whilst many SCPLs have carboxypeptidase activity (Li et al., 2001; Casamitjana-Martínez et al., 2003), some catalyse transacylation reactions rather than cleaving carboxyterminal peptide bonds (Mugford and Milkowski, 2012). All Arabidopsis SCPLs contain signal peptides targeting them for secretion (Fraser et al., 2005) and many SCPLs are detected in the apoplast (Sueldo et al., 2014; Grosse-Holz et al., 2018).

The MEROPS database divides proteases into a further three smaller classes, in addition to the four major classes discussed above. These are asparagine peptide lyases, glutamic proteases and threonine proteases. Asparagine peptide lyases and glutamic proteases have not been studied extensively and plant members are yet to be identified (Rawlings et al., 2011). Threonine proteases such as Arabidopsis PBA1 form subunits of the 26S proteasome that mediates protein degradation (Tanaka, 2009). PBA1 has caspase-3-like activity and is involved in the induction of PCD upon infection with avirulent bacteria (Hatsugai et al., 2009), but is not an apoplastic immune protease. These three protease classes are not later discussed in this review because they do not contain apoplastic immune proteases.

2.4 Meta-analysis of apoplastic immune proteases

Scientific advances have identified and characterised an increasing number of apoplastic immune proteases. We undertook a meta-analysis of proteases that are both apoplastic and involved in immunity. We identified 46 putative apoplastic immune proteases, summarised in **Table 2.1**. For the purpose of the analysis, we counted orthologs of a gene in different species separately. Closely related paralogs from the same species that show indistinguishable immune phenotypes or act redundantly, *CathB1*, *-2* and *-3* in Arabidopsis for instance (McLellan et al., 2009), are counted only once.

To qualify as an apoplastic immune protease, experimental evidence is required for each of these three defining words: apoplastic, immune and protease. This can be summarised as the ABC criteria: (A) apoplastic location; (B) biological function in immunity; and (C) catalytic activity as a protease. We critically evaluated each of the 46 putative apoplastic immune proteases for fulfilling these criteria, summarised in **Table 2.1** and discussed below.

Table 2.1: Criteria for apoplastic immune proteases. 46 proteases are evaluated against the ABC criteria for apoplastic immune proteases: (A) apoplastic location; (B) biological function in immunity; and (C) catalytic activity as a protease. *As*, *Avena sativa; At*, *Arabidopsis thaliana*; *Cp*, *Carica papaya; Cs*, *Citrus sinensis*; *Gb*, *Gossypium babardense*; *Gm*, *Glycine max*; *Hb*, *Hevea brasiliensis; Hv*, *Hordeum vulgare*; *Mj*, *Mirabilis jalapa*; *Nb*, *Nicotiana benthamiana*; *Nt*, *Nicotiana tabacum*; *Os*, *Oryza sativa*; *Sl*, *Solanum lycopersicum*; *St*, *Solanum tuberosum*; *Ta*, *Triticum aestivum; Zm*, *Zea mays*; Y (Yes), evidence that protein meets criteria; **N** (No), evidence that protein does not meet criteria; -, protein not tested against criteria; *, not shown *in planta*. For reference numbers, refer to bibliography.

			A	**B1**	**B2**	**B3**	**B4**	**B5**	**C1**	**C2**	
Name	MEROPS Family	Organism	Apoplastic?	Genetically required?	Induced?	Inhibited?	Diversifying selection?	Secretion prevented?	Protease?	Activity required?	Reference
AED1	A01	*At*	Y	-	Y	-	-	-	-	-	43
*Gm*AP1	A01	*Gm*	Y	Y	-	-	-	Y	Y	Y	147
*St*AP1/3	A01	*St*	Y	-	Y	-	-	-	Y	-	142-145, 252, 270
*Os*AP77	A01	*Os*	-	Y	Y	-	-	-	-	-	2
*Le*AspP	A01	*Sl*	-	-	Y	-	-	-	-	-	324
CDR1	A01	*At*	Y	Y	Y	-	-	-	Y	Y	349, 415
		Os	Y	-	Y	-	-	-	Y	Y	300
SAP1/2	A01	*At*	Y	Y	Y	-	-	-	Y	Y	401
C14	C1A	*Sl*	Y	-	Y	Y	**N**	Y	Y	-	41, 153, 184, 201, 341
		St	-	-	Y	-	Y	-	-	-	16, 184, 185
CathB	C1A	*At*	Y*	Y	Y	-	-	-	Y	-	122, 251, 299
		Nb	Y	Y	Y	-	-	-	Y	-	126
		St	-	-	Y	-	-	-	-	-	17
CP1/2	C1A	*Zm*	Y	-	Y	Y	-	-	Y	-	258, 268, 428
CP14	C1A	*Nb*	Y*	Y	-	-	-	-	Y	-	41, 184, 281
Mir1	C1A	*Zm*	Y	-	Y	Y	-	-	Y	Y	110, 232, 233, 263, 287, 288, 393
MRP1/2	C1A	*Mj*	Y	-	-	Y	-	-	Y	-	93
Papain	C1A	*Cp*	Y	-	Y	Y	-	-	Y	-	18, 101, 146, 197
Pip1	C1A	*Sl*	Y	Y	Y	Y	-	-	Y	-	169, 296, 336, 341, 374
*Cs*RD21a	C1A	*Cs*	Y	-	Y	Y	-	-	Y	-	65
Rcr3	C1A	*Sl*	Y	Y	Y	Y	Y	-	Y	-	89, 93, 169, 202, 234, 286, 312, 336, 341, 352
*Cs*SAG12-1	C1A	*Cs*	-	-	Y	-	-	-	Y	-	65
XCP2	C1A	*Os*	-	Y	Y	-	-	-	-	-	273

		Zm	Y	-	Y	Y	-	-	Y	-	268, 389
At-MMPs	M10	*At*	Y	Y	Y	-	-	-	Y	-	239, 243, 425
*Gm*MMP2	M10	*Gm*	-	-	Y	-	-	-	Y	-	228
*Nt*MMP1	M10	*Nt*	Y	-	Y	-	-	-	Y	-	241, 328
Sl-MMPs	M10	*Sl*	Y	Y	Y	-	-	-	Y	-	218, 429
*Hv*PR-17a/-17b	M10?	*Hv*	Y	-	Y	-	-	-	-	-	64
*Nb*PRp27	M10?	*Nb*	-	Y	Y	-	-	-	-	-	418
*Nt*PRp27	M10?	*Nt*	Y	-	Y	-	-	-	-	-	276
WCI-5	M10?	*Ta*	-	-	Y	-	-	-	-	-	131, 332
*Os*BISCPL1	S10	*Os*	-	-	Y	-	-	-	-	-	225
P69B	S8	*Sl*	Y	-	Y	Y	-	-	Y	Y	135, 178, 286, 296, 372, 373, 377, 399, 426, 429
P69C	S8	*Sl*	Y	-	Y	-	-	-	Y	-	178, 296, 376
*Sl*Phyt-1/-2	S8	*Sl*	Y	-	-	-	-	-	Y	-	29, 309
Phytaspase	S8	*Nt* *Os*	Y -	Y -	Y -	- -	- -	- -	Y Y	- Y	61, 62 62
SAS-1/-2	S8	*As*	Y	-	**N**	-	-	-	Y	-	68
*Gb*SBT1	S8	*Gb*	Y	Y	Y	-	-	-	-	-	94
SBT3	S8	*Sl*	Y	Y	Y	-	-	-	Y	-	254, 255
SBT3.3	S8	*At*	Y	Y	Y	-	-	-	Y	Y	302
SBT3.5	S8	*At*	Y	-	-	-	-	-	Y	-	35, 334
*Nb*SBT5.2	S8	*Nb*	Y	-	-	-	-	-	Y	-	286, 399
*St*SBTc-3	S8	*St*	Y	-	Y	-	-	-	Y	Y	108, 109
*Hb*SPA	S8	*Hb*	Y	-	Y	Y	-	-	Y	-	98

2.4.1 Criterium A (Apoplast): Apoplastic location can be subjective and dynamic

In total, 35 of the 46 identified proteins (76%) have been shown to be secreted, although whether a protein is considered apoplastic is dependent on definition. We consider a protease to be apoplastic if its catalytic domain is located outside of the plasma membrane. This encompasses the extracellular space and the xylem, but also the cell wall and latex. The picture is complicated when considering that proteins are often found in multiple locations within and outside the cell. The papain C14, for example, is found in the vacuoles,

vesicles, endoplasmic reticulum and apoplast of tomato (Bozkurt et al., 2011). We define a protease as apoplastic if the mature protein is located, not necessarily exclusively, in the apoplast. Therefore, we exclude peptide fragments of proteases that have an apoplastic immune function, if the full-length protein is not apoplastic. This is exemplified by *Drosera capensis* aspartic proteases known as Droserasins that are post-translationally cleaved to release small antimicrobial peptides, but are themselves not apoplastic (Sprague-Piercy et al., 2020).

The literature is abundant with examples of proteases whose apoplastic location is predicted on the basis of the extracellular location of orthologous proteases, or the use of prediction software such as ApoplastP, which utilises machine learning to predict the location based on amino acid enrichment and depletion patterns (Sperschneider et al., 2018), and SignalP, which predicts signal peptides and their cleavage sites (Armenteros et al., 2019). These methods of prediction are not infallible and experimental evidence is usually obtained to confirm the location of the protease. This might include detection of the protease from apoplastic fluid or confocal microscopy with fluorescent fusion proteins.

Protein location is also dynamic, and both import to and export from the apoplast are inducible upon both abiotic and biotic stress. Proteases are released from the vacuole into the apoplast upon PCD induced by avirulent bacteria (Hatsugai et al., 2009). Conversely, phytaspase is constitutively secreted into the apoplast of tobacco and rice before being physically relocalised into the cell upon PCD (Chichkova et al., 2010). Similarly, cotton subtilase *Gb*SBT1 relocates from the apoplast to the cytoplasm during defence against the fungus *Verticillium dahliae* (Duan et al., 2016). Extracellular *Gb*SBT1 interacts with the secreted *V. dahliae* effector prohibitin, which may trigger the movement of *Gb*SBT1 into the cell (Duan et al., 2016).

2.4.2 Criterium B (Biological role)

B1: Seventeen proteases are genetically required for immunity

We classified a protease as genetically required for the immune response if knockdown or knockout of the gene in question resulted in increased pathogen susceptibility. Genetic requirement for pathogen resistance has been demonstrated for 17 of the 46 identified proteases (37%). For example, antisense *Pip1* tomato plants are highly susceptible to *Cladosporium fulvum*, *Pseudomonas syringae* and *Phytophthora infestans* (Ilyas et al., 2015). Likewise, hairpin silencing of tomato *SBT3* increases the growth of *Manduca sexta* larvae (Meyer et al., 2016a) and depletion of *NbPRp27* by VIGS increases susceptibility to *P. syringae* pv. *tabaci* (Xie and Goodwin, 2009).

In contrast to the 17 confirmed proteases contributing positively to immunity, the APOPLASTIC, EDS1-DEPENDENT 1 (AED1) Asp protease in Arabidopsis might be suppressing immune responses (Breitenbach et al., 2014). *AED1* silencing results in elevated transcripts of the SAR marker gene *PR1*, as well as severe stunting, indicative of a constitutive defence phenotype. However, disease assays showing significantly increased resistance of silenced plants compared to wild-type plants have not yet been reported.

Redundancy amongst closely related immune proteases can make it difficult to untangle immune functions. For instance, studies on five MMP genes in Arabidopsis showed that triple mutants had a stronger defect in immunity when compared to single mutants to both *Botrytis cinerea* and *Golovinomyces orontii* (Zhao et al., 2017). Similarly, Arabidopsis *CathB1*, *-B2* and *-B3* show high sequence identity and are redundantly involved in basal resistance and the development of PCD (McLellan et al., 2009).

Genetic requirement should be demonstrated through knockdown or knockout of the gene in question and cannot be inferred from lines that naturally accumulate different levels of the protease. For instance, the protease Mir1 accumulates in resistant but not susceptible maize lines and there is a negative correlation between Mir1 protein concentration and larval weight (Pechan et al., 2000). However, this cannot be used as evidence for the genetic requirement of Mir1 since there are likely to be other differences between these lines. Overexpression of a protease is also used to infer an immune function, but these experiments must also be interpreted with caution since they do not demonstrate the endogenous role of the protease.

B2: Protease induction at transcript/protein level is common

Protease induction upon biotic stressed can be inferred through experimental techniques measuring an increase in transcript levels, such as RNA sequencing, or protein abundance, such as western blotting or mass-spectrometry. In total 38 of the 46 proteases (83%) are induced at the transcript and/or protein level. This suggests that nearly all immune proteases are PR proteins, or alternatively that proteases that are not induced, but do function in immunity, are being overlooked. For instance, mRNA corresponding to the tomato Asp protease *Le*AspP is induced in leaves upon wounding (Schaller and Ryan, 1996), and there is a rapid accumulation of soybean *GmMMP2* transcripts upon infection with *Phytophthora sojae* and *P. syringae* pv. *glycinea* (Liu et al., 2001). Likewise, experiments with coffee cultivars showed an increase in apoplastic Ser protease activity upon *Hemileia vastratrix* infection, particularly in resistant cultivars (Guerra-Guimarães et al., 2015), and activity-based protein profiling (ABPP, explained in section C1) uncovered an increased activity of Cys and Ser proteases Pip1, P69B and P69C in tomato upon *Ralstonia solanacearum* infection (Planas-Marquès et al., 2018). However, not all immune proteases are induced. The oat subtilases SAS-1 and SAS-2 are constitutively transcribed

and present in the cell but apoplastic activity is induced by relocation into the apoplast at the onset of PCD induced by the fungal toxin victorin (Coffeen and Wolpert, 2004).

B3: Identification of pathogen-derived inhibitors has been restricted to Cys and Ser proteases

Inhibition by pathogen-derived inhibitors has been described for eleven of the 46 immune proteases (24%). Notably, nine of these eleven proteases are Cys proteases. In fact, the Cys proteases Rcr3, Pip1 and C14 are each targeted by multiple inhibitors (Tian et al., 2007; Shabab et al., 2008; Kaschani et al., 2010; Lozano-Torres et al., 2012; Shindo et al., 2016), with the same inhibitor often targeting multiple Cys proteases (Clark et al., 2018). The concept of adaptation of a pathogen and its inhibitor repertoire to its host is neatly demonstrated by the case of *Phytophthora mirabilis*, an oomycete closely related to *P. infestans*, which infects the four-o'clock flower (*Mirabilis jalapa*). Whilst EPIC1 of *P. infestans* inhibits Solanum Rcr3, *Pm*EPIC1 of *P. mirabilis* has specialised to inhibit the Rcr3-related proteases MRP1 and MRP2 of *M. jalapa*. The specialisation of each effector to its corresponding protease was underpinned by a single amino acid polymorphism in the host protease along with a reciprocal single amino acid change in the pathogen effector (Dong et al., 2014).

Despite the bias in the literature towards the identification of Cys protease inhibitors, there are also some known examples of Ser protease inhibitors. Tomato P69B is inhibited by two Kazal-like Ser protease inhibitors of *P. infestans*, EPI1 and EPI10 (Tian et al., 2004, 2005). These inhibitors are distinct, differing in the number and sequence of the Kazal-like domains they possess. Inhibition of P69B by two divergent inhibitors suggests this is an important infection strategy for the pathogen. The *Phytophthora palmivora* homolog of EPI10 is secreted into the apoplast during infection of rubber tree (*Hevea brasiliensis*) (Chinnapun et al., 2009) and inhibits the apoplastic subtilase *Hb*SPA, which may otherwise mediate

resistance to the pathogen (Ekchaweng et al., 2017). Whilst inhibitors of apoplastic Asp and metalloproteases have not yet been reported, there is no inherent reason why they could not be targeted by pathogen-derived inhibitors.

B4: Selection pressure acting on immune proteases is rarely investigated

Only two of the 46 immune proteases (4%) have been shown to be under diversifying selection: Rcr3 and *St*C14 (Shabab et al., 2008; Kaschani et al., 2010; Kaschani and van der Hoorn, 2011). Their variant residues locate around the substrate binding site as a footprint of an arms race with pathogen-derived inhibitors. The positions of the variant residues in Pip1 and P69B are also consistent with the presence of diversifying selection caused by pathogen-derived inhibitors (Shabab et al., 2008; Hörger and van der Hoorn, 2013). This low number is not because of negative results for the remaining proteases, but rather because this aspect has not been investigated for most immune proteases. Only *Sl*C14 is confirmed to be under stabilising, rather than diversifying, selection (Shabab et al., 2008). The difference in selection pressure between tomato and potato C14 likely reflects the specialisation of *P. infestans* to wild potato, its natural host (Kaschani et al., 2010).

B5: Two proteases are prevented from secretion into the apoplast

The prevention of protease secretion into the apoplast has been identified for two of the 46 proteases (4%). Secretion of the tomato Cys protease C14 is prevented by the *P. infestans* RxLR effector AvrBlb2, which accumulates around haustoria. An *AvrBlb2* mutant impaired in haustorial localisation allowed apoplastic C14 accumulation and was unable to promote infection symptoms of *P. infestans* (Bozkurt et al., 2011). Likewise *P. sojae*, the cause of soybean stem and root rot, secretes the plasma membrane-localised RxLR-type effector *Ps*Avr240 that prevents the secretion of the soybean Asp protease *Gm*AP1 into the apoplast (Guo et al., 2019). *Gm*AP1 positively contributes to resistance against

Phytophthora species, and so by preventing its secretion, *Gm*AP1-mediated defence is compromised. In both instances, however, the underlying molecular mechanism is unknown.

2.4.3 Criterium C (Catalytic activity):

C1: Protease activity is shown for most candidates

Protease activity has been confirmed for 34 of the 46 identified proteases (74%). In particular, catalytic activity has been confirmed for the majority of the identified Cys proteases (81%). This likely reflects the relatively thorough characterisation of papains and the tools available to monitor their activity.

Catalytic activity is demonstrated by the ability of a protease to degrade a biological or commercial substrate. For instance, gelatin and casein are general protease substrates that were used to confirm the protease activity of tomato Rcr3 and potato *St*SBTc-3, respectively (Krüger et al., 2002; Fernández et al., 2015). Similarly, myelin basic protein and Z-Leu-Arg-MCA have confirmed the catalytic activity of soybean metalloprotease *Gm*MMP2 (Liu et al., 2001) and *Nicotiana benthamiana* Cys protease CP14 (Paireder et al., 2016) , respectively. Protease activity can also be inferred using ABPP. This technique uses chemical probes that mimic substrates but covalently bind to the active site of proteases as a readout for their activity (Morimoto and van der Hoorn, 2016). For example, ABPP labelling was used to infer the catalytic activity of *Citrus sinensis* RD21a (Clark et al., 2018), tomato P69C (Planas-Marquès et al., 2018) and *Nb*SBT5.2 (Paulus et al., 2020). Finally, catalytic activity is implicit if criteria C2 is satisfied, even if the activity has not been shown directly – for instance, an active-site mutant of soybean Asp protease *Gm*AP1 no longer confers resistance to *Phytophthora capsici*, indicating that the wild-type protease must display catalytic activity (Guo et al., 2019).

C2: The requirement of catalytic activity for biological function is rarely shown

The active site of proteases has been shown to be required for the biological function of only nine of the 46 immune proteins (20%). The requirement of catalytic activity can primarily be shown by a catalytically inactive mutant no longer being able to perform the described immune function. For instance, catalytic mutants of Asp protease SAP1 are no longer able to suppress *P. syringae* growth (Wang et al., 2019c). Similarly, tobacco silenced for PCD-promoting phytaspase show an abolished tobacco mosaic virus (TMV)-induced HR that can be restored by complementation with wild-type rice phytaspase, but not its catalytic mutant (Chichkova et al., 2010).

Alternatively, the requirement for catalytic activity can be shown through the use of an inhibitor preventing the biological function of the protease. However, this can only be taken as evidence if only the protease in question is being inhibited. Since most commercial inhibitors are not specific to a single protease, the protease must be purified and inhibition studied *in vitro*. For instance, papain itself is released into the latex of papaya upon wounding, where it provides a strong toxicity and growth inhibition against a range of lepidopteran pests (Konno et al., 2004). Papaya leaves painted with the papain inhibitor E-64 support significantly greater larval growth, but this is not proof of the catalytic requirement of papain itself since E-64 may also inhibit other papain-like Cys proteases present in latex (Konno et al., 2004).

Likewise, the antimicrobial activity of extracellular Asp proteases *St*AP1 and *St*AP3 was demonstrated by *in vitro* experiments showing the inhibition of *P. infestans* cyst and *Fusarium solani* conidia germination upon incubation with the purified proteases (Guevara et al., 2002, 2004). This antimicrobial activity can be abolished by the addition of the Asp protease inhibitor pepstatin A to the purified proteases (Guevara et al., 2002, 2004). Addition of Pepstatin A to apoplastic fluid also increases susceptibility to *F. solani*, but this

is not enough evidence that these proteases have antimicrobial activity *in vivo*, and that catalytic activity is required for this.

2.5 Six functions of secreted immune proteases

The molecular mechanism by which apoplastic proteases confer immunity appears resolved in eight cases: *St*AP1/3, SAP1/2, Mir1, Papain, Rcr3, P69B, *Sl*Phyt-1/-2 and SBT3.5, although genetic requirement for the immune response has not yet been demonstrated for *St*AP1/3, Papain and *Sl*Phyt-1/-2. We divide these mechanisms into four groups: antimicrobial activity, immune hydrolase activation, damage-associated molecular pattern (DAMP) release and effector perception. A single protease may act on multiple substrates and hence perform multiple functions, as is the case for tomato P69B (Wang et al., 2019a; Paulus et al., 2020).

2.5.1 Apoplastic proteases display direct antimicrobial activity

Apoplastic proteases are in a perfect place to directly damage the pathogen, impeding growth and proliferation (Konno et al., 2004; Mendieta et al., 2006). One of the first papains to be characterised, Mir1 from maize, has direct antimicrobial activity against insect pests. This was first indicated by growth inhibition of fall armyworm and tobacco budworm larvae feeding on callus expressing *Mir1* (Pechan et al., 2000). Direct antimicrobial activity was later demonstrated by a sharp increase in the permeability of *Spodoptera frugiperda* (fall armyworm) peritrophic matrix to Blue Dextran upon the addition of purified Mir1 (Mohan et al., 2006). Mir1 accumulates at the wound site within one hour of larval feeding, assisted by the protease's movement through the plant vascular tissues (Lopez et al., 2007). The protease inhibits larval growth by degrading Insect Intestinal Mucin (IIM), which crosslinks the chitin fibrils in the peritrophic matrix (Fescemyer et al., 2013). This induces IIM

permeabilization, which impairs digestion and nutrient absorption (Pechan et al., 2002; Mohan et al., 2006). Larvae compensate for this damage by altering their midgut transcriptome to upregulate IIM replacement components (Fescemyer et al., 2013) and produce Cys protease inhibitors in the midgut (Li et al., 2009). Mir1 also provides enhanced resistance to corn leaf aphids above-ground, and western corn rootworm below-ground (Louis et al., 2015; Varsani et al., 2016).

Direct antimicrobial activity has also been shown for secreted aspartic protease 1 and 2 (SAP1 and SAP2) in Arabidopsis. Purified SAP1 and SAP2 are capable of suppressing *P. syringae* growth *in vitro*, demonstrating their antimicrobial activity (Wang et al., 2019c). SAP1 and SAP2 contribute redundantly to defence against *P. syringae* through the cleavage of the bacterial protein MucD, which is required for bacterial growth (Wang et al., 2019c). Cleavage of MucD by SAP1 and SAP2 suppresses bacterial growth without causing bacterial death. *SAP* homologs are found throughout the Brassicaceae family as well as in tomato and rice, suggesting this role in immunity could be evolutionarily conserved (Wang et al., 2019c).

2.5.2 Apoplastic proteases activating immune hydrolases

Apoplastic proteases are able to activate other immature hydrolases by removing inhibitory prodomains. For instance, tomato subtilase P69B cleaves after Asp residues to remove the prodomain of Rcr3, thereby activating this immune protease (Paulus et al., 2020). *N. benthamiana* subtilase SBT5.2, which is from a different subfamily to P69B, can also process proRcr3 into mature Rcr3 (Paulus et al., 2020). This suggests that activation of immune proteases by subtilases is common in Solanaceous plants.

Likewise, Arabidopsis subtilase SBT3.5 activates pectin methylesterases (PMEs) such as PME17 (Sénéchal et al., 2014). PMEs are found in the apoplast and are responsible for the

demethylation of homogalacturonan, the major constituent of pectin in the cell wall. Altering the cell wall properties such as pH and rigidity can have dramatic consequences for the resistance of plants to pathogens, which may use cell wall degradation as an infection strategy (Lionetti et al., 2007), There is evidence of both positive and negative roles for PMEs in immunity (Lionetti et al., 2007; Körner et al., 2009). PME17 is required for immunity because its transcripts are upregulated in response to *P. syringae* and *Alternaria brassicicola* infection, and *pme17* mutants are more susceptible to *P. syringae* (Bethke et al., 2014). This implicates SBT3.5 in immunity through the activation of a cell wall-modifying enzyme.

2.5.3 Apoplastic proteases mediating DAMP release

Another function of apoplastic proteases is mediating the release of peptides that act as DAMPs (Hou et al., 2019). Tomato phytaspases *Sl*Phyt-1 and *Sl*Phyt-2 can process the defence peptide systemin from its precursor, prosystemin (Beloshistov et al., 2018). Systemin release is required for wound signalling, which is critical in the response to herbivory (Savatin et al., 2014). Prosystemin is found in the cell cytoplasm whilst phytaspases are apoplastic (Chichkova et al., 2010). Therefore the processing of prosystemin can occur only upon wounding, when cellular integrity is disrupted and the proteins can interact (Beloshistov et al., 2018). The diffusion of phytaspases into the cell during PCD (Chichkova et al., 2010) could also trigger systemin activation, providing a link between PCD and the systemic wound response in tomato (Ryan, 2000).

Maize papains are required for the processing of the propeptide Prozip1 to release Zip1, a small peptide DAMP that activates SA signalling (Ziemann et al., 2018). Zip1 release induces papain activation, thus establishing a positive feedback loop, and promotes SA-mediated defence responses including the upregulation of defence-related genes such as those encoding chitinases and β-1,3-glucanases, and the mitigation of infection by

biotrophic fungi (Ziemann et al., 2018). However, the individual protease responsible for Prozip1 processing has not yet been identified.

2.5.4 Apoplastic proteases perceive pathogen effectors

Two apoplastic immune proteases act in the perception of pathogen effectors. The tomato papain-like Rcr3 is critical for recognition of the pathogen effector Avr2 produced by the fungus *C. fulvum*. The complex formed when Avr2 inhibits Rcr3 is perceived by the leucine-rich repeat receptor-like protein Cf2, triggering the HR (Rooney et al., 2005). Rcr3 is essential for Avr2 perception and in the absence of Cf2, Rcr3 does not contribute to immunity to *C. fulvum*, suggesting that it acts as a decoy mimicking the more abundant Rcr3 paralog Pip1 (Ilyas et al., 2015). However, Rcr3 contributes to *P. infestans* resistance in the absense of Cf2, indicating also a direct role in immunity (Ilyas et al., 2015). Like *C. fulvum*, *P. infestans* secretes effectors to inhibit Rcr3 and other papains. Yet unlike Avr2, EPIC1 and EPIC2B are 'stealthy' effectors that inhibit host proteases without being detected by Cf2 (Song et al., 2009).

The second protease involved in effector perception utilises a very different mechanism. The Cys-rich secreted protein PC2 produced by *P. infestans* is cleaved by apoplastic subtilases including P69B, triggering an immune response including cell death, the accumulation of ROS and the upregulation of defence-related genes (Wang et al., 2019a). This cleavage is essential for the PC2-triggered immune response and presumably produces a small peptide that is recognised at the cell surface. Interestingly, *P. infestans* is able to inhibit PC2 cleavage and therefore cell death by producing Ser protease inhibitors such as EPI1 (Wang et al., 2019a).

2.5.5 Apoplastic proteases required for the HR

Several apoplastic proteases contribute to HR, although relatively little is understood about the mechanisms by which they regulate and initiate this process. For instance, overexpression and silencing of tobacco phytaspase results in TMV-induced lesions that are larger or smaller, respectively, than those of wildtype plants, providing evidence of a clear involvement of phytaspase in the HR. How this is achieved at the mechanistic level has not yet been elucidated (Chichkova et al., 2010).

The first subtilases associated with PCD, SAS-1 and SAS-2, were identified in 2004 and have caspase-6-like activity. These saspases are thought to be involved in a signalling cascade leading to the cleavage of RuBisCO (Coffeen and Wolpert, 2004). Similarly, increased caspase-3-like activity is implicated in the production of necrotic lesions in potato leaves that restrict *P. infestans* growth (Fernández et al., 2012). This activity was later attributed to potato subtilase *St*SBTc-3 which was isolated from *P. infestans*-infected leaves (Fernández et al., 2015). A role in PCD for *St*SBTc-3 is further suggested by the ability of the purified protease to induce cytoplasm shrinkage and decrease the viability of tomato cell cultures *in vitro* (Fernández et al., 2015). Likewise, the tomato phytaspases *Sl*Phyt-2, -3, -4, -5 and -6 were able to trigger cell death, observed by trypan blue staining, when overexpressed in tomato leaves (Reichardt et al., 2018).

Cathepsin B (CathB) is a papain implicated in PCD in both plants and animals. Silencing of *CathB* in *N. benthamiana* restricts HR triggered by both *Erwinia amylovora* and *P. syringae*, compromising resistance (Gilroy et al., 2007). In Arabidopsis, three *CathB* genes have caspase-3-like activity and contribute redundantly to HR (McLellan et al., 2009; Ge et al., 2016). However, the importance of CathB in HR appears to be context dependent. For instance, *Nb*CathB induces HR triggered by the Avr/R combination Avr3a/R3a, but is not required for HR triggered by Avr4/Cf4 (Gilroy et al., 2007). Likewise, *AtCathB* mutants are

more susceptible to virulent *P. syringae*, yet despite a reduction in AvrB/RPM1-mediated HR, *AtCathB* mutant plants are not compromised in reducing bacterial growth (McLellan et al., 2009). In spite of the evidence that CathB participates in HR regulation, the location of CathB action - apoplastic or intracellular - remains unclear. Studying the role of proteases during the HR is challenged by the fact that protease location cannot be resolved whilst the cell is undergoing PCD.

2.5.6 Apoplastic proteases mediate SAR and priming

Three apoplastic proteases (AED1, CDR1 and SBT3.3) are involved in signalling leading to local and systemic defence responses, as well as priming the plant for future pathogen invasion. In each case, the substrates of the immune proteases and their position within the signalling cascade are not known.

Constitutive Disease Resistance 1 (CDR1) is an “atypical” Arabidopsis pepsin-like Asp protease identified by T-DNA activation tagging (Xia et al., 2004). *CDR1* overexpression results in increased resistance to virulent *P. syringae* as well as a phenotype mimicking constitutive SAR activation, whilst antisense *CDR1* lines show enhanced bacterial susceptibility (Xia et al., 2004). Upon pathogen invasion, CDR1 accumulates in the apoplast, where it induces both local and systemic defence responses in a SA-dependent manner. Activation of the systemic defence response can be achieved by a mobile elicitor present in extracellular fluids and thought to be generated by CDR1, but its identity is still unknown (Xia et al., 2004). Likewise, rice *OsCDR1* induces the expression of defence-related genes and enhances disease resistance to multiple pathogens when overexpressed in both rice and Arabidopsis (Prasad et al., 2009). Local *OsCDR1* expression in Arabidopsis induces a systemic defence response, suggesting that CDR1 has a conserved function in SA-mediated disease resistance (Prasad et al., 2009). The contrasting roles for CDR1 and

AED1 (Criterium B1) raise fascinating questions regarding their evolution and substrate selectivity.

Arabidopsis subtilase SBT3.3 is involved in the regulation of immune priming (Ramírez et al., 2013). Priming is the process by which plants mount a stronger and faster immune response. The expression of *SBT3.3* is induced upon pathogen invasion and *sbt3.3* mutants are more susceptible to *P. syringae* and *Hyaloperonospora arabidopsidis*. SBT3.3 primes plants for the transcriptional activation of defence-related genes following pathogen invasion by inducing chromatin remodelling in the form of activating histone marks at the promoters of SA-regulated defence-related genes including *PR1*, and at its own promoter, initiating a positive-feedback loop (Ramírez et al., 2013). However, the substrate and mechanism of SBT3.3 activity remain enigmatic.

2.6 Discussion

There is no doubt that proteases play important roles in plant immunity, and the emerging picture is that these roles are very diverse. Unravelling these different roles holds several major challenges.

The first challenge lies in unravelling a robust proteolytic network with intrinsic redundancies. Genetic redundancy improves the robustness of defence when multiple proteins, each with different sensitivities to e.g. pathogen-derived inhibitors, act on one or several substrates (Whitacre, 2012; Fares, 2015). A similar robust network has been described for diverse “helper” and “sensor” NLRs that confer immunity to a broad range of plant pathogens (Wu et al., 2017). The expansion of the *P69* family in tomato (Jordá et al., 2000; Reichardt et al., 2018) as well as the clustering of papains in several plant families (Richau et al., 2012) support the concept of selection for redundant protease networks. Compensation between different protease classes, such as Asp and Cys proteases, is also increasingly likely because redundant proteases may cleave at different sites within the same region of a substrate to produce the same outcome.

A second challenge is to understand how apoplastic proteases are regulated. Activation of apoplastic proteases may be dependent on endogenous regulators (Zimmermann et al., 2016), proteolytic cascades (Paulus et al., 2020), pH (Meyer et al., 2016b), or redox status (Balakireva and Zamyatnin, 2019). Understanding how these elements coordinate protease function during pathogen invasion remains a challenge for future research.

The third, obvious challenge is the identification of biologically relevant substrates. Substrate identification techniques can return multiple candidates, but not all of these substrates may contribute to the observed immune phenotype. This can be tested

experimentally, for instance using uncleavable mutant substrates. However, redundancy amongst substrates providing collective immunity may mask the role of individual substrates.

A fourth challenge is to determine if the prevalence of Cys and Ser proteases, particularly papains and subtilases, is due to their relative importance in immunity, or the result of a research bias, sparked by leading examples and supported by robust detection assays. Future efforts should also include unbiased approaches to identify secreted immune proteases and consider less well-characterised proteases. In addition, the lack of research into apoplastic proteases from basal plant species (**Table 2.1**) should be noted. This data gap prevents our understanding of the evolution of apoplastic defence, although the lack of research into plant immunity in basal plant species is beginning to be addressed (Mamaeva et al., 2023).

In addition, we are left with several intriguing questions. For instance, which apoplastic proteases are responsible for DAMP and PAMP release *in vivo*? For instance, proteases responsible for releasing the bacterial PAMPs from flagellin and EF-Tu remain to be identified. Furthermore, how do secreted proteases act collectively and consecutively on substrates? In addition, how do plant proteases distinguish between plant and pathogen substrates in order to prevent self-degradation? Are extracellular protease repertoires different between plant species and is this important for co-evolution with secreted pathogen proteins? Or for being a non-host? Finally, in what way do secreted proteases from pathogens or endophytes influence the catalytic activity of the apoplast? These are just a few of the fascinating remaining questions waiting to be answered.

2.7 Contributions

This review was entirely written by myself. Professor Renier van der Hoorn gave suggestions, assisted editing and drew **Figure 2.1**.

Chapter 3: Screen of a selection of suppressed hydrolases

3.1 Abstract

Plants are threatened by invading pathogens including bacteria, fungi and oomycetes, putting agriculture at risk of considerable yield loss. A critical factor determining the outcome of plant-pathogen interactions is defence of the apoplast, the extracellular space in leaves. Previous work in the van der Hoorn group used activity-based proteomics to monitor hydrolase dynamics in the *Nicotiana benthamiana* apoplast upon infection with *Pseudomonas syringae* pv. *tomato* DC3000∆*hQ* (*Pto*DC3000∆*hQ*).

Sixty plant hydrolases were suppressed at the activity level upon infection, including the previously described immune ß-galactosidase BGAL1. We hypothesised that, like BGAL1, the other hydrolases may be inhibited by *P. syringae* to prevent their immune function. We tested six of the suppressed hydrolases in 'agromonas' assays. Overexpression of two hydrolases conferred bacterial resistance in unexpected ways. This included *Nb*PR3, which conferred bacterial resistance despite its annotation as an endochitinase, and *Nb*RD21, which conferred resistance to *Pto*DC3000 only when the strain carried the HopQ1-1 effector and triggered effector-triggered immunity (ETI).

3.2 Introduction

Previous work in the van der Hoorn group looked to uncover novel hydrolase dynamics in the *Nicotiana benthamiana* apoplast during *Pseudomonas syringae* infection (Sueldo et al., 2023). This made use of activity-based protein profiling (ABPP) as a tool to monitor apoplastic hydrolase activities. ABPP uses chemical probes that covalently bind to the active site of specific enzymes. Since different enzymes have different substrate specificities, a chosen probe enables specific labelling of active enzymes of a particular class. Each probe is attached to a reporter tag. Fluorescent tags enable visualisation of proteins separated on acrylamide gels that are scanned for fluorescence, whilst an affinity tag such as biotin allows the proteins to be purified and identified by mass-spectrometry (MS; Morimoto and van der Hoorn, 2016).

To simultaneously monitor the activity of multiple classes of hydrolase upon *P. syringae* pv. *tomato* DC3000Δ*hQ* infection, a 'probe cocktail' was used. This consisted of three different biotinylated probes: DCG-04 (Greenbaum et al., 2000), FP-biotin (Liu et al., 1999) and JJB111 (Chandrasekar et al., 2014), which label cysteine proteases (CPs), serine hydrolases (SHs), and glycosyl hydrolases (GHs) respectively. Apoplastic fluid was isolated from *N. benthamiana* two days after infection with either *Pto*DC3000Δ*hQ* or water in N=4 replicates. The apoplastic proteome was labelled with the probe cocktail, purified and analysed by MS (**Figure 3.1A**). The experiment identified 171 target hydrolases (**Figure 3.1B**), of which 92% were differentially labelled between the mock and *Pto*DC3000Δ*hQ* treatment (**Figure 3.1C**; Sueldo et al., 2023). Many hydrolases (97) increased in activity upon infection, but interestingly, 60 hydrolases were suppressed (**Figure 3.1D**). This included 24 SHs, 27 GHs, and nine CPs (**Figure 3.1E**).

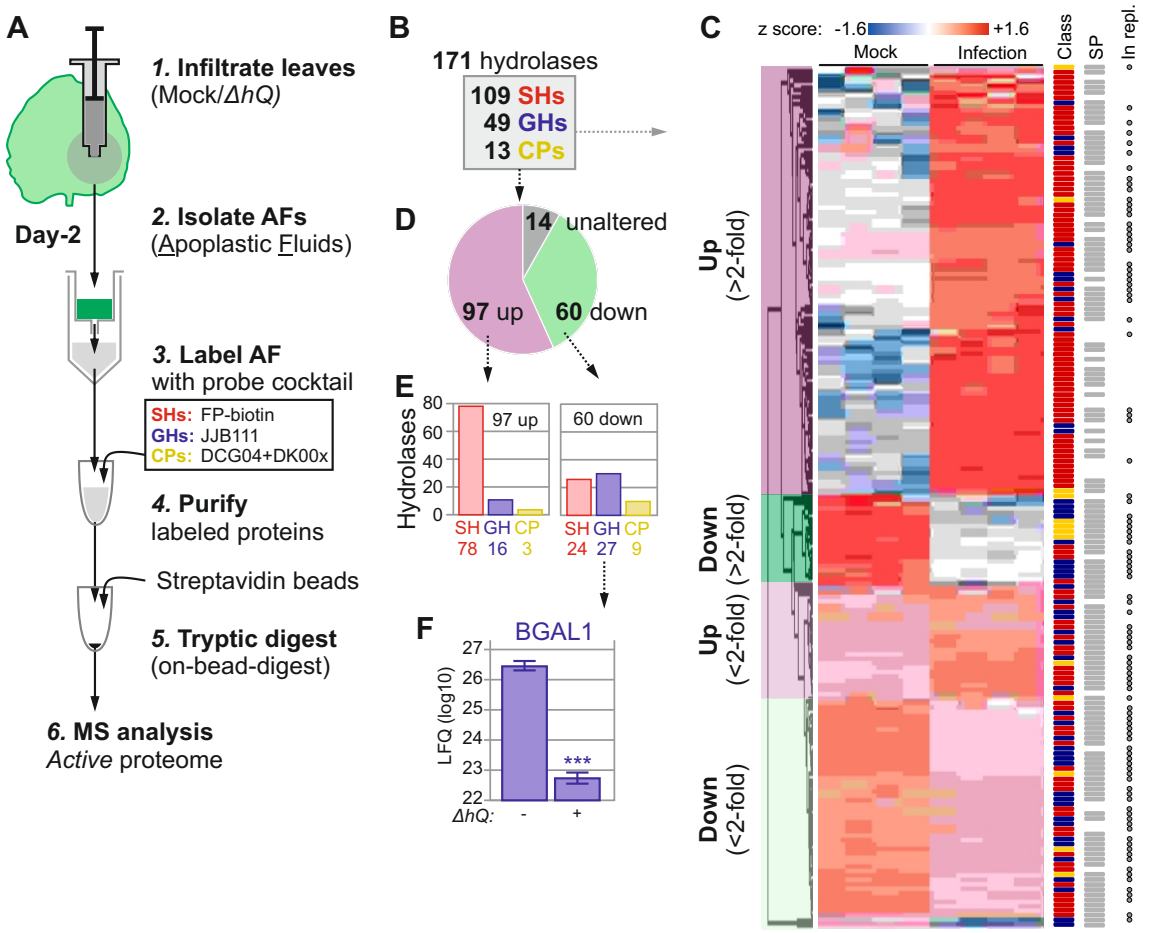


Figure 3.1: Analysis of *N. benthamiana* hydrolase dynamics during *P. syringae* infection
A: Experimental design. Leaves were infiltrated with water (Mock) or *Pto*DC3000Δ*hQ* (Δ*hQ*).Two days later, apoplastic fluid was collected and labelled with the probe cocktail. Labelled proteins were purified and analysed by mass spectrometry with N=4.
B: Classification of 171 identified hydrolases
C: Heatmap of 171 identified hydrolases. Hydrolases were annotated according to fold-change, class, presence of signal peptide, and detection in independent experimental replicate.
D: Summary of activity changes of 171 identified hydrolases.
E: Summary of hydrolase classes significantly up- or down-regulated upon infection.
F: BGAL1 activity is significantly reduced upon infection in this dataset.
Data collected and figure produced by Dr. Daniela Sueldo.

Among these suppressed hydrolases was BGAL1, a ß-galactosidase previously shown to be suppressed during *Pto*DC3000Δ*hQ* infection (**Figure 3.1F**; Buscaill et al., 2019). BGAL1 acts in immunity by de-glycosylating flagellin, thereby enabling the release of the flg22 elicitor whose perception by FLS2 triggers the immune response (Buscaill et al., 2019). This suggests that some of the other suppressed hydrolases we identified may, like BGAL1, be involved in plant defence, and bacterial inhibition has evolved in response to this.

We selected six suppressed hydrolases to test this hypothesis (**Table 3.1**). Their suppression is not a result of changes in protein levels because these proteins accumulate upon infection (Sueldo et al., 2023). Gene names for the suppressed hydrolases were assigned by taking the name of the closest homolog in *Arabidopsis thaliana* (Arabidopsis), identified through a BLAST search (Johnson et al., 2008). These hydrolases were selected due to having a predicted signal peptide (Armenteros et al., 2019), their robust suppression at the activity level over two independent experiments (**Figure 3.2**), and the relative ease with which they could be cloned.

Table 3.1: List of six selected proteins suppressed upon infection in *Nicotiana benthamiana*. Names were assigned from the closest homolog in *Arabidopsis thaliana* identified through a BLAST search (Johnson et al., 2008).

Class	Family	Accession number	Name (*Nb*)
Cysteine protease	Papain-like cysteine protease	NbD007909.1	RD19
		NbD027122.1	RD21
Serine hydrolase	Subtilase	NbD006086.1	SBT1.7
	Serine carboxypeptidase-like	NbD049241.1	SCPL20
		NbD034870.1	SCPL48
Glycosyl hydrolase	Glycosyl hydrolase family 19	NbD015584.1	PR3

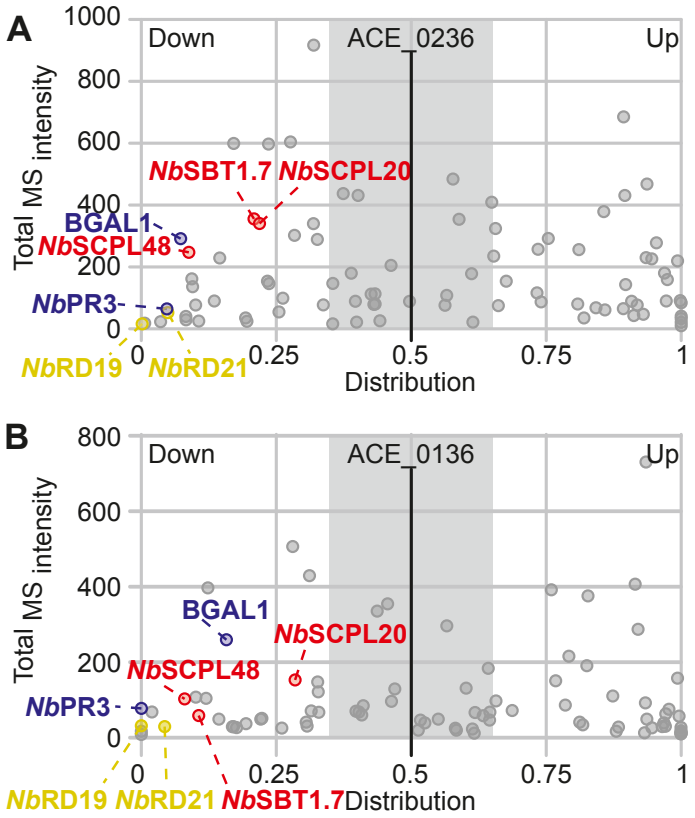


Figure 3.2: Selected hydrolases are robustly suppressed over two independent experiments. Data from the experiment shown in Figure 3.1 (**A**) was compared to a replicate experiment (**B**) and plotted in distribution graphs. Total MS/MS spectra for mock and infected samples were combined and plotted against the distribution of each protein in mock and infected samples, calculated by $LFQ_{infected}/(LFQ_{mock} + LFQ_{infected})$. The six selected hydrolases, as well as BGAL1, are labelled and coloured according to their hydrolase class. Data collected, and figure produced, by Dr. Daniela Sueldo.

The six hydrolases include two CPs (*Nb*RD19, *Nb*RD21), three SHs (*Nb*SBT1.7, *Nb*SCPL20, *Nb*SCPL48), and one GH (*Nb*PR3). None of these hydrolases have been studied in *N. benthamiana* before. However, their functions are somewhat characterised in other species.

The Arabidopsis homolog of the papain-like cysteine protease (PLCP) *Nb*RD19 functions in plant immunity, albeit inside the cell. Upon *Ralstonia solanacearum* infection, *AtRD19* expression is induced, and the protein relocates to the nucleus, where it mediates the interaction between the type III effector PopP2 and its cognate R protein RRS1-R (Bernoux et al., 2008).

Several orthologs of the PLCP *NbRD21* have been implicated in plant immunity. *StC14*, the potato ortholog of *NbRD21*, is under diversifying selection in potato, the natural host of *Phytophthora infestans* (Kaschani et al., 2010). Further, tomato and potato C14 are inhibited by Cip1 from *P. syringae* (Shindo et al., 2016) as well as EPIC1 and EPIC2B from the oomycete *P. infestans* (Kaschani et al., 2010), which also produces the effector AvrBlb2 to prevent secretion of C14 into the tomato apoplast (Bozkurt et al., 2011). Similarly, Arabidopsis RD21A is targeted by effectors 4E02, produced by the sugar beet cyst nematode *Heterodera schachtii*, and Mc1194, produced by the root-knot nematode *Meloidogyne chitwoodi*, presumably to impede its immune function (Pogorelko et al., 2019; Davies et al., 2015). *At*RD21A is further implicated in resistance to the fungus *Botrytis cinerea*, and to *P. syringae* during conditions of drought stress (Shindo et al., 2012; Liu et al., 2020).

Arabidopsis SCPL20 belongs to clade IB of the serine carboxypeptidase-like (SCPL) family and shows high similarity to a stress-inducible SCPL protein from tomato (Fraser et al., 2005). Further, *At*SCPL20 has a predicted role in peroxisomal β-oxidation and is detected in the apoplast upon *Verticillium longisporum* infection (Floerl et al., 2012). Arabidopsis SCPL48 belongs to SCPL clade IV, and is similar to CPY from yeast (*Saccharomyces cerevisiae*; Fraser et al., 2005). *AtSCPL48* is upregulated during developmental programmed cell death (PCD; Olvera-Carrillo et al., 2015), although no immune function has been described. In contrast, the Arabidopsis homolog of subtilase *NbSBT1.7* increases in abundance following methyl jasmonate treatment (Golldack et al., 2003).

Finally, *Nb*PR3 belongs to GH family 19 and is annotated as an acidic endochitinase. Endochitinases conventionally function in antifungal immunity (Jashni et al., 2015a). However, overexpression of *NtPR-Q*, the tobacco ortholog of *NbPR3*, enhances the

expression of defence genes such as *NtPR1a* and *NtPR2*, and confers resistance to the bacteria *R. solanacearum* (Tang et al., 2017).

In this chapter, we tested six suppressed hydrolases in 'agromonas' assays to determine if this suppression was because they have a role in the plant immune response. This is a novel technique pioneered in the van der Hoorn group whereby the growth of *P. syringae* infiltrated into agroinfiltrated leaves is measured using a cocktail of antibiotics to select for only *P. syringae* growth (Buscaill et al., 2021). From this screen we identified two candidates, each contributing to plant immunity in a surprising way. This included *Nb*PR3, which appears to function in bacterial immunity despite its annotation as an endochitinase, and *Nb*RD21, whose immune function appears to be dependent on effector-triggered immunity (ETI).

3.3 Results

3.3.1 Silencing candidate genes by VIGS

To determine a role in immunity for these candidate hydrolases, we initially used virus-induced gene silencing (VIGS, Lu et al., 2003). Fragments from suppressed hydrolase genes were cloned into the binary TRV2 vector and transformed into *N. benthamiana* seedlings along with TRV1 by agroinfiltration (Senthil-Kumar and Mysore, 2014). Five-weeks later, leaves were infiltrated with *P. syringae* cultures and bacterial growth measured to determine if hydrolase silencing increased bacterial growth, indicating a function in defence. However, silencing of the hydrolases was extremely detrimental to the growth of the plants (**Supplementary Table 3.1**). In contrast to control plants silenced for *GFP*, hydrolase silencing resulted in a high proportion of the seedlings showing necrotic phenotypes and therefore being unable to use.

3.3.2 Creation of selected overexpressed hydrolases

Instead, a role in immunity for the candidates was tested by overexpressing the candidate hydrolases. We used GoldenGate cloning (Engler et al., 2008) to assemble overexpression constructs for candidate genes, where expression was driven by the 35S promoter. Six hydrolases were cloned into overexpression constructs (**Table 3.1**). Along with the relative ease with which they could be cloned, the six candidates were selected based on having robustly suppressed hydrolase activity over two independent experiments, the presence of a signal peptide, interesting immune phenotypes of homologous genes in other plant species and coming from a diverse range of hydrolase families. Following confirmation of construct assembly by Sanger sequencing, we confirmed expression of the six hydrolases *in planta* using ABPP and western blotting (**Figure 3.3**).

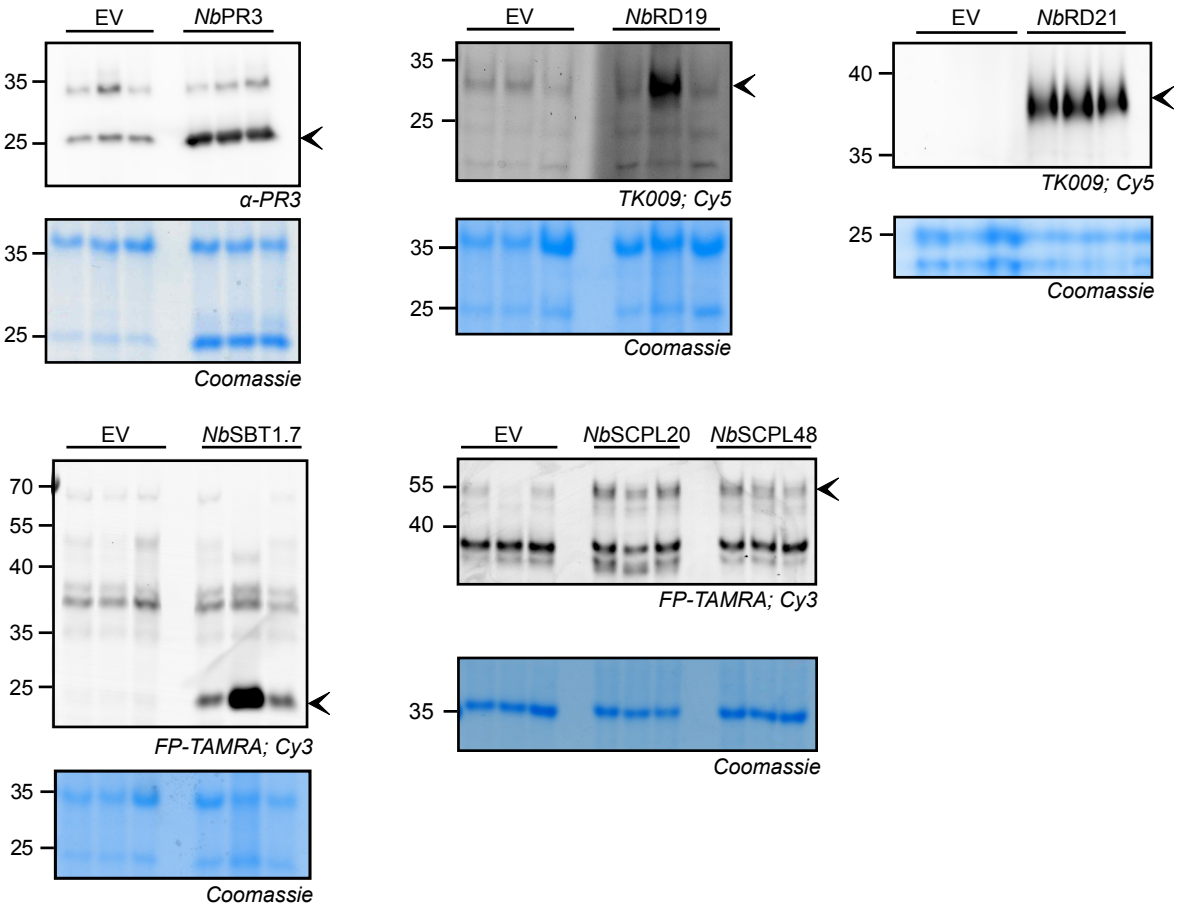


Figure 3.3: Confirmation of hydrolase expression. Suppressed hydrolases were transiently co-expressed with the silencing inhibitor P19 by agroinfiltration of *N. benthamiana*. Apoplastic fluid was isolated four days later from three biological replicates and labelled with fluorescent probes TK009 (CPs) or FP-TAMRA (SHs). Labelled samples were separated by SDS-PAGE, scanned for fluorescence and stained with Coomassie. Accumulation of *Nb*PR3 was detected using an α-PR3 antibody and Coomassie staining.

3.3.3 Agromonas screen of suppressed hydrolases

To determine a role in immunity for the selected hydrolases, we made use of the recently developed 'agromonas' assay (**Figure 3.4A**; Buscaill et al., 2021). In this experiment, *N. benthamiana* leaves transiently expressing the selected hydrolases along with the silencing inhibitor P19 were infected with10^6 CFU/mL *Pto*DC3000*ΔhQ* using a needleless syringe. Three days later, extracts were taken from leaves and serial dilutions were plated on selective media. Bacterial growth was measured by counting colonies and compared to a control agroinfiltrated with an empty-vector (EV). Each construct was tested in three independent experiments, using six plants (biological replicates) per experiment (**Figure**

3.4B). We found that only *NbPR3* increased resistance to *Pto*DC3000*ΔhQ* when overexpressed.

We also cloned overexpression constructs for three additional suppressed hydrolases: the GHs *Nb*BGLU40 (NbD047288.1), *Nb*Fla1 (NbD030889.1) and *Nb*Fla8 (NbD005008.1). These hydrolases were included in 'agromonas' assays (**Figure 3.5**). Although *Nb*Fla1 increased susceptibility and *Nb*Fla8 increased resistance to *Pto*DC3000*ΔhQ*, we were unable to confirm expression of the overexpressed proteins and so they are not discussed further in the thesis.

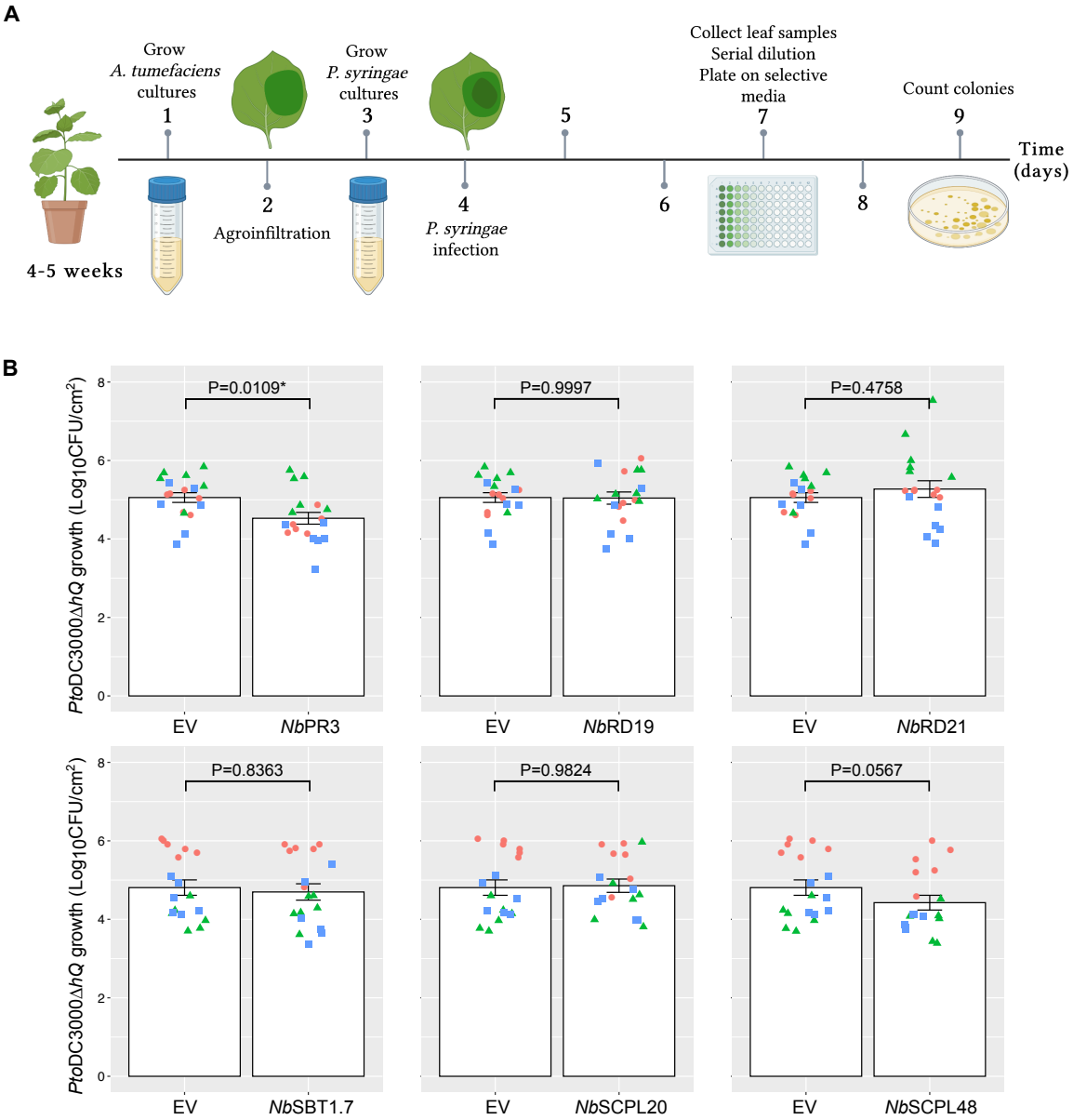


Figure 3.4: Only *NbPR3* expression increases bacterial immunity.

A: Agromonas timeline. 4-5 week-old *N. benthamiana* plants were agroinfiltrated with P19 plus hydrolase overexpression constructs at OD_{600} = 0.5. Two days later, the same leaves were infiltrated with *P. syringae* cultures at 10^6 CFU/mL. Three days later, leaf discs were collected, lysed, and plated in serial dilution on selective media. Plates were incubated at 28°C for two days before counting colonies. Figure created with BioRender.com.

B: Screen of six suppressed hydrolases. Hydrolases were transiently co-expressed by agroinfiltration in four-week-old plants along with silencing inhibitor P19. Empty-vector (EV) was included as a negative control. Two days later, the same leaves were infiltrated with 10^6 CFU/mL *Pto*DC3000Δ*hQ*. Bacterial growth in colony-forming units (CFU) was measured three days later. Bars represent mean ± SE of all biological replicates over three experiments; biological replicates from the same experiment have the same shape and colour. P-values were calculated by two-way ANOVA followed by post-hoc comparison using the Dunnett test to examine the effect of construct overexpression on bacterial growth. *, P<0.05.

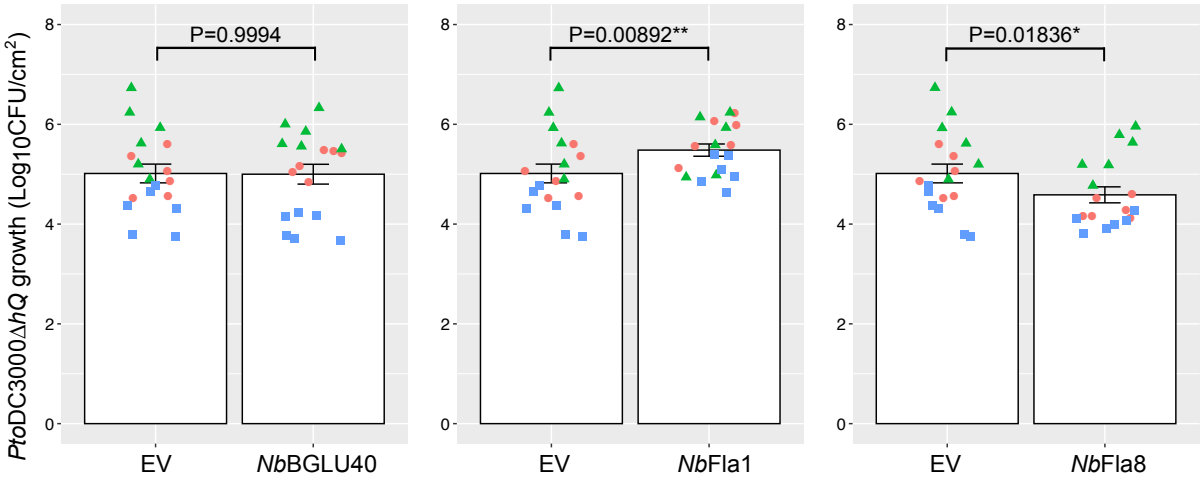


Figure 3.5: Screen of three suppressed GHs. *NbBGLU40*, *NbFla1* and *NbFla8* were transiently co-expressed by agroinfiltration in four-week-old plants along with silencing inhibitor P19. Empty-vector (EV) was included as a negative control. Two days later, the same leaves were infiltrated with 10^6 CFU/mL *Pto*DC3000Δ*hQ*. Bacterial growth in colony-forming units (CFU) was measured three days later. Bars represent mean ± SE of all biological replicates over three experiments; biological replicates from the same experiment have the same shape and colour. P-values were calculated by two-way ANOVA followed by post-hoc comparison using the Dunnett test to examine the effect of construct overexpression on bacterial growth. *, P<0.05; **, P<0.01.

3.3.4 *Nb*PR3 confers resistance to multiple *P. syringae* strains

To further investigate a role for *Nb*PR3 in bacterial immunity, we performed disease assays using wildtype *Pto*DC3000, and two additional *P. syringae* strains, pv. *syringae* B728a (*Psy*B728a), which is naturally pathogenic on bean, and pv. *tabaci* 6605 (*Pta*6605), which naturally infects tobacco (Vinatzer et al., 2006; Lee et al., 2013). *Nb*PR3 was found to confer resistance to wildtype *Pto*DC3000 (**Figure 3.6A**). Furthermore, *NbPR3* overexpression slightly but significantly conferred resistance to *Pta*6605 (**Figure 3.6B**), but not to *Psy*B728a (**Figure 3.6C**). From these results, we have taken *Nb*PR3 forward for further analysis to determine its immune function (**Chapter 4**).

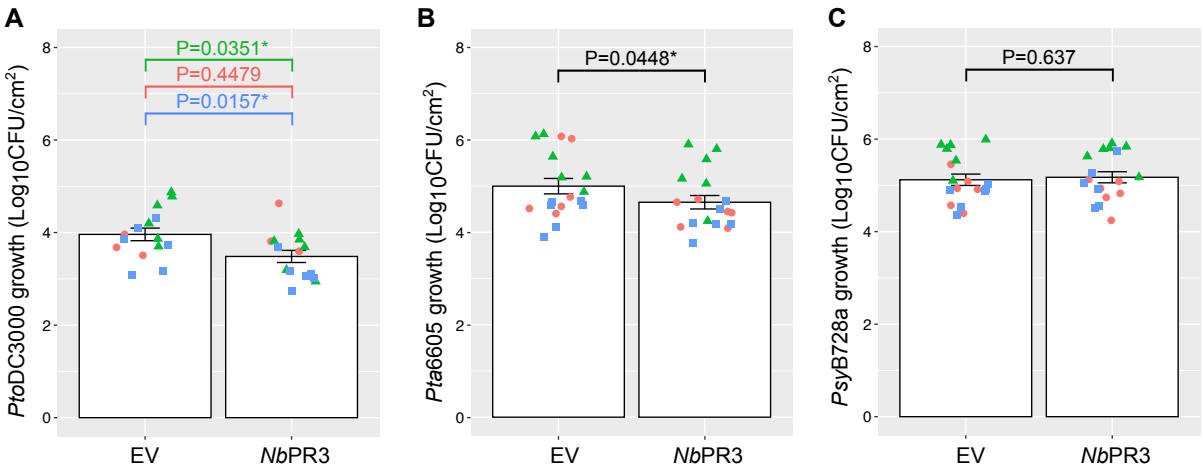


Figure 3.6: *Nb*PR3 confers resistance to *Pto*DC3000 and *Pta*6605, but not *Psy*B728a. *NbPR3* was transiently co-expressed by agroinfiltration in four-week-old plants along with silencing inhibitor P19. Empty-vector (EV) was included as a negative control. Two days later, the same leaves were infiltrated with 10^6 CFU/mL *Pto*DC3000 (**A**), *Pta*6605 (**B**), or *Psy*B728a (**C**). Bacterial growth in colony-forming units (CFU) was measured three days later. Bars represent mean ± SE of all biological replicates over three experiments; biological replicates from the same experiment have the same shape and colour. P-values were calculated by individual *t*-tests (**A**) or two-way ANOVA (**B**, **C**) to examine the effect of construct overexpression on bacterial growth. *, P<0.05.

3.3.5 ETI-dependent role for *Nb*RD21 in plant immunity

A lack of immune phenotype for *Nb*RD21 in response to *Pto*DC3000Δ*hQ* infection was somewhat surprising, given the well-documented immune phenotypes of its orthologs (Kaschani et al., 2010; Shindo et al., 2012; Liu et al., 2020). To clarify this contradiction, we tested whether *NbRD21* overexpression could confer resistance to additional *P. syringae* strains. We tested wildtype *Pto*DC3000 which, unlike the virulent *Pto*DC3000Δ*hQ*, secretes the type III effector HopQ1-1. This effector is recognised by the *N. benthamiana* R protein Roq1 and triggers ETI and the hypersensitive response (HR) (Schultink et al., 2017). We also tested *Psy*B728a and *Pta*6605, which like *Pto*DC3000Δ*hQ* are virulent on *N. benthamiana* (Vinatzer et al., 2006; Lee et al., 2013).

Interestingly, overexpression of *NbRD21* strongly conferred resistance to the wildtype avirulent *Pto*DC3000, but not to the virulent strains *Pta*6605 and *Psy*B728a (**Figure 3.7**).

Due to this unique resistance phenotype, *Nb*RD21 was also taken forward for further study (**Chapters 5** & **6**).

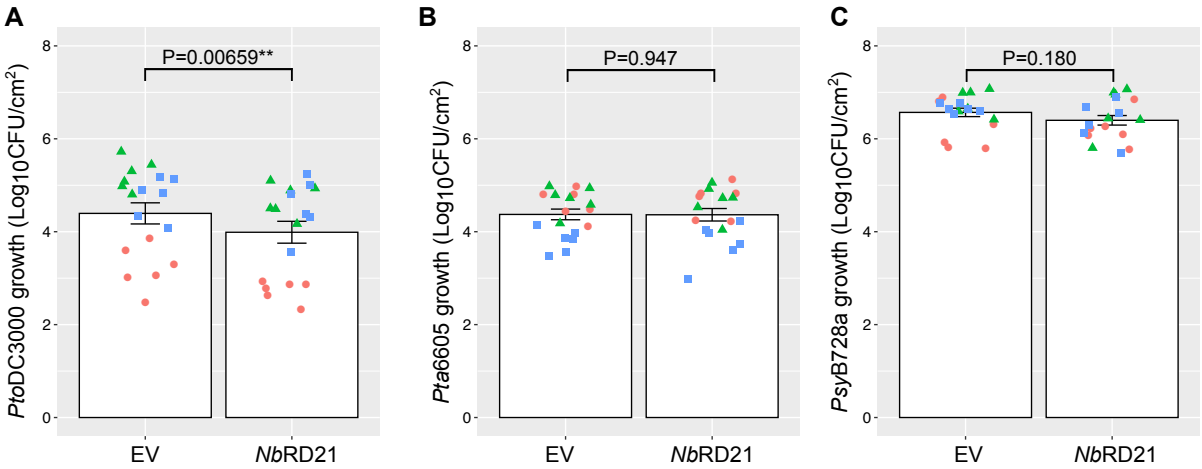


Figure 3.7: Transient *Nb*RD21 expression increases immunity to *Pto*DC3000 but not *Pta*6605 or *Psy*B728a. *NbRD21* was transiently co-expressed by agroinfiltration in four-week-old plants along with silencing inhibitor P19. Empty-vector (EV) was included as a negative control. Two days later, the same leaves were infiltrated with 10^6 CFU/mL *Pto*DC3000 (**A**), *Pta*6605 (**B**), or *Psy*B728a (**C**). Bacterial growth in colony-forming units (CFU) was measured three days later. Bars represent mean ± SE of all biological replicates over three experiments; biological replicates from the same experiment have the same shape and colour. P-values were calculated by two-way ANOVA to examine the effect of construct overexpression on bacterial growth. **, P<0.01.

3.3.6 Testing the ETI-dependence of *Nb*RD21 immune function

Our results indicated that *Nb*RD21 immune function is dependent on either HopQ1-1 or ETI. To test this hypothesis, we determined if transient *NbRD21* expression could confer resistance to *Psy*B728a expressing HopQ1-1. Wildtype *Psy*B728a lacks this effector and is therefore virulent on *N. benthamiana* (Wei et al., 2007). We hypothesised that the addition of HopQ1-1 into *Psy*B728a would lead to avirulence and resistance upon transient *NbRD21* expression. Indeed, we observed tissue collapse upon infection with *Psy*B728a expressing HopQ1-1, indicative of the HR. However, we found that *NbRD21* overexpression did not confer resistance to *Psy*B728a expressing HopQ1-1 (**Figure 3.8**).

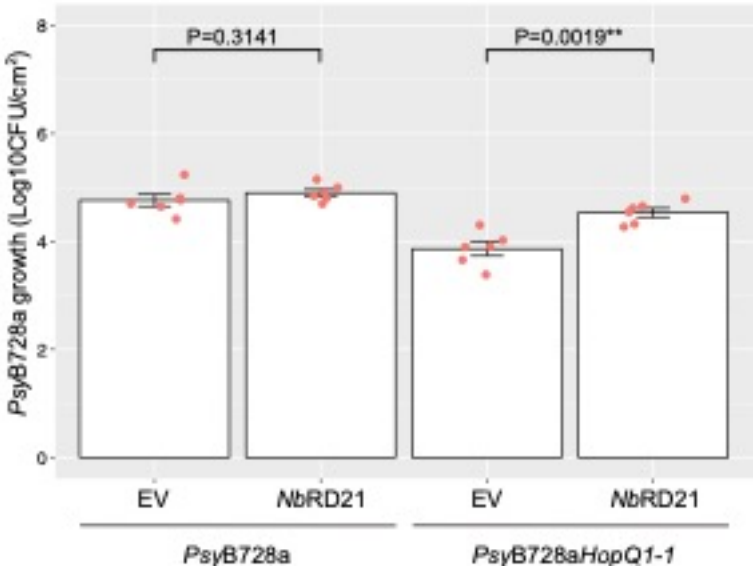


Figure 3.8: *NbRD21* overexpression does not confer resistance to avirulent *Psy*B728a. *NbRD21* was transiently co-expressed by agroinfiltration in four-week-old plants along with silencing inhibitor P19. Empty-vector (EV) was included as a negative control. Two days later, the same leaves were infiltrated with 10^6 CFU/mL *Psy*B728a or *Psy*B728aHopQ1-1. Bacterial growth in colony-forming units (CFU) was measured three days later. Bars represent mean ± SE of N=6 biological replicates. P-values were calculated by *t*-tests. **, P<0.01.

3.4 Discussion

This thesis is based on previous data identifying hydrolases suppressed during infection with *Pto*DC3000Δ*hQ*. In this chapter, six of these hydrolases were tested for their role in resistance to bacterial infection. Our results identified two exciting candidates: *Nb*PR3, an annotated endochitinase which appears to function in bacterial immunity, and *Nb*RD21, a PLCP with a hypothesised ETI-dependent resistance phenotype.

VIGS was unsuccessful

Initial attempts to determine an immune function for the candidate proteins utilised VIGS. Here, we found necrotic phenotypes in our silenced plants compared to *GFP*-silenced controls, consistent with previous findings that VIGS silencing can lead to necrosis, dwarfed growth and death (Dommes et al., 2019). These are summarised in **Supplementary Table 3.1**. Necrotic symptoms could be a result of the size of the silencing fragment cloned into the TRV2 vector, inoculation method or *Agrobacterium* concentration (Broderick and Jones, 2014; Hartl et al., 2008; Shi et al., 2021).

There are alternative methods of gene silencing that we could have utilised, such as transient silencing using hairpin RNA (Watson et al., 2005). However, we reasoned that gene silencing was not an optimal method to determine a role in immunity for the candidates. The candidates were identified on the basis that they were suppressed during *P. syringae* infection. Silencing platforms would compare bacterial growth between silenced plants, which do not produce the hydrolase, and control plants where hydrolase activity is suppressed. Depending on the extent of the suppression, this could result in no difference in resistance between the control and silenced plants.

Confirmation of hydrolase expression

Instead, we determined if the suppressed proteins could confer resistance when transiently expressed. We generated overexpression constructs for the six hydrolases and confirmed their expression *in planta* using a variety of biochemical methods. Of particular interest are *Nb*PR3 and *Nb*SBT1.7. *NbPR3* overexpression was confirmed using a commercial antibody raised against tobacco class I chitinases CHNA and CHNB (Agrisera), which are expected to label at a molecular weight of 32-35 kDa. The antibody labels additional signals in *N. benthamiana* at ~35kDa, in addition to our *Nb*PR3 of interest (**Figure 3.3**). The upper band on the blot could be derived from modification of *Nb*PR3, such as glycosylation. However, this seems unlikely given that the intensity of this signal is similar to the EV control. Instead, it seems more likely that the upper band corresponds to class I chitinases, which are larger than class II chitinases such as *Nb*PR3 due to the presence of the chitin-binding domain (Araki and Torikata, 1995).

Another interesting result came from the labelling of overexpressed *NbSBT1.7*. Apoplastic fluid from plants overexpressing *NbSBT1.7* was labelled with the FP-TAMRA probe, resulting in an intense signal at ~22 kDa which was absent in control AF. This suggests the signal corresponds to active *Nb*SBT1.7. However, this size of protein is unusually small for a subtilase, contrasting with a predicted weight of 69 kDa for mature *Nb*SBT1.7. Indeed, the purified mass of Arabidopsis SBT1.7 is 76.1 kDa (Hamilton et al., 2003). We saw no differential signal between *Nb*SBT1.7 and EV samples at 70 kDa (**Figure 3.3**). A potential explanation for this discrepancy is that full-length *Nb*SBT1.7 is cleaved *in planta*, possibly after probe binding has taken place, given that proteins identified through ABPP are by definition active. To test whether *Nb*SBT1.7 is cleaved in the absence of the fluorescent probe, or indeed if cleavage retains subtilase activity, we could test the subtilase activity of AF from plants overexpressing *NbSBT1.7* using a fluorescent substrate such as FITC-Casein. Alternatively, the signal could be an alternative 22 kDa SH that is activated by

*Nb*SBT1.7. These hypotheses were not pursued further given the lack of phenotype for *Nb*SBT1.7 in agromonas assays.

Endochitinase *Nb*PR3 functions in bacterial immunity

We found that the GH *Nb*PR3, despite being annotated as an endochitinase, functions in bacterial immunity. This is complementary to the finding that the tobacco ortholog *NtPR-Q* also functions in bacterial immunity when overexpressed in transgenic tobacco (Tang et al., 2017). This is discussed in detail in the following chapter. It is important to note that both this study and Tang *et al* only studied the effects of increased hydrolase expression. These experiments should therefore be complemented with disease assays using catalytically-inactive or *pr3* knockout plants. We are in the process of generating *Nbpr3* knockouts by genome editing of *N. benthamiana*, but unfortunately were unable to obtain these in time for the present study.

We found that *NbPR3* overexpression strongly confers resistance to *Pto*DC3000, slightly but significantly confers resistance to *Pta*6605, and does not confer resistance to *Psy*B728a (**Figure 3.4**, **3.6**). This discrepancy could be due to differences in inhibitor repertoires, or the strength of inhibitor expression, between different strains. *Psy*B728a may produce a particularly potent inhibitor, which overexpression of *NbPR3* is unable to overcome. Supporting this, almost 1000 protein-encoding genes are found in the *Psy*B728a genome that are absent in *Pto*DC3000, including several type III effectors (Feil et al., 2005). In addition, *Psy*B728a may be more robust to the immune activity of *Nb*PR3 due to differences in its toxin and hormone repertoire (Feil et al., 2005; Howden et al., 2009).

Alternatively, *Nb*PR3 may confer immunity by acting on a bacterial substrate produced by *Pto*DC3000 and *Pta*6605, but not by *Psy*B728a. For example, the substrate may be downregulated by *Psy*B728a as a strategy to avoid recognition, similar to flagellin gene

expression when this bacteria colonises *Phaseolus vulgaris* (Yu et al., 2013). Alternatively, *Psy*B728a may be evading *Nb*PR3-dependent immunity by substrate polymorphism or glycan shielding (Buscaill and van der Hoorn, 2021). An interesting example is the ß-galactosidase BGAL1, which promotes the release of immunogenic peptides from the flagellin of *Pto*DC3000 and *Pta*6605 through recognition of a terminal modified viosamine (mVio) in the flagellin O-glycan (Buscaill et al., 2019). *Psy*B728a evades this detection by replacing the mVio with a putative *N*-acetylglucosamine, which is not recognised by BGAL1. A similar mechanism may be in place to prevent detection of the *Nb*PR3 substrate. Given the pattern of resistance we observed upon *NbPR3* overexpression, (**Figure 3.4**, **3.6**) it is even possible that *Nb*PR3 is functioning in the same flagellin recognition pathway.

*Nb*RD21 has an ETI-dependent resistance function

The second candidate we took forward for further study is the PLCP *Nb*RD21. Previous studies have discussed *NbRD21* homologs in the context of plant immunity, but specific immune functions or substrates have not been identified (Kaschani et al., 2010; Shindo et al., 2012; Liu et al., 2020). Further, *Nb*RD21 has not been studied before. Interestingly, we found that *NbRD21* overexpression was able to confer resistance to avirulent *Pto*DC3000, but not the virulent strains *Pto*DC3000Δ*hQ*, *Pta*6605 or *Psy*B728a (**Figure 3.4**, **3.7**). Most intriguing is the contrasting phenotypes of resistance versus susceptibility when *NbRD21*-overexpressing plants are infected with wildtype *Pto*DC3000 compared to the *hopq1-1* mutant. These two strains differ only in a single effector protein, but this difference manifests in ETI and the HR for *Pto*DC3000, and disease for *Pto*DC3000Δ*hQ.*

One possible explanation for this phenotype is that the effector HopQ1-1 is a substrate of *Nb*RD21. For example, *Nb*RD21 may be required to specifically mediate the interaction between HopQ1-1 and its R protein Roq1, triggering ETI and the HR (Schultink et al., 2017). However, given the high level of activity of *Nb*RD21 (**Figure 3.3**), as well as the

nucleocytoplasmic localisation of HopQ1-1 (Li et al., 2013), this hypothesis is unlikely. PLCPs tend to have a wide substrate repertoire, and require tight regulation – spatial, temporal, or via inhibitors – to prevent indiscriminate cleavage of plant proteins (van der Linde et al., 2012; Petushkova et al., 2022; Rustgi et al., 2017).

Combined with the fact that RD21 is predominantly vacuolar (Lampl et al., 2013), the *Nb*RD21 resistance phenotype might be better explained by membrane fusion-mediated immunity (Hatsugai et al., 2009). During infection with avirulent bacteria, the large vacuole, containing antibacterial proteins and cell death-promoting factors, fuses with the plasma membrane, releasing these contents into the apoplast (Hatsugai et al., 2009). The released hydrolytic enzymes attack proliferating bacteria and eventually trigger the HR (Hatsugai et al., 2009). In this model, during infection with virulent bacteria, *Nb*RD21 is present in the apoplast at insufficient levels to overcome its inhibition and confer resistance. Upon infection with avirulent bacteria such as *Pto*DC3000, ETI is triggered, and vacuolar contents are released into the apoplast. This leads to a large increase in apoplastic *Nb*RD21, which both enables it to overcome its inhibition as well as encounter new substrates, thereby conferring immunity. Therefore, we propose that spatial regulation is used to modulate *Nb*RD21 immune function until pathogen invasion in an ETI-dependent manner (**Figure 3.9**).

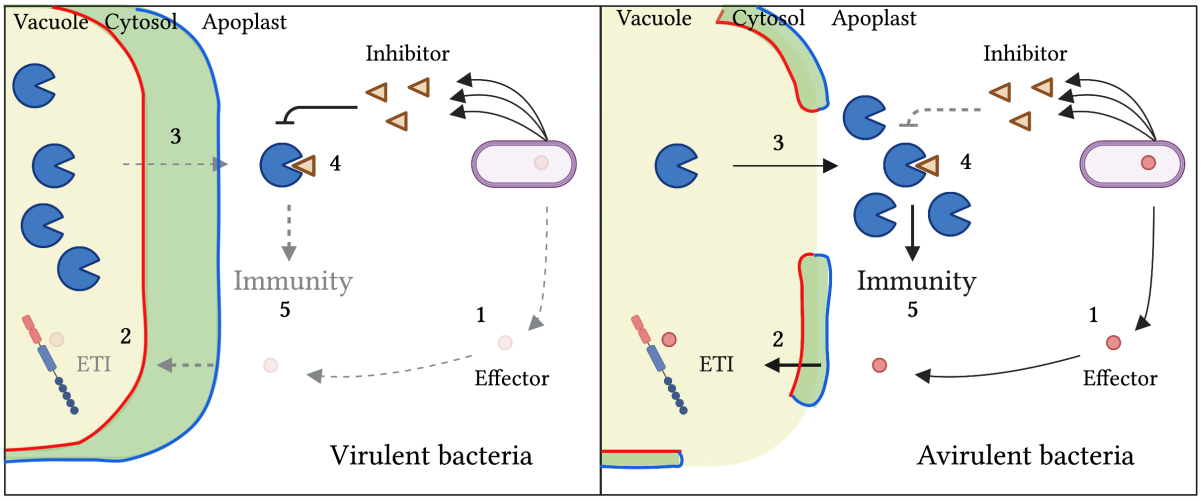


Figure 3.9: Hypothesis for the ETI-dependent immune function of *Nb*RD21.
Pathogenic bacteria proliferate in the *N. benthamiana* apoplast. Avirulent bacteria (right) produce effectors (**1**) which are recognised by receptors leading to effector-triggered immunity (ETI; **2**). During ETI, the large vacuole fuses with the plasma membrane, releasing *Nb*RD21 (blue) into the apoplast. In the absence of ETI (left), *Nb*RD21 remains in the vacuole (**3**). Pathogenic bacteria secrete inhibitors targeting apoplastic *Nb*RD21 (**4**). If membrane fusion has taken place, apoplastic *Nb*RD21 can overcome this inhibition and confer immunity to the pathogen (**5**). Figure created with BioRender.com.

To confirm that the role of *Nb*RD21 is dependent on HopQ1-1 or ETI, we tested if *NbRD21* overexpression could confer resistance to *Psy*B728a expressing *HopQ1-1*. We hypothesised that *Nb*RD21 would now confer resistance to this avirulent *Psy*B728a strain. In contrast, bacterial growth was significantly increased upon *NbRD21* overexpression compared to the EV control (**Figure 3.8**). This result makes it more unlikely that HopQ1-1 is the specific substrate of *Nb*RD21, although it might still be possible that the lack of resistance upon *NbRD21* overexpression is due to effective inhibition by *Psy*B728a. An alternative explanation for this result is that *Nb*RD21 acts on *Pto*DC3000 substrates that are not produced by *Psy*B728a. This is possible given the differences in protein-encoding genes from these two strains (Feil et al., 2005). This would mean despite its relocation to the apoplast upon ETI, *Nb*RD21 could still be unable to confer resistance to *Psy*B728a.

Future experiments should look to confirm the ETI-dependence of *Nb*RD21 immune function by using alternative effectors to trigger ETI and membrane fusion. For instance,

we would expect *NbRD21* overexpression to increase immunity to virulent *Pto*DC3000Δ*hQ* before tissue collapse triggered by co-infiltration with genes encoding the potato receptor Rx and the potato virus X coat protein elicitor CP, compared to virulent *Pto*DC3000Δ*hQ* with Rx alone (Bendahmane et al., 1999). If this was successful, it would also rule out *Nb*RD21 immune function being dependent on HopQ1-1, rather than ETI in general.

Lack of phenotypes for four suppressed hydrolases

Despite being suppressed at the activity level during *Pto*DC3000Δ*hQ* infection, four of the hydrolases (*Nb*RD19, *Nb*SBT1.7, *Nb*SCPL20, *Nb*SCPL48) showed no phenotype in agromonas assays. There are several possible reasons for his. First, overexpression of the hydrolases may be insufficient in overcoming their suppression by the pathogen. This would prevent the hydrolases from producing an immune phenotype. This could be the case for *Nb*RD19 and *Nb*SCPL48, since they showed varying activity levels between biological replicates upon overexpression when compared to EV (**Figure 3.3**). In fact, the level of resistance upon *NbSCPL48* overexpression was almost significant, so this warrants further investigation (**Figure 3.4**). Another possibility is that these hydrolases function in immunity against untested *P. syringae* strains, or indeed other pathogen species entirely. For instance, if the proteins were able to confer resistance to wildtype *Pto*DC3000, in a similar way to *Nb*RD21, this would support the suggestion of a general mechanism of ETI-dependent resistance. Indeed, Arabidopsis RD19 is normally localised in the vacuole, supporting this hypothesis (Bernoux et al., 2008).

A lack of phenotype could be due to limitations in our infection assays. Agroinfiltration is known to induce the immune response, including an upregulation of PR proteins, xylanase inhibitors and leucine-rich repeat (LRR)-containing receptors (Grosse-Holz et al., 2018). Indeed, *N. benthamiana* receptor *Nb*CSPR recognises the csp22 epitope derived from Cold Shock Protein (CSP) of *Agrobacterium tumefaciens* to mount an age-dependent immune

response, which limits transformation efficiency (Saur et al., 2016). The mounting immune response may reduce both hydrolase transformation and *P. syringae* growth, preventing the detection of immune phenotypes.

Finally, these four immune hydrolases may simply not function in immunity. Their suppressed activity may be a result of large-scale changes in the apoplast upon pathogen invasion, rather than due to specific inhibition by bacteria in response to an immune function (Kesten et al., 2019; Masachis et al., 2016; O'Leary et al., 2016; Tahir et al., 2019). Despite buffering the apoplastic fluid used in the MS experiment to minimise disruption of apoplastic conditions, changes will inevitably occur. Apoplastic protease activity is sensitive to environmental changes, which could include post-translational modifications, or changes in pH or metabolite levels (Tahir et al., 2019; Wang et al., 2020).

3.5 Conclusion

In summary, from this chapter we have identified two suppressed hydrolases with antibacterial immune functions. We identified *Nb*PR3, which confers bacterial resistance when overexpressed, despite its annotation as an endochitinase. The immune function of *Nb*PR3 is investigated in **Chapter 4**. We also identified *Nb*RD21, which confers bacterial resistance to avirulent *Pto*DC3000. The functions of overexpressed and endogenous *Nb*RD21 are investigated in **Chapter 5**. Finally, in **Chapter 6** we begin to characterise the bacterial inhibitor of *Nb*RD21.

3.6 Contributions

Professor Renier van der Hoorn conceived the project and contributed to experimental design and data interpretation. Dr. Daniela Sueldo, Dr. Farnusch Kaschani and Professor Markus Kaiser performed the initial mass spectrometry and subsequent analysis to identify the suppressed hydrolases. Dr. Pierre Buscaill cloned VIGS constructs and the *NbRD21* overexpression construct, and provided technical assistance during the first months of my PhD. *Ps*yB728aHopQ1-1 was produced by Rohini Chawla.

3.7 Supplementary Figures

Supplementary Table 3.1: Phenotypes of VIGS plants

Silenced gene	Plasmid (+ TRV1)	Phenotype
GFP (negative control)	TRV2::GFP	Slight growth stunting
*Nb*BGLU40	pPB057	Severe growth stunting Leaf deformation Necrosis Death
*Nb*Fla1	pPB048	
*Nb*Fla8	pPB049	
*Nb*PR3	pPB036	
*Nb*RD19	pPB068	
*Nb*RD21	pPB038	
*Nb*SBT1.7	pPB058	
*Nb*SCPL20	pPB060	
*Nb*SCPL48	pPB051	

3.8 Methods

Plant growth conditions – *N. benthamiana* was grown in a growth chamber at room temperature with a 16-hour light cycle and 60% humidity and watered on alternating days.

Bacterial strains – bacterial strains used in this chapter are summarised in **Table 3.2**.

Table 3.2: Bacterial strains used in this chapter.

Name	Description	Reference
P. syringae pv. *tomato* DC3000	Wildtype	Buell et al., 2003
P. syringae pv. *tomato* DC3000ΔhQ	*P. syringae* pv. *tomato* DC3000 lacking the *hopQ1-1* effector	Wei et al., 2007
P. syringae pv. *syringae* B728a	Wildtype	Feil et al., 2005
P. syringae pv. *tabaci* 6605	Wildtype	Matsui et al., 2021
P. syringae pv. *syringae* B728a HopQ1-1	*P. syringae* pv. syringae B728a expressing the HopQ1-1 effector	This study, Rohini Chawla
A. tumefaciens GV3101	Derivative of *A. tumefaciens* C58 carrying pMP90 plasmid	Koncz and Schell., 1986
E. coli DH10B	Chemically competent *E. coli*	Thermo Fisher Scientific EC0113

Virus-induced gene silencing – Fragments of suppressed hydrolases were cloned into binary TRV2 vector (Liu et al., 2002) and transformed into *Agrobacterium tumefaciens*. Primers for amplifying VIGS fragments are summarised in **Table 3.3**. Overnight cultures were resuspended in agroinfiltration buffer (10 mM $MgCl_2$, 10 mM MES, 150 µM acetosyringone) to a final OD_{600} of 0.5. All constructs were co-expressed with bacteria containing TRV1 (Liu et al., 2002). *TRV2::GFP* was used as a negative control and *TRV2::PDS*, which causes photo-bleaching, was used as a silencing marker (Liu et al., 2002). *N. benthamiana* seedlings were infiltrated at ten days old and were grown for 4-5 weeks before use.

Cloning of hydrolases – Overexpression constructs for six candidate hydrolases were built by GoldenGate Assembly (Engler et al., 2008). The full-length genes were amplified from cDNA using primers summarised in **Table 3.3**. Binary vectors were generated in a Golden Gate reaction with 35S promoter (pICH51288) and 35S terminator (pICH41414; Engler et al., 2014) into binary backbone pJK001c (Paulus et al., 2020) using BsaI restriction sites, resulting in binary clones summarized in **Table 3.4**. Binary vectors were transformed into *Agrobacterium tumefaciens* GV3101 (pMP90) by freeze-thawing and selection for kanamycin and gentamicin resistance.

Table 3.3: Primers used in this chapter. Incorporated substitutions are shown in red. Overhangs are shown in lower-case.

Name	Purpose	Sequence (5' - 3')
*Nb*BGLU40_VIGS_F	Clone *NbBGLU40* VIGS construct	ttggtctcaattcGAATTCAACCATATGTAACA
*Nb*BGLU40_VIGS_R	Clone *NbBGLU40* VIGS construct	ttggtctcaatccGTAGTAGATTATGAGTAACAATG
*Nb*Fla1_VIGS_F	Clone *NbFla1* VIGS construct	ttggtctcaattcTGTGCAAAATGACGGTAACGT
*Nb*Fla1_VIGS_R	Clone *NbFla1* VIGS construct	ttggtctcaatccTCCGCCGTCGAATCCGCA
*Nb*Fla8_VIGS_F	Clone *NbFla8* VIGS construct	ttggtctcaattcAACGGCAACTTAGGTTCCGT
*Nb*Fla8_VIGS_R	Clone *NbFla8* VIGS construct	ttggtctcaatccCTCAATGGCAGTTTGATACGTC
*Nb*PR3_VIGS_F	Clone *NbPR3* VIGS construct	ttggtctcaattcTGGTTCCCTGAGTGCAGAACC
*Nb*PR3_VIGS_R	Clone *NbPR3* VIGS construct	ttggtctcaatccCGATTCGCCGCCTGATC
*Nb*RD21_VIGS_F	Clone *NbRD21* VIGS construct	ttggtctcaattcCCACTGATCGTCGCAGGTT
*Nb*RD21_VIGS_R	Clone *NbRD21* VIGS construct	ttggtctcaatccTTTTAATGATGAAATCAAAGGCAT
*Nb*SBT1.7_VIGS_F	Clone *NbSBT1.7* VIGS construct	ttggtctcaattcGCCGGACACGTGGATC
*Nb*SBT1.7_VIGS_R	Clone *NbSBT1.7* VIGS construct	ttggtctcaatccAACTTTATATGTTCCAGCCG
*Nb*SCPL20_VIGS_F	Clone *NbSCPL20* VIGS construct	ttggtctcaattcACTACTCTATGCAACGGAAATTTC
*Nb*SCPL20_VIGS_R	Clone *NbSCPL20* VIGS construct	ttggtctcaatccGCCATTGAGAATCTCAGGCC
*Nb*SCPL48_VIGS_F	Clone *NbSCPL48* VIGS construct	ttggtctcaattcTCTCATATTGCTCTTTCATT
*Nb*SCPL48_VIGS_R	Clone *NbSCPL48* VIGS construct	ttggtctcaatccGAACATCCTTGAAGCTTTAG
*Nb*BGLU40_F1	Clone *NbBGLU40* from cDNA, remove BsaI	tggtggtctcaaATGTTAAAGAAGAGAGACATTGCTC
*Nb*BGLU40_R1	Clone *NbBGLU40* from cDNA, remove BsaI	ttcgtggtctcaGCGAAGTATCCTTTCACGTTGCA
*Nb*BGLU40_F2	Clone *NbBGLU40* from cDNA, remove BsaI	tggtggtctcaTCGCGTGGTCACTGATGG
*Nb*BGLU40_R2	Clone *NbBGLU40* from cDNA, remove BsaI	ttcgtggtctcaaagcCTAAGCAGATCCAAGGAAATTCTT
*Nb*Fla1_F	Clone *NbFla1* from cDNA	tggtggtctcaaATGCAGCTCCGGTCAGCC
*Nb*Fla1_R	Clone *NbFla1* from cDNA	ttcgtggtctcaaagcTTACAGCAATACAAAGAAAAACCAC
*Nb*Fla8_F	Clone *NbFla8* from cDNA	tggtggtctcaaATGGGCGCACTACACATT
*Nb*Fla8_R	Clone *NbFla8* from cDNA	ttcgtggtctcaaagcCTAGGACAAATAAACGGACACA
*Nb*PR3_F	Clone *NbPR3* from cDNA	tggtggtctcaaATGGAGTTTTCTGGATCACCACTGG
*Nb*PR3_R	Clone *NbPR3* from cDNA	ttcgtggtctcaaagcCTAGCCCTGGGCGAAGTTCCTT
*Nb*RD19_F	Clone *NbRD19* from cDNA	tggtggtctcaaATGGCACTTCATTATGCTTTAAT
*Nb*RD19_R	Clone *NbRD19* from cDNA	ttcgtggtctcaaagctcaGTGTGAGCTGGTACTAA
*Nb*RD21_F	Clone *NbRD21* from cDNA	tggtggtctcaaATGGCAAATCATAGCTCCACTCTCA
*Nb*RD21_R	Clone *NbRD21* from cDNA	ttcgtggtctcaaagcTCAAGAACTGCTCTTCCGTCCT
*Nb*SBT1.7_F1	Clone *NbSBT1.7* from cDNA, remove BsaI	tggtggtctcaaATGTCTAGATACCCAGTAATACTTG
*Nb*SBT1.7_R1	Clone *NbSBT1.7* from cDNA, remove BsaI	ttcgtggtctcaACCCTTCTCCATAGCAGCAA
*Nb*SBT1.7_F2	Clone *NbSBT1.7* from cDNA, remove BsaI	tggtggtctcaGGGTATTTTGGTGTCTTGTTCAGC
*Nb*SBT1.7_R2	Clone *NbSBT1.7* from cDNA, remove BsaI	ttcgtggtctcaaagcTCATGTCCAAGAAATTGCCACAG
*Nb*SCPL20_F	Clone *NbSCPL20* from cDNA	tggtggtctcaaATGGCAAGAATAAATGC
*Nb*SCPL20_R	Clone *NbSCPL20* from cDNA	ttcgtggtctcaaagcTCATATGTTCTTGCCCTC
*Nb*SCPL48_F	Clone *NbSCPL48* from cDNA	tggtggtctcaaATGGCTTCTTCTTTCTCTC

*Nb*SCPL48_R	Clone *NbSCPL48* from cDNA	ttcgtggtctcaaagcCTAGGACAATTTGCCTTG

Table 3.4: Constructs used in this chapter

Name	Description	Reference
TRV1	Binary TRV1	Liu et al., 2002
TRV2::GFP	Binary TRV2::GFP	Liu et al., 2002
TRV2::PDS	Binary TRV2::PDS	Liu et al., 2002
pPB057	Binary TRV2::*Nb*BGLU40	This work
pPB048	Binary TRV2::*Nb*Fla1	This work
pPB049	Binary TRV2::*Nb*Fla8	This work
pPB036	Binary TRV2::*Nb*PR3	This work
pPB068	Binary TRV2::*Nb*RD19	This work
pPB038	Binary TRV2::*Nb*RD21	This work
pPB058	Binary TRV2::*Nb*SBT1.7	This work
pPB060	Binary TRV2::*Nb*SCPL20	This work
pPB051	Binary TRV2::*Nb*SCPL48	This work
pICH51288	pL0M-PU-35S-TMV-3-5128835S	Engler et al., 2014
pICH41414	pL0M-T-35S-1-4141435S	Engler et al., 2014
P19	Binary 35S::P19	Van der Hoorn et al., 2003
pJK001c	Binary empty-vector (EV)	Paulus et al., 2020
pAG002	Binary 35S::*Nb*BGLU40	This work
pAG008	Binary 35S::*Nb*Fla1	This work
pAG009	Binary 35S::*Nb*Fla8	This work
pAG001	Binary 35S::*Nb*PR3	This work
pAG010	Binary 35S::*Nb*RD19	This work
pPB034	Binary 35S::*Nb*RD21	This work
pAG003	Binary 35S::*Nb*SBT1.7	This work
pAG004	Binary 35S::*Nb*SCPL20	This work
pAG005	Binary 35S::*Nb*SCPL48	This work

Agroinfiltration – *Agrobacterium* cultures were grown in LB media (kanamycin 50 µg/mL and gentamicin 10 µg/mL) overnight at 28°C. The next day, cultures were centrifuged at 4,000 *g* for 10 minutes at room temperature and resuspended in agroinfiltration buffer (10 mM $MgCl_2$, 10 mM MES, 150 µM acetosyringone) to a final OD_{600} of 0.5. All constructs were co-expressed with the silencing suppressor P19, and empty-vector (EV) was used as a

negative control. *N. benthamiana* plants were infiltrated when 4-5 weeks-old, and 2-3 fully expanded leaves were infiltrated per plant.

Apoplastic fluid (AF) isolation – AF was isolated from plants four days after agroinfiltration. Leaves were removed and infiltrated with ice-cold milliQ water and centrifuged at 1,000 *g* for 15 minutes and 4°C. AF was used immediately, or flash-frozen in liquid nitrogen and stored at -20°C.

Protein analysis – Apoplastic fluid was isolated from *N. benthamiana* plants transiently expressing hydrolases at 4 days-post infiltration (dpi). The presence of active serine hydrolases and cysteine proteases was measured by ABPP using the FP-TAMRA probe (Thermo Fisher Scientific) and TK009 (Sueldo et al., 2023), respectively. To label hydrolases, apoplastic fluid samples were incubated in a 50 µl reaction with 0.2 µM FP-TAMRA (for serine hydrolases), or a 250 µl reaction with 2 µM TK009 (for cysteine proteases), in the presence of 5 mM DTT and 50 mM sodium acetate pH 5 at room temperature for one hour (serine hydrolases) or four hours (for cysteine proteases). After labelling, the reaction was stopped by precipitation in 4x ice-cold acetone followed by resuspension in 4x gel loading buffer (200 mM Tris-HCl pH 6.8, 400 mM dithiotreitol, 8% SDS, 40% glycerol, 0.04% bromophenol blue) and heating at 90°C for 5 minutes. Samples were separated by SDS-PAGE and visualised using a Typhoon scanner with Cy3 filter (serine hydrolases) or Cy5 filter (cysteine proteases). Coomassie staining was used to check protein loading. *Nb*PR3 was detected by western blot using α-PR3 antibody raised against tobacco PR3 isoforms (Agrisera; 1:2500 in PBS-T), and α-rabbit-HRP secondary antibody (GE Healthcare).

Agromonas assays – Hydrolases were transiently expressed in *N. benthamiana* by agroinfiltration. Six plants were used per overexpression construct. Plants were covered

overnight with a transparent lid to increase humidity. Two days later, *P. syringae* cultures grown in LB media for 24 hours were washed and resuspended in milliQ water at 10^6 CFU/mL. Agroinfiltrated leaves were then infiltrated with *P. syringae* using a needleless syringe. Three days later, leaf discs were punched with a cork borer from each infected leaf, and surface-sterilised with 15% hydrogen peroxide for 2 minutes. Leaf discs were then washed twice in MilliQ and dried. Leaf discs were placed into a 1.5 mL safe-lock Eppendorf tube with three 3 mm diameter metal beads and 1 mL of MilliQ. Tubes were placed in tissue lyser for five minutes at 30 Hertz per second. 200 µL of the lysed tissue was transferred to the first row (A) of a 96-well plate and then serial 10-fold dilutions were made until the last row (20 µL tissue + 180 µL MilliQ). 20 µL of undiluted tissue and serial dilutions were plated on LB-agar plates containing *Pseudomonas* CFC Agar Supplement (10 µg/mL cetrimide, 10 µg/mL fucidin and 50 µg/mL cephaloridine, Oxoid SR0103). Plates were allowed to dry, incubated at 28°C for two days and then colonies were counted. Colonies counted were converted into $Log_{10}CFU/cm^2$.

Experiments were performed in groups of three constructs, including an EV control each time. Results from three experiments were pooled to give a final N=18 for each construct. P-values were calculated by two-way ANOVA to correct for variation between experiments, followed by post-hoc comparison using the Dunnett test to examine the effect of the overexpression constructs on bacterial growth. When individual experiments used different numbers of biological replicates (**Figure 3.6A**) or experiments were not repeated (**Figure 3.8**), P-values were calculated by *t*-tests.

Chapter 4: Analysis of the role of *Nb*PR3 in immunity

4.1 Abstract

Plant chitinases hydrolyse chitin, a polymer of ß-1,4-*N*-acetyl-D-glucosamine found in fungal cell walls. *Nb*PR3 is annotated as an acidic endochitinase, but we found it lacks this activity *in vitro*. In this chapter, we investigated alternative functions for *Nb*PR3 in bacterial immunity. We showed that *Nb*PR3 immune function is dependent on both its catalytic activity, and a *Nicotiana*-specific mutation in the catalytic general base. *Nb*PR3 was unable to hydrolyse a range of potential monosaccharide substrates, and we showed that *Nb*PR3 does not have lysozyme activity, does not directly damage bacterial growth *in vitro*, and does not activate the immune response. However, we identified an exciting potential role for *Nb*PR3 in elicitor release.

4.2 Introduction

Chitinases hydrolyse chitin, a polymer of ß-1,4-*N*-acetyl-D-glucosamine that is found in fungal cell walls and animal exoskeletons (Dahiya et al., 2006). Plant chitinases have diverse roles in plant development and responses to both biotic and abiotic stress (Grover, 2012). Much of the evidence for the role of chitinases in pathogen resistance concerns antifungal immunity (Collinge et al., 1993). Chitinases are grouped into two families, glycosyl hydrolase (GH) family 18 and GH 19, based on the sequence of their catalytic domain (Grover, 2012). InterProScan prediction suggests *Nb*PR3 belongs to GH family 19 (Jones et al., 2014). GH 19 family members show structural similarity to lysozymes and share characteristic deletions and auxiliary domains (Tyler et al., 2010).

According to the CAZy database, members of GH 19 use two catalytic glutamate (Glu) residues to hydrolyse their substrates (Cantarel et al., 2009). One Glu serves as the catalytic general acid, and is found within a characteristic -SHETT- sequence (Tang et al., 2004). Chitinase activity is abolished when this residue is mutated (Chaudet et al., 2014; Han et al., 2016). In contrast, some hydrolytic activity is retained upon substitution of the second Glu residue, which serves as the catalytic general base (Andersen et al., 1997; Tang et al., 2004). Catalysis is supported by several additional conserved active site residues which impair chitinolytic activity when mutated (Garcia-Casado et al., 1998; Tang et al., 2004; Ubhayasekera et al., 2009). Many roles have been described for GH 19 family members in antifungal immunity (Kawase et al., 2006; Martínez-Caballero et al., 2014), but some antibacterial functions have also been described, including bacterial agglutination and lysozyme activity (Guan et al., 2008; Subroto et al., 1999). Indeed, the tobacco ortholog of *NbPR3*, *NtPR-Q*, confers resistance to the bacterium *Ralstonia solanacearum* when overexpressed (Tang et al., 2017).

Chitinases are divided into seven classes based on amino acid sequence similarities (Grover, 2012). The difference between the otherwise very similar class I and class II chitinases lies in the presence (class I) or absence (class II) of the chitin-binding domain (CBD) at the N-terminus. The CBD is not thought to be essential for the catalytic activity of chitinases, but rather is required for the affinity and binding of the chitinase to its substrate (Beintema, 1994). Accordingly, class I chitinases tend to have higher chitinase activity than those from class II (Sela-Buurlage et al., 1993). In fact, removal of the CBD from class I tomato chitinases *Sl*Chi1 and *Sl*Chi13 by the fungus *Fusarium oxysporum* significantly reduces their chitinase and antifungal activity, suggesting it is used by the fungus as an infection strategy (Jashni et al., 2015a). Phylogenetic analysis of *Nb*PR3 suggests it is a class II chitinase because it lacks a CBD (**Figure 4.1**).

The annotation of *Nb*PR3 as an endochitinase is at odds with antibacterial activity because they lack chitin. In this chapter, we aimed to identify the function of *Nb*PR3 in antibacterial immunity.

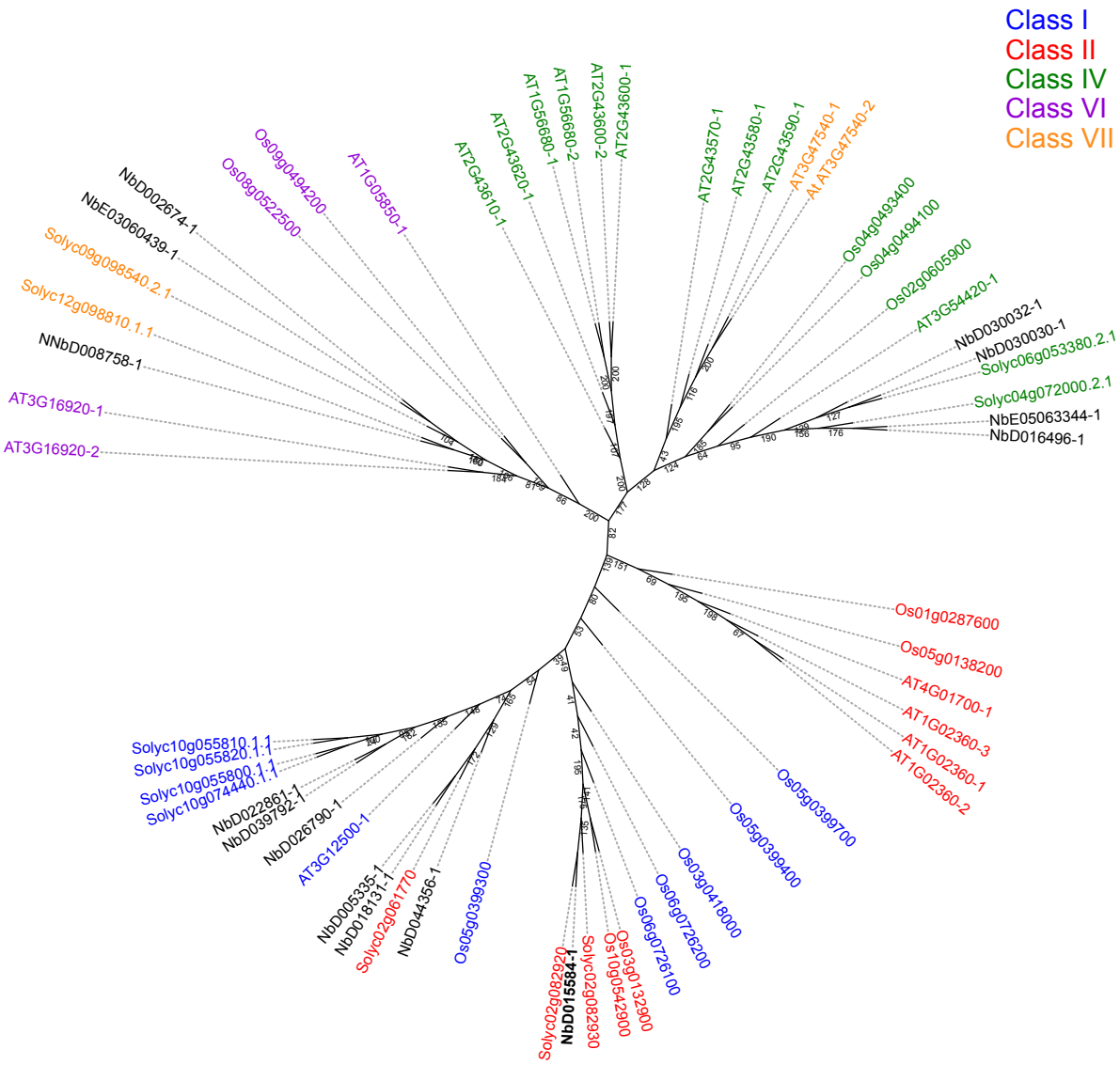


Figure 4.1: Phylogenetic tree of full-length GH19 proteins. GH19 sequences with the Pfam/InterPro IDs PF00182, IPR000726 and IPR016283 were identified from *Arabidopsis thaliana* (AT), *Solanum lycopersicum* (Solyc), *Oryza sativa* (Os) and *Nicotiana benthamiana* (Nb) genomes using InterProScan. Truncated proteins were manually removed and sequences were aligned by ClustalO (Sievers et al., 2011) followed by TrimAl (Capella-Gutiérrez et al., 2009). Phylogenetic analyses were performed in NGPhylogeny.fr (Lemoine et al., 2019) using the maximum-likelihood method with 200 bootstrap replicates. The tree was annotated using iTOL (Letunic and Bork, 2016). Proteins are coloured as per the legend according to their previous assignment in the literature to one of the five GH19 chitinase classes (Tyler et al., 2010; Jashni et al., 2015a); proteins in black correspond to *N. benthamiana* proteins, which are currently unassigned. *Nb*PR3 (NbD015584-1) is highlighted in bold.

4.3. Results

4.3.1 *Nb*PR3 accumulates in the apoplast upon infection

As a pathogenesis-related (PR) protein, *Nb*PR3 is expected to accumulate upon pathogen invasion (Ali et al., 2018). However, in **Chapter 3** we found that *Nb*PR3 was suppressed at the activity level during *Pseudomonas syringae* pv. *tomato* DC3000Δ*hQ* (*Pto*DC3000Δ*hQ*) infection. We also found that transiently expressed *Nb*PR3 can be labelled with an antibody raised against tobacco PR3 isoforms (**Figure 3.3**). To determine if *Nb*PR3 accumulates upon infection, we inoculated *Nicotiana benthamiana* with 10^6 CFU/mL *Pto*DC3000Δ*hQ* or a mock control of water. Two days later, we isolated apoplastic fluid (AF) and detected *Nb*PR3 accumulation with α-PR3. This experiment confirmed that *Nb*PR3 protein increases upon infection, despite its suppression at the activity level (**Figure 4.2**).

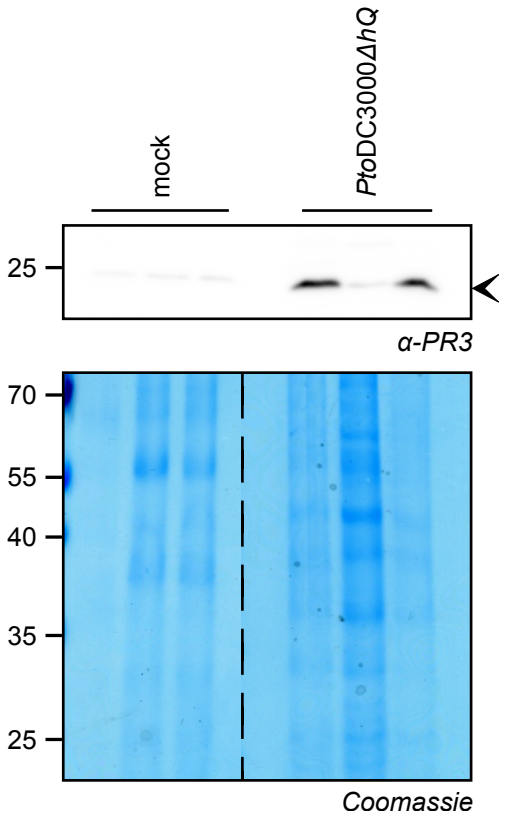


Figure 4.2: *Nb*PR3 accumulates in the apoplast upon *Pto*DC3000Δ*hQ* infection. AF was isolated from *N. benthamiana* leaves infiltrated with water (mock) or 10^6 CFU/mL *Pto*DC3000*ΔhQ* in N=3 biological replicates at 2 dpi. Proteins were separated by SDS-PAGE, analysed with western blot using α-PR3 raised against tobacco PR3 and stained with Coomassie. *Nb*PR3 is indicated with the arrowhead.

4.3.2 Catalytic activity is required for the immune function of *Nb*PR3

We next determined if *Nb*PR3 immune function is dependent on its catalytic activity. The catalytic general acid (Glu) appears to be the most important residue for catalytic activity of GH 19 enzymes (Chaudet et al., 2014; Han et al., 2016; Tang et al., 2004). We identified this residue in *Nb*PR3 as E92, which residues within the characteristic -SHETT- motif. We used site-directed mutagenesis using 35S::*Nb*PR3 (pAG001) as a template to substitute the catalytic general acid E92 into alanine (E92A), creating *Nb*PR3^{E92A}. Since *Nb*PR3 is abundant in AF, we confirmed this construct is expressed *in planta* by Coomassie staining (**Figure 4.3A**).

Next, we tested whether transiently expressed *NbPR3*^{E92A} provides resistance to *Pto*DC3000Δ*hQ* in 'agromonas' assays. In this experiment, *N. benthamiana* leaves transiently expressing *NbPR3*^{E92A} were infected with *Pto*DC3000Δ*hQ* cultures, and bacterial growth was measured three days later. Empty-vector (EV) and wildtype *NbPR3* were used as negative and positive controls, respectively. In contrast to wildtype *Nb*PR3, the catalytic mutant no longer conferred resistance to *Pto*DC3000Δ*hQ* (**Figure 4.3B**), indicating that *Nb*PR3 requires catalytic activity to perform its immune function.

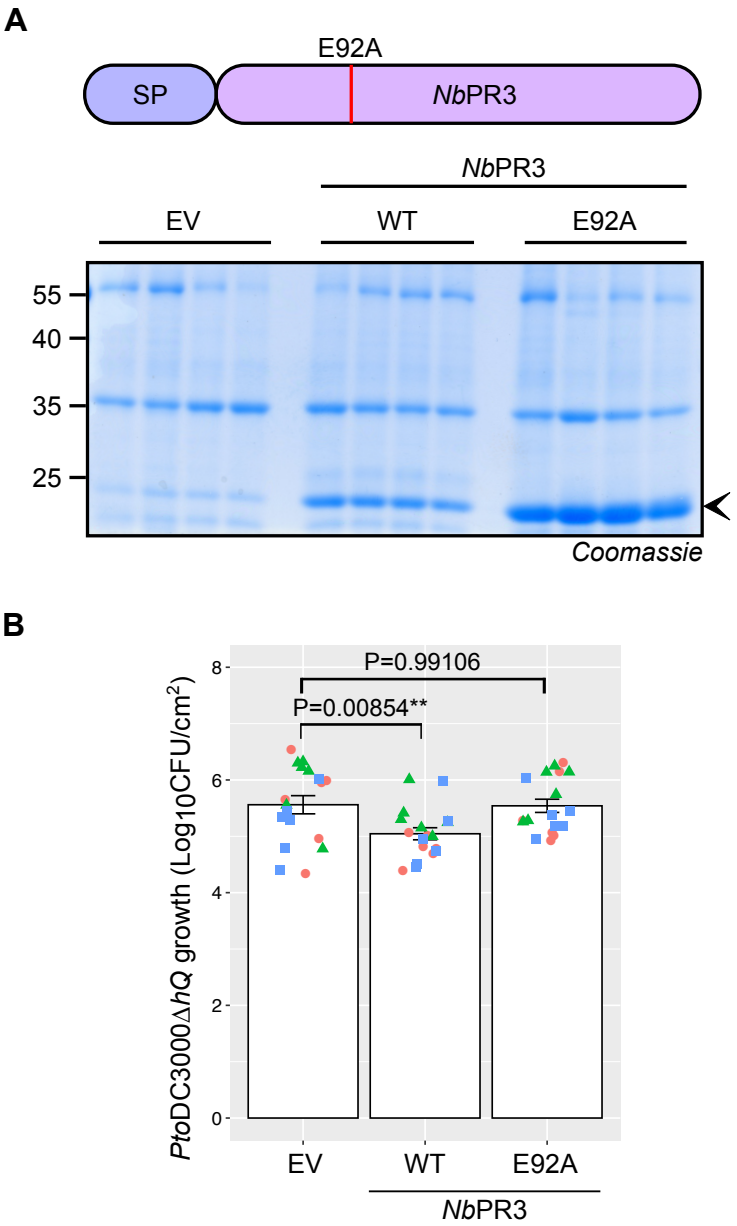


Figure 4.3: *Nb*PR3 requires catalytic activity for its immune function.
A: The *Nb*PR3 catalytic mutant accumulates in the apoplast of agroinfiltrated *N. benthamiana* leaves. *Nb*PR3 and its catalytic mutant (E92A), shown schematically, along with the empty-vector (EV) control, were agroinfiltrated with the silencing inhibitor P19 into *N. benthamiana* leaves. Apoplastic fluid was isolated at day 4 from N=4 replicates, separated by SDS-PAGE and analysed by Coomassie staining. The arrowhead indicates *Nb*PR3 protein.
B: Transient overexpression of *NbPR3* but not its catalytic mutant suppresses bacterial growth of *Pto*DC3000*ΔhQ*. *NbPR3*, its catalytic site E92A mutant, and the EV control were transiently co-expressed with the silencing inhibitor P19 by agroinfiltration into *N. benthamiana* leaves. Two days later, the same leaves were infiltrated with 10^6 CFU/mL *Pto*DC3000*ΔhQ*. Bacterial growth in colony-forming units (CFU) was measured at 3 dpi. Bars represent mean ± SE of all biological replicates over three experiments; biological replicates from the same experiment have the same shape and colour. P-values were calculated by two-way ANOVA followed by post-hoc comparison using the Dunnett test to examine the effect of construct overexpression on bacterial growth. **, P<0.01.

4.3.3 *Nb*PR3 does not have endochitinase activity

Next, we tested whether *Nb*PR3 is a functional endochitinase. We tested whether AF isolated from plants overexpressing EV, *NbPR3* or *NbPR3*^{E92A} could degrade the fluorogenic endochitinase substrate 4-methylumbelliferyl-β-D-N,N′,N″-triacetylchitotrioside (4-MU-GlcNac$_3$, **Figure 4.4A**) *in vitro*. A commercial endochitinase from the fungus *Trichoderma viride* was used as a positive control. Neither *Nb*PR3 nor its catalytic mutant were able to hydrolyse the substrate (**Figure 4.4B**), indicating that *Nb*PR3 lacks endochitinase activity.

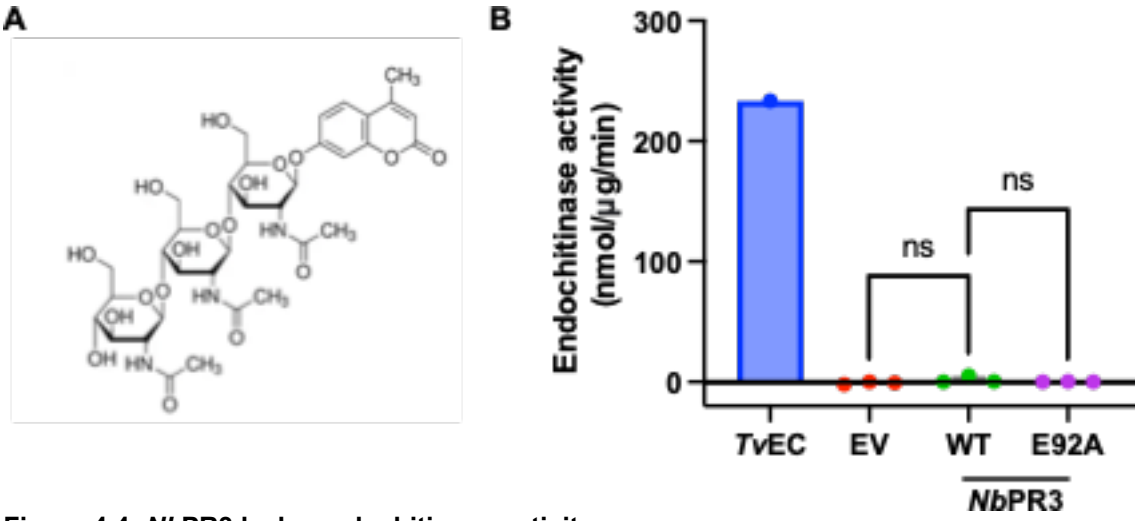


Figure 4.4: *Nb*PR3 lacks endochitinase activity.
A: Structure of 4-MU-GlcNAc$_3$. Taken from commercial website (Sigma-Aldrich, M5639).
B: Endochitinase activity assay. Apoplastic fluid from plants transiently co-expressing *NbPR3*, its catalytic mutant E92A or an empty-vector (EV) control with the silencing inhibitor P19 was isolated at 4 dpi and incubated with 18 µM 4-MU-GlcNac$_3$ at 37°C. The rate of hydrolysis was measured at 355ex/450em and calculated per µg *Nb*PR3 protein estimated by Coomassie staining (**Supplementary Figure 4.1**). The endochitinase of *Trichoderma viride* (*Tv*EC) was included as a positive control. Error bars represent mean ± SE of N=3 biological replicates. P-values were calculated by one-way ANOVA followed by post-hoc comparison using the Dunnett test. Ns, not significant.

4.3.4 Identifying residues important for the lack of chitinase activity

We compared the protein sequence of *Nb*PR3 with that of the closest homolog in *Nicotiana tabacum* with demonstrated chitinase activity, CHN-A (Suarez et al., 2001). We investigated differences between the sequences that could explain the lack of chitinase activity for *Nb*PR3 (**Figure 4.5**).

There are many differences between the proteins, but only two of these were previously shown to be important catalytic residues. The serine residue S198 in CHN-A is a threonine residue T128 in *Nb*PR3, and the catalytic general base E167 in CHN-A is replaced with glutamine Q112 in *Nb*PR3. The former mutation is unlikely to be important for the loss of endochitinase activity. Polymorphism at this site is common, with both serine or threonine residues conferring chitinase activity (Garcia-Casado et al., 1998; Passarinho and de Vries, 2002; Suarez et al., 2001).

On the other hand, Q112 in *Nb*PR3 is likely to be detrimental to chitinase activity. Site-directed mutagenesis of the catalytic general base from Glu to Gln almost abolishes the activity of active chitinases (Andersen et al., 1997; Garcia-Casado et al., 1998). Therefore, we hypothesised that Q112 in *Nb*PR3 is important for its lack of endochitinase activity.

```
NbPR3 27   IGSIVTSDLFNEMLKNRNDVRCPANGFYTYDAFIAAANSFPGFGTTGDDTARRKEIA  83
CHN-A 80   LGSIISSSMFDQMLKHRNDNACQGKGFYSYNAFINAARSFPGFGTSGDTTARKREIA  136

NbPR3 84   AFFGQTSHETTGGSLSAE--PFTGGYCFVRQNDQ---------------SERYYGRG  123
CHN-A 137  AFFAQTSHETTGGWATAPDGPYAWGYCWLREQGSPGDYCTPSGQWPCAPGRKYFGRG  193

NbPR3 124  PIQLTNRNNYEKAGTAIQQDLVNNPDLVATDATISFKTAIWFWMTAQDNKPSSHDVI  180
CHN-A 194  PIQISHNYNYGPCGRAIGVDLLNNPDLVATDPVISFKSALWFWMTPQSPKPSCHDVI  250

NbPR3 181  IGSWTPSAADQAANRVPGYGVITNIINGGIECGMGRNDAVEDRIGYYRRYCGMLNVA  237
CHN-A 251  IGRWQPSAGDRAANRLPGFGVITNIINGGLECGRGTDSRVQDRIGFYRRYCSILGVS  307

NbPR3 238  PGENLDCYNQRNFAQG  253
CHN-A 308  PGDNLDCGNQRSFGNG  323
```

Figure 4.5: Alignment of *Nb*PR3 with CHN-A. The *Nb*PR3 protein sequence was BLASTed (Johnson et al., 2008) against the *Nicotiana tabacum* proteome. The most homologous protein with demonstrated endochitinase activity was CHN-A (Sela-Buurlage et al., 1993). Residues important for catalytic activity are shown in green, the catalytic general acid and base are underlined. Differences to *Nb*PR3 are highlighted in grey.

4.3.5 A *Nicotiana*-specific mutation at the catalytic general base

Comparison of the protein sequence of chitinases has shown the majority contain Glu at their catalytic general base (Q112, Tang et al., 2004). However, *Nt*PR-Q, like its ortholog *Nb*PR3, also has Gln at its catalytic general base and has low chitinase activity (Brunner et al., 1998). Given that *Nt*PR-Q is also involved in bacterial resistance (Tang et al., 2017), we hypothesised that this mutation is important for *Nicotiana* PR3 proteins to gain a novel antibacterial function.

We determined if the catalytic Gln residue is found throughout the *Nicotiana* genus by aligning the protein sequences of putative *NbPR3* orthologs from several *Nicotiana* species, as well as Arabidopsis, pepper (*Capsicum annuum*), potato (*Solanum tuberosum*), tomato (*Solanum lycopersicum*) and rice (*Oryza sativa*) (**Figure 4.6**, **Supplementary Figure 4.2**).

Interestingly, we found Q112 is conserved throughout the *Nicotiana* genus, but not found in other species. This suggests that the E into Q substitution occurred in the *Nicotiana* common ancestor ~ 50 million years ago.

```
Nbenthamiana        77 ARRKEIAAFFGQTSHETTGGSL-SA-EPFTGGYCFVRQNDQ------ 115
Ntabacum            77 ARRKEIAAFFGQTSHETTGGSL-SA-EPFTGGYCFVRQNDQ------ 115
Nattenuata          77 ARRKEIAAFFGQTSHETTGGSL-SA-EPFTGGYCFVRQNDQ------ 115
Nsylvestris         77 ARRKEIAAFFGQTSHETTGGSL-SA-EPFTGGYCFVRQNDQ------ 115
Ntomentosiformis    77 ARRKEIAAFFGQTSHETTGGSL-SA-EPFTGGYCFVRQNDQ------ 115
Cannuum             75 ARKTEIAAFFGQTSHETTGGSL-SADGPFAGGYCFVREGNQ------ 114
Stuberosum          75 ARKKEIAAFFGQTSHETTGGSL-SADGPFAGGYCFLREGNQ------ 114
Slycopersicum       69 ARKKEIAAFFGQTSHETTGGSL-SADGPFAGGYCFVREGNQ------ 108
Athaliana          123 TRKKEVAAFFGQTSHETTGGWATAPDGPYSWGYCFKQEQNPASDYCE 169
Osativa             83 LIRRELAAFFGQTSHETTGGTR-GSSDQFQWGYCFKEEINKA----- 123
```

Figure 4.6: Alignment of *Nb*PR3 with putative orthologs. The *Nb*PR3 protein sequence was BLASTed (Johnson et al., 2008) against the proteomes of *Nicotiana* species (*N. benthamiana*, *N. tabacum*, *N. attenuata*, *N. sylvestris*, *N. tomentosiformis*), pepper (*Capsicum annuum*), potato (*Solanum tuberosum*), tomato (*Solanum lycopersicum*), Arabidopsis (*Arabidopsis thaliana*) and rice (*Oryza sativa*). The top hit from each species was selected and aligned using ClustalO (Sievers et al., 2011) at NGPhylogeny.fr (Lemoine et al., 2019). Key catalytic residues are shown in green, the catalytic general acid and base are underlined. Differences to *Nb*PR3 are highlighted in grey.

4.3.6 *Nicotiana*-specific glutamine is required for antibacterial resistance

To determine if the E112Q mutation was important for antibacterial activity, we generated a Q112E substitution mutant (*Nb*PR3^{Q112E}) by site-directed mutagenesis using 35S::*Nb*PR3 (pAG001) as a template. We confirmed the expression of this mutant *in planta* by Coomassie staining (**Figure 4.7A**).

We next tested whether transiently overexpressed *Nb*PR3^{Q112E} is still able to confer resistance to *Pto*DC3000Δ*hQ* in 'agromonas' assays. EV and wildtype *Nb*PR3 were used as negative and positive controls, respectively. Importantly, *Nb*PR3^{Q112E} no longer conferred resistance to *Pto*DC3000Δ*hQ* (**Figure 4.7B**), demonstrating that the *Nicotiana*-specific Q112 residue is essential for the acquisition of antibacterial activity.

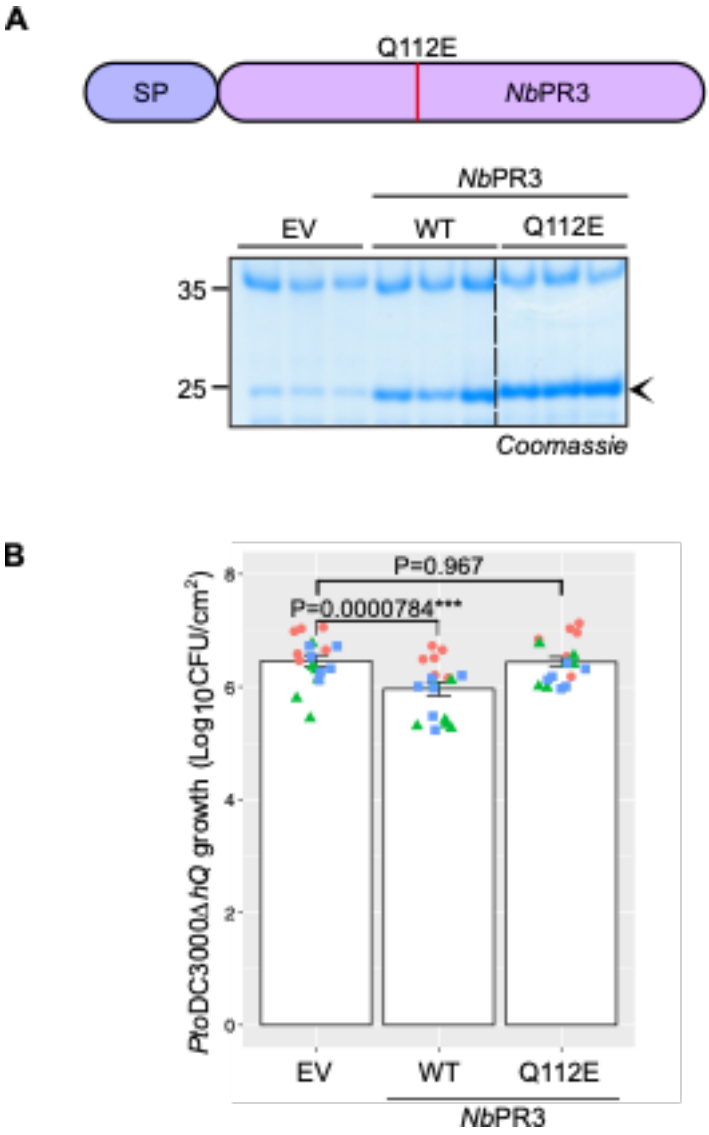


Figure 4.7: *Nb*PR3 requires Q112 for its immune function.

A: *Nb*PR3^{Q112E} accumulates in the apoplast of agroinfiltrated *N. benthamiana* leaves. *Nb*PR3 and the Q112E substitution mutant, shown schematically, along with the empty-vector (EV) control, were transiently co-expressed with the silencing inhibitor P19 in *N. benthamiana* leaves by agroinfiltration. Apoplastic fluid was isolated at day 4 from N=3 replicates, separated by SDS-PAGE and analysed by Coomassie staining. The arrowhead indicates *Nb*PR3 protein.

B: Transient overexpression of *NbPR3* but not the Q112E mutant suppresses bacterial growth of *Pto*DC3000*ΔhQ*. *NbPR3*, the substitution mutant Q112E, and the EV control were transiently co-expressed with the silencing inhibitor P19 in *N. benthamiana* leaves by agroinfiltration. Two days later, the same leaves were infiltrated with 10^6 CFU/mL *Pto*DC3000*ΔhQ*. Bacterial growth in colony-forming units (CFU) was measured at 3 dpi. Bars represent mean ± SE of all biological replicates over three experiments; biological replicates from the same experiment have the same shape and colour. P-values were calculated by two-way ANOVA followed by post-hoc comparison using the Dunnett test to examine the effect of construct overexpression on bacterial growth. ***, P<0.001.

4.3.7 Q112E is insufficient to restore endochitinase activity

Next, we tested whether endochitinase activity was restored in *Nb*PR3^{Q112E} using the fluorogenic endochitinase substrate 4-MU-GlcNac$_3$ *in vitro*. However, we found that *Nb*PR3^{Q112} lacked endochitinase activity when compared to the positive control, the endochitinase of *Trichoderma viride* (**Figure 4.8**). Furthermore, there was no significant difference in endochitinase activity between wildtype *Nb*PR3 and *Nb*PR3^{Q112E} (one-way ANOVA with Dunnett test, P=0.7355). This indicates that other residues must have been involved in the loss of endochitinase activity.

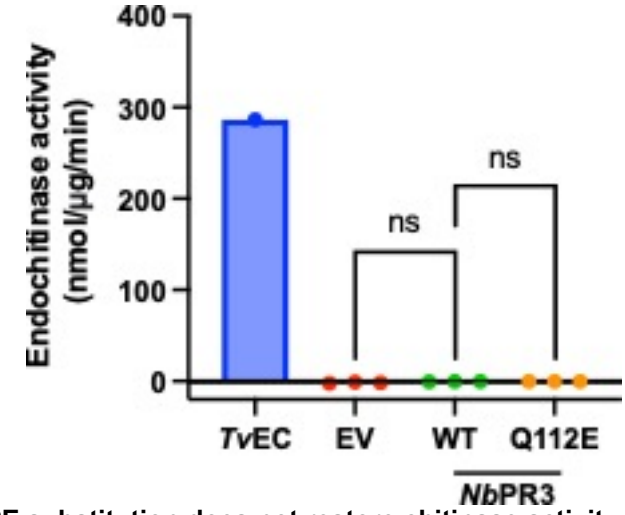


Figure 4.8: The Q112E substitution does not restore chitinase activity in *Nb*PR3.
Apoplastic fluid from plants transiently co-expressing wildtype (WT) *NbPR3*, substitution mutant *NbPR3*^{Q112E} (Q112E), or an empty-vector (EV) control with the silencing inhibitor P19 was isolated at 4 dpi and incubated with 18 µM 4-MU-GlcNac$_3$ at 37ºC. The rate of hydrolysis was measured at 355ex/450em and calculated per µg *Nb*PR3 protein estimated by Coomassie staining (**Supplementary Figure 4.3**). The endochitinase of *Trichoderma viride* (*Tv*EC) was included as a positive control. Error bars represent mean ± SE of N=3 biological replicates. P-values were calculated by one-way ANOVA followed by post-hoc comparison using the Dunnett test. Ns, not significant.

4.3.8 Biochemical approaches to identify the substrate of *Nb*PR3

Given that *Nb*PR3 lacks endochitinase activity, we next set out to find an alternative substrate for *Nb*PR3. Aside from Q112, *Nb*PR3 retains all the important catalytic residues, and so we predict it still acts on a glycan. However, glycosyl hydrolase substrates are incredibly diverse (Davies and Henrissat, 1995), making it challenging to test every potential substrate. We used a biochemical approach to narrow down the possible *Nb*PR3 substrate.

4.3.8.1 *Nb*PR3 is unable to hydrolyse a range of monosaccharide substrates

We made use of twelve 4-nitrophenyl-conjugated monosaccharide substrates previously used to determine the substrate specificity of the ß-galactosidase BGAL1 (Buscaill et al., 2019). Cleavage of these substrates by an appropriate hydrolase produces a yellow colour that can be detected using a spectrophotometer. We isolated AF from plants transiently expressing EV or *NbPR3* and confirmed expression was successful (**Figure 4.9A**). We then incubated this AF with 4-nitrophenyl-conjugates and calculated hydrolytic activity (**Figure 4.9B**). BGAL1 was used as a positive control for hydrolysing ß-galactopyranoside. There was no significant difference in hydrolytic activity between *Nb*PR3 and the EV control for any of the substrates (*t*-tests with False Discovery Rate correction), suggesting that *Nb*PR3 was unable to hydrolyse any of the tested monosaccharides *in vitro*.

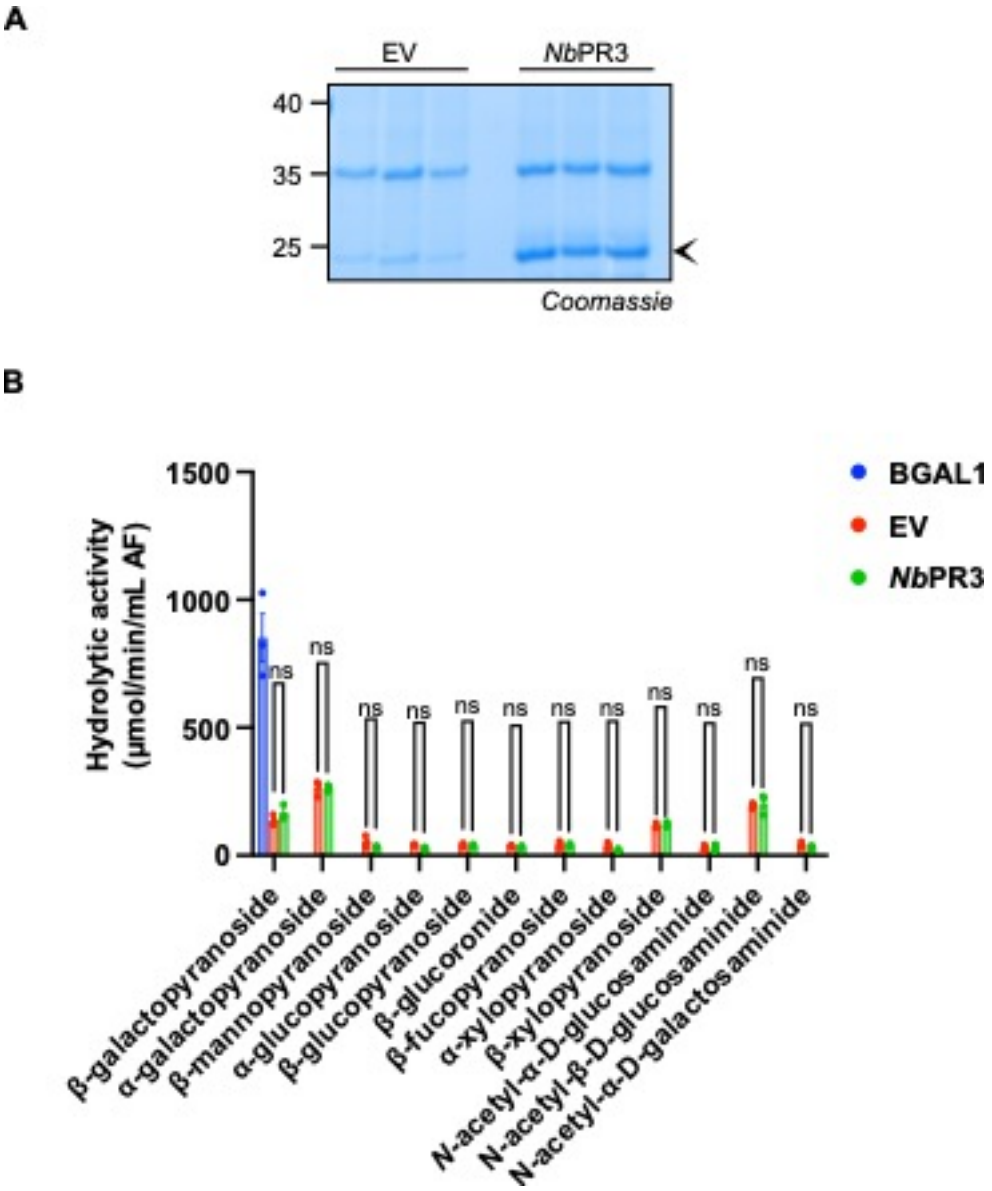


Figure 4.9: *Nb*PR3 was unable to hydrolyse a range of monosaccharide substrates.
A: Transient expression of *NbPR3* for this experiment was successful. *NbPR3* or an empty-vector (EV) control were agroinfiltrated with the silencing inhibitor P19 into *N. benthamiana* leaves. Apoplastic fluid was isolated at day 4 from N=3 replicates, separated by SDS-PAGE and analysed by Coomassie staining. The arrowhead indicates *Nb*PR3 protein.
B: *Nb*PR3 cannot hydrolyse 4-nitrophenyl-monosaccharide conjugates. Apoplastic fluid from plants transiently co-expressing the silencing inhibitor P19 and *NbPR3*, or the positive and negative controls *BGAL1* and EV, was incubated with 1 mM 4-nitrophenyl-monosaccharide conjugates at room temperature for 10 minutes. The reaction was stopped with 100 mM Na_2CO_3 and the A_{450} was measured. Error bars represent mean ± SE of N=3 biological replicates. P-values were calculated by multiple *t*-tests followed by False Discovery Rate correction. Ns, not significant.

4.3.8.2 Glycan array to identify *Nb*PR3 substrate

Since the potential substrate range of *Nb*PR3 is so broad, we planned to utilise a glycan array to identify substrates. This consisted of a glass slide onto which 300 different representative glycans were printed, allowing us to simultaneously test their affinity to *Nb*PR3 (RayBiotech GA-Glycan-300, Blixt et al., 2004). We planned to hybridise catalytically inactive, His-tagged *Nb*PR3 to the glass slide, and detect His-tagged *Nb*PR3 using a biotinylated α-His antibody and Cy3-conjugated streptavidin (**Figure 4.10**).

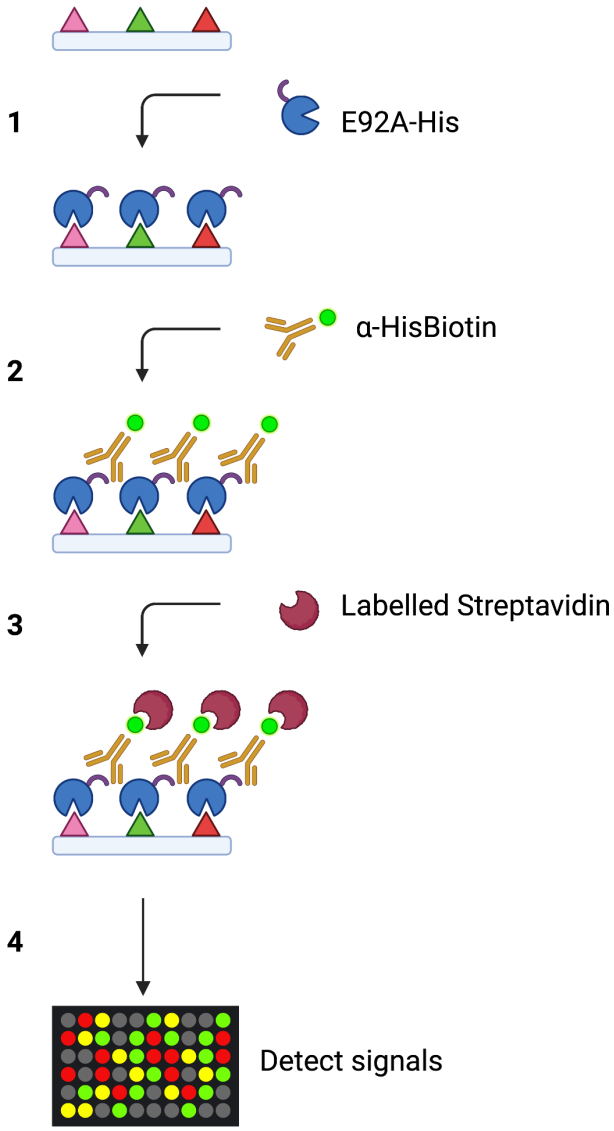


Figure 4.10: Sandwich-based procedure for glycan array. *Nb*PR3^{E92A}-His (E92A-His) is purified from apoplastic fluid and incubated on the glycan microarray slide (**1**). Biotinylated antibody (α-HisBiotin) is incubated on the slide and attaches to bound E92A-His (**2**). Cy3-conjugated streptavidin complexes with biotinylated proteins (**3**). Signals are detected using a fluorescent scanner (**4**). Adapted from RayBio Glycan Array 300 User Manual. Created with BioRender.com.

We generated an expression construct for *Nb*PR3^{E92A}-His (E92A-His) and verified expression of this His-tagged protein in AF by western blot (**Figure 4.11A**). Next, we purified His-tagged *Nb*PR3^{E92A} protein from AF using Nickel NTA agarose beads (**Figure 4.11B**). Our yield following purification was always 410-480 µg/mL, which is expected for purification of secreted proteins, and well within the required 50-500 µg/mL starting material

required for the glycan array (Schuster et al., 2022, RayBiotech GA-Glycan-300). The elution fraction was stained with Coomassie and appears clean with only a single band (**Figure 4.11B**), and reasonable purification efficiency given the intense band in earlier fractions will also correspond to endogenous *Nb*PR3.

We cannot rule out that this elution contains contaminants, which could bind to glycans in the array and give false positive signals. However, we hoped to subtract this background by purifying and testing Pip1^{mut}-His, a catalytically inactive tomato immune papain-like cysteine protease, to use as the negative control in the glycan array (Kourelis et al., in prep). We tested the α-HisBiotin antibody on different amounts of purified E92A-His and Pip1^{mut}-His proteins (0.05-50 ng; **Figure 4.11C**). We observed strong signals of 50 ng Pip1^{mut}-His, and weak labelling with 5 ng Pip1^{mut}-His, but we were unable to detect purified E92A-His in any of the tested conditions. However, we found that AF from plants transiently expressing *E92A-His* could be labelled with α-HisBiotin, suggesting the lack of signal is due to a problem with E92A-His purification (**Figure 4.11D**). Due to these issues, we were unable to make further progress with the glycan array.

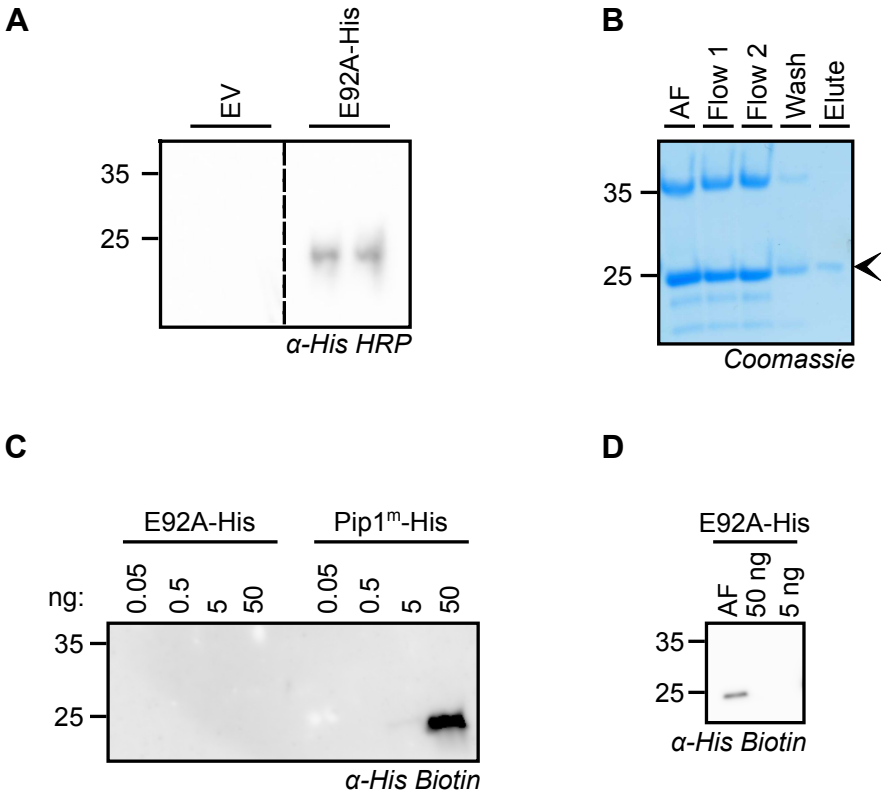


Figure 4.11: Optimising E92A-His for glycan array.
A: His-tagged *Nb*PR3^{E92A} (E92A-His) is expressed in apoplastic fluid (AF). AF from plants transiently co-expressing *E92A-His* or an empty-vector (EV) control with the silencing inhibitor P19 was isolated at 4 dpi from N=3 biological replicates and pooled. Proteins were separated in duplicate by SDS-PAGE and visualised by western blotting with α-His HRP.
B: Purification of E92A-His. AF from plants transiently co-expressing *E92A-His* with the silencing inhibitor P19 was passed through a Nickel NTA column to purify E92A-His. Samples were taken at each stage in the purification process, proteins were separated by SDS-PAGE and stained with Coomassie. *Nb*PR3 proteins are indicated by the arrowhead.
C: Labelling of E92A-His with biotinylated antibody. Varying amounts of purified E92A-His and Pip1^{mut}-His were ran on an acrylamide gel and labelled with α-HisBiotin.
D: E92A-His in AF can be labelled with α-HisBiotin. E92A-His before and after Nickel NTA purification was ran on an acrylamide gel and labelled with α-HisBiotin.

4.3.9 Hypothesis-driven approaches to identify the substrate of *Nb*PR3

As we were unable to identify the substrate of *Nb*PR3 biochemically, we took a hypothesis-driven approach to test ways in which *Nb*PR3 may function in bacterial immunity. We hoped that by identifying the molecular function of *Nb*PR3, we could work backwards to identify the substrate.

4.3.9.1 *Nb*PR3 does not have lysozyme activity

First, we tested if *Nb*PR3 functions as a lysozyme. Lysozymes hydrolyse peptidoglycan, which is composed of alternating residues of ß-1,4-*N*-acetyl-D-glucosamine and *N*-acetylmuramic acid (Liu et al., 2014). Peptidoglycan forms part of the bacterial cell wall and is essential for cell structure and stability (Vollmer et al., 2008). Some plant chitinases, including GH 19 family members, have additional lysozyme activity which triggers bacterial immunity through cell lysis or triggering PAMP-triggered immunity (PTI; Liu et al., 2014; Scheltinga et al., 1994; Subroto et al., 1999).

We hypothesised that *Nb*PR3 may have changed substrate specificity from chitin to peptidoglycan. Peptidoglycan hydrolysis can be indirectly measured as lytic activity on *Micrococcus lysodeikticus*, which has peptidoglycan in its cell wall (Lee and Yang, 2002). We incubated AF from plants transiently expressing *NbPR3* and its mutants with *M. lysodeikticus* cells and measured the change in absorbance. Lysozyme from chicken egg white (LCEW) and EV were included as positive and negative controls, respectively. In contrast to the positive control, *Nb*PR3 had no lysozyme activity *in vitro* (**Figure 4.12**). Further, there was no significant difference in lysozyme activity between *Nb*PR3 and EV (one-way ANOVA with Dunnett's T3 correction, P=0.9784), *Nb*PR3^{E92A} (P=0.535) or *Nb*PR3^{Q112E} (P=0.1541).

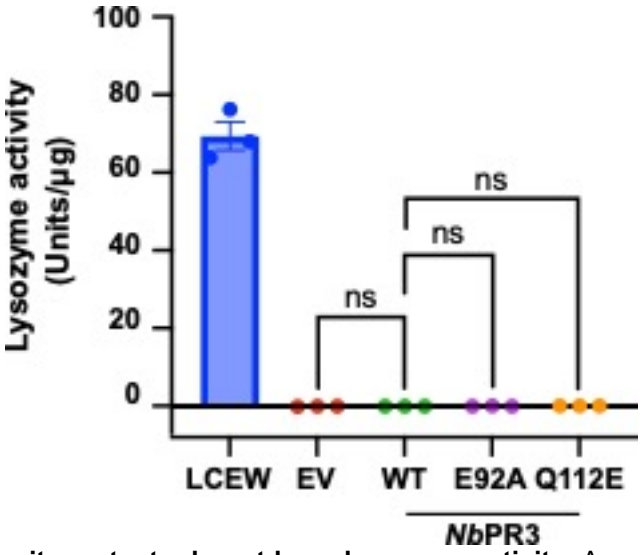


Figure 4.12: *Nb*PR3 or its mutants do not have lysozyme activity. Apoplastic fluid from plants transiently co-expressing *NbPR3*, mutants *NbPR3*^{E92A} (E92A) and *NbPR3*^{Q112E} (Q112E), or an empty-vector (EV) control along with the silencing inhibitor P19 was isolated at 4 dpi and incubated with *Micrococcus lysodeikticus* cells in potassium phosphate buffer. The change in A_{450} was measured and converted to units per µg *Nb*PR3 protein estimated by Coomassie staining (**Supplementary Figure 4.3**). 0.01 mg/mL lysozyme from chicken egg white (LCEW) was included as a positive control. Error bars represent mean ± SE of N=3 biological replicates. P-values were calculated by one-way ANOVA followed by post-hoc comparison using the Dunnett test. Ns, not significant.

4.3.9.2 *Nb*PR3 does not directly damage *Pto*DC3000 *in vitro*

Second, we tested if *Nb*PR3 can directly inhibit bacterial growth *in vitro*. This resistance strategy has already been described for several plant hydrolases. For instance, maize papain Mir1 inhibits the growth of insect pathogens by degrading insect intestinal mucin, and secreted aspartic protease 1 (SAP1) and SAP2 can suppress *P. syringae* growth *in vitro* (Fescemyer et al., 2013; Wang et al., 2019c). Furthermore, animal lysozymes can directly prevent pathogen growth by triggering bacterial lysis (Davis et al., 2011). We tested whether AF from plants transiently expressing *NbPR3* could directly inhibit bacterial growth, similar to experiments done previously (O'Leary et al., 2016; Wang et al., 2019c).

We isolated AF from plants transiently expressing EV, *NbPR3* or its catalytic mutant and confirmed expression was successful by Coomassie staining (**Figure 4.13A**). We incubated this AF with 10^6 CFU/mL *Pto*DC3000*ΔhQ* for eight hours. Samples were taken every two

hours and plated in dilution series to measure bacterial growth as colony-forming units (CFU). LCEW was included as a positive control since lysozymes can directly inhibit bacterial growth (Davis et al., 2011). In contrast to the positive control, *Nb*PR3 was unable to significantly reduce bacterial growth *in vitro* (**Figure 4.13B**). Further, there was no significant difference between wildtype *Nb*PR3 and its catalytic mutant. Therefore, we concluded that *Nb*PR3 does not function by direct bacterial damage.

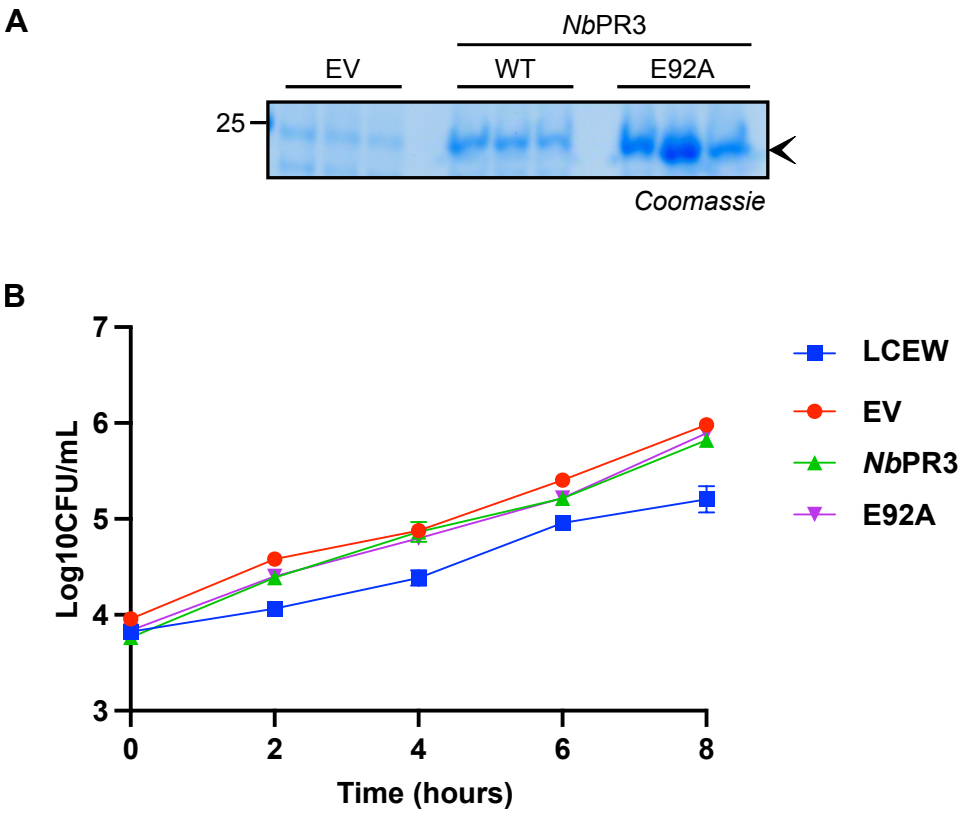


Figure 4.13: *Nb*PR3 does not prevent bacterial growth *in vitro*.
A: Transient expression of *NbPR3* for this experiment was successful. *NbPR3* and its catalytic mutant (E92A) along with the empty-vector (EV) control, were agroinfiltrated with the silencing inhibitor P19 into *N. benthamiana* leaves. Apoplastic fluid was isolated at day 4 from N=3 replicates, separated by SDS-PAGE and analysed by Coomassie staining. The arrowhead indicates *Nb*PR3 protein.
B: *Nb*PR3 does not reduce bacterial growth *in vitro*. 10^6 CFU/mL *Pto*DC3000*ΔhQ* was incubated at 25°C in apoplastic fluid from plants transiently co-expressing *NbPR3*, *NbPR3*^{E92A} or EV control along with the silencing inhibitor P19. 1 mg/mL lysozyme from chicken egg white (LCEW) was used as a positive control. Samples were taken at 2-hour intervals and plated in serial dilution with CFC antibiotic. Bacterial growth in colony-forming units (CFU) was counted 2 days later. Lines represent mean ± SE of N=3 biological replicates.

4.3.9.3 *Nb*PR3 does not induce PR protein accumulation

Third, we tested if *Nb*PR3 activates the immune response. PR proteins are key components of plant defence that are induced upon pathogen invasion (Ali et al., 2018). They are grouped into 17 families based on protein sequence and function, including antifungal (PR1), ß-1,3-glucanases (PR2) and chitinases (PR3) (van Loon et al., 2006). The association of their expression with pathogen invasion make PR proteins, particularly PR1 and PR2, routinely used markers of defence response initiation (Ali et al., 2018). Plant immune hydrolases have been implicated in PR protein activation (Ramírez et al., 2013; Xia et al., 2004). In fact, overexpression of the tobacco ortholog of *NbPR3*, *NtPR-Q*, induced expression of *NtPR1a/b* and *NtPR2* (Tang et al., 2017).

We monitored PR protein accumulation upon *NbPR3* overexpression. We tested this in both wildtype and *NahG*-transgenic *N. benthamiana*. In *NahG*-transgenic plants, salicylic acid (SA) is degraded by salicylate hydroxylase (Anand et al., 2008). We therefore tested whether *Nb*PR3-induced PR protein expression was dependent on SA. AF from plants overexpressing *NbPR3* and its mutants, or an EV control was labelled with antibodies raised against PR2 and PR3 proteins (**Figure 4.14A**). Band intensity was quantified relative to wildtype EV samples (**Figure 4.14B**). Expression of *NbPR3* did not induce PR2 levels in wildtype plants. In contrast, PR2 accumulated significantly less when *NbPR3* and its mutants were overexpressed, compared to the EV control. PR2 accumulation was significantly less in *NahG* plants and was again unaffected by *NbPR3* expression.

As expected, PR3 protein accumulation is higher in wildtype plants overexpressing *NbPR3* proteins compared to EV. PR3 protein accumulation is reduced in *NahG* plants, presumably because of reduced endogenous *NbPR3* expression, and because the promoter driving *NbPR3* overexpression is partly SA-dependent (Redman et al., 2002). Overall, we conclude that *Nb*PR3 does not induce PR protein expression.

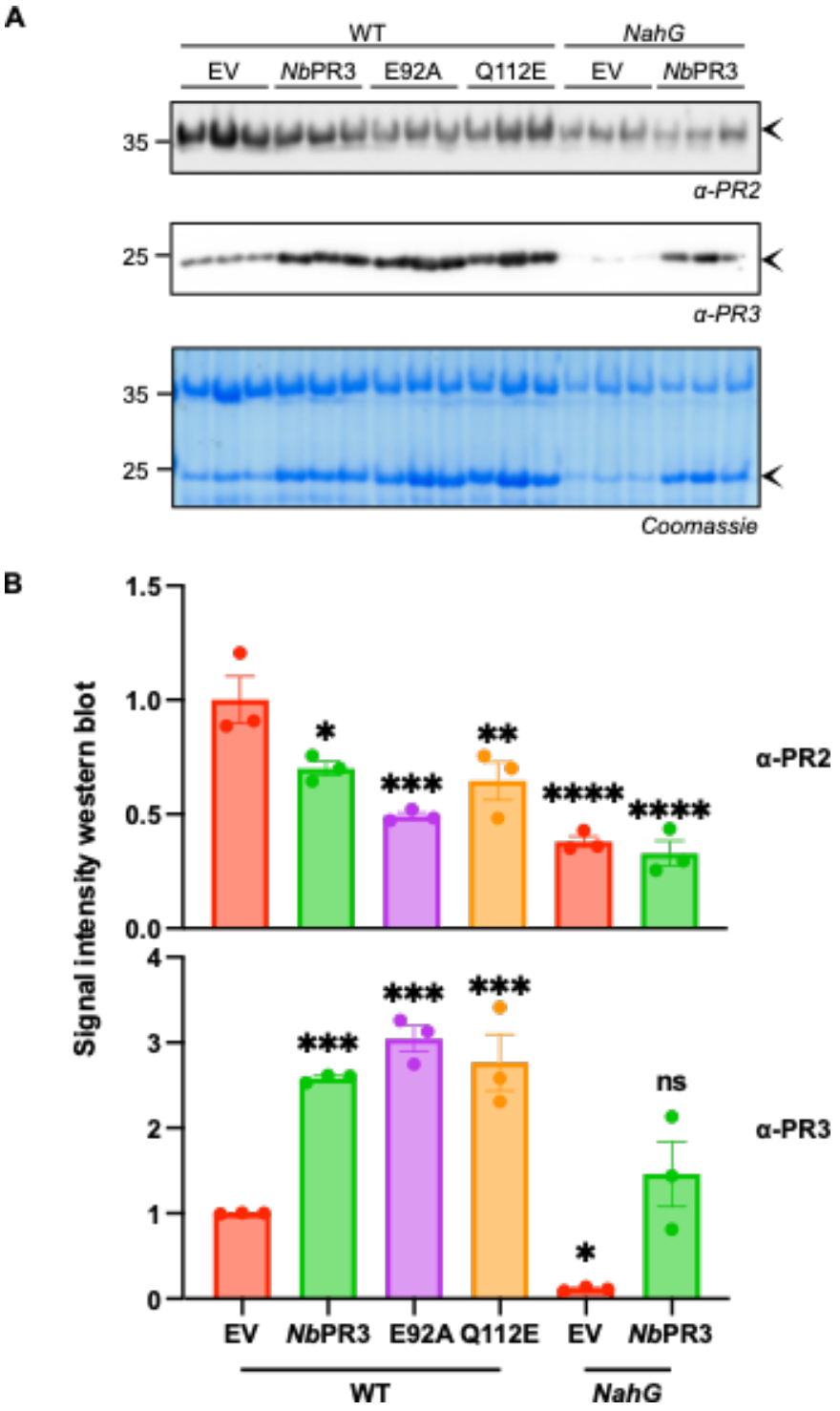


Figure 4.14: *Nb*PR3 does not induce PR protein accumulation.
A: Acrylamide gels showing accumulation of PR2 and PR3 proteins. AF from wildtype (WT) and *NahG*-transgenic *N. benthamiana* transiently co-expressing *NbPR3* and its mutants *NbPR3*^{E92A} (E92A) and *NbPR3*^{Q112E} (Q112E), or an empty-vector (EV) control along with the silencing inhibitor P19 was isolated at 4 dpi with N=3 biological replicates. Proteins were separated by SDS-PAGE and visualised by Coomassie staining and western blotting with α-PR2 and α-PR3. PR2 and PR3 proteins are indicated with arrowheads.
B: Western blot signals were quantified and normalised to the intensity of the WT EV controls. Bars represent mean ± SE of N=3 biological replicates. P-values comparing signal intensity to the WT EV control are the result of one-way ANOVA with Dunnett correction for multiple comparisons. *, P<0.05; **, P<0.01; ***, P<0.001; ****, P<0.0001; ns, not significant.

4.3.9.4 Potential role for *Nb*PR3 in elicitor release

Finally, we tested whether *Nb*PR3 functions in the release of a bacterial elicitor to trigger the reactive oxygen species (ROS) burst (Torres et al., 2006). *Pto*DC3000*ΔhQ* cultures were incubated in AF from plants transiently overexpressing *NbPR3* or an EV control. The mixture was added to naïve leaf discs and used to measure the ROS burst in the presence of luminol and horseradish peroxidase (HRP; **Figure 4.15**).

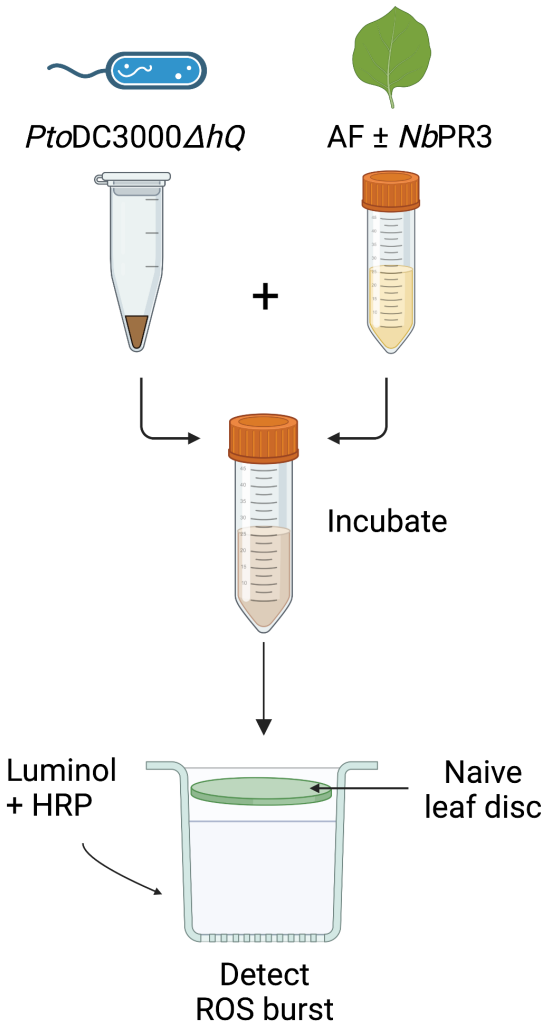


Figure 4.15: Elicitor release assay. 5 x 10^6 CFU/mL *Pto*DC3000*ΔhQ* was incubated for 90 minutes in apoplastic fluid from plants transiently co-expressing *NbPR3* proteins or an empty-vector control along with the silencing inhibitor P19. The mixture was centrifuged and resuspended in sterile water with 25 ng/µL luminol and 25 ng/µL HRP. The solution was added to naïve leaf discs in a 96-well plate and chemiluminescence was immediately measured using a plate reader. Figure created with BioRender.com, adapted from Buscaill et al., 2019.

Our first experiment showed that *NbPR3* overexpression increased both the primary and secondary ROS burst to whole *Pto*DC3000*ΔhQ* cultures compared to the EV control, suggesting a role for *Nb*PR3 in bacterial elicitor release (**Figure 4.16A**). This oxidative burst was dependent on the presence of *Pto*DC3000*ΔhQ*, rather than triggered by *Agrobacterium* in the AF, since it did not occur in the absence of *P. syringae* (**Figure 4.17**).

However, subsequent repeats of this experiment were inconsistent. First, we were able to replicate an increased secondary, but not primary, oxidative burst upon *NbPR3* overexpression (**Figure 4.16B**). In a final repeat, we found that *NbPR3* overexpression did increase the primary oxidative burst compared to EV, but this result was also found upon overexpression of the catalytic mutant $NbPR3^{E92A}$ (**Figure 4.16D**). This is contradictory to our previous finding that *Nb*PR3 requires catalytic activity to confer bacterial resistance. However, $NbPR3^{E92A}$ accumulated much higher than wildtype *Nb*PR3 in AF for this assay (**Figure 4.16D**). Overall, we have found some evidence of a role for *Nb*PR3 in elicitor release, but our results are inconsistent and necessitate further experimentation and optimisation of transient *NbPR3* expression.

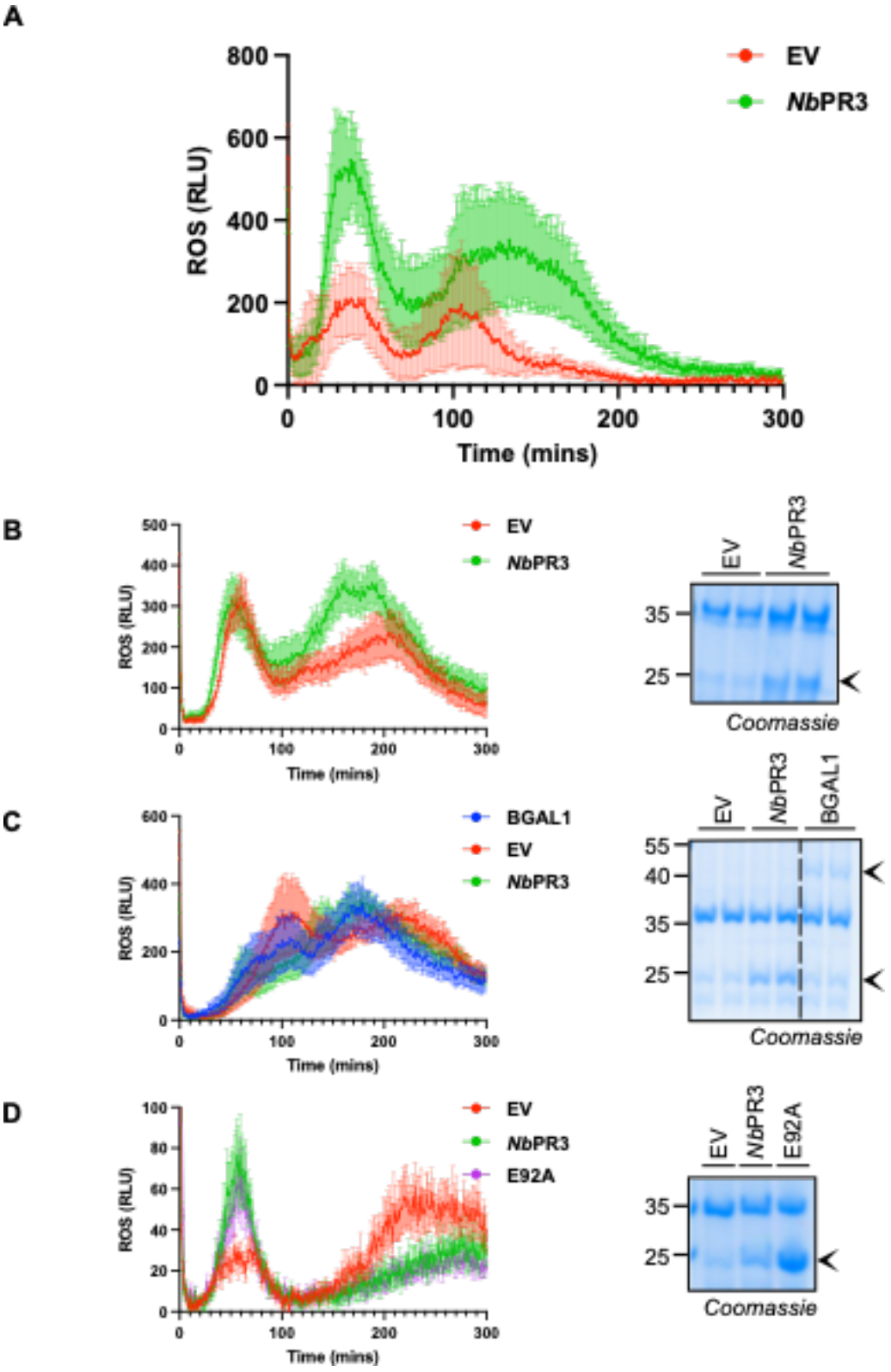


Figure 4.16: Effect of *NbPR3* overexpression on the oxidative burst. Apoplastic fluid (AF) from plants transiently co-expressing *NbPR3* (**A**-**D**), *BGAL1* (**C**) *NbPR3*^{E92A} (E92A; **D**) or an empty-vector (EV) control, along with the silencing inhibitor P19, was isolated at 4 dpi and pooled. *Pto*DC3000*ΔhQ* cultures were incubated in AF at 5 x 10^6 CFU/mL before adding to naïve leaf discs to monitor the oxidative burst. Lines on plots represent mean ± SE of N=5 (**A**) or N=7 (**B**-**D**) biological replicates. Protein expression was checked by Coomassie staining (**B**-**D**), expected protein sizes are indicated with arrowheads.

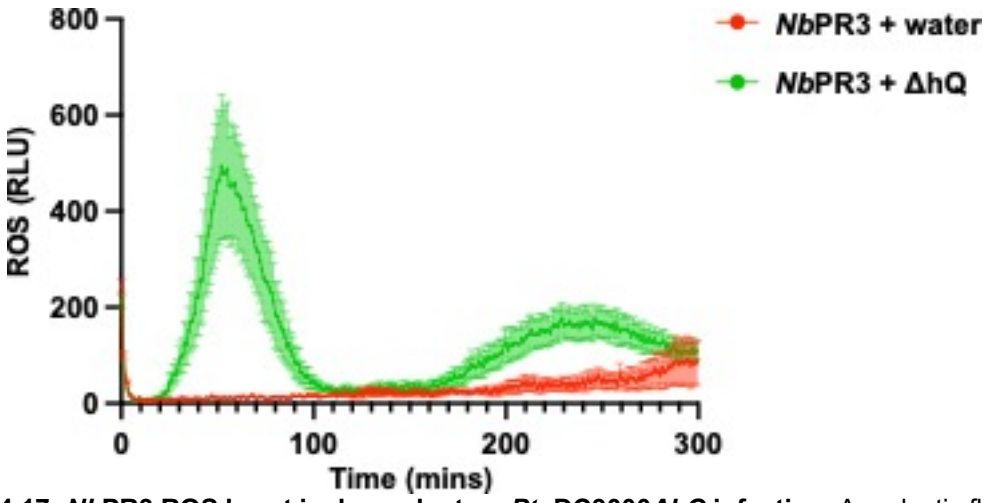


Figure 4.17: *Nb*PR3 ROS burst is dependent on *Pto*DC3000*ΔhQ* infection. Apoplastic fluid from plants transiently co-expressing *NbPR3* and the silencing inhibitor P19 was isolated at 4 dpi and pooled. Water or 5 x 10^6 CFU/mL *Pto*DC3000*ΔhQ* was incubated in AF at before adding to naïve leaf discs to monitor the oxidative burst. Lines on plots represent mean ± SE of N=7 biological replicates.

4.4 Discussion

In this chapter we investigated the immune function of *Nb*PR3. We found that *Nb*PR3 lacks endochitinase activity and has gained a new function in bacterial resistance, which is dependent on a *Nicotiana*-specific Q112 residue. We were unable to identify the substrate of *Nb*PR3 through biochemical approaches, but we uncovered a potential role for *Nb*PR3 in elicitor release.

*Nb*PR3 activity is reduced despite protein accumulation

In the previous chapter, we identified *Nb*PR3 as being suppressed at the activity level upon infection with *Pto*DC3000*ΔhQ*. This appeared contradictory to *Nb*PR3 being a PR protein, which should accumulate upon pathogen invasion. We tested this by monitoring *Nb*PR3 accumulation in the apoplast of infected leaves (**Figure 4.2**). The fact that *Nb*PR3 accumulates upon infection makes the overall reduction in *Nb*PR3 activity even more remarkable. Future work could identify inhibitors of *Nb*PR3. This requires an assay to monitor the activity of *Nb*PR3. Unfortunately, the original probe JJB111 used to monitor *Nb*PR3 activity by activity-based protein profiling is no longer available. Our assays on 4-nitrophenyl-monosaccharides did not uncover a substrate for *Nb*PR3 either. The discovery of the *Nb*PR3 inhibitor represents an exciting research direction once a substrate and activity assay are established.

Antibacterial activity is dependent on *Nicotiana*-specific Q112

We determined that *Nb*PR3 requires catalytic activity to perform its immune function, and that *Nb*PR3 has no endochitinase activity *in vitro* (**Figure 4.3**, **4.4**). We found that the catalytic general base in *Nb*PR3 is Gln (Q112) rather than Glu (**Figure 4.5**). Gln is isosteric with Glu, but whilst Gln is neutral, Glu is negatively charged. Glu to Gln mutation of the

catalytic general base is severely detrimental to chitinase activity (Andersen et al., 1997; Garcia-Casado et al., 1998). This is unlikely due to significant structural alterations. For example, mutation of the catalytic general base of a barley endochitinase from Glu to Gln did not impact structural integrity or behaviour during ion-exchange chromatography (Andersen et al., 1997). This suggests that the difference in *Nb*PR3 substrate specificity could be driven by differences in charge rather than structure.

The presence of Gln at the catalytic general base is conserved throughout *Nicotiana* species but absent in other Solanaceous species that we tested (**Figure 4.6**). This includes *Nt*PR-Q, which also functions in antibacterial resistance (Tang et al., 2017). Importantly, this residue is essential for the antibacterial activity of *Nb*PR3 (**Figure 4.7**). This suggests that the Q112 substitution was critical for the neo-functionalisation of an ancestral PR3 chitinase in the *Nicotiana* ancestor. Indeed, it would be interesting to test if other *Nicotiana* *NbPR3* orthologs also confer bacterial immunity.

However, the *Nb*PR3^{Q112E} mutant had no endochitinase activity *in vitro*, suggesting that this residue alone was not responsible for the change in substrate specificity (**Figure 4.8**). There are additional sequence polymorphisms specific to the *Nicotiana* genus (**Supplementary Figure 4.2**). Whilst these are not found in important catalytic residues, they may contribute structurally to the neo-functionalised PR3.

<u>The substrate of *Nb*PR3 remains enigmatic</u>

A lack of endochitinase activity for *Nb*PR3 is unsurprising, given that bacteria do not contain chitin. However, *Nb*PR3 was also unable to hydrolyse twelve different monosaccharide substrates (**Figure 4.9**). Given the unfeasibility of testing the vast diversity of carbohydrate substrates, we opted to use a glycan array to test the affinity of *Nb*PR3 to 300 representative

substrates simultaneously. This method was successfully used to examine the substrate specificity of the chitin-binding effector Ecp6 (Jonge et al., 2010).

We chose to use catalytically inactive *Nb*PR3 as it can bind glycan substrates without hydrolysis. We successfully His-tagged and purified E92A-His, however, it proved difficult to establish the optimal conditions for antibody labelling (**Figure 4.11**). Despite the seemingly successful purification, we could not label E92A-His with α-HisBiotin at any concentration (0.05-50 ng; **Figure 4.11C**). However, transiently expressed *E92A-His* in AF could be labelled (**Figure 4.11D**), as could purified Pip1^{mut}-His, suggesting a problem with E92A-His purification. We stored purified proteins at -20^{o}C, which we have found stable for proteases such as *Nb*RD21 and Pip1. We hypothesised that *Nb*PR3 or its tag may be unstable at -20^{o}C and degraded over time. Alternatively, the purified protein may precipitate out upon thawing. We tested this by keeping fresh purifications at 0^{o}C (on ice in a 4^{o}C cold-room) and analysing them by western blot 24 hours later. We also adjusted the pH of the AF from 6.5 to 7.15 with PBS prior to purification. The His-tag shows highest affinity to Nickel NTA at neutral pH, and PBS buffer also provides NaCl, which reduces nonspecific binding to the resin (Bornhorst and Falke, 2000). Finally, we tried detecting 500 ng of E92A-His protein with α-HisBiotin. Despite these efforts, we were unable to label E92A-His with α-HisBiotin and so could not make further progress with the glycan array. In the future, batch purification methods, whereby AF from *E92A-His*-expressing plants is incubated in Nickel NTA resin, should be attempted. This method is more efficient than column purification at low concentrations of protein (Bornhorst and Falke, 2000; Spriestersbach et al., 2015). Alternatively, *Nb*PR3 purification using a bacterial or yeast expression system may yield more favourable results (Demain and Vaishnav, 2009).

Hypothesis-driven approaches to *Nb*PR3 substrate identification

Given the similarity between chitin and peptidoglycan, and the dual functionality of some chitinases having additional lysozyme activity, we hypothesised that a change in substrate specificity from chitin to peptidoglycan would be a relatively simple change to evolve in the PR3 ancestor. We tested if *Nb*PR3 was able to lyse *M. lysodeikticus* cells in an established lysozyme activity assay (**Figure 4.12**). We found that neither *Nb*PR3 nor its mutants were able to lyse the bacterial cells *in vitro*, suggesting *Nb*PR3 does not have lysozyme activity. Consistent with this, *Nb*PR3 was unable to reduce *P. syringae* growth *in vitro*, in contrast to a lysozyme control (**Figure 4.13**), although in this experiment we did not standardise protein abundance. Indeed, the peptidoglycan layer of *P. syringae*, a gram-negative bacterium, is embedded beneath the outer membrane and is therefore less accessible to lysozymes (Nash et al., 2006).

We tested if *Nb*PR3 activated immune responses by monitoring accumulation of PR2 proteins, ß-glucanases abundant in the *N. benthamiana* apoplast (Goulet et al., 2010). Previous work found that *NbPR-Q* overexpression confers bacterial resistance and the upregulation of defence gene transcripts (Tang et al., 2017). *NbPR3* overexpression was unable to induce PR2 accumulation (**Figure 4.14**). In fact, PR2 accumulation was significantly reduced when *NbPR3* or its mutants were overexpressed, compared to the control. This could be due to saturation of protein synthesis machinery. Importantly, there was no difference in PR2 accumulation between overexpressed *NbPR3* and its mutants. The authors speculated that constitutive *NtPR-Q* expression led to the accumulation of unfolded proteins in the endoplasmic reticulum (ER). ER stress can trigger the unfolded protein response (UPR), initiating plant defence and the expression of PR proteins (Bao and Howell, 2017; Wan and Jiang, 2016). However, we found that *Nb*PR3 mutants E92A and Q112E accumulate as well as wildtype *Nb*PR3 without conferring bacterial resistance, arguing against this hypothesis (**Figure 4.3**, **4.7**).

Finally, we tested whether *Nb*PR3 releases an elicitor to trigger the oxidative burst. The primary oxidative burst involves a rapid generation of apoplastic H_2O_2 that occurs within minutes of pathogen perception. The secondary oxidative burst typically comes from the chloroplast upon effector recognition following infection with avirulent pathogens (Lamb and Dixon, 1997; Shapiguzov et al., 2012). For instance, tobacco shows a biphasic oxidative burst upon infection with avirulent *P. syringae* pv. *syringae* (Keppler et al., 1989). However, the secondary oxidative burst can also be triggered upon pathogen-associated molecular pattern (PAMP) recognition. For instance, a *P. syringae* pv. *tomato* DC3000*ΔhrpA* mutant, which is unable to produce the type III secretion system, triggers a chloroplastic ROS burst, supporting secondary PAMP-triggered responses (de Torres Zabala et al., 2015). Furthermore, perception of fatty acid metabolites derived from lipopolysaccharides (LPS), which are PAMPs found in the outer membrane of gram-negative bacteria, triggers a biphasic oxidative burst in Arabidopsis that is partially dependent on the receptor kinase LORE (Kutschera et al., 2019; Shang-Guan et al., 2018; Zhang et al., 2013).

We found some preliminary evidence for virulent PtoDC3000*ΔhQ* triggering both the primary and secondary ROS burst upon incubation with *Nb*PR3 (**Figure 4.16**). Interestingly, LPS can trigger a secondary oxidative burst response in *N. benthamiana*, despite the restriction of the LPS receptor LORE to Brassicaceae (Ranf et al., 2015; Shang-Guan et al., 2018). *Nb*PR3 might mediate the release and perception of the fatty acid moiety from LPS that is thought to trigger the secondary oxidative burst (Kutschera et al., 2019; Shang-Guan et al., 2018). Alternatively, if we infer that *Nb*PR3 does not release an elicitor from *Psy*B728a due to the lack of a phenotype in our disease assays (**Chapter 3**), *Nb*PR3 could be involved in the release of the flagellin elicitor along with BGAL1. BGAL1 releases the flagellin elicitor from *Pto*DC3000 and *Pta*6605, but not from *Psy*B728a, caused by differences in the glycosylation pattern of bacterial flagellin (Buscaill et al., 2019, 2021). It is possible that *Nb*PR3 acts redundantly with BGAL1, although they do not appear to have

the same substrate specificity (**Figure 4.9B**), suggesting that *Nb*PR3 might act at a different stage of flagellin elicitor release. To test this, we should confirm that *Nb*PR3 triggers an oxidative burst to *Pta*6605, but not *Psy*B728a.

Future work should confirm the existence of, and subsequently identify, the elicitor released by *Nb*PR3. For example, we can monitor the oxidative burst response of leaf discs taken from *N. benthamiana* lacking FLS2 to determine if *Nb*PR3 acts in flagellin perception (Wu et al., 2022). Alternatively, we can test if *Nb*PR3 can release the flagellin elicitor from the *fliC* mutant of *P. syringae* (Kvitko et al., 2009). To determine a role in LPS recognition, we could monitor the secondary oxidative burst in response to purified LPS (Shang-Guan et al., 2018). In case the *Nb*PR3 substrate is derived from neither flagellin nor LPS, we can determine if the elicitor is perceived by a pattern recognition receptor (PRR) kinase or a leucine-rich repeat receptor-like protein (LRR-RLP) by detecting the ROS burst in the absence of *BAK1* or *SOBIR1*, respectively (Kim et al., 2013; Zhang and Thomma, 2013). Mutants for *BAK1* and *SOBIR1* in *N. benthamiana* have been recently reported (Huang et al., 2020; Sun et al., 2022). However, prior to further investigation we need to establish a more robust assay for measuring elicitor release by *Nb*PR3. There is inconsistency in *Nb*PR3 triggering the primary and secondary oxidative burst, both, or neither (**Figure 4.16**). This could be partially due to often poor expression of *NbPR3* (**Figure 4.16C**). Indeed, *BGAL1* overexpression only increases the oxidative burst in the *bgal1* mutant background because wildtype plants have endogenous BGAL1 (**Figure 4.16C**, Buscaill et al., 2019). This suggests poor transient expression along with high endogenous *Nb*PR3 expression, or more effective hydrolase inhibition *in vitro*, could be contributing to the variable phenotypes in our assays.

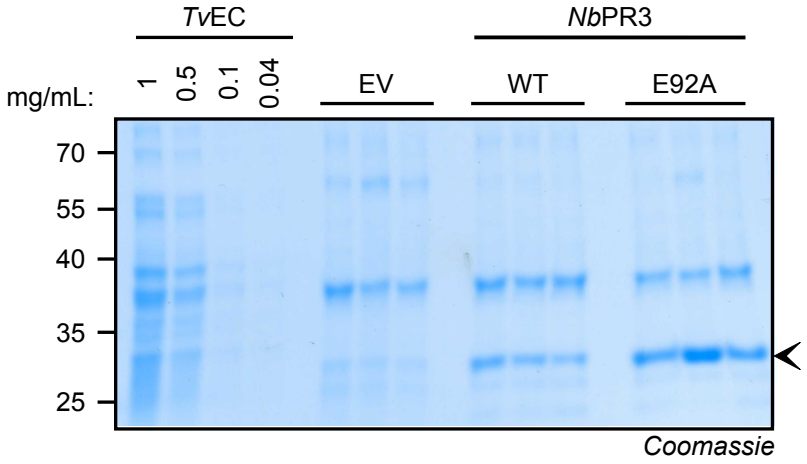
4.5 Conclusion

We propose that *Nb*PR3 has gained a novel function in bacterial immunity underpinned by an E→Q substitution at the catalytic general base. This mutation likely occurred in the *Nicotiana* common ancestor since it is found throughout the *Nicotiana* genus. We showed that *Nb*PR3 does not have endochitinase or lysozyme activity and does not induce PR protein expression. We have uncovered an exciting potential role for *Nb*PR3 in elicitor release.

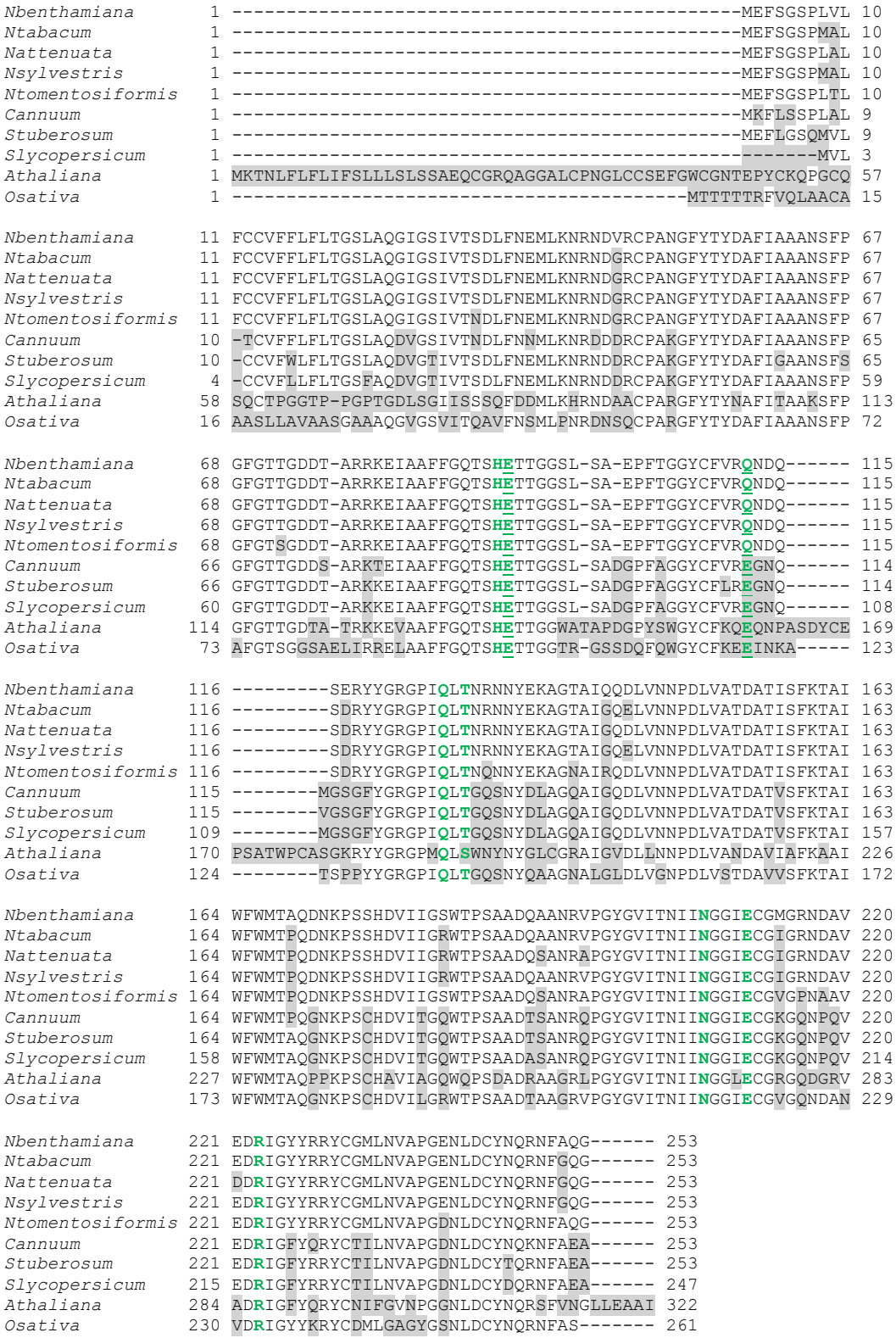
4.6 Contributions

Plasmid pJK187 was generated by Dr. Jiorgos Kourelis.

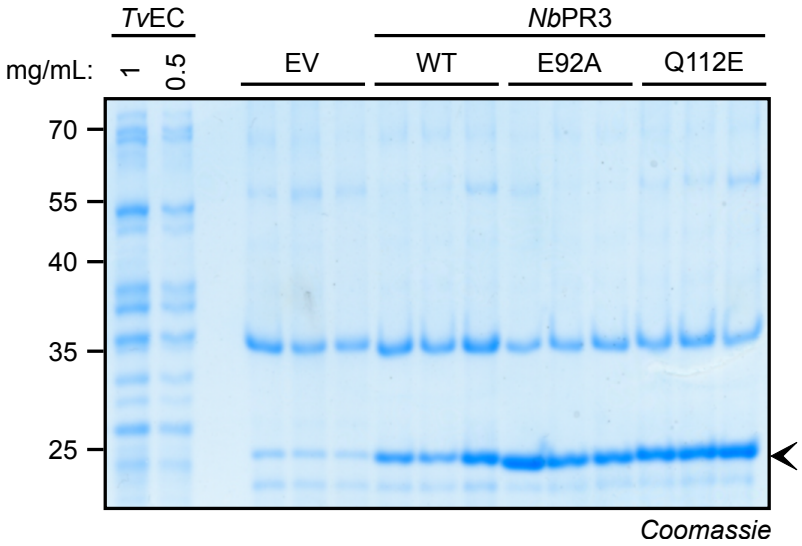
4.7 Supplementary Figures



Supplementary Figure 4.1: Estimation of *Nb*PR3 concentration.
Apoplastic fluid from *N. benthamiana* transiently co-expressing wildtype *NbPR3* or its catalytic mutant *NbPR3*^{E92A} (E92A), or an empty-vector (EV) control along with the silencing inhibitor P19 was isolated at 4 dpi with N=3 replicates. Proteins were separated by SDS-PAGE alongside known concentrations of endochitinase from *Trichoderma viride* (*Tv*EC, Sigma-Aldrich C8241) and stained with Coomassie. Band intensity was quantified using Fiji (Schindelin et al., 2012) relative to the 30 kDa 1 mg/mL TvEC signal. *Nb*PR3 protein is indicated with the arrowhead. Used to estimate protein concentration for **Figure 4.4**.



Supplementary Figure 4.2: Alignment of *Nb*PR3 with putative orthologs. The *Nb*PR3 protein sequence was BLASTed (Johnson et al., 2008) against the proteomes of *Nicotiana* species, pepper (*Capsicum annuum*), potato (*Solanum tuberosum*), tomato (*Solanum lycopersicum*), Arabidopsis and rice (*Oryza sativa*). The top hit from each species was selected and aligned using ClustalO (Sievers et al., 2011) at NGPhylogeny.fr (Lemoine et al., 2019). Key catalytic residues are shown in green, the catalytic general acid and base are underlined.



Supplementary Figure 4.3: Estimation of *Nb*PR3 concentration.
Apoplastic fluid from *N. benthamiana* transiently co-expressing *NbPR3* or its mutants *NbPR3*^{E92A} (E92A) and *NbPR3*^{Q112E} (Q112E), or an empty-vector (EV) control along with the silencing inhibitor P19 was isolated at 4 dpi with N=3 replicates. Proteins were separated by SDS-PAGE alongside known concentrations of endochitinase from *Trichoderma viride* (*Tv*EC, Sigma-Aldrich C8241) and stained with Coomassie. Band intensity was quantified using Fiji (Schindelin et al., 2012) relative to the 30 kDa 1 mg/mL TvEC signal. *Nb*PR3 protein is indicated with the arrowhead. Used to estimate protein concentration for **Figure 4.8**, **4.12**.

4.8 Methods

Phylogenetic tree – GH 19 sequences with the Pfam/InterPro IDs PF00182, IPR000726 and IPR016283 were identified from *Arabidopsis thaliana*, *Solanum lycopersicum*, *Oryza sativa* and *Nicotiana benthamiana* genomes using InterProScan (Jones et al., 2014). Truncated proteins were manually removed and sequences were aligned by ClustalO (Sievers et al., 2011) followed by TrimAl (Capella-Gutiérrez et al., 2009). Phylogenetic analyses were performed in NGPhylogeny.fr (Lemoine et al., 2019) using the maximum-likelihood method with 200 bootstrap replicates. The tree was annotated using iTOL (Letunic and Bork, 2016). Proteins were annotated according to their previous assignment in the literature to one of the five GH19 chitinase classes (Tyler et al., 2010; Jashni et al., 2015a).

Plant growth conditions – *N. benthamiana* was grown in a growth chamber at room temperature with a 16-hour light cycle and 60% humidity and watered on alternating days.

Strains – strains used in this chapter are summarised in **Table 4.1**.

Table 4.1: Strains used in this chapter.

Name	Description	Reference
P. syringae pv. *tomato* DC3000ΔhQ	*P. syringae* pv. *tomato* DC3000 lacking the *hopQ1-1* effector	Wei et al., 2007
A. tumefaciens GV3101	Derivative of *A. tumefaciens* C58 carrying pMP90 plasmid	Koncz and Schell., 1986
E. coli DH10B	Chemically competent *E. coli*	Thermo Fisher Scientific EC0113

Molecular cloning – Primers used are summarised in **Table 4.2**. Constructs used in this chapter are summarised in **Table 4.3**. *NbPR3*^{E92A} and *NbPR3*^{Q112E} were created by site-directed mutagenesis using pAG001 as template. Overlapping primers incorporating the desired mutations were designed and the fragments amplified by PCR using Q5

Polymerase (New England Biolabs). DpnI was used to digest the methylated template. *NbPR3*^{E92A}*-His* was generated by amplification of *NbPR3*^{E92A} sequence from pAG006 with primers incorporating the polyhistidine tag. The fragment was cloned into pJK187 in a GoldenGate reaction using BbsI (Engler et al., 2008). Purified PCR products were transformed into competent *Escherichia coli* DH10β. Sanger sequencing was used to verify the constructs before transformation into *Agrobacterium tumefaciens* GV3101 (pMP90) and selection for kanamycin and gentamicin resistance.

Table 4.2: Primers used in this chapter. Incorporated substitutions are shown in red. Overhangs are shown in lower-case.

Name	Purpose	Sequence (5' - 3')
E92A_F	Clone *NbPR3*^{E92A} from pAG001	CTTCTCATGCAACTACTGGTGGTTCCCTGAGTGCAGAACC
E92A_R	Clone *NbPR3*^{E92A} from pAG001	CCACCAGTAGTTGCATGAGAAGTTTGACCGAAAAAGGCAGC
Q112E_F	Clone *NbPR3*^{Q112E} from pAG001	GCTTTGTTCGGGAAAATGACCAGAGTGAAAGATATTATGGTAGAGGACCCATCC
Q112E_R	Clone *NbPR3*^{Q112E} from pAG001	CACTCTGGTCATTTTCCCGAACAAAGCAATATCCTCCTGTAAATGGTTCTGC
E92A_His_F	Clone *NbPR3*^{E92A}*-His* from pAG011	ttgaagacaaaATGGAGTTTTCTGGATCACCACTGGTATTG
E92A_His_R	Clone *NbPR3*^{E92A}*-His* from pAG011	ttgaagacaaaagctcaatgatgatgatgatgatggccaccGCCCTGGGCGAAGTTCCTTTG

Table 4.3: Constructs used in this chapter

Name	Description	Reference
P19	Binary 35S::P19	Van der Hoorn et al., 2003
pJK001c	Binary empty vector (EV)	Paulus et al., 2020
pAG001	Binary 35S::*Nb*PR3	This work
pAG006	Binary 35S::*Nb*PR3^{E92A}	This work
pAG007	Binary 35S::*Nb*PR3^{Q112E}	This work
pJK646	Binary 35S::BGAL1	Buscaill et al., 2019
pJK187	Binary 35S promoter and terminator	This work, Dr. Jiorgos Kourelis
pAG011	Binary 35S::*Nb*PR3^{E92A}-His	This work
pJK169	Binary 35S::Pip1^{mut}-His	Kourelis et al., in prep

Agroinfiltration – Agroinfiltration was performed as previously described (**Chapter 3.8**).

Apoplastic fluid (AF) isolation – AF isolation was performed as previously described (**Chapter 3.8**).

Western blot and Coomassie staining – Proteins from AF were precipitated in 4x ice-cold acetone and resuspended in 2x gel-loading buffer (100 mM Tris-HCl pH 6.8, 200 mM dithiotreitol, 4% SDS, 20% glycerol, 0.02% bromophenol blue). Proteins were loaded onto 12% acrylamide gels and separated by SDS-PAGE. For western blotting, proteins were transferred to PVDF membranes using a Trans-Blot Turbo Transfer System (Bio-Rad). Membranes were blocked in 5% (w/v) milk in PBS-T (phosphate buffered saline, 0.1% Tween-20) at room temperature for one hour or 4°C overnight before addition of primary antibody in 5% milk in PBS-T for two hours at room temperature or overnight at 4°C (α-PR2 and α-PR3, Agrisera AS07 208/ AS07 207, 1:2500; α-His HRP, Invitrogen MA1-21315-HRP, 1:5000; α-His Biotin, Thermo Fisher Scientific MA1-21315-BTIN, 1:1000). Where appropriate, membranes were washed and incubated in secondary antibody for one hour at room temperature (α-Rabbit HRP, GE Healthcare NA934V, 1:1000, 5% milk in PBS-T; streptavidin-HRP, Sigma S2438, 1:1000, 5% BSA in PBS-T). Clarity Western ECL substrate (Bio-Rad) was used for signal detection For Coomassie staining, acrylamide gels were stained overnight with Coomassie Brilliant Blue G-250. Band intensity was quantified using Fiji (Schindelin et al., 2012).

Agromonas assays – Agromonas assays were performed as previously described (**Chapter 3.8**).

Endochitinase activity assay – AF was isolated at 4 days-post infiltration and used to test endochitinase activity as described previously, using the fluorescent substrate 4-methylumbelliferyl-β-D-*N,N′,N″*-triacetylchitotrioside (4-MU-GlcNac$_3$; Hollis et al., 1997; Libantová et al., 2009). 4-MU-GlcNac$_3$ was resuspended in 0.1 M sodium acetate. We combined 20 µL AF with 30 µL substrate solution to a final substrate concentration of 18 µM in a black 96-well plate. Measurements were taken every minute for an hour in an Infinite M200 plate reader (Tecan) using 355 nm excitation and 450 nm emission. We used an endochitinase mixture from the fungus *Trichoderma viride* (Sigma-Aldrich C8241) as a

positive control at a final concentration of 0.04 mg/mL. Protein concentration was estimated by Coomassie staining and band intensity quantification using Fiji (Schindelin et al., 2012). Graphs were made using GraphPad Prism 9.

Colourimetric substrate assay – The assay to test the activity of *Nb*PR3 towards twelve 4-nitrophenyl monosaccharide substrates (β-D-galactopyranoside, α-D-galactopyranoside, β-D-mannopyranoside, β-D-glucopyranoside, α-D-glucopyranoside, β-D-glucuronide, β-D-xylopyranoside, α-D-xylopyranoside, β-D-fucopyranoside, *N*-acetyl-β-D-glucosaminide, *N*-acetyl-α-D-glucosaminide, and *N*-acetyl-α-D-galactosaminide, Sigma-Aldrich) was performed as previously published (Buscaill et al., 2019). Substrates were prepared as 10 mM stock solutions in milliQ water. 40 µL AF from plants transiently overexpressing *NbPR3*, *BGAL1* or an EV control with the silencing inhibitor P19 was isolated at 4 dpi and incubated with 1 mM 4-nitrophenyl conjugates in the presence of 50 mM MES pH 5. Samples were incubated for ten minutes at room temperature and the reaction was stopped by adding 1 M Na_2CO_3. Absorbance was monitored at 420 nm using an Infinite M200 plate reader (Tecan). Graph was made using GraphPad Prism 9.

Protein purification – His-tagged proteins were purified from AF using Nickel NTA agarose beads (Sigma-Aldrich) as previously described (Schuster et al., 2022). Briefly, AF was isolated from plants transiently expressing His-tagged proteins and pooled. Nickel NTA resin was added to a column and equilibrated with ice-cold purification buffer (50 mM Tris/HCl pH 7.4, 150 mM NaCl). AF was applied to the column and the column was washed (50 mM Tris/HCl pH 7.4, 150 mM NaCl, 50 mM imidazole). Proteins were eluted in purification buffer (50 mM Tris/HCl pH 7.4, 150 mM NaCl, 250 mM imidazole). Protein concentration was measured using the DC Assay (Bio-Rad).

Lysozyme activity assay – AF was isolated at 4 days-post infiltration and used to test lysozyme activity according to the manufacturer's protocol. *Micrococcus lysodeikticus* cells (Sigma-Aldrich M3770) were resuspended in 50 mM potassium phosphate buffer pH 6.24 at 0.15 mg/mL and the A_{450} adjusted to 0.6-0.7. We mixed 10 µL AF with 250 µL cell solution and recorded the A_{450} at 15 second intervals for five minutes at 25°C using an Infinite M200 plate reader (Tecan). We used 0.1 µg lysozyme from chicken egg white (Sigma-Aldrich L6876) as a positive control. We calculated the maximum linear rate of A_{450} decrease and converted this into units of enzyme activity per µg protein, estimated by Coomassie staining. Graph was made using GraphPad Prism 9.

In vitro growth assay – *Pto*DC3000*ΔhQ* cultures were grown overnight in LB media and then incubated in a 96-well plate in 200 µL AF from plants transiently expressing *NbPR3*, *NbPR3*^{E92A} or an EV control with the silencing inhibitor P19 at 10^6 CFU/mL. AF from EV-expressing plants supplemented with 1 mg/mL lysozyme from chicken egg white (Sigma-Aldrich L6876) was used as a positive control. Three biological replicates were used per treatment. The plate was incubated at 25°C at 100 rpm and 20 µL of each sample was removed immediately, and at two-hour intervals thereafter. Samples were plated in serial dilution on LB-agar plates containing *Pseudomonas* CFC Agar Supplement (10 µg/mL cetrimide, 10 µg/mL fucidin and 50 µg/mL cephaloridine, Oxoid SR0103) and incubated at 28°C. Colonies were counted after two days and used to calculate bacterial growth in $Log_{10}CFU/cm^2$.

Oxidative burst – We used a protocol previously developed in the group to measure the ROS burst (Buscaill et al., 2019). The protocol is based on the detection of light emitted when horseradish peroxidase (HRP) oxidises luminol in the presence of H_2O_2. Luminol (Sigma-Aldrich 123072) and HRP (Thermo Fisher Scientific 31490) stocks were resuspended in dimethyl sulfoxide or milliQ water at 10 mg/mL. Leaf discs (6 mm diameter)

were punched from leaves of untreated *N. benthamiana* plants (5 or 7 biological replicates) and incubated overnight in milliQ water. *Pto*DC3000*ΔhQ* cultures grown in LB media were centrifuged and the pellet resuspended in 5 mL AF pooled from plants transiently overexpressing *BGAL1*, *NbPR3*, *NbPR3*^{E92A} or an EV control with the silencing inhibitor P19 at 5 x 10^6 CFU/mL. After incubation for 90 minutes at room temperature on a rotor, bacterial mixtures were centrifuged, and the pellets resuspended in 2.5 mL of assay solution containing 25 ng/µL luminol and 25 ng/µL HRP. Leaf discs were transferred to a 96-well plate with 3 technical replicates per biological replicate. 100 µL assay solution was added to each leaf disc. Chemiluminescence was recorded by an Infinite M200 plate reader (Tecan) every minute for five hours. Graphs were made using GraphPad Prism 9.

Chapter 5: Analysis of the role of *Nb*RD21 in immunity

5.1 Abstract

*Nb*RD21 is an active and abundant papain-like cysteine protease (PLCP) found in multiple cellular locations. The functions of *Nb*RD21 orthologs have previously been studied in both a developmental and immune context, although *Nb*RD21 has not been studied before. In this chapter, we used both transient expression and CRISPR-Cas9 genome editing to investigate *Nb*RD21 activity. We showed that *Nb*RD21 requires catalytic activity to perform its immune function but does not confer resistance to *Phytophthora infestans*. *Nb*RD21 also does not directly damage bacterial growth *in vitro*, activate the immune response nor activate the oxidative burst. However, proteomics data identified a role for *Nb*RD21 in receptor-like kinase (RLK) processing.

5.2 Introduction

Responsive-to-Desiccation 21 (RD21) belongs to the papain-like cysteine protease (PLCP) class of cysteine proteases, which are typified by their stability and proteolytic activity in harsh environments (Richau et al., 2012). PLCPs are found across the breadth of all kingdoms of life, and perform a broad range of functions, from regulating plant seed germination to human antigen processing (Petushkova et al., 2022). Plant PLCPs consist of an α-helix and a β-sheet domain that fit together to create a substrate binding groove containing the catalytic triad (Cys-His-Asn; Richau et al., 2012).

*Nb*RD21 belongs to PLCP subfamily 1 and contains a C-terminal extension consisting of a proline-rich domain followed by a cysteine-rich granulin domain (Richau et al., 2012). The exact role of the granulin domain is not known, but it shares homology to animal granulins, which act as growth hormones released during wounding or inflammation (Bateman and Bennett, 2009). The *NbRD21* ortholog in *Arabidopsis thaliana* (Arabidopsis; *AtRD21A*) has been studied most intensely as a responsive-to-desiccation gene (Koizumi et al., 1993). *Nb*RD21 is synthesised with an N-terminal autoinhibitory prodomain (**Figure 5.1A**). Maturation of RD21 first involves removal of the pro-peptide domain to produce intermediate RD21 (iRD21). This process is not autocatalytic and relies on other proteases (Yamada et al., 2001). Conversely, removal of the C-terminal granulin domain to produce mature RD21 (mRD21) relies on catalytic activity and is almost abolished in a substitution mutant lacking the catalytic cysteine (Gu et al., 2012). Whilst mRD21 is a soluble protease, Arabidopsis iRD21 forms a stable aggregate in vacuoles (Yamada et al., 2001). Nevertheless, both iRD21 and mRD21 are active and can degrade rubisco *in vitro* (Gu et al., 2012). The RD21 catalytic triad consists of a cysteine residue, supported by histidine and asparagine (**Figure 5.1B**, Gu et al., 2012)

Arabidopsis RD21A is a highly active and abundant protease, found in multiple locations at the cellular and subcellular level (Richau et al., 2012; van der Hoorn et al., 2004). *At*RD21A negatively regulates sphingolipid-induced cell death (Ormancey et al., 2019), and its trafficking through the vacuoles to endothelial cells with Protein Disulfide Isomerase-5 is thought to regulate programmed cell death during seed development (Andème Ondzighi et al., 2008).

The functions of *NbRD21* orthologs in plant immunity have been explored previously. *RD21* mutant Arabidopsis plants (*Atrd21a*) are more susceptible to the necrotrophic fungus *Botrytis cinerea* (Shindo et al., 2012), and a subsequent study identified a role for *At*RD21A in resistance to *Pseudomonas syringae* during drought stress (Liu et al., 2020). The tomato and potato orthologs of *NbRD21*, *SlC14* and *StC14*, are implicated in resistance to the oomycete *Phytophthora infestans*. The pathogen secretes the cystatin-like proteins EPIC1/EPIC2B, and the RxLR effector AvrBlb2, which inhibit the activity of *Sl*C14, and prevent its secretion into the apoplast, respectively (Kaschani et al., 2010; Bozkurt et al., 2011). Further, *St*C14 is under diversifying selection that is thought to be driven by its antagonistic interactions with pathogen-derived inhibitors (Kaschani and van der Hoorn, 2011). The *Nicotiana benthamiana* PLCP *NbC14*, originally thought to be orthologous to *SlC14*, is required for resistance to *P. infestans* (Bozkurt et al., 2011). However, *Nb*C14 was later renamed *Nb*CP14 because it is unrelated to *Nb*RD21 and its orthologs discussed here. *Nb*CP14 is actually orthologous to *Nt*CP14, a PLCP that regulates programmed cell death during tobacco embryogenesis (Paireder et al., 2016). Finally, *P. syringae* pv. *tomato* DC3000 secretes Cip1, a chagasin-like inhibitor targeting *Sl*C14 (Shindo et al., 2016). The high degree of similarity in protein sequence between *Nb*RD21 and its orthologs *At*RD21A, *Sl*C14, *St*C14 and *Triticum aestivum* triticain-α (**Figure 5.2**) lends further support to the hypothesis that *Nb*RD21 also functions in immunity.

In this chapter, we combined transient expression and genome editing of *NbRD21* to uncover the function of *Nb*RD21 during both pathogen invasion and unchallenged conditions. We first utilised a hypothesis-driven approach to identify the immune function of *Nb*RD21. We then used liquid chromatography tandem mass-spectrometry (LC-MS/MS) to uncover changes in the proteome of *Nbrd21* knockout plants. From this analysis, we identified a role for *Nb*RD21 in the processing of receptor-like kinases (RLKs).

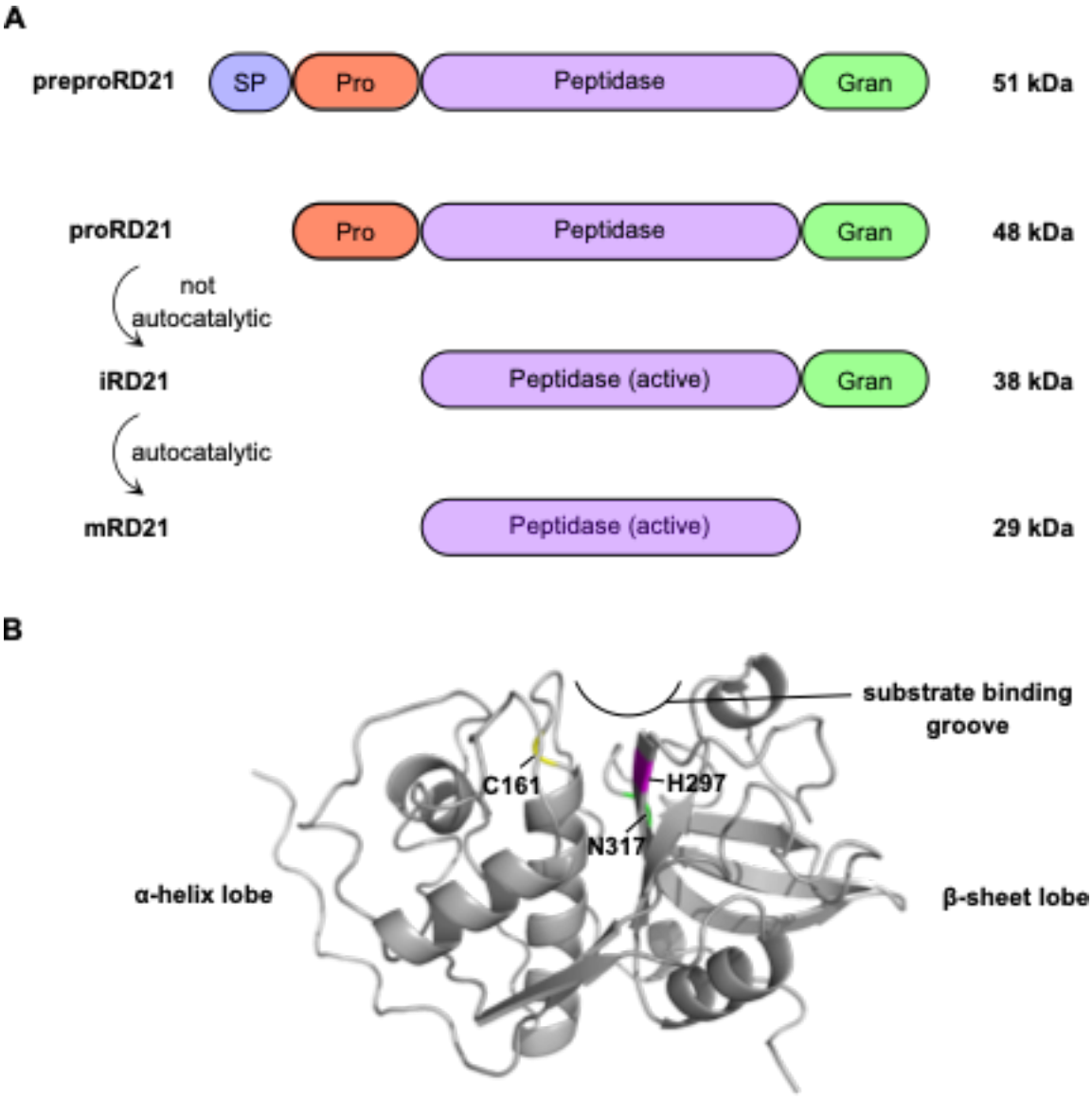


Figure 5.1: Structure and processing of *Nb*RD21.
A: Maturation of *Nb*RD21. PreproRD21 is synthesised with an N-terminal signal peptide (SP), an inhibitory pro-peptide (Pro), and a C-terminal granulin (Gran) domain. Following signal peptide removal, the pro-peptide domain of *Nb*RD21 is removed by another protease to produce intermediate RD21 (iRD21). Autocatalytic removal of the granulin domain produces mature RD21 (mRD21). Predicted molecular weights in kilodaltons are indicated on the right. Adapted from Yamada et al., 2001.
B: Alphafold prediction of mature *Nb*RD21 structure. Residues of the catalytic triad are coloured (yellow, Cys 161; pink, His 297; green, Asn 317). Annotated in PyMOL.

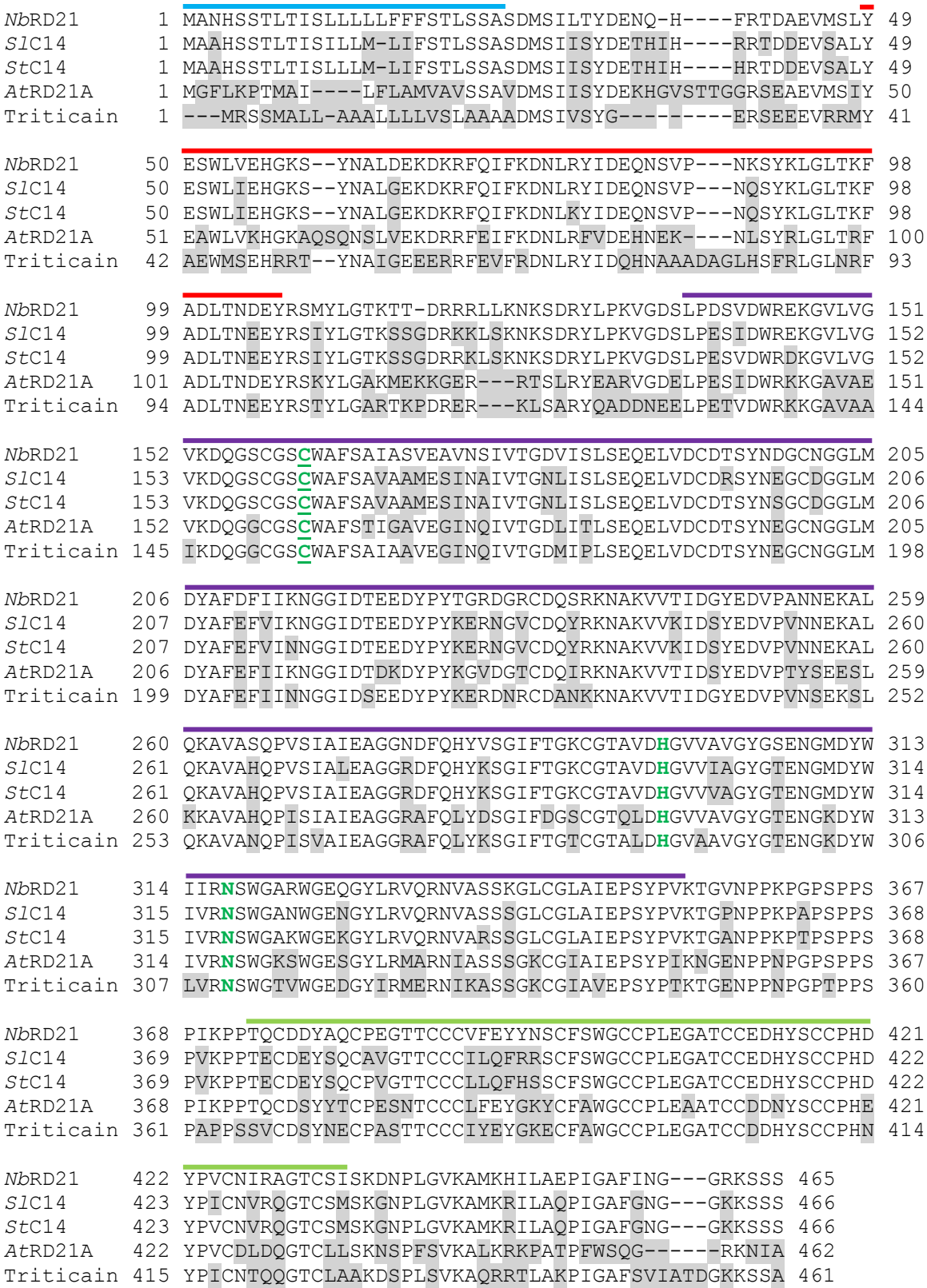


Figure 5.2: Alignment of *Nb*RD21 with putative orthologs. The *Nb*RD21 protein sequence was BLASTed (Johnson et al., 2008) against the proteomes of tomato (*Solanum lycopersicum*), potato (*Solanum tuberosum*), Arabidopsis and wheat (*Triticum aestivum*). The top hit from each species was selected and aligned using ClustalO (Sievers et al., 2011) at NGPhylogeny.fr (Lemoine et al., 2019). Key catalytic residues are shown in green, the catalytic cysteine is underlined. Differences to *Nb*RD21 are highlighted in grey. Key domains of *Nb*RD21, predicted by InterProScan (Jones et al.,

2014), are annotated above the sequence. Blue, signal peptide; red, prodomain; purple, peptidase domain; green, granulin domain.

5.3 Results

5.3.1 Preparing tools for studying *Nb*RD21 function

Before determining *Nb*RD21 function, we first established a rapid assay for measuring *Nb*RD21 activity. Activity-based protein profiling (ABPP) can be used to monitor cysteine protease activity, but labelling requires a three-hour incubation period and separation by SDS-PAGE. Cleavage of the fluorescent cysteine protease substrate Z-Leu-Arg-7-amino-4-methylcoumarin (zLR-AMC; **Figure 5.3A**) can be used to more rapidly monitor cysteine protease activity in a plate reader (Sijwali et al., 2001). To test if *Nb*RD21 activity can be monitored using zLR-AMC, we isolated apoplastic fluid (AF) from *N. benthamiana* transiently expressing *NbRD21* or an empty-vector (EV) control at 4 days-post infiltration and detected a linear increase in fluorescence over time (**Figure 5.3B**). AF samples containing transiently expressed *Nb*RD21 had significantly higher cysteine protease activity than AF from plants transiently expressing EV (**Figure 5.3C**; *t*-test, P=0.0298), indicating that cleavage of zLR-AMC can be used to monitor *Nb*RD21 activity.

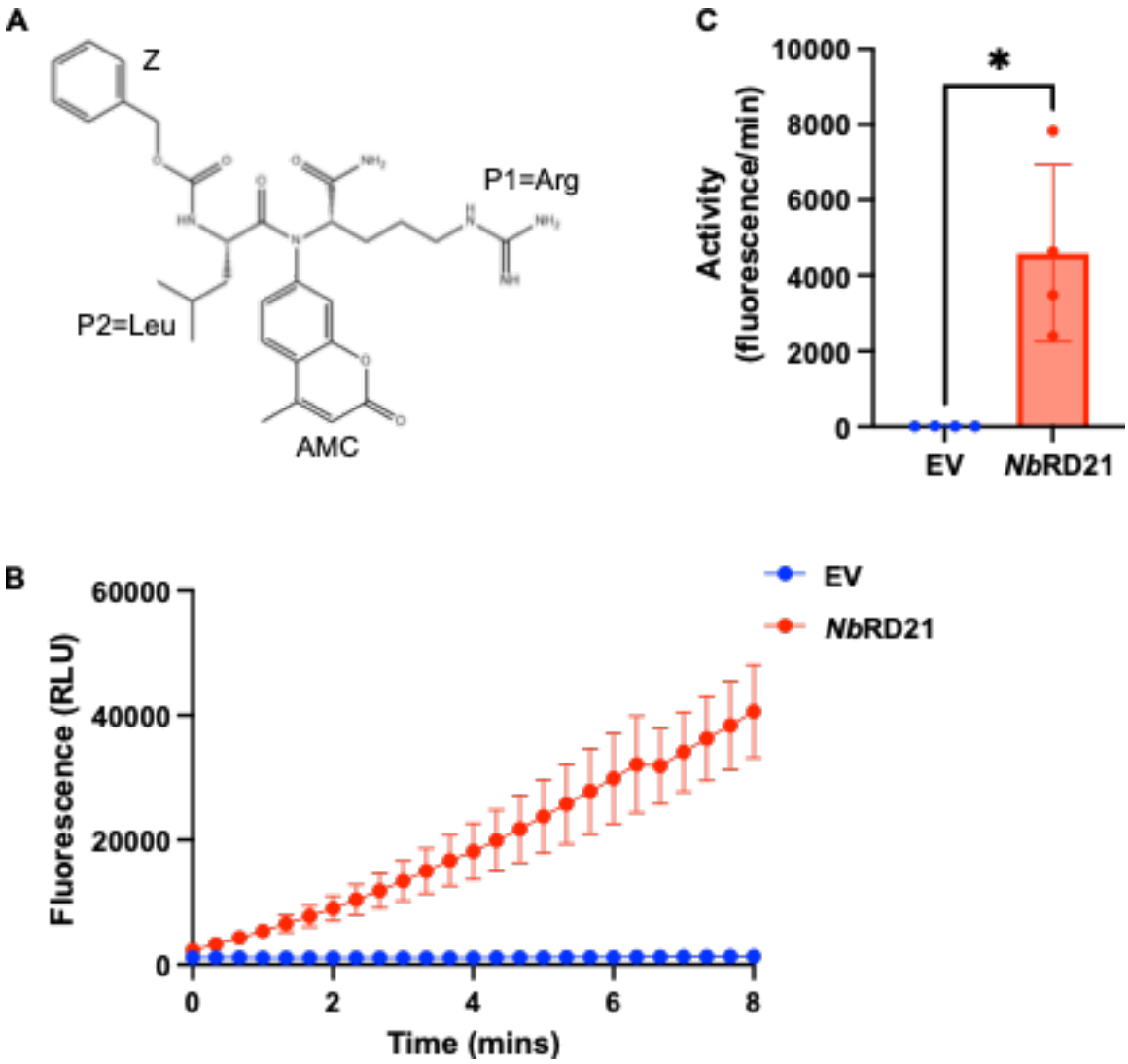


Figure 5.3: *Nb*RD21 activity can be measured with fluorescent substrate.
A: Structure of Z-Leu-Arg-AMC. Adapted from chemicalbook.com. Release of fluorescent 7-amino-4-methylcoumarin can be detected with a plate reader.
B,C: Significantly increased cysteine protease activity upon transient expression of *NbRD21*. Apoplastic fluid from plants transiently co-expressing *NbRD21* or empty-vector (EV) with the silencing inhibitor P19 was isolated and 4 dpi and mixed with 40 μM zLR-AMC in the presence of 2.5 mM DTT and 31.25 mM sodium acetate pH 5. Fluorescence at 380ex/460em was measured in relative light units (RLU) at 20 second intervals for 8 minutes at room temperature in a plate reader (**B**). Activity was calculated by fluorescence per minute (**C**). Error bars represent mean ± SE of N=4 biological replicates. Statistical significance was calculated by *t*-test; *, P<0.05.

Next, we generated catalytically inactive *Nb*RD21 to determine if immune function is dependent on catalytic activity. The catalytic cysteine residue of *Nb*RD21 was identified by InterProScan (Jones et al., 2014) and comparison with orthologs (Gu et al., 2012). We used site-directed mutagenesis using 35S::*Nb*RD21 (pPB034) as a template to substitute the catalytic cysteine C161 into alanine (C161A), creating *Nb*RD21^{C161A}. We confirmed this

construct is expressed *in planta* by western blotting using the α-C14 antibody (**Figure 5.4A**; Kaschani et al., 2010). As previously described for Arabidopsis RD21A (Gu et al., 2012), *Nb*RD21^{C161A} mostly accumulates as iRD21 because granulin domain removal is autocatalytic (**Figure 5.4A**). In contrast to wildtype *Nb*RD21, AF from plants transiently expressing *NbRD21*^{C161A} had significantly reduced cysteine protease activity on zLR-AMC (*t*-test, P=0.0234), comparable to that of the EV control (**Figure 5.4B**).

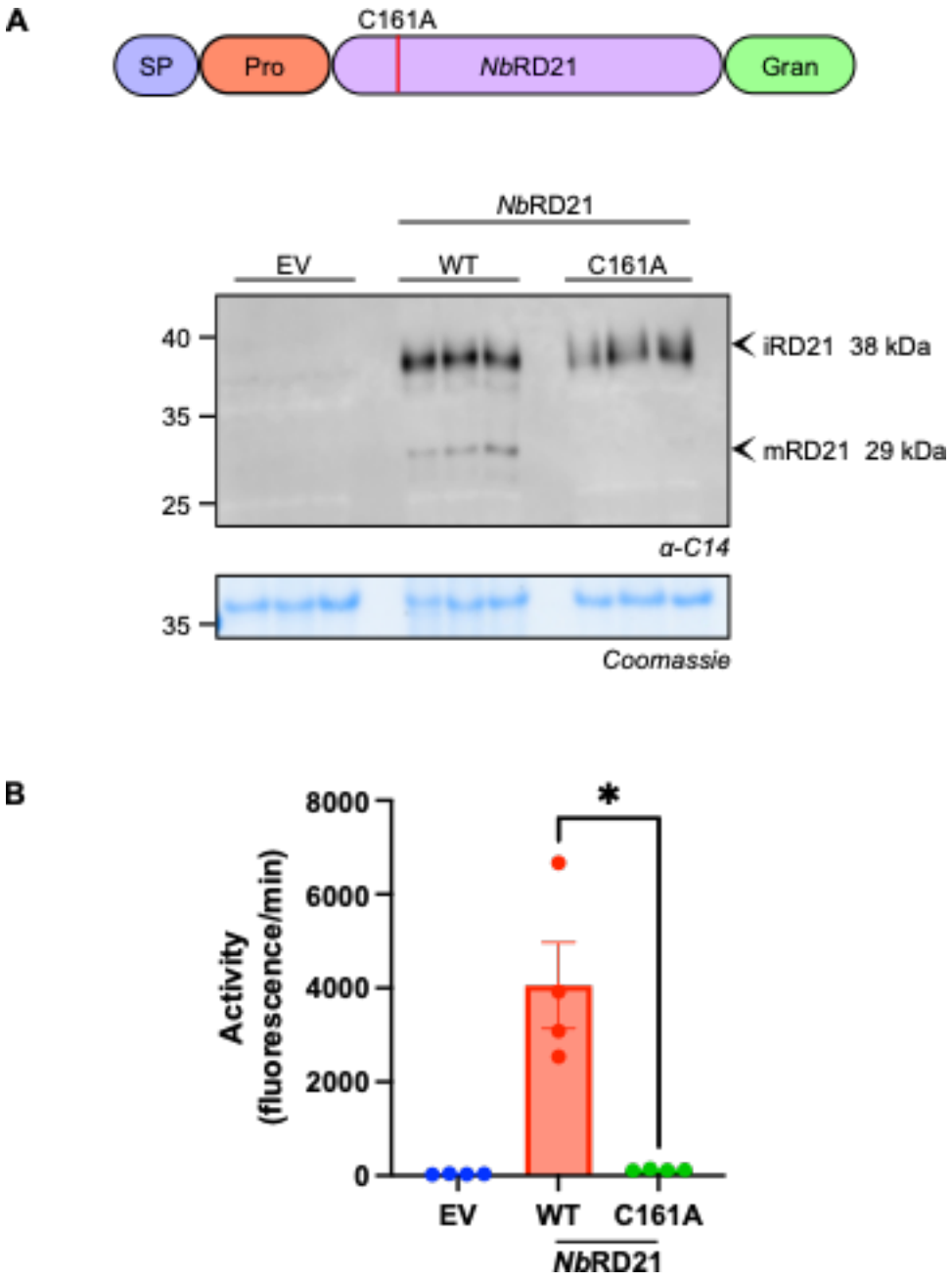


Figure 5.4: Generation of *Nb*RD21 catalytic mutant.
A: The *Nb*RD21 catalytic mutant accumulates in the apoplast of agroinfiltrated *N. benthamiana* leaves. *Nb*RD21 and its catalytic mutant (C161A), shown schematically, along with the empty-vector (EV) control, were agroinfiltrated with the silencing inhibitor P19 and apoplastic fluid was isolated at day 4 from N=3 replicates, separated by SDS-PAGE and analysed by western blotting with α-C14 and Coomassie staining. The arrowheads indicate intermediate (i) and mature (m) *Nb*RD21 protein. **B:** *Nb*RD21^{C161A} has significantly reduced catalytic activity. AF from plants transiently co-expressing wildtype *NbRD21*, the catalytic mutant *NbRD21*^{C161A} or an EV control with the silencing inhibitor P19 was isolated at 4 dpi and mixed with 40 μM zLR-AMC in the presence of 2.5 mM DTT and 31.25 mM sodium acetate pH 5. Fluorescence at 380ex/460em was measured at 20 second intervals for 10 minutes at room temperature in a plate reader. Error bars represent mean ± SE of N=4 biological replicates. Statistical significance was calculated by *t*-test; *, P<0.05.

Next, we tested whether transiently expressed *NbRD21*^{C161A} increases resistance to *Pto*DC3000 in 'agromonas' assays. In this experiment, *N. benthamiana* leaves transiently expressing *NbRD21*^{C161A} were infected with *Pto*DC3000, and bacterial growth was measured three days later. EV and wildtype *NbRD21* were used as negative and positive controls, respectively. In contrast to *Nb*RD21, the catalytic mutant no longer conferred resistance to *Pto*DC3000 (**Figure 5.5**). Therefore, we concluded that *Nb*RD21 requires catalytic activity to perform its immune function.

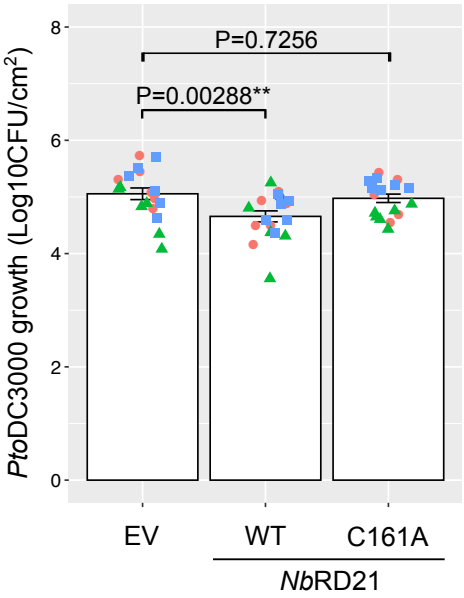


Figure 5.5: *Nb*RD21 requires catalytic activity for its immune function.
NbRD21, its catalytic site C161A mutant, and the empty-vector (EV) control were transiently co-expressed by agroinfiltration in 4 week-old *N. benthamiana* along with the silencing inhibitor P19. Two days later, the same leaves were infiltrated with 10^6 CFU/mL *Pto*DC3000. Bacterial growth in colony-forming units (CFU) was measured at 3 dpi. Bars represent mean ± SE of all biological replicates over three experiments; biological replicates from the same experiment have the same shape and colour. P-values were calculated by two-way ANOVA followed by post-hoc comparison using the Dunnett test. **, P<0.01.

5.3.2 Generation of *Nbrd21* knockouts

To determine the function of endogenous *Nb*RD21, we used CRISPR-Cas9 to generate *rd21* knockout lines (Ma et al., 2016). We expressed two sgRNAs targeting *NbRD21* (NbD027122.1) in *N. benthamiana* by agroinfiltration and generated transgenic plants by tissue culture. One sgRNA (sgRNA1; GCAGTGAACTCGATAGTCAC) successfully introduced mutations in *NbRD21* in two independent knockout lines, *4#1-6* and *1#2-6*, which contain a four base pair deletion and a single base pair insertion, respectively (**Figure 5.6A**). The growth of these lines is phenotypically indistinguishable from wildtype plants (**Figure 5.6B**).

Next, we checked for off-target cuts using Cas-OFFinder (Bae et al., 2014). We identified 34 additional sequences in the *N. benthamiana* genome with three or fewer mismatches to our sgRNA sequences (**Supplementary Table 5.1**, **5.2**). Two of the sequences were located within homologs of *NbRD21* (NbD031661 and NbD048751). We sequenced these two genes in both knockout lines and found no mutations at the potential off-target cut sites (**Supplementary Figure 5.1**).

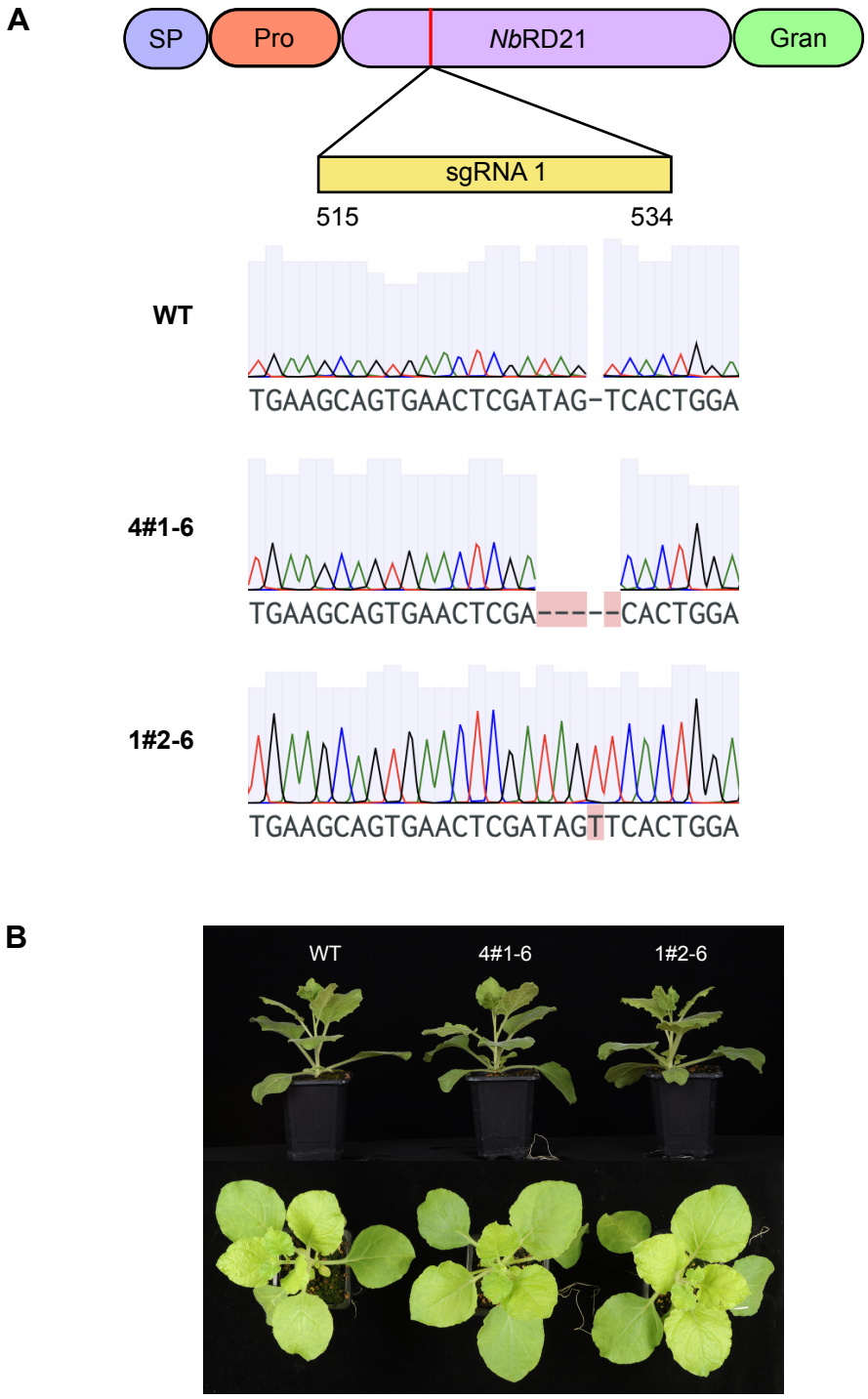


Figure 5.6: Generation of *rd21* knockout lines by CRISPR-Cas9.
A: sgRNA targeting *NbRD21* generated two independent knockouts. Sequencing of sgRNA target site in wildtype (WT) and *rd21* knockout *N. benthamiana* revealed two independent knockout lines. *4#1-6* and *1#2-6* have a 4 bp deletion and a 1 bp insertion, respectively. Bases differing from wildtype are shown in red. Sequencing results analysed at Benchling.com.
B: No phenotypic difference in *rd21* knockout lines. Representative photos of wildtype, *4#1-6* and *1#2-6* 4 week-old *N. benthamiana* plants.

To test if *rd21* lines have reduced cysteine protease activity, we isolated total extract (TE) from wildtype and *rd21* knockout *N. benthamiana* and incubated with 2 μM TK009 (Sueldo et al., 2023). Plants from both *rd21* lines lacked a ~38 kDa signal present in wildtype plants, which suggests this signal corresponds to iRD21 (**Figure 5.7A**). Interestingly, a 35 kDa signal is more intense in *rd21* samples compared to wildtype, suggesting compensatory upregulation of a redundant cysteine protease. As further confirmation of reduced cysteine protease activity in *rd21* plants, we monitored cleavage of the fluorescent cysteine protease substrate zLR-AMC by TE isolated from wildtype and *rd21* mutant *N. benthamiana* (**Figure 5.7B**). Both *rd21* lines had significantly reduced cysteine protease activity compared to wildtype plants (one-way ANOVA with Dunnett correction, $P<0.0001$).

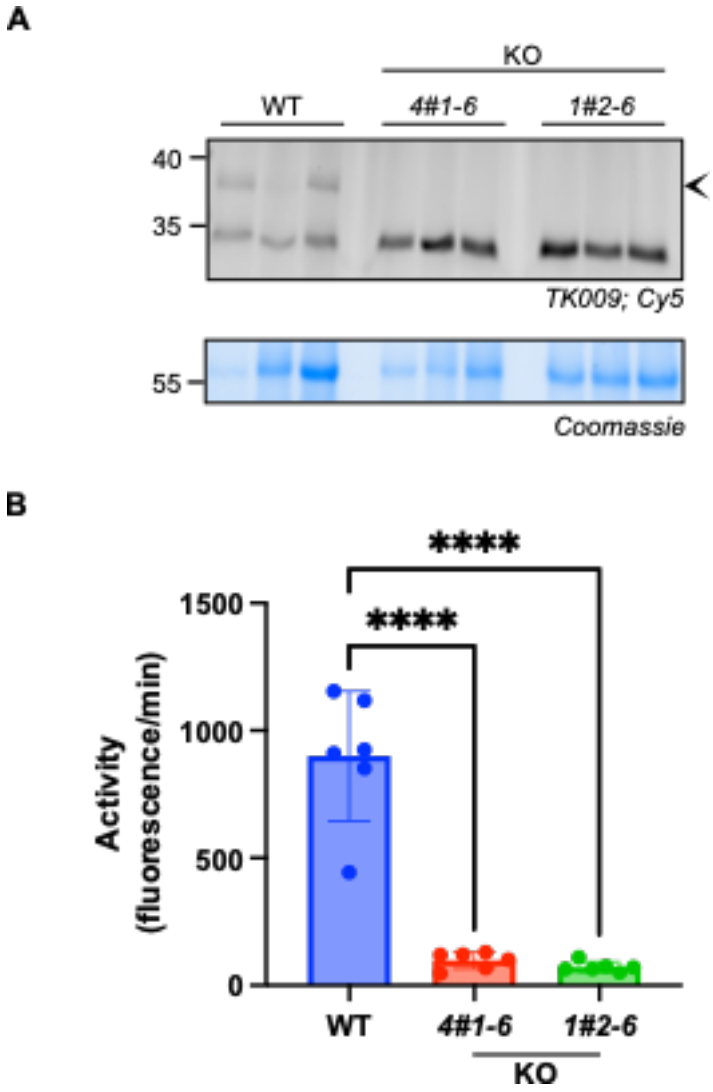


Figure 5.7: *rd21* mutants have significantly reduced cysteine protease activity
A: *Nb*RD21 signal is absent in protease activity profile of *rd21* knockouts (KO). Total extract was isolated from 4 week-old wildtype and *rd21* mutant *N. benthamiana* and 100 µg protein was labelled with 2 µM TK009 in the presence of 5 mM DTT and 50 mM sodium acetate pH 5 at room temperature for 4 hours. Labelled samples were separated by SDS-PAGE, scanned for fluorescence with Cy5 setting and stained with Coomassie. The expected size for iRD21 is indicated with the arrowhead.
B: *rd21* mutants have significantly reduced catalytic activity. Total extract was isolated from 4 week-old wildtype and *rd21* mutant *N. benthamiana* and mixed with 40 µM zLR-AMC in the presence of 2.5 mM DTT and 31.25 mM sodium acetate pH 5. Fluorescence at 380ex/460em was measured at 1 minute intervals for 1 hour at room temperature in a plate reader. Error bars represent mean ± SE of N=6 biological replicates. Statistical significance was calculated by one-way ANOVA followed by post-hoc comparison using the Dunnett test. ****, P<0.0001. Data collected by Msc student Lauren Eddie.

Next, we tested whether the *rd21* lines are more susceptible to *Pto*DC3000 infection. Wildtype *N. benthamiana* and both *rd21* lines were infected with *Pto*DC3000 cultures, and bacterial growth was measured three days later. We found a subtle but significant increase in susceptibility of both *rd21* knockout lines to *Pto*DC3000, suggesting endogenous *Nb*RD21 functions in bacterial immunity (**Figure 5.8**).

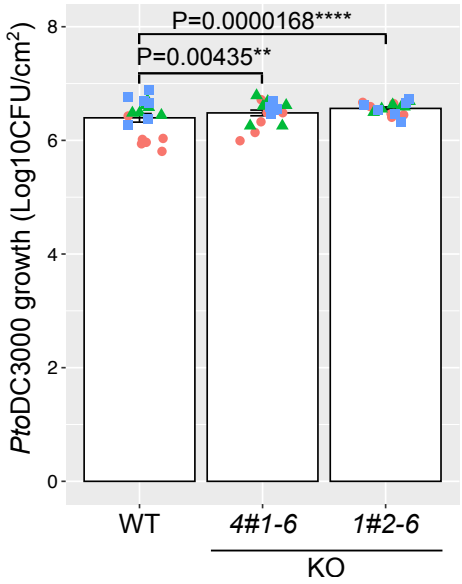


Figure 5.8: *rd21* knockouts are more susceptible to *Pto*DC3000
Wildtype (WT) and *rd21* knockout (KO) lines *4#1-6* and *1#2-6* were infiltrated with 10^7 CFU/mL *Pto*DC3000. Bacterial growth in colony-forming units (CFU) was measured at 3 dpi. Bars represent mean ± SE of all biological replicates over three experiments (N=18); biological replicates from the same experiment have the same shape and colour. P-values were calculated by two-way ANOVA followed by post-hoc comparison using the Dunnett test. **, P<0.01; ****, P<0.0001. Data collected by Msc student Lauren Eddie.

5.3.3 Hypothesis-driven approaches to identify the substrate of *Nb*RD21

5.3.3.1 *Nb*RD21 does not provide resistance to *Phytophthora infestans*

To determine if the immune function of *Nb*RD21 is specific to *P, syringae*, we next tested whether the *rd21* knockout lines are more susceptible to the oomycete *Phytophthora infestans*. Detatched leaves of wildtype and *rd21* plants were drop-inoculated with 10^6 zoospores/mL of *P. infestans* isolate 90128, and necrotic lesion size was measured either four or six days later. In both experiments, there was no significant difference in lesion size between *rd21* and wildtype plants (**Figure 5.9**). This suggests *Nb*RD21 does not function in *P. infestans* resistance.

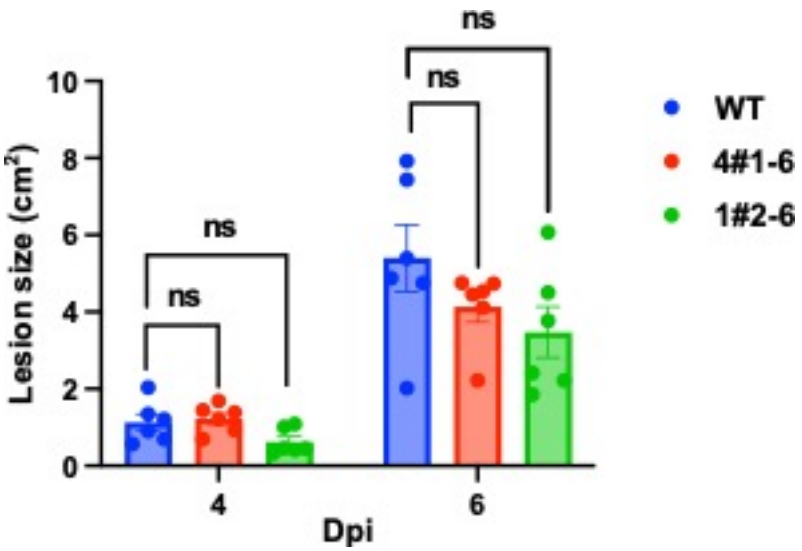


Figure 5.9: *P. infestans* growth is unaffected by *rd21* knockout
P. infestans 90128 was drop-inoculated at 10^6 zoospores/mL onto detached leaves of wildtype (WT) and *rd21* mutant *N. benthamiana*. After incubation at 18°C for 4 or 6 days, leaves were scanned and necrotic lesion size measured using Fiji (Schindelin et al., 2012). Error bars represent mean ± SE of N=6 biological replicates. Statistical significance was calculated by one-way ANOVA followed by post-hoc comparison using the Dunnett test. Ns, not significant at $P<0.05$. Data collected by Msc student Lauren Eddie.

5.3.3.2 *Nb*RD21 does not reduce *Pto*DC3000 growth *in vitro*

We next tested if *Nb*RD21 can directly reduce growth of *Pto*DC3000. We incubated 10^6 CFU/mL *Pto*DC3000 cultures in AF isolated from plants transiently expressing EV, *NbRD21* or *NbRD21*^{C161A} for eight hours. Samples were taken every two hours and plated in dilution series to measure bacterial growth as colony-forming units (CFU). Lysozyme from chicken egg white (LCEW) was included as a positive control because lysozymes can directly inhibit bacterial growth (Davis et al., 2011). We found that *Nb*RD21 was unable to significantly reduce bacterial growth *in vitro*, in contrast to the positive control (**Figure 5.10**). At eight hours, bacterial growth was slightly increased upon *NbRD21* expression compared to the EV control. Therefore, we concluded that *Nb*RD21 does not function by directly reducing bacterial growth.

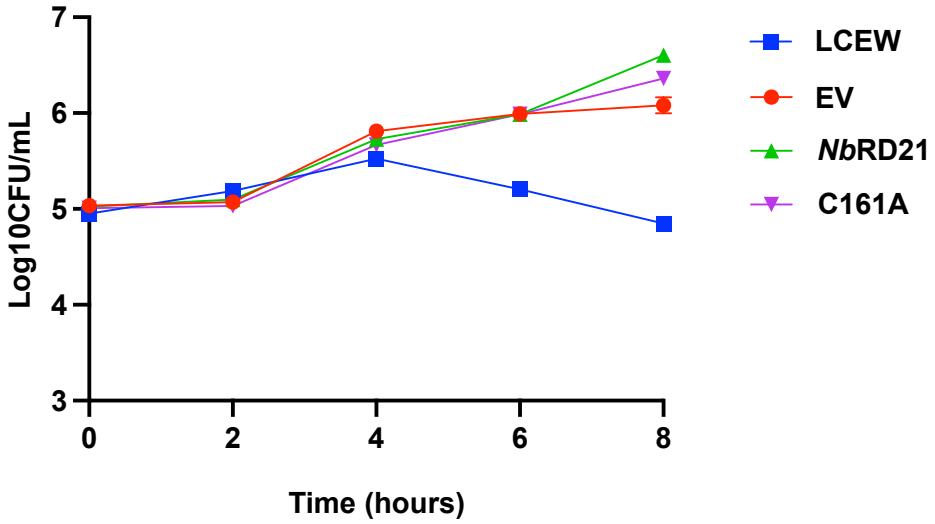


Figure 5.10: *Nb*RD21 does not reduce bacterial growth *in vitro*.
10^6 CFU/mL *Pto*DC3000 was incubated at 25°C in AF from plants transiently co-expressing *NbRD21*, *NbPR3*^{C161A} or an empty-vector (EV) control with the silencing inhibitor P19. 1 mg/mL lysozyme from chicken egg white (LCEW) was used as a positive control. Samples were taken at 2-hour intervals and plated in serial dilution with CFC antibiotic. Bacterial growth in colony-forming units (CFU) was counted 2 days later. Lines represent mean ± SE of N=3 biological replicates. Data collected by Msc student Lauren Eddie.

5.3.3.3 *Nb*RD21 does not induce PR protein accumulation

To test if *Nb*RD21 acts in immunity by activating the immune response, we monitored the accumulation of PR1, PR2 and PR3 in wildtype and *rd21* mutant plants treated with the salicylic acid mimic Bion (Lavergne et al., 2017).

Bion treatment induced the accumulation of PR proteins compared to water-treated plants (**Figure 5.11A**). However, there was no significant difference in PR1 accumulation between wildtype and *rd21* mutants (**Figure 5.11A**), although this experiment was not repeated. Further, there were significant differences in PR2 and PR3 accumulation between wildtype and *rd21* mutant plants, but these were not consistent between replicate experiments. For example, PR2 accumulation is significantly reduced in both *rd21* mutant lines compared to wildtype in two experiments, but unchanged in a third (**Figure 5.11B**). Further, in three separate experiments PR3 accumulation was significantly increased, decreased, and unchanged in *rd21* line *1#2-6* compared to wildtype (**Figure 5.11B**, **Supplementary Figure 5.2**). The lack of consistency in these results led us to conclude that *Nb*RD21 does not activate the immune response.

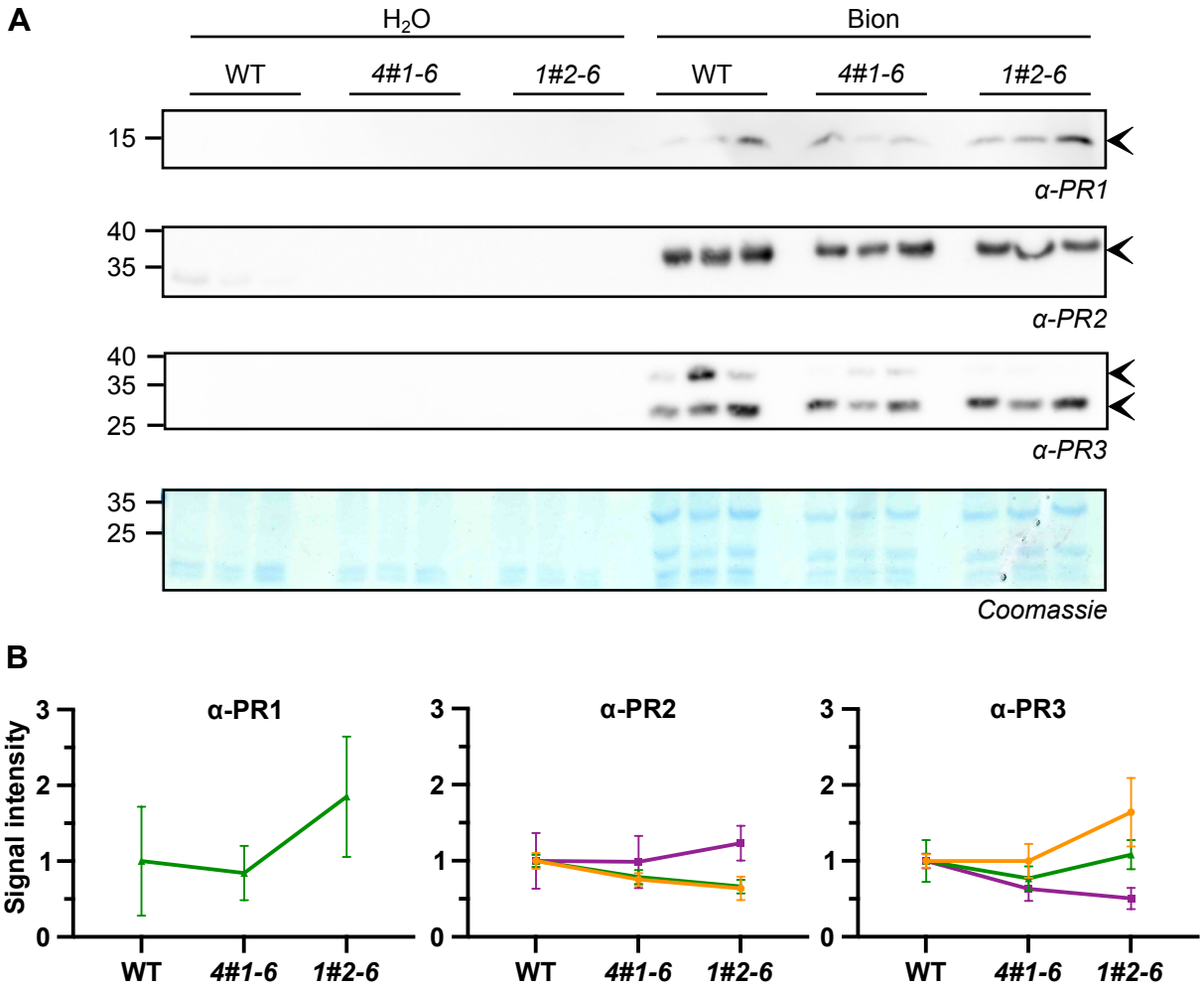


Figure 5.11: *Nb*RD21 does not induce PR protein accumulation.
A: Acrylamide gels showing accumulation of PR proteins. Wildtype (WT) and *rd21* plants were treated with water or 0.42 mg/mL Bion for 3 days. Apoplastic fluid was collected 4 days later, proteins were separated by SDS-PAGE and visualised by Coomassie staining and western blotting with α-PR1, α-PR2 and α-PR3. Expected protein sizes are indicated with arrowheads. Data collected by Msc student Lauren Eddie.
B: Trends in PR protein accumulation are inconsistent between experiments. Western blot signals were quantified and normalised to the intensity of the wildtype Bion-treated control. Colours represent three replicate experiments. Error bars represent mean ± SE of, N=3 (rep 1; green, **Figure 5.11A**), N=4 (rep 2; purple, **Supplementary Figure 5.2A**), and N=6 (rep 3; orange, **Supplementary Figure 5.2B**) replicates.

5.3.3.4 *Nb*RD21 does not release elicitors from *P. syringae*

The oxidative burst is the rapid production of reactive oxygen species (ROS) that occurs upon pathogen perception (Torres et al., 2006). We tested whether *Nb*RD21 releases an elicitor from *P. syringae* to activate the oxidative burst. AF from plants transiently expressing *NbRD21* or an EV control was pooled, and expression confirmed using the fluorescent

cysteine protease substrate zLR-AMC (**Figure 5.12A**). *Pto*DC3000 cultures were incubated in the AF and the mixture was added to leaf discs of wildtype *N. benthamiana* to measure the ROS burst in the presence of luminol and horseradish peroxidase (**Figure 5.12B**). There was no significant difference in the oxidative burst upon *NbRD21* overexpression. Therefore, we concluded that *Nb*RD21 does not release elicitors from *Pto*DC3000.

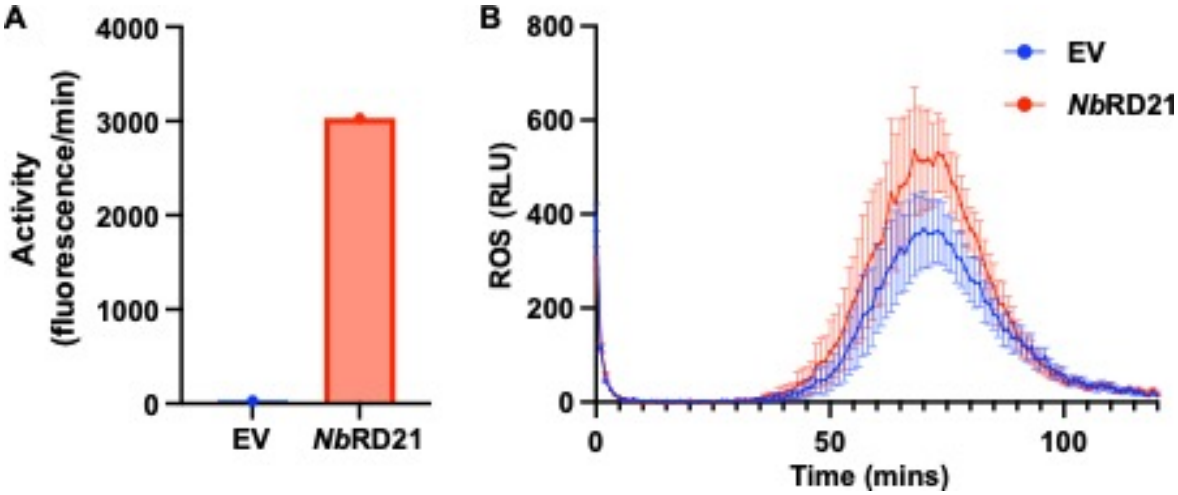


Figure 5.12: *NbRD21* overexpression does not release an elicitor from *P. syringae*.
A: Transient *NbRD21* expression was successful. AF from plants transiently co-expressing *NbRD21* or an empty-vector (EV) control with the silencing inhibitor P19 was isolated at 4 dpi, pooled and mixed with 40 μM zLR-AMC in the presence of 2.5 mM DTT and 31.25 mM sodium acetate pH 5. Fluorescence at 380ex/460em was measured at 1-minute intervals for 25 minutes at room temperature in a plate reader.
B: Transient *NbRD21* expression does not affect the ROS burst. *Pto*DC3000 cultures were incubated in AF at 5 x 10^6 CFU/mL before adding to leaf discs to monitor the ROS burst. Lines on plots represent mean ± SE of N=7 biological replicates.

5.3.4 Proteomic approach to substrate identification

As we were unable to identify the function of *Nb*RD21 using a hypothesis-driven approach, we used a proteomic approach to substrate identification. We looked for differences between the proteomes of wildtype and *rd21* mutant *N. benthamiana* by liquid chromatography tandem mass-spectrometry (LC-MS/MS). Total extract (TE) was isolated from leaves of three 4-week-old plants per genotype and prepared for MS analysis by

methanol-chloroform precipitation followed by trypsin digest. Peptides were sent to Essen, Germany for analysis.

Our analysis identified a total of 4440 protein groups across nine samples. After removing contaminants, we identified 4183 protein groups, including 2070 that were found in all samples. To increase the power of our analysis, we combined the two *rd21* knockout lines into one functional group ('knockout'). We selected only proteins with at least two valid values in at least one functional group (wildtype or knockout), resulting in 2951 protein groups. The data was log-transformed and used to produce a volcano plot (**Figure 5.13**). We found that 55 protein groups showed significant differential accumulation between wildtype and knockout (FDR = 0.05, S0 = 0.1; **Figure 5.13**, **Table 5.1**).

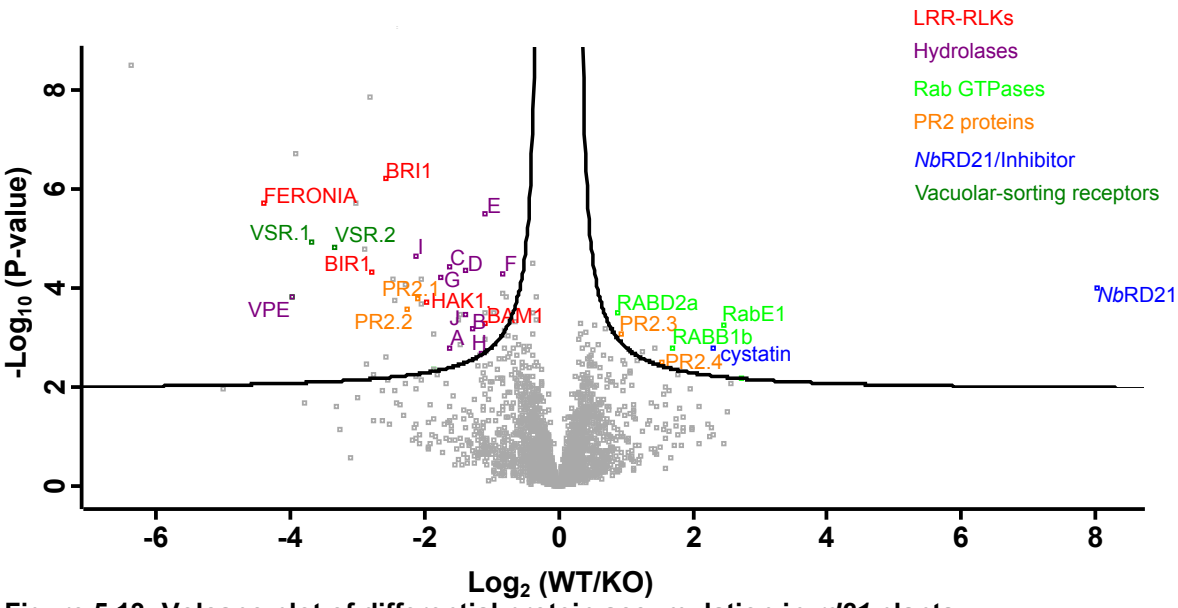


Figure 5.13: Volcano plot of differential protein accumulation in *rd21* plants
Volcano plots of proteins identified in total extract of wildtype (WT; N=3) and *rd21* knockout (KO; N=6; *4#1-6* and *1#2-6*) plants. Samples were digested with trypsin and analysed by LC-MS/MS. Proteins above the black line have significant Log_2(WT/KO) (*t*-test, FDR = 0.05, S0 = 0.1). Proteins of interest are colour-coded according to legend. Adapted from figure produced by Msc student Lauren Eddie.

Table 5.1: Proteins with significant differential accumulation in *rd21* plants. Proteins are ordered by difference in LFQ intensity between wildtype (WT) and knockout (KO). Functional annotations correspond to the key (**Figure 5.13**). Localisation predicted using TargetP (Armenteros et al., 2019). S, secreted; M, mitochondria; C, chloroplast; O, other. Adapted from table generated by Msc student Lauren Eddie.

Protein IDs	Fasta headers	-log10(P-value)	Difference (WT - KO)	Predicted localisation	Functional annotation
NbD030674.1	nicotinate-nucleotide pyrophosphorylase [carboxylating], chloroplastic-like	8.49	-6.36	C	
NbD027854.1	receptor-like protein kinase FERONIA	5.71	-4.39	S	FERONIA
NbE05062848.1; +2	vacuolar-processing enzyme-like	3.82	-3.96	S	VPE
NbD050007.1	40S ribosomal protein S4-like	6.71	-3.93	O	
NbD020924.1; +1	vacuolar-sorting receptor 1-like isoform X1	4.94	-3.69	S	VSR.1
NbD002077.1	vacuolar-sorting receptor 3-like	4.82	-3.32	S	VSR.3
NbE03060165.1; +2	hexokinase-2-like	5.69	-3.03	O	
NbD022440.1; +1	NEDD8-conjugating enzyme Ubc12	4.79	-2.88	O	
NbD007942.1	50S ribosomal protein L4, chloroplastic	2.46	-2.86	C	
NbE03060488.1; +4	aldose 1-epimerase-like isoform X4	7.84	-2.82	S	
NbE03059933.1	probably inactive leucine-rich repeat receptor-like protein kinase At5g48380	4.32	-2.79	S	BIR1
NbD011968.1; +2	temperature-induced lipocalin-1-like	2.24	-2.76	O	
NbD003233.1	nucleoside diphosphate kinase 3-like	2.59	-2.58	M	
NbE03062097.1; +1	BRI1 protein	6.21	-2.56	S	BRI1
NbD004448.1; +1	40S ribosomal protein S12-like isoform X1	4.18	-2.47	O	
NbD021087.1	40S ribosomal protein S4-like	3.75	-2.44	O	
NbD049300.1; +1	uncharacterized protein LOC107782810	4.09	-2.29	C	
NbD004581.1; +3	glucan endo-1,3-beta-glucosidase 4	3.58	-2.27	S	PR2.2
NbD021520.1	LOW QUALITY PROTEIN: serine carboxypeptidase-like 7	4.65	-2.12	S	I
NbE03054370.1; +6	beta-glucosidase 18-like isoform X2	3.79	-2.09	O	PR2.1
NbD026305.1	UDP-D-apiose/UDP-D-xylose synthase 2-like	4.18	-2.05	O	
NbD010989.1; +1	Partial, hexokinase	3.66	-2.04	O	
NbE44070930.1; +2	probable LRR receptor-like serine/threonine-protein kinase At1g06840 isoform X1	3.72	-1.97	S	HAK1
NbD053013.1; +2	protein disulfide isomerase-like 2-3	2.37	-1.87	S	
NbE05064110.1; +1	histidinol dehydrogenase, chloroplastic isoform X1	3.05	-1.86	O	
NbD004239.1	cyprosin-like	4.23	-1.75	S	G
NbE03055263.1; +1	uncharacterized protein LOC107785953	2.77	-1.63	O	A
NbD045213.1	bifunctional purple acid phosphatase 26-like	4.42	-1.62	S	C
NbD036894.1; +4	hexokinase-2-like	3.35	-1.51	O	
NbD008781.1	RNA-binding protein 2-like	2.86	-1.48	O	
NbD041018.1	Partial, apyrase 1-like	3.47	-1.47	O	
NbD020626.1; +2	serine carboxypeptidase-like	3.46	-1.38	S	J
NbD031156.1	bifunctional purple acid phosphatase 26-like	4.37	-1.38	S	D
NbD028744.1	probable inactive purple acid phosphatase 1 isoform X1	3.19	-1.27	S	B
NbD030419.1	serine/threonine-protein phosphatase 4 regulatory subunit 2-like	2.66	-1.17	O	
NbD038993.1; +2	serine carboxypeptidase-like	2.67	-1.16	S	H
NbD042626.1; +1	protein TIC 40, chloroplastic	2.96	-1.11	O	
NbE44071249.1; +2	protein fluG	3.51	-1.10	O	
NbD028383.1; +1	leucine-rich repeat receptor-like serine/threonine-protein kinase BAM1	3.28	-1.10	S	BAM1
NbE03058205.1; +1	subtilisin-like protease SBT1.7	5.48	-1.09	S	E
NbD006784.1	uncharacterized protein LOC109225373	3.50	-0.98	S	
NbD026141.1	30S ribosomal protein S1, chloroplastic	3.90	-0.84	C	
NbE05066551.1; +1	tripeptidyl-peptidase 2 isoform X1	4.28	-0.84	C	F
NbD014118.1	50S ribosomal protein L10, chloroplastic-like	3.84	-0.78	C	
NbD039658.1	5-methyltetrahydropteroyltriglutamate--homocysteine methyltransferase-like	3.31	-0.74	O	
NbD009650.1; +5	ras-related protein RABD2a-like	3.49	0.87	O	RABD2a
NbD018865.1; +1	glucan endo-1,3-beta-glucosidase 14	3.08	0.94	S	PR2.3
NbD003757.1; +3	abscisic acid and environmental stress-inducible protein TAS14-like isoform X2	2.72	1.25	O	
NbD019138.1; +1	Aminocyclopropanecarboxylate oxidase	2.78	1.43	O	
NbD008120.1; +2	glucan endo-1,3-beta-glucosidase, acidic isoform GI9-like	2.49	1.54	S	PR2.4
NbD050026.1; +2	ras-related protein RABB1b isoform X1	2.79	1.71	O	RABB1b
NbD048893.1; +2	cysteine proteinase inhibitor 6-like	2.77	2.30	S	cystatin
NbD019532.1; +7	RabE1	3.24	2.45	O	RabE1

NbD052338.1; +1	uncharacterized protein At2g27730, mitochondrial-like	2.19	2.73	M	
NbD027122.1	papain-like cysteine proteinase 6	4.01	8.01	S	*Nb*RD21

*Nb*RD21 is significantly reduced in the knockout group, providing independent confirmation of the generation of our knockout lines. We BLASTed the remaining protein groups to functionally categorise them (**Table 5.1**; Johnson et al., 2008). We found that a cystatin was reduced in the knockout group, possibly in response to a diminished need to regulate its target *Nb*RD21 (Martinez and Diaz, 2008). We also found three Rab GTPases, important regulators of membrane trafficking, were downregulated in the knockout lines (Woollard and Moore, 2008).

We identified PR2 proteins that were significantly upregulated and downregulated in our knockout group. This is in line with our previous finding that PR protein accumulation upon Bion treatment is inconsistent in *rd21* plants (**Figure 5.11B**). Many more proteins were significantly upregulated in the absence of *Nb*RD21, suggesting they could be *Nb*RD21 substrates. We identified eleven hydrolases, two vacuolar-sorting receptors and five receptor-like kinases (RLKs).

5.3.5 No detected difference in VPE activity in *rd21* mutants

One of the upregulated hydrolases is a vacuolar processing enzyme (VPE). To test if we could detect increased VPE activity in *rd21* mutants, total extract was isolated from wildtype and *rd21* plants and incubated with 0.25 μM DK-004, which detects VPEs (Thomas, 2020). Active *N. benthamiana* VPEs mostly accumulate at 37-38 kDa (Thomas, 2020). However, we found no detectable differences in VPE labelling in either of our *rd21* lines compared to wildtype *N. benthamiana* (**Figure 5.14**).

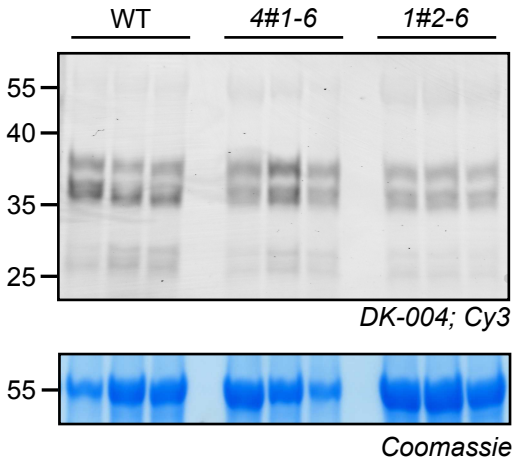


Figure 5.14: VPE activity is unaltered in *rd21* plants
Total extract was isolated from wildtype (WT) and *rd21* plants (lines *4#1-6* and *1#2-6*) into PBS containing 5 mM DTT and 50 mM sodium acetate pH 5 and protein concentrations between samples were standardised. Samples were incubated with 0.25 µM DK-004 in the dark for 3 hours. Proteins were concentrated by acetone precipitation, separated by SDS-PAGE, scanned for fluorescence with Cy3 setting and stained with Coomassie.

5.3.6 *Nb*RD21 is involved in RLK regulation

Based on the upregulation of five RLKs in *rd21* plants, we hypothesised that *Nb*RD21 might play a role in RLK homeostasis. We therefore monitored the degradation of a Myc- and YFP-tagged Arabidopsis leucine-rich repeat (LRR)-RLK, *At*RLK902, in wildtype and *rd21* plants. *At*RLK902 regulates plant immunity by phosphorylating BSK1 (Zhao et al., 2019). A previous study monitored the *in vivo* degradation of transiently expressed *AtRLK902* in *N. benthamiana* by western blot using α-GFP and α-Myc (**Figure 5.15**; Villamor-Sernestrand, 2016). Interestingly, this degradation could be prevented with the addition of the inhibitor E64, suggesting it is controlled by a cysteine protease.

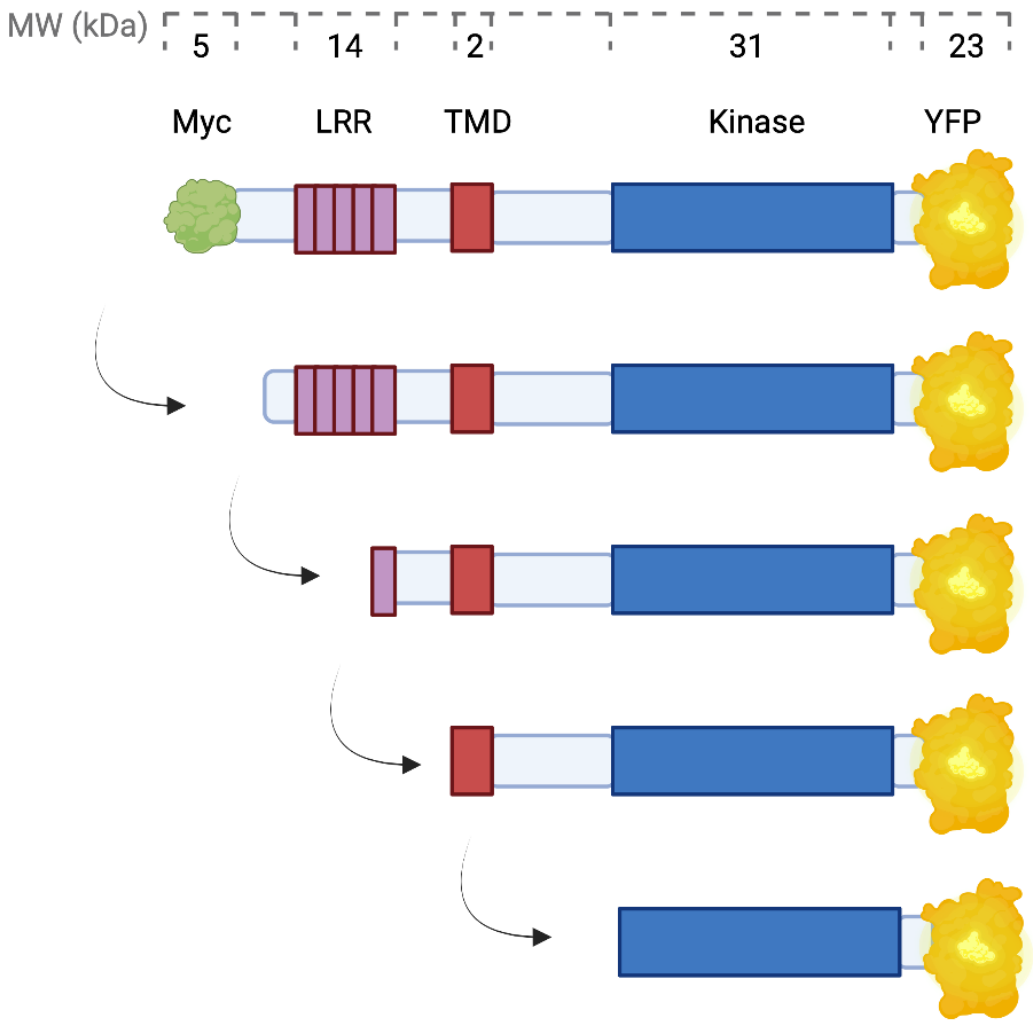


Figure 5.15: Putative processing of *At*RLK902. Structure of the full-length *At*RLK902 protein, Myc-tagged at the N-terminus and YFP-tagged at the C-terminus. Cleavage of the protein results in successively smaller fragments. LRR, leucine-rich repeat; TMD, transmembrane domain. The predicted unglycosylated molecular weights are displayed in kDa. Adapted from Villamor-Sernestrand, 2016. Created with BioRender.com.

To test if *At*RLK902 degradation is altered in *rd21* plants, we transiently expressed the tagged *AtRLK902* into wildtype and *4#1-6 N. benthamiana* with three biological replicates and isolated total extracts at 1, 2, 3, 4 and 5 days-post infiltration (dpi). Samples were extracted into denaturing gel loading buffer to prevent *ex vivo* processing of samples. Western blot analysis with α-GFP revealed both an increased signal intensity, and the accumulation of higher molecular weight signals in *rd21* plants compared to wildtype plants

(**Figure 5.16A**). This was consistent across three replicates (**Supplementary Figure 5.3**), indicating reduced RLK degradation in the absence of *Nb*RD21.

We next tested if degradation of transiently expressed *At*RLK902 is increased upon co-expression of *NbRD21* compared to an EV control. We isolated total extracts from four biological replicates at five days-post infiltration and boiled samples to reduce *ex vivo* processing. By isolating samples at five days-post infiltration rather than over a time course, we were able to simultaneously load all samples on a single gel, hence preventing the arbitrary pairing of wildtype and *rd21* knockout samples. We analysed proteins with α-GFP western blot (**Figure 5.16B**). Consistent with the previous finding, we detected reduced accumulation of higher molecular weight signals upon transient *NbRD21* expression (**Figure 5.16B**). Full-length *At*RLK902 (150 kDa) was detected in all control samples but absent when co-expressed with *NbRD21*. Further, we detected increased accumulation of lower molecular weight fragments when *NbRD21* was expressed compared to the EV control. This suggests that transient *NbRD21* expression promotes *At*RLK902 degradation.

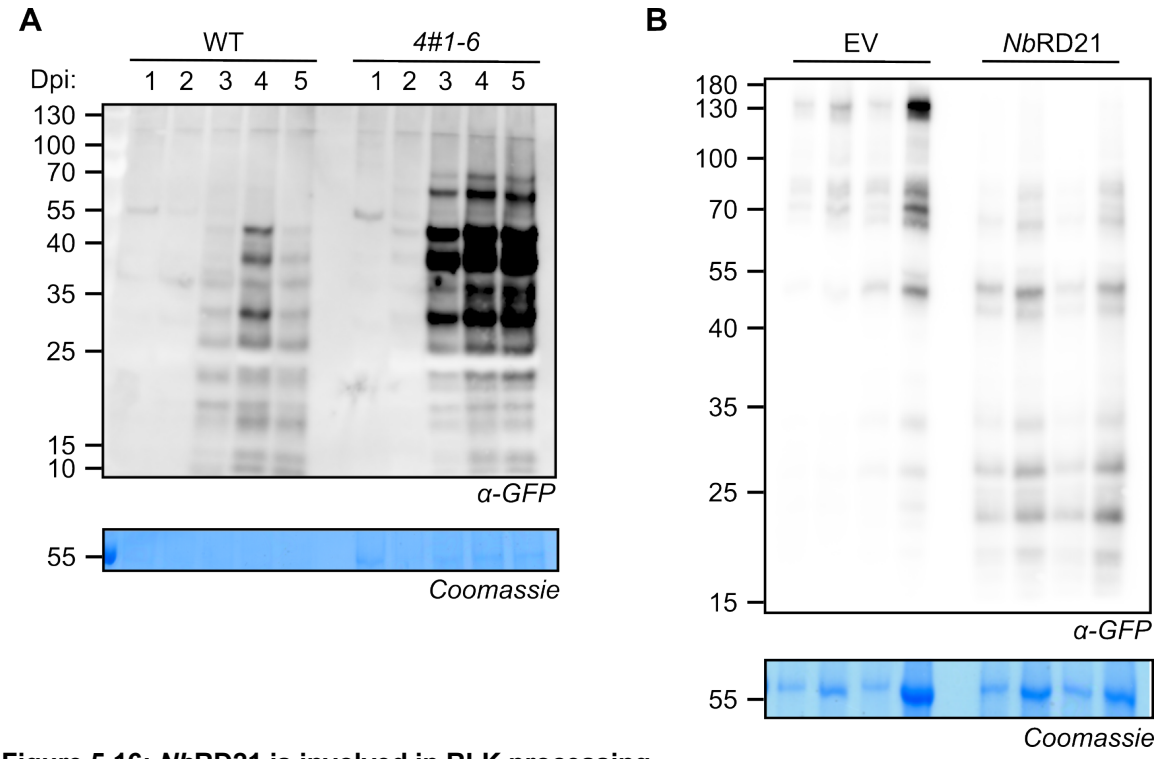


Figure 5.16: *Nb*RD21 is involved in RLK processing.
A: Increased RLK accumulation in *rd21* mutants. Total extract from wildtype (WT) and *rd21* mutant (line *4#1-6*) *N. benthamiana* transiently co-expressing YFP-tagged *AtRLK902* with the silencing inhibitor P19 was isolated at 1, 2, 3, 4 and 5 dpi. Proteins were separated by SDS-PAGE, labelled with α-GFP and stained with Coomassie. Blot shows one biological replicate per treatment with 3 minutes exposure. Blots for all replicates with 30 seconds exposure are found in **Supplementary Figure 5.3**. Data collected by Msc student Lauren Eddie.
B: Reduced RLK accumulation upon transient *NbRD21* expression. Total extracts from plants transiently co-expressing *NbRD21* or an empty-vector (EV) control, along with *AtRLK902* and the silencing inhibitor P19, was isolated at 5 dpi with N=4 biological replicates. Proteins were separated by SDS-PAGE, labelled with α-GFP and stained with Coomassie.

Finally, we monitored processing of two RLKs identified by proteomics. When we monitored *At*RLK902 degradation, samples were extracted directly into gel loading buffer, which has a deep blue colour. Therefore, protein concentrations could not be measured and hence standardised using the colourimetric DC assay. This resulted in unequal protein loading between samples (**Figure 5.16B**). Our subsequent experiments with *Nb*BAM1 and *Nb*FERONIA therefore used alternative methods to detect RLK processing. GFP-tagged *NbBAM1* and *NbFERONIA* were cloned and expressed in wildtype and *rd21* plants by agroinfiltration. Compared to wildtype plants, GFP fluorescence was significantly increased in the *rd21* plants upon transient expression of *NbBam1* (**Figure 5.17A, Supplementary Figure 5.4**), consistent with increased *Nb*BAM1 accumulation in the absence of *Nb*RD21.

We were unable to detect fluorescent GFP signals with our *NbFERONIA-eGFP* construct (**Supplementary Figure 5.4**). However, transient *NbFERONIA* expression causes necrosis and a reduction in leaf autofluorescence that can be measured in the red light spectrum (Xi et al., 2021). We detected a significant reduction in red fluorescence upon *NbFERONIA* expression in both of our *rd21* lines compared to wildtype plants, accompanied by increased cell death (**Figure 5.17B, Supplementary Figure 5.4**). The increased necrosis would be consistent with increased *Nb*FERONIA levels in the absence of *Nb*RD21. Overall, this data provides support that *Nb*RD21 regulates homeostasis of *Nb*BAM1 and *Nb*FERONIA.

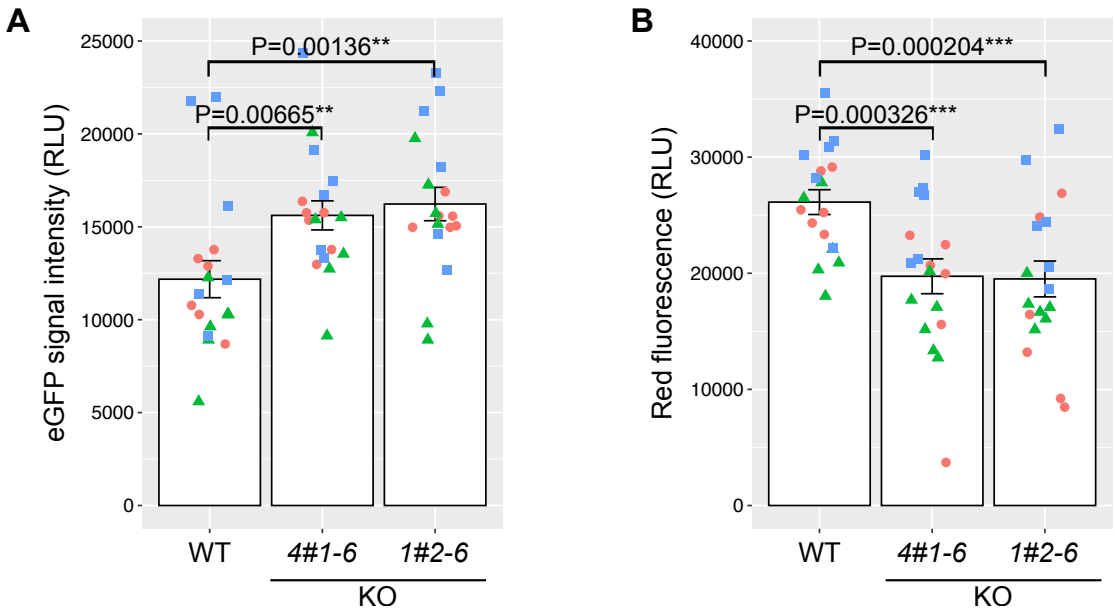


Figure 5.17: *Nb*BAM1 and *Nb*FERONIA levels are increased in *rd21* plants
Leaves from wildtype and *rd21* plants transiently expressing *NbBAM1-eGFP* (**A**) or *NbFERONIA-eGFP* (**B**) were isolated at 3 or 4 dpi and scanned with Cy2 (**A**) or Cy5 (**B**) setting. Bars represent mean ± SE of all biological replicates over three experiments; biological replicates from the same experiment have the same shape and colour. P-values were calculated by two-way ANOVA followed by post-hoc comparison using the Dunnett test. **, P<0.01; ***, P<0.001. Data collected by Dr Mariana Schuster.

5.4 Discussion

In this chapter, we investigated the function of *Nb*RD21. We demonstrated that *Nb*RD21 requires catalytic activity to perform an immune function against *P. syringae,* which is not extended to *P. infestans*. We found no evidence that *Nb*RD21 can directly reduce bacterial growth, cause PR protein accumulation or bacterial elicitor release. We generated two independent *rd21* mutant lines with reduced cysteine protease activity that are significantly more susceptible to *Pto*DC3000. Interestingly, we identified a role for *Nb*RD21 in RLK homeostasis during unchallenged conditions.

Subtle susceptibility phenotype of *rd21* lines

We generated two independent *rd21* knockout lines by CRISPR-Cas9 and used Cas-OFFinder to locate sites of potential off-target mutations. A previous study found that off-target mutations occurred at a rate of only 0.09% when there were at least four mismatches between the sgRNA sequence and the potential off-target (Modrzejewski et al., 2020). We therefore used a cut-off of three mismatches in our analysis. Although we cannot exclude the possibility of mutations elsewhere in the genome, the prediction tool only identified potential mutation sites in two of the *NbRD21* homologs, NbD031661 and NbD048751. We confirmed these genes are wildtype in both *rd21* lines by Sanger sequencing (**Supplementary Figure 5.1**). Therefore, we predict that both of our *rd21* lines are single gene knockouts, at least for *NbRD21* homologs. The subtle susceptibility phenotype of both rd21 lines to *P. syringae* could be due to redundancy with homologs such as NbD031661 and NbD048751.

Interestingly, activity labelling of *rd21* mutant lines showed an increased activity at ~34 kDa that was consistent across all biological replicates (**Figure 5.7A**). This signal could correspond to another hydrolase that is upregulated to compensate for loss of *Nb*RD21.

Redundancy between plant immune proteases has been described (McLellan et al., 2009; Paulus et al., 2020). The signal could correspond to *Nb*RD19, which also labels at 34 kDa (**Figure 3.3**). Our proteomics analysis detected *Nb*RD19 in only two of our *rd21* samples, but in none of our wildtype samples, which is not inconsistent with this hypothesis. Functional redundancy between hydrolases, along with effective inhibition of endogenous *Nb*RD21 in wildtype plants, could explain the surprisingly subtle disease phenotype of the *rd21* mutants (**Figure 5.8**), despite their drastic biochemical phenotype (**Figure 5.7B**). We found no immune phenotype for *Nb*RD19 in our experiments with virulent *Pto*DC3000Δ*hQ* (**Figure 3.4B**). However, the role of *Nb*RD19 in resistance to wildtype avirulent *Pto*DC3000 was not explored, and *Nb*RD19 function could be ETI-dependent, like *Nb*RD21. Indeed, Arabidopsis RD19 is required for resistance to avirulent *Ralstonia solanacearum* (Bernoux et al., 2008). Nevertheless, our proteomics and ABPP experiments used uninfected plants. Further experimentation is required to determine if *Nb*RD19 compensates for *Nb*RD21 in infected conditions.

On the other hand, the signal could be an artefact of reduced competition for probe binding in the *rd21* plants, given that equal amounts of protein were labelled from each sample. Supporting this, both *rd21* lines have a drastic biochemical phenotype which suggests no compensatory activity by a PLCP that can cleave zLR-AMC (**Figure 5.7B**). Furthermore, our proteomics data did not identify significantly upregulated PLCPs in *rd21* plants (**Figure 5.13**). Despite this, there is significantly less accumulation of a cystatin in the *rd21* mutants, which could lead to increased activity of other PLCPs without changing their abundance.

<u>*Nb*RD21 immune function warrants further investigation</u>

Our hypothesis-driven approach failed to identify an immune function for *Nb*RD21. We found no role for *Nb*RD21 in reducing bacterial growth or promoting elicitor release.

Nevertheless, in future these experiments should be conducted using purified *Nb*RD21 rather than *Nb*RD21 in apoplastic fluid, as AF isolation may dilute the protease and limit potential interactions with the bacteria. We found no role for *Nb*RD21 in resistance to *P. infestans*. However, due to the subjectivity of measuring lesion size, future experiments should confirm this by additionally measuring hyphal growth and spore count in *rd21* plants upon *P. infestans* inoculation. We also found contradictory results for the role of *Nb*RD21 in immune activation, with contrasting trends of PR protein accumulation across experimental replicates (**Figure 5.11**). This is echoed by our proteomics data finding PR2 proteins were both significantly upregulated and downregulated in the *rd21* lines (**Figure 5.13**), although it is important to note that this data came from unchallenged plants. These inconsistencies suggest no role for *Nb*RD21 in PR protein activation, or at least that another factor determines the outcome. Further avenues for exploring *Nb*RD21 immune function include the activation of the MAP kinase cascade, which is pivotal for plant immune signalling (Meng and Zhang, 2013), and manipulation of the apoplastic environment through pH or redox changes, which could influence the activity of both host and pathogen proteins (Grosse-Holz et al., 2018; Matika and Loake, 2014). These apoplastic alterations can be monitored by co-expressed pHluorin (Jutras et al., 2018) and infiltrating Amplex Red (Tian et al., 2016), respectively.

rd21 mutants have a significantly altered proteome

We used proteomics to uncover substrates and interacting partners of *Nb*RD21. We only detected proteins in total extracts since preparation of apoplastic fluid samples was unsuccessful. During proteome analysis there were high levels of variability between the total extract samples. This necessitated combining our two independent *rd21* lines into a single functional group to detect significant changes. This should not be problematic, given both lines behaved identically in our previous experiments. However, future experiments

should include six replicates per treatment. Another potential source of variation might be in endogenous *Nb*RD21 levels between wildtype plants. This could be addressed with complementary experiments measuring changes in the *N. benthamiana* proteome upon *P. syringae* infection using purified *Nb*RD21 in *rd21* mutants to control for protein expression. Finally, in this experiment we isolated samples from unchallenged plants, and so any immune-specific substrates could be missed. This is particularly important given our hypothesis that *Nb*RD21 is relocalised upon infection with avirulent bacteria.

Our proteomics data showed significant upregulation of eleven hydrolases in *rd21* plants compared to wildtype, including predicted serine, cysteine and aspartic proteases (**Figure 5.13**). Some of these proteins may act redundantly with *Nb*RD21 and are upregulated as a compensatory mechanism. Redundancy is even possible between different protease classes since cleavage of different areas of a substrate could produce an equivalent outcome. Alternatively, the upregulated hydrolases may be substrates of *Nb*RD21 that accumulate in its absence. Regulation of hydrolase activity through proteolytic cleavage has previously been described (Zimmermann et al., 2016).

On the other hand, upregulated proteases in *rd21* plants may be activators of *Nb*RD21. Pro-peptide domain removal in *Nb*RD21 is not autocatalytic, suggesting that activation is achieved by another protease. The region between the pro-peptide and peptidase domains of *Nb*RD21 is rich in Asp residues. VPEs, cysteine proteases which favour cleavage after Asp (Vorster et al., 2019), have already been implicated in RD21 activation. Whilst *At*RD21A maturation persists in Arabidopsis *vpe* quadruple mutants (Gu et al., 2012), recent proteomics data showed increased N-terminal *Nb*RD21 processing and activation upon overexpression of a VPE (Thomas, 2020). Functional redundancy could explain why VPEs are not necessary for RD21 activation (Gu et al., 2012). For instance, tomato Rcr3 can slowly mature autocatalytically, but is more efficiently matured by tomato subtilase

P69B and can also be processed by *N. benthamiana* SBT5.2 (Paulus et al., 2020). Like VPEs, subtilases are good candidates for *Nb*RD21 pro-peptide removal given many can cleave after Asp residues (Paulus et al., 2020; Reichardt et al., 2018). The *N. benthamiana* ortholog of *P69B*, or the upregulated subtilase SBT5.2 from our proteomics data, are important future lines of inquiry to address this question.

The VPE we identified in our proteomics data may be upregulated as a compensatory mechanism to increase the amount of active *Nb*RD21 in response to *NbRD21* knockout. This could occur at both the transcription or translation level. For instance, *Nb*RD21 knockout may influence global chromatin restructuring that favours the expression of VPE genes, or induce cellular stress that promotes VPE translation (El-Brolosy and Stainier, 2017). Despite this, we were unable to detect increased VPE activity in our *rd21* plants, suggesting the upregulation is not coupled with activation, for example due to post-transcriptional modifications or endogenous inhibition of the VPE (**Figure 5.14**).

A role for *Nb*RD21 in RLK degradation

Most importantly, our proteomics data uncovered five RLKs significantly upregulated in *rd21* plants. RLKs function in a multitude of plant processes, including development, growth, and responses to abiotic and biotic stress (Liu et al., 2017). Homologs of three detected RLKs have described immune functions. *At*FERONIA confers resistance by regulating the oxidative burst (Liao et al., 2017), *At*BIR1 interacts with *At*BAK1 to negatively regulate cell death and defence responses (Gao et al., 2009), and homologs of *NbHAK1* in both soybean and Arabidopsis mediate resistance to herbivory (Uemura et al., 2020). Functions of the remaining detected RLKs have so far only been described in a developmental context. *At*BRI1 is involved in brassinosteroid signal transduction (Ali et al., 2022), and *At*BAM1 modulates root xylem patterning (Fan et al., 2021).

The upregulation of RLKs, along with previous data showing cysteine protease-dependent degradation of an Arabidopsis RLK (Villamor-Sernestrand, 2016) led us to hypothesise that *Nb*RD21 may function in RLK degradation. Indeed, we found reduced degradation of transiently expressed *At*RLK902 in *rd21* plants (**Figure 5.16A**). However, in this experiment we were unable to detect full-length *At*RLK902, and we also detected increased low molecular weight fragments compared to previous data (Villamor-Sernestrand, 2016). In the wildtype samples, this is likely due to excessive *ex vivo* processing. Whilst we extracted samples directly into denaturing gel loading buffer (GLB), SDS in the buffer may have actually promoted *Nb*RD21 activation in wildtype plants (Gu et al., 2012).

We found a significant increase in GFP fluorescence in both *rd21* lines upon transient expression of *NbBAM1-eGFP* (**Figure 5.17A**). This hints at increased *Nb*BAM1 stability in the absence of *Nb*RD21. We were unable to detect GFP fluorescence upon expression of *NbFERONIA-eGFP*, although we observed a strong necrosis phenotype (**Supplementary Figure 5.4**) which probably limited *NbFERONIA-eGFP* expression (Shrawat and Lörz, 2006). We found a significant reduction in red light fluorescence in both of our *rd21* lines (**Figure 5.17B**). This indirectly suggests an increased accumulation of functional *Nb*FERONIA in the absence of *Nb*RD21. These datasets support a role of *Nb*RD21 in RLK homeostasis. However, western blotting is still required to verify that the increased fluorescence and necrosis corresponds to increased intact RLK accumulation in the absence of *Nb*RD21. Furthermore, future experiments should monitor endogenous RLK processing to exclude the possibility that degradation is an artefact of overexpression.

The mode of action for *Nb*RD21-mediated RLK processing is unclear. One possibility is receptor ectodomain shedding. Ectodomain shedding is a means of regulating membrane-bound protein activity through proteolytic cleavage of extracellular or cytosolic domains to release signalling molecules (Hayashida et al., 2010). Whilst extensively described in animals, only a few examples have been described in the plant kingdom (Park and Ronald,

2012; Petutschnig et al., 2014). However, the extensive cleavage profile of *At*RLK902 suggests RLK degradation rather than a single cleavage event indicative of shedding (**Figure 5.16**). Western blotting is required to determine if *Nb*BAM1 and *Nb*FERONIA are also processed in this way.

Instead, we propose that *Nb*RD21 promotes RLK degradation by receptor-mediated endocytosis (RME; **Figure 5.18**). In RME, receptors are sorted at the plasma membrane (PM) into vesicles which travel through the endosomal system and are either recycled back to the PM, or taken to the vacuole for degradation or interaction with their downstream signalling components (Claus et al., 2018). Supporting this hypothesis, we found not only an upregulation of RLKs in *rd21* lines, but also a significant upregulation of vacuolar-sorting receptors, which sort proteins into transport vesicles, and a downregulation of Rab GTPases, which promote vesicle trafficking and fusion. Furthermore, *At*RD21A localises in lytic vacuoles and the trans-golgi network (TGN; Andème Ondzighi et al., 2008). Finally, previous data showed that addition of the cysteine protease inhibitor E64 to tobacco BY-2 cells caused endosomal accumulation (Yamada et al., 2005), suggesting a cysteine protease such as *Nb*RD21 promotes endosomal trafficking to the vacuole. Endosomal accumulation could explain the observed upregulation of membrane-localised vacuolar-sorting receptors, and downregulation of vesicle fusion-mediating Rab GTPases, in the *rd21* lines. Future work should verify that endosomes do indeed accumulate in our *rd21* lines.

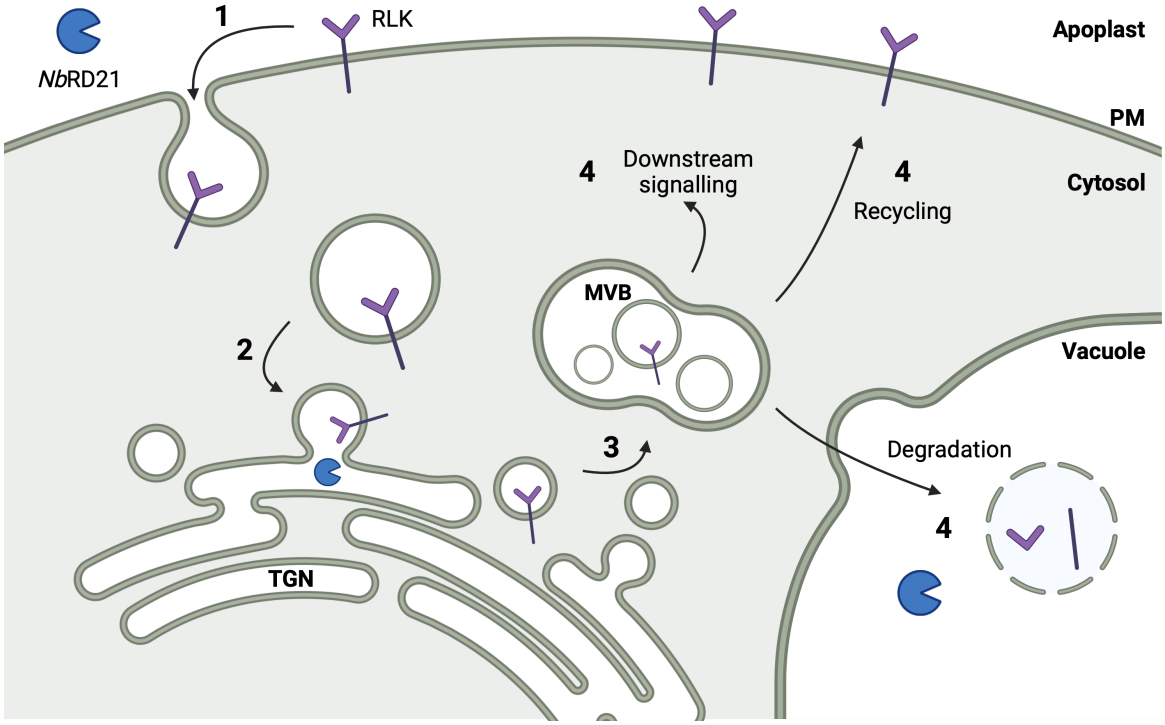


Figure 5.18: Putative pathways for *Nb*RD21-mediated RLK regulation. RLKs (purple) located at the plasma membrane (PM) are internalised into vesicles by endocytosis (**1**). Vesicles travel to the vacuole via the trans-golgi network (TGN; **2**) and multivesicular bodies (MVB; **3**), where they are degraded, recycled or engage in downstream signalling (**4**). *Nb*RD21 (blue) may promote endocytosis from the apoplast, TGN or vacuole. Adapted from figure created by Msc student Lauren Eddie. Created with BioRender.com.

Reconciling different modes of *Nb*RD21 function

The HR-dependent immune function of *Nb*RD21 uncovered in **Chapter 3** appears at odds with the evidence presented here. However, it is possible that we have uncovered two independent functions of *Nb*RD21. The strong biochemical phenotype of our *rd21* knockout lines suggests *Nb*RD21 is a highly active protease (**Figure 5.7B)**. Indeed, *At*RD21A rapidly degrades rubisco upon SDS treatment (Gu et al., 2012). This activity, coupled with the identification of several endogenous inhibitors that regulate RD21 activity (**Figure 5.13**, Andème Ondzighi et al., 2008; Rustgi et al., 2017) suggests *Nb*RD21 cleaves substrates in a relatively nonspecific manner. Therefore, it seems likely that *Nb*RD21 function is determined more by external regulation such as controlled localisation than by its substrate

specificity, in stark contrast to other classes of proteases (Reichardt et al., 2018, Thomas, 2016). Given that the proteomics data was collected from unchallenged plants, and that *NbRD21* depletion caused the accumulation of developmental as well as immune RLKs, RLK processing could represent a housekeeping function for *Nb*RD21 that is separate to its role in the immune response.

Nonetheless, the upregulation of three immune RLKs in our proteomics data, coupled with our subsequent experiments suggesting reduced processing of immune RLKs in the absence of *Nb*RD21 (**Figure 5.16, 5.17B**) should not be overlooked. Although RME leads to constitutive degradation and recycling of inactive RLKs, it is also a vital part of the signalling process for activated RLKs involved in both development, such as BRI1, and immunity, such as FLS2 and PEPR1 (Claus et al., 2018). Following endosomal signalling, activated RLKs are ultimately degraded in the vacuole. This process is known as ligand-induced endocytosis (Claus et al., 2018). For instance, PM-localised FLS2 triggers early immune responses such as the oxidative burst, whilst later events including callose deposition are thought to be regulated by endosomal FLS2 (Claus et al., 2018). By suppressing *Nb*RD21, *Pto*DC3000 could be preventing endosomal RLK immune signalling. The activation status of the observed differential RLKs identified here, including *Nb*BAM1 and *Nb*FERONIA, is unknown. Therefore, it would be interesting to clarify whether *Nb*RD21 promotes RME as part of RLK homeostasis, or mediates ligand-induced endocytosis upon pathogen recognition. For instance, activation of RLKs could be monitored with the use of fluorescent ligands. In fact, a fluorescent brassinosteroid analogue was previously developed to monitor endocytosis of ligand-bound BRI1 in Arabidopsis (Irani et al., 2012).

5.5 Conclusion

In this chapter, we found that *Nb*RD21-mediated resistance is dependent on its catalytic activity, although we could not identify an immune function using our hypothesis-driven approach. We identified a potential role for *Nb*RD21 in RLK processing via receptor-mediated endocytosis, which may be distinct from its role in bacterial defence. We propose that *Nb*RD21 is a highly active and nonspecific protease whose activity is determined by spatial and temporal regulation rather than substrate specificity.

5.6 Contributions

Dr. Philippe Varennes-Jutras designed and cloned the *NbRD21* sgRNAs. Urszula Pyzio assisted with tissue culture of *rd21* knockouts. Dr Farnusch Kaschani and Professor Markus Kaiser performed the mass-spectrometry. Rotation student Bergthor Traustason and Msc student Lauren Eddie assisted in genotyping *rd21* lines under my supervision. Knockout activity characterisation, proteomics sample preparation and analysis, knockout disease assays, *in vitro* growth assay, PR accumulation experiment and an *At*RLK902 experiment were performed by Msc student Lauren Eddie under my supervision. Cloning of GFP-tagged *Nb*FERONIA and *Nb*BAM1 and their resulting experiments were performed by Dr Mariana Schuster, who also provided guidance with proteomics sample preparation and *P. infestans* disease assays.

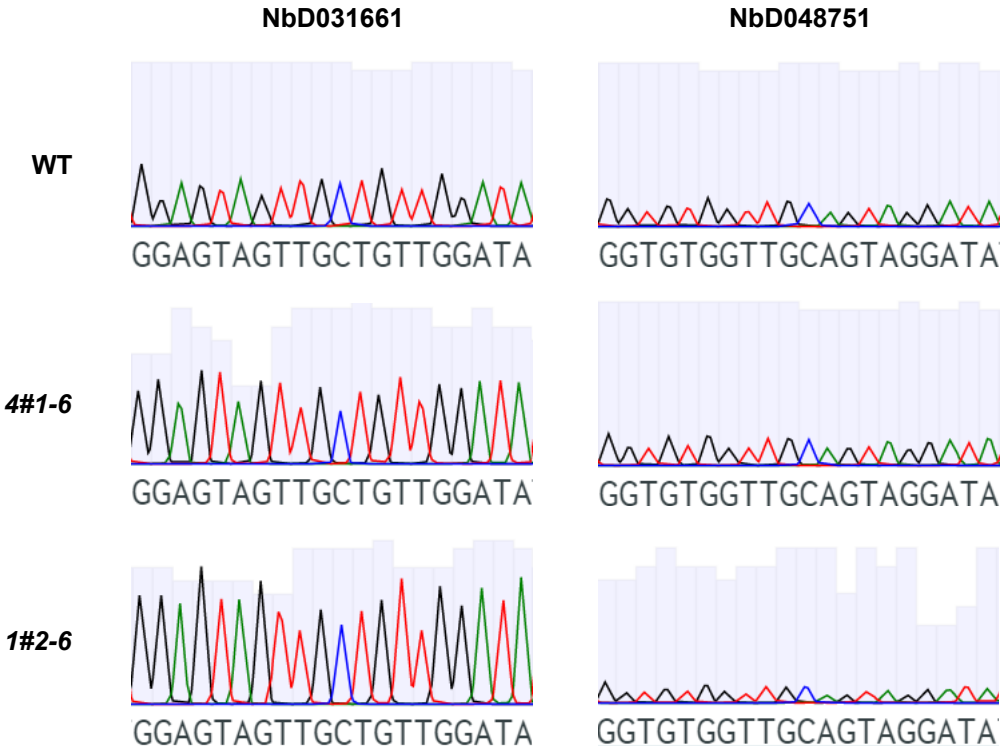
5.7 Supplementary figures

Supplementary Table 5.1: Identification of sequences with 3 or fewer mismatches to sgRNA1. Cas-OFFinder (Bae et al., 2014) was used to identify sequences in the *N. benthamiana* genome with 3 or fewer mismatches to the sgRNA1 sequence (GCAGTGAACTCGATAGTCAC) followed by the PAM sequence NRG. Mismatches are coloured in red.

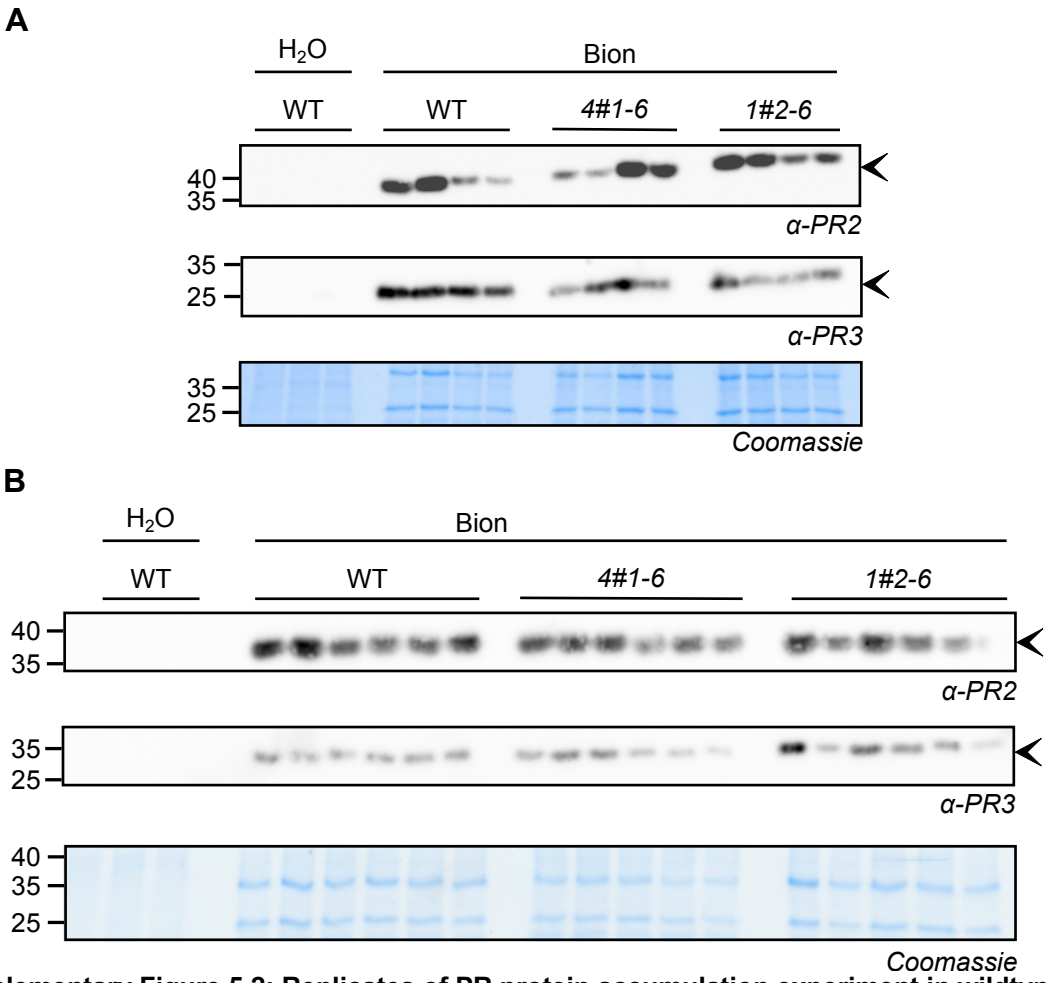
Location	Alignment with sgRNA1
NbD027122.1	GCAGTGAACTCGATAGTCAC TGG
Niben101Scf00151	GCAGTGCACTCGATATTCAC AAG
Niben101Scf15995	GCAGTGATCTCAATAGTCAC CGG
Niben101Scf00217	GCAGGGATCTCAATAGTCAC TGG
Niben101Scf01109	GCAGGGATCTCAATAGTCAC CGG
Niben101Scf01623	GCAGTGAATTCGCTTGTCAC CAG
Niben101Scf02407	GCAGGGATCTCAATAGTCAC CAG
Niben101Scf02549	GCAGCGATCTCAATAGTCAC CAG
Niben101Scf04379	GCAGTGAACTCGAGAGGCAT CAG
Niben101Scf04432	GCAGGGATCTCAATAGTCAC CGG
Niben101Scf05087	GCAGGGATCTCAATAGTCAC TGG
Niben101Scf05472	GCAGTGAACTCGAGAGTAAT CAG
Niben101Scf06867	GCAGAGATCTCAATAGTCAC CGG
Niben101Scf08777	GCAGTGCAGTCGACAGTCAC GGG
Niben101Scf10381	GCAGTGATCTCAACAGTCAC CGG
Niben101Scf11785	GCAGGGATCTCAATAGTCAC CGG
Niben101Scf12361	GCAGTAAAATCGATAATCAC AAG
Niben101Scf17947	GCAGTGATCTCAACAGTCAC AAG

Supplementary Table 5.2: Identification of sequences with 3 or fewer mismatches to sgRNA2. Cas-OFFinder (Bae et al., 2014) was used to identify sequences in the *N. benthamiana* genome with 3 or fewer mismatches to the sgRNA2 sequence (GGTGTGGTAGCTGTTGGATA) followed by the PAM sequence NRG. Mismatches are coloured in red.

Location	Alignment with sgRNA2
NbD027122.1	GGTGTGGTAGCTGTTGGATA TGG
NbD031661	GGAGTAGTTGCTGTTGGATA TGG
NbD048751	GGTGTGGTTGCAGTAGGATA TGG
Niben101Scf00182	GGTTTGGTGGCTGTTGGATT GAG
Niben101Scf02026	GAGGTGGTAGCTGTTGGATC TAG
Niben101Scf02164	GGGGGGGTAGCTGTTTGATA TAG
Niben101Scf02844	GGTTTAGTAGCTGTTGGATT GGG
Niben101Scf04537	GGTGTGGTTGCTGTGAGATA TAG
Niben101Scf05226	GGAGTGGCAGCAGTTGGATA TGG
Niben101Scf05402	GGTAAAGTAGCTGTTGGATA TGG
Niben101Scf06397	GGTTTGGTAGCCGTTGGATT AAG
Niben101Scf07353	GGTGGGGAAGCTGTTCGATA GAG
Niben101Scf08041	CGTTTGGTAGCTGTTGGAGA CGG
Niben101Scf09334	GTTGTGGTTGCTGTTGGAGA GGG
Niben101Scf10999	TGTGTGGTAGATGTTGGCTA TAG
Niben101Scf13041	GGTTTAGTAGCTGTTGGATT GGG
Niben101Scf14634	GGTGTGCAAGCTATTGGATA AAG
Niben101Scf22099	GGAGTGGTAGATGTTGTATA TGG

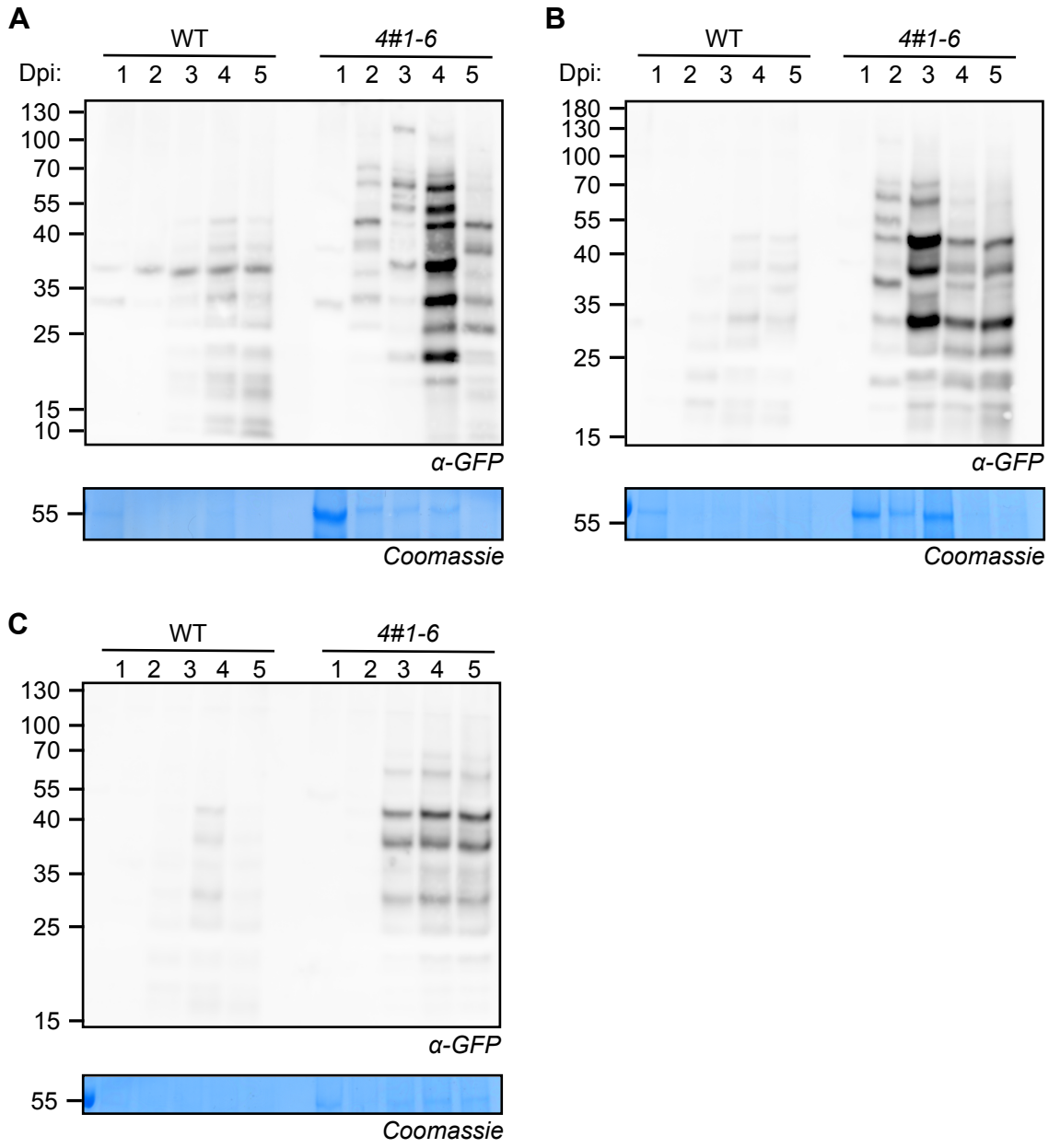


Supplementary Figure 5.1: *rd21* mutants show no off-target cuts in tested genes. Cas-OFFinder identified sequences in the *N. benthamiana* genome with ≤3 mismatches with either sgRNA targeting NbD027122.1, returning genes NbD031661 and NbD048751. Genes from wildtype (WT) and *rd21* (*4#1-6*, *1#2-6*) *N. benthamiana* were sequenced and analysed using Benchling.com.

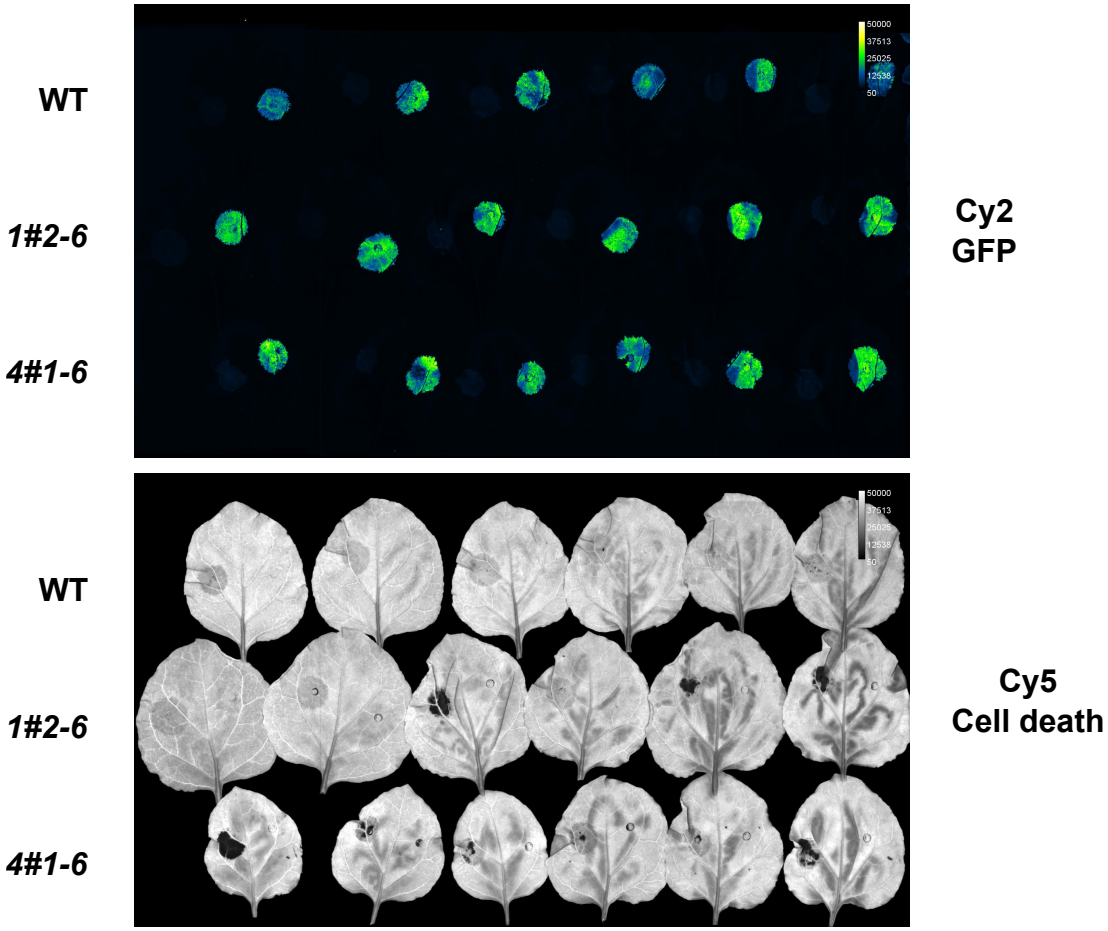


Supplementary Figure 5.2: Replicates of PR protein accumulation experiment in wildtype and *rd21* plants

Wildtype (WT) and *rd21* mutant plants were treated with water or 0.42 mg/mL Bion for 3 days with N=4 (**A**) or N=6 (**B**) replicates. AF was collected 4 days later, proteins were separated by SDS-PAGE and visualised by Coomassie staining and western blotting with α-PR2 and α-PR3. Expected protein sizes are indicated with arrowheads. Data collected by Msc student Lauren Eddie.



Supplementary Figure 5.3: Consistently increased RLK accumulation in *rd21* plants.
Total extract from wildtype (WT) and *rd21* mutant (*4#1-6*) plants transiently expressing YFP-tagged *AtRLK902* was isolated at 1-4 dpi at N=3. Proteins were separated by SDS-PAGE, labelled with α-GFP and stained with Coomassie. Each blot shows a separate pair of biological replicates with 30 seconds exposure. (**C**) corresponds to **Figure 5.16A**. Data collected by Msc student Lauren Eddie.



Supplementary Figure 5.4: Fluorescent scanning of leaves transiently expressing eGFP-tagged *NbBAM1* and *NbFERONIA*.
Leaves of wildtype (WT) and *rd21* (*4#1-6* and *1#2-6*) plants transiently expressing *NbBAM1-eGFP* (right side of leaves) and *NbFERONIA-eGFP* (left side of leaves) were detached at 3 dpi and scanned with Cy2 filter to detect GFP fluorescence, and Cy5 filter to detect cell death. Data collected by Dr Mariana Schuster.

5.8 Methods

Plant growth conditions – *N. benthamiana* was grown in a growth chamber at room temperature with a 16-hour light cycle and 60% humidity and watered on alternating days.

Strains – strains used in this chapter are summarised in **Table 5.2**.

Table 5.2: Strains used in this chapter.

Name	Description	Reference
P. syringae pv. *tomato* DC3000	Wildtype	Buell et al., 2003
P. infestans isolate 90128	A2 mating type, race 1.3.4.7.8.9.10.11	Tian et al., 2007
A. tumefaciens GV3101	Derivative of *A. tumefaciens* C58 carrying pMP90 plasmid	Koncz and Schell., 1986
E. coli DH10B	Chemically competent *E. coli*	Thermo Fisher Scientific EC0113

Molecular cloning – Primers used are summarised in **Table 5.3**. Constructs used in this chapter are summarised in **Table 5.4**. *NbRD21*^{C161A} was created by site-directed mutagenesis using pPB034 as template. Overlapping primers incorporating the desired mutations were designed and the fragments amplified by PCR using Q5 Polymerase (New England Biolabs). DpnI was used to digest the methylated template. To generate binary constructs expressing C-terminally tagged RLKs, the Cf-4 sequence of pJK227 was replaced by the coding sequences of the candidate RLKs as follows. A pJK227 backbone was amplified via PCR. The coding sequences of *NbFeronia* (NbE05064351) and *NbBam1* (NbD028383) were obtained by PCR on coding DNA obtained from *N. benthamiana* leaf tissue. The resulting sequences contained overlapping stretches with the backbone and the coding sequence of the RLK without the signal peptide and stop regions. These inserts were subsequently cloned into the pJK227 backbone via Gibson assembly (Gibson et al., 2009). Purified PCR products were transformed into competent *Escherichia coli* DH10β. Sanger sequencing was used to verify the constructs before transformation into

Agrobacterium tumefaciens GV3101 (pMP90) and selection for kanamycin and gentamicin resistance.

Table 5.3: Primers used in this chapter. Incorporated substitutions are shown in red.

Name	Purpose	Sequence (5' - 3')
C161A_F	Clone *Nb*RD21C161A from pPB034	CTGTGGGAGTGCTTGGGCATTCTCTGCAATTGC
C161A_R	Clone *Nb*RD21C161A from pPB034	GCCCAAGCACTCCCACAGCTTCCTTGATCC
RD21_C_F	Genotyping *rd21*	GACTCGACGGGCCTTCTAAA
RD21_C_R	Genotyping *rd21*	AGAAAGAATGGCAAGCAACATGC
NbD031661_F	Genotyping NbD031661	GTGGGAGATGCGACCAAAATCG
NbD031661_R	Genotyping NbD031661	AGATGGAGGAGAACGGCCAG
NbD048751_F	Genotyping NbD048751	CAACTTAGTGGGGTCTGGGAAGG
NbD048751_R	Genotyping NbD048751	AGGTGGCTTGACTGGTGAAGG
MS72	Amplifying pJK227	GGTGGCATGGTGAGCAAGGG
MS73	Amplifying pJK227	ACCTCCTGCACATCAACAAA
MS82	Amplifying *Nb*FERONIA from cDNA	TTTGTTGATGTGCAGGAGGTCAAAATTCTGCAACTGGTGA
MS83	Amplifying *Nb*FERONIA from cDNA	CCCTTGCTCACCATGCCACCGCGTCCTTTTGGATTCATGA
MS88	Amplifying NbBAM1 (NbD028383) from cDNA	TTTGTTGATGTGCAGGAGGTAGACAACCCCGTATACCTGA
MS89	Amplifying NbBAM1 (NbD028383) from cDNA	CCCTTGCTCACCATGCCACCGATGCTGAGTAGGTCAGGTG

Table 5.4: Constructs used in this chapter

Name	Description	Reference
P19	Binary 35S::P19	Jutras et al., 2018
pJK001c	Binary empty vector (EV)	Paulus et al., 2020
pJK309	Cas9 vector for *Agrobacterium* expression	This work
pPJ064	2xsgRNA *Nb*RD21 with Cas9	This work
pPB034	Binary 35S::*Nb*RD21	This work
pAG011	Binary 35S::*Nb*RD21^{C161A}	This work
pPJ064	CRISPR-Cas9 of *NbRD21*	This work
pJV007	Binary 35S::4xMyc-*At*RLK902-YFP	Villamor-Sernestrand, 2016
pJK227	pL2M-P19-2x35S::Cf-4-GFP	This work
pMS021	pL2M-P19-2x35S::*Nb*FERONIA-eGFP	This work
pMS024	pL2M-P19-2x35S::*Nb*BAM1-eGFP	This work

Generation of *rd21* lines – Two independent sgRNA sequences targeting NbD027122.1 (sgRNA1: GCAGTGAACTCGATAGTCAC; sgRNA2: GGTGTGGTAGCTGTTGGATA) were cloned into the Cas9 vector pJK309 to produce pPJ064. *Agrobacterium* cultures were grown in LB media (kanamycin 50 μg/mL and gentamicin 10 μg/mL) overnight at 28°C. The next day, cultures were centrifuged at 4000 *g* for 10 minutes at room temperature and resuspended in agroinfiltration buffer (10 mM $MgCl_2$, 10 mM MES, 150 μM acetosyringone) to a final OD_{600} of 0.1. 4-week-old *N. benthamiana* plants were infiltrated and three days later, leaf discs were punched from infiltrated leaves, settled in distilled water for one hour and soaked in 10% bleach for ten minutes. Leaf discs were grown on shooting media without antibiotics for three days before transferring to media containing kanamycin. Shoots were transferred to fresh shooting media every 1-2 weeks until growth in rooting media from week 6. Once roots were established, plantlets were potted and grown in the growth chamber. Seeds of heterozygous primary transformants (*4#1* and *1#2*) were sown and plants genotyped. Two homozygous secondary transformants (*4#1-6* and *1#2-6*) were identified and their progeny was used in this chapter.

Agroinfiltration – Agroinfiltration was performed as previously described (**Chapter 3.8**).

Apoplastic fluid (AF) isolation – AF isolation was performed as previously described (**Chapter 3.8**).

Total extract (TE) isolation – Leaf discs (1 cm diameter) were punched from leaves and flash-frozen in liquid nitrogen. Leaf tissue was ground to a powder with a plastic pestle and resuspended in phosphate-buffered saline (PBS, 1:3 w:v). Samples were centrifuged at 14,000 *g* for 10 minutes at 4°C and either used immediately or stored at -20°C.

Fluorescent cysteine protease activity assay – Cysteine protease activity was measured using the fluorogenic substrate Z-Leu-Arg-7-amino-4-methylcoumarin (zLR-AMC, R&D Systems). AF or TE was mixed with 40 μM zLR-AMC in a black 96-well plate in the presence of 2.5 mM DTT and 31.25 mM sodium acetate pH 5 at a final reaction volume of 100 µL. Fluorescence at 380 nm excitation / 460 nm emission was recorded in a plate reader (Tecan Infinite M200) at 20-60 second intervals for 10-60 minutes. Activity was calculated by change in fluorescence over time. P-values were determined by *t*-test or one-way ANOVA with Dunnett correction.

Western blotting and Coomassie staining – Western blotting was performed as previously described (**Chapter 4.8**). Briefly, membranes were blocked in 5% (w/v) milk in PBS-T before addition of primary antibody in 5% milk in PBS-T (α-C14, Kaschani et al., 2010; 3:10,000; α-PR1, Agrisera AS10 687, 1:2500; α-GFP-HRP, Abcam ab6663, 1:2500). Where appropriate, membranes were washed and incubated in secondary antibody for one hour at room temperature (α-Rabbit HRP, GE Healthcare NA934V, 1:1000, 5% milk in PBS-T). Clarity Western ECL substrate (Bio-Rad) was used for signal detection For Coomassie staining, acrylamide gels were stained overnight with Coomassie Brilliant Blue G-250. Band intensity was quantified using Fiji (Schindelin et al., 2012).

Activity-based protein profiling (ABPP) – Total extract was isolated from leaves of wildtype and *rd21* plants with N=3 biological replicates. Protein concentration was measured using the DC assay (Bio-Rad). For detecting PLCPs, 100 µg protein was labelled with 2 μM TK009 (Sueldo et al., 2023) in the presence of 5 mM DTT and 50 mM sodium acetate pH 5 at room temperature for 4 hours. For detecting VPEs, TE samples were isolated directly into PBS containing 5 mM DTT and 50 mM sodium acetate pH 5. Equal protein quantities were incubated with 0.25 μM DK-004 (Thomas, 2020) in the dark for 3 hours. After labelling, the reaction was stopped by precipitation in 4x ice-cold acetone followed by resuspension

in 4x gel loading buffer (200 mM Tris-HCl pH 6.8, 400 mM dithiotreitol, 8% SDS, 40% glycerol, 0.04% bromophenol blue) and heating at 90°C for 5 minutes. Labelled samples were separated by SDS-PAGE, scanned for fluorescence with Cy5 filter (PLCPs) or Cy3 filter (VPEs) and stained with Coomassie.

Agromonas assays – See **Chapter 3.8**.

Phytophthora infestans infection assay – Disease assays were based on a previous study (Karki and Halterman, 2021). *P. infestans* isolate 90128 was grown on Rye A media at 18°C in the dark. Two weeks later, plates were flooded with cold water to release zoospores. Motile zoospores were quantified with a haemocytometer. Six detached leaves of wildtype and *rd21* (*4#1-6* and *1#2-6*) *N. benthamiana* plants were drop-inoculated with a 10^6 zoospores/mL. Leaves were stored on wet paper towels in sealed plates in a growth cabinet at 18°C for four or six days. Necrotic lesions were identified by fluorescent scanning with Cy5 filter (Amersham Typhoon) and lesion area was quantified using Fiji (Schindelin et al., 2012). Linear regression found no effect of leaf size on necrotrophic lesion area ($F_{(1,16)}$=0.182, P=0.6754). Therefore, the effect of genotype on lesion size was determined by one-way ANOVA with Dunnett correction. Graph was produced using GraphPad Prism 9.

In vitro growth assay – See chapter **Chapter 4.8**.

PR protein accumulation – Wildtype and *rd21* (*4#1-6* and *1#2-6*) *N. benthamiana* plants were top-watered with 10 mL water or 0.42 mg/mL Bion 50 WG (Syngenta) every day for three days to induce PR protein accumulation (Lavergne et al., 2017). AF was isolated four days after the final treatment. Proteins were precipitated with ice-cold acetone, resuspended in 2x gel loading buffer (100 mM Tris-HCl pH 6.8, 200 mM dithiotreitol, 4% SDS, 20% glycerol, 0.02% bromophenol blue), boiled at 90°C for five minutes and

separated by SDS-PAGE. PR protein accumulation was monitored by western blotting with antibodies against PR1, PR2 and PR3.

Oxidative burst – See **Chapter 4.8**.

Proteomics – sample preparation – AF and TE were isolated from wildtype and *rd21* (*4#1-6* and *1#2-6*) *N. benthamiana* plants with N=3 replicates. Protein concentration was measured using the DC assay (Bio-Rad). For AF, samples were adjusted to 1 mL due to low protein concentration; TE samples contained 200 μg protein in 100 μL. Halt Protease Inhibitor Cocktail (Thermo Fisher Scientific 78429) was added to samples at 1:100 to prevent proteolytic degradation. Samples were carbamidomethylated by reduction with 5 mM DTT for 30 minutes at 37°C followed by alkylation with 20 mM 2-chloroacetamide for 30 minutes at room temperature. Proteins were precipitated using methanol and chloroform (Wessel and Flügge, 1984), pellets were air-dried and proteins were eluted by sonicating in 6 M urea. Proteins were digested with trypsin/LysC at 1:40 enzyme:proteome for three hours at 37°C. Samples were then diluted in 50 mM Tris-HCl pH 8 (until <1 M urea) and incubated overnight at 37°C with shaking. The pH of the samples was adjusted to <3 with heptafluorobutyric acid (HFBA) and 100 μg protein was desalted on stage tips (Bond Elut OMIX C18, Agilent A57003100) first with 50% acetonitrile, then with 1% and 0.1% HFBA. The next day, peptides were eluted in 0.1% formic acid and 75% acetonitrile before being dried for 2 hours (SpeedVac).

Proteomics – data analysis – Peptides were analysed by liquid chromatography tandem mass-spectrometry at the Analytics Core Facility, Essen using a Thermo Orbitrap Fusin Lumos coupled with a Thermo EASY-nLC 1200 liquid chromatography instrument. Data was searched against the NbDE proteome database (Kourelis et al., 2019) and a contaminants database implemented in MaxQuant (v. 2.0.2.0, Cox et al., 2011). Perseus (v. 2.0.3.0, Tyanova et al., 2016) was used for data analysis, filtering, statistics and

annotation of the volcano plot. Wildtype and knockout categorical groups were compared by *t*-tests (FDR=0.05, S0=0.1, 250 randomisations). Significant hits were functionally annotated using BLAST (Johnson et al., 2008), InterPro (Hunter et al., 2009), Pfam (Finn et al., 2014), UniProt (The UniProt Consortium, 2017) and TAIR (Berardini et al., 2015).

RLK processing – *Agrobacterium* cultures containing *AtRLK902*, *NbBAM1-eGFP* and *NbFERONIA-eGFP* were prepared as described in **Chapter 3.8** to a final OD_{600} of 1 (**Figure 5.16A**/**Supplementary Figure 5.3**: P19 + *AtRLK902*; **Figure 5.16B**: P19 + *AtRLK902* + EV/*NbRD21*) or 0.5 (**Figure 5.17**: *NbBAM1-eGFP* and *NbFERONIA-eGFP*). *N. benthamiana* plants were infiltrated when 4-5 weeks-old, and 2-3 fully expanded leaves were infiltrated per plant. For *At*RLK902 experiments, samples were taken every day for five days (**Figure 5.16A**/**Supplementary Figure 5.3**) or at 5 days-post infiltration (**Figure 5.16B**) directly into 1x gel loading buffer to prevent ex vivo degradation. Samples were boiled at 90^{o}C for five minutes (**Figure 5.16B**). Proteins were separated by SDS-PAGE and detected with α-GFP-HRP (Abcam ab6663, 1:2500). For *Nb*BAM1 and *Nb*FERONIA, six plants per genotype were infiltrated with each RLK. Leaves were collected at 3 days-post infiltration and scanned for fluorescence with an Amersham Typhoon using filters Cy2 (GFP), Cy3 (red fluorescence) and Cy5 (cell death).

Chapter 6: Characterisation of *Nb*RD21 inhibition

6.1 Abstract

Inhibition of host immune proteases is a common strategy used by many plant pathogens. Previous data showed that *Nb*RD21 activity is reduced during *Pseudomonas syringae* infection. In this chapter, we confirmed that this reduction in activity is due to *Nb*RD21 inhibition. We developed a rapid and high-throughput method of monitoring *Nb*RD21 inhibition in a plate reader and used it to begin characterisation of the inhibitor. Finally, we found evidence that the *Nb*RD21 inhibitor is novel and is secreted by multiple bacterial species.

6.2 Introduction

Upon colonisation of its host, *Pseudomonas syringae* produces effector proteins, toxins and other virulence factors to promote pathogenesis (Xin et al., 2018). Effector proteins encoded by *avr* and *hop* genes have diverse functions in pathogenicity, including suppression of PAMP-triggered immunity (PTI), hormone manipulation and inhibition of host proteins (Collmer et al., 2000; Cunnac et al., 2009). For example, HopF2 ADP ribosylates *Arabidopsis thaliana* (Arabidopsis) MAP kinase kinase-5, which inhibits the induction of PTI-induced MAP kinase cascades (Wang et al., 2010), and AvrPto inhibits the Arabidopsis pattern-recognition receptors FLS2 and EFR (Xiang et al., 2008). The majority of these proteins are imported into the host cell via the type III secretory system (T3SS), a needle-like structure largely regulated by *hrp* genes found in a pathogenicity island (Collmer et al., 2000). The exception is AvrD, which directs production of cell death-eliciting syringolides (Kobayashi et al., 1990; Mucyn et al., 2014; Preston, 2000). In addition, other unrelated genes encode effector proteins secreted into the host apoplast, to contribute to bacterial virulence (Shindo et al., 2016).

Toxins and other small virulence factors are also crucial weapons in pathogen invasion. Firstly, *P. syringae* can manipulate its host through the production of plant hormone mimics. Coronatine structurally and functionally mimics the plant hormone jasmonic acid to antagonise salicylic acid (SA) signalling, which is critical for the plant defence response to hemibiotrophic pathogens such as *P. syringae* (Geng et al., 2014). Furthermore, *P. syringae* synthesises indole-3-acetic acid to mimic host auxin and inhibit SA-dependent induction of defence pathways (McClerklin et al., 2018). Lipopeptides are secondary metabolite toxins containing a peptide and a fatty acid tail (Girard et al., 2020). The lipopeptides syringomycin and syringopeptin, encoded by the *syr* and *syp* gene clusters, become imbedded in the host plasma membrane and induce necrosis (Bender and Scholz-Schroeder, 2004). Antimetabolite toxins such as mangotoxin and phaseolotoxin are derived

from peptides and interfere with the biosynthesis of amino acids in the host resulting in chlorotic zones or necrotic lesions (Arrebola et al., 2011). Finally, the toxin syringolin prevents SA-mediated immunity and pathogen-induced stomatal closure through inhibition of the proteasome (Misas-Villamil et al., 2013; Schellenberg et al., 2010). Production of these toxins utilises polyketide synthesis and non-ribosomal peptide synthase pathways (Bender et al., 1999). Expression of many virulence factors is regulated by the GacA/GacS system, composed of a sensor kinase and a transcription regulator, which also inhibits gene expression in the *hrp* pathogenicity island (Heeb and Haas, 2001; O'Malley and Anderson, 2021).

Pathogens secrete inhibitors of host defence hydrolases as an infection strategy (Misas-Villamil and van der Hoorn, 2008). The *Nicotiana benthamiana* β-galactosidase BGAL1 is inhibited by galactosyrin to prevent the release of the immunogenic flg22 elicitor from the glycosylated flagellin of *P. syringae* (Buscaill et al., 2019). *Phytophthora sojae* secretes glucanase inhibitor proteins (GIPs) to inhibit the soybean β-1,3-endoglucanase EGaseA from releasing glucan elicitors from the pathogen cell wall (Rose et al., 2002). Finally, the apoplastic tomato serine hydrolase P69B is inhibited by kazal-like inhibitors EPI1 and EPI10 of *Phytophthora infestans* (Tian et al., 2005, 2004).

Whilst *Nb*RD21 inhibition has not been directly studied before, there is evidence for inhibition of its orthologs. The tomato ortholog of *Nb*RD21, *Sl*C14, is inhibited by the chagasin-like protein Cip1 of *P. syringae*, and the cystatin-like proteins EPIC1 and EPIC2B of *P. infestans* (Kaschani et al., 2010; Shindo et al., 2016). In fact, these EPICs are thought to be the catalyst for diversifying selection of C14 in potato, the natural host of *P. infestans* (Kaschani and van der Hoorn, 2011). Whist direct inhibitors of Arabidopsis RD21 have not been identified, this protease does interact with pathogen virulence proteins. For example, *At*RD21A directly interacts with the Mc1194 effector secreted by the root-knot nematode *Meloidogyne chitwoodi* (Davies et al., 2015). Whilst the biological consequences of this

interaction have not been established, Arabidopsis *rd21a* mutants are more susceptible to *M. chitwoodi*, suggesting that *At*RD21A inhibition could be an infection strategy (Davies et al., 2015). Furthermore, *Xanthomonas oryzae* secretes the type III effector AvrRxo1 which can physically interact with both *At*RD21A and the E3 ligase SINAT4 to promote *At*RD21A degradation (Liu et al., 2020). Finally, the localisation of *Sl*C14 and *At*RD21A is regulated by the RxLR effector AvrBlb2 of *P. infestans*, and the 4E02 effector of *Heterodera schachtii*, respectively (Bozkurt et al., 2011; Pogorelko et al., 2019), presumably to prevent interaction between these defence proteases and their substrates. Overall, the manipulation of *Nb*RD21 orthologs by plant pathogens indicates they are important components of the plant immune system.

*Nb*RD21 activity is reduced in the *N. benthamiana* apoplast upon infection with *P. syringae* pv. tomato DC3000 *ΔhopQ1-1* (*Pto*DC3000*ΔhQ*), suggesting this protease is also inhibited by plant pathogens (Sueldo et al., 2023). In this chapter, we began to characterise the inhibitor of *Nb*RD21. We developed and optimised a method to monitor *Nb*RD21 inhibition during *Pto*DC3000*ΔhQ* infection. We used this method to begin biochemical characterisation of the *Nb*RD21 inhibitor. Finally, we investigated the breadth of *Nb*RD21 inhibitor production in different bacteria.

6.3. Results

6.3.1 *Nb*RD21 inhibition can be detected by convolution ABPP

First, we tested if *Nb*RD21 inhibition could be measured by convolution activity-based protein profiling (ABPP; **Figure 6.1A**). In this technique, a proteome containing putative inhibitors is mixed with a proteome containing proteins of interest before (mix-label, ML) or after (label-mix, LM) labelling with a fluorescent probe that binds to active proteins of a given class (Chandrasekar et al., 2017). Proteins are separated by SDS-PAGE and scanned for fluorescence. If inhibition takes place, then mixing proteomes prior to labelling results in a significant reduction in the detected fluorescent signal compared to mixing labelled samples (Chandrasekar et al., 2017). To prepare ML samples, apoplastic fluid (AF) isolated from *N. benthamiana* transiently expressing *NbRD21* at 4 days-post infiltration was incubated for 30 minutes with an equal volume of the supernatant of *Pto*DC3000*ΔhQ* grown overnight in mannitol-glutamate (MG) media. Unmixed proteomes (AF containing *Nb*RD21 and supernatant containing putative inhibitors) and ML samples were labelled for three hours with the papain-like cysteine protease probe TK009 (Sueldo et al., 2023). Prior to separation by SDS-PAGE, LM samples were created by mixing equal volumes of labelled unmixed proteomes.

We detected a 38 kDa signal in the AF samples corresponding to the intermediate isoform of *Nb*RD21 (iRD21) which was absent in the unmixed bacterial supernatant sample (**Figure 6.1B**). As expected, relative intensity of this signal was reduced by 49% when the AF samples and supernatant were mixed after labelling (LM, **Figure 6.1C**). Importantly, signal intensity was significantly reduced in the ML condition compared to LM (**Figure 6.1C**; paired one-tail *t*-test, P=0.0427). This confirms that *Pto*DC3000*ΔhQ* secretes an inhibitor of *Nb*RD21.

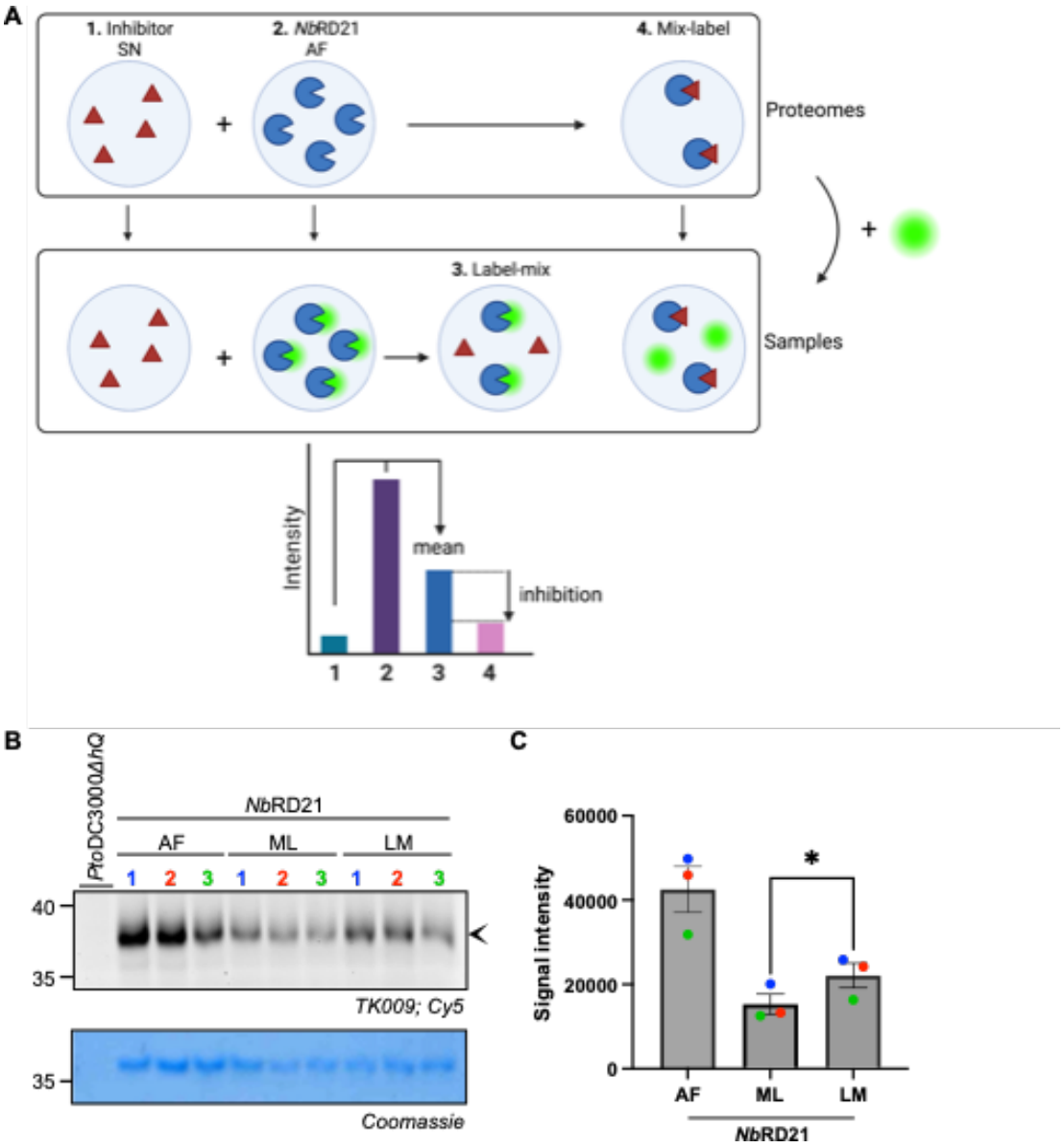


Figure 6.1: *Nb*RD21 inhibition can be detected by convolution ABPP.
A: Convolution ABPP workflow. Bacterial supernatant (SN; 1) containing putative inhibitors (triangles) is mixed with apoplastic fluid (AF) from *N. benthamiana* transiently co-expressing the silencing inhibitor P19 and *NbRD21* (blue pacman; 2) prior to labelling with fluorescent cysteine protease probe TK009 (green) to create a mix-label sample (ML; 4). As a control, samples 1 and 2 are mixed after labelling (label-mix, LM; 3). Samples are separated by SDS-PAGE and scanned for fluorescence to detect signal intensity. If there is inhibition, signal intensity in the ML condition is less than in the LM control condition. Adapted from Chandrasekar et al., 2017. Figure created with BioRender.com.
B: Addition of inhibitor to *Nb*RD21 prior to labelling reduces signal in protease activity profile. AF was isolated from *N. benthamiana* transiently co-expressing *NbRD21* with the silencing inhibitor P19 in N=3 biological replicates at 4 dpi. Samples were mixed with supernatant of *Pto*DC3000*ΔhQ* grown in mannitol-glutamate media before (ML) or after (LM) labelling with 2 µM TK009 for three hours. Samples were separated by SDS-PAGE, scanned for fluorescence with Cy5 setting and stained with Coomassie. Unmixed supernatant and AF were included as controls. Biological replicates are numbered and colour-coded. Intermediate *Nb*RD21 is indicated with the arrowhead.
C: Quantification of signal intensities. Relative intensities of the *Nb*RD21 activity signal indicated with the arrowhead (**B**) were quantified using Fiji (Schindelin et al., 2012) and displayed graphically using GraphPad Prism 9. Error bars represent mean ± SE of N=3 paired biological replicates, which are distinguished by colour. Statistical significance was calculated by paired one-tail *t*-test. *, P<0.05.

6.3.2 Establishing a fluorescent activity assay to monitor *Nb*RD21 inhibition

Whilst the previous result is promising, we wanted to develop a faster and higher throughput method of monitoring *Nb*RD21 inhibition. We established a method of monitoring *Nb*RD21 inhibition in a plate reader using the fluorescent cysteine protease substrate Z-Leu-Arg-7-amino-4-methylcoumarin (zLR-AMC; **Figure 5.3A**). This method combined our previous zLR-AMC protocol (**Chapter 5**) with elements of convolution ABPP to establish a method for detecting *Nb*RD21 inhibition by a secreted bacterial inhibitor (**Figure 6.2**).

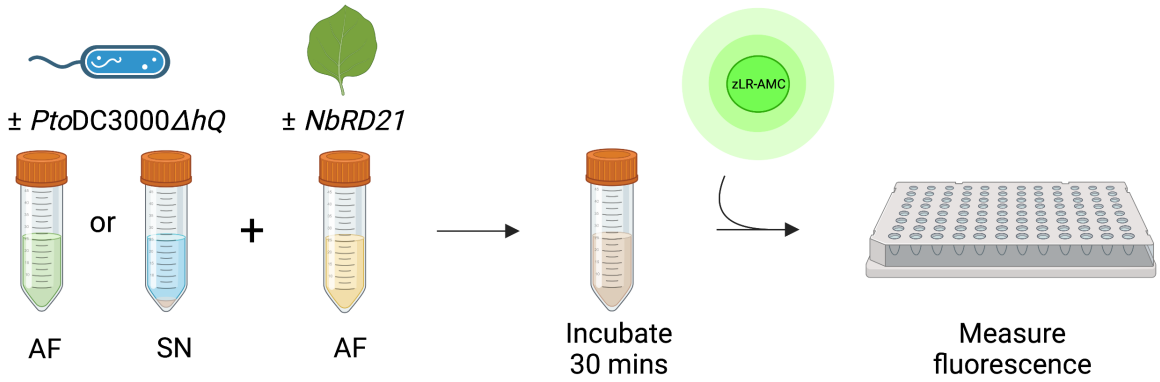


Figure 6.2: Fluorescent *Nb*RD21 inhibition assay. Apoplastic fluid (AF) from *N. benthamiana* transiently co-expressing *NbRD21* with the silencing inhibitor P19 was mixed 1:1 with either AF isolated at 2 dpi from *N. benthamiana* infected with 10^6 CFU/mL *Pto*DC3000*ΔhQ*, or the supernatant (SN) of *Pto*DC3000*ΔhQ* cultured in growth media overnight at OD_{600} = 1. AF from mock (water)-infiltrated plants, or growth media without bacteria, was used as a negative control. Samples were incubated for 30 minutes at room temperature and then mixed with 40 µM Z-Leu-Arg-AMC in the presence of 5 mM DTT and 31.25 mM sodium acetate pH 5. Fluorescence at 380ex/460em was measured in a plate reader. AF from plants transiently expressing empty-vector was subtracted as background. Figure created with BioRender.com.

First, we monitored whether *Nb*RD21 can be inhibited by AF from plants infected with 10^6 CFU/mL *Pto*DC3000*ΔhQ*. AF was isolated from infected *N. benthamiana* at 2 days-post infiltration and passed through a 0.22 µM pore syringe filter to remove bacteria. AF isolated from mock (water)-infiltrated plants was used as a control. Equal volumes of AF from infected plants were mixed with AF from plants transiently expressing *NbRD21* or an empty-vector (EV) control. After 30 minutes incubation, we monitored cleavage of the fluorescent

cysteine protease substrate zLR-AMC. There was a significant reduction in cysteine protease activity when both EV (repeated-measures one-way ANOVA with Šidák correction, P=0.0387) and *Nb*RD21 (P=0.0281) samples were mixed with AF from infected plants compared to AF isolated from mock-infiltrated plants, which is indicative of cysteine protease inhibition (**Figure 6.3**).

Importantly, the cysteine protease activity of EV samples was only ~2% of that of the *Nb*RD21 samples in control conditions. This suggests that transiently expressed *Nb*RD21 accounts for 98% of the measured cysteine protease activity in its AF, confirming this method can be used to approximate the activity of purified *Nb*RD21. Nonetheless, in subsequent experiments we subtracted the activity of EV samples and putative inhibitor samples as background to improve the accuracy of our activity measurements. For simplicity, the cysteine protease activity of AF isolated from plants transiently expressing *NbRD21* will henceforth be referred to as *Nb*RD21 activity.

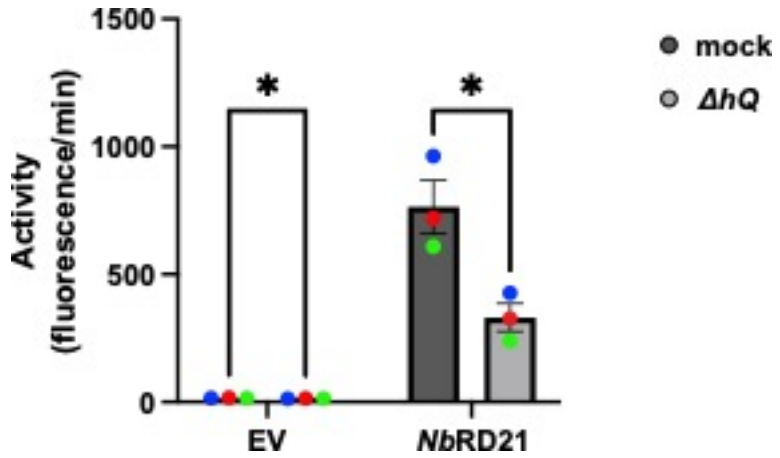


Figure 6.3: Significant reduction in *Nb*RD21 activity in the presence of AF from *Pto*DC3000*ΔhQ*-infected plants. Apoplastic fluid (AF) from wildtype *N. benthamiana* transiently co-expressing *NbRD21* with the silencing inhibitor P19 was isolated at 4 dpi, passed through a 0.22 µM pore syringe filter and mixed with AF pooled at 2 dpi from *N. benthamiana* infected with 10^6 CFU/mL *Pto*DC3000*ΔhQ* or a water (mock) control. After 30 minutes incubation, samples were mixed with 40 µM Z-Leu-Arg-AMC and fluorescence at 380ex/460em was measured in a plate reader. Cysteine protease activity of AF from plants transiently expressing an empty-vector (EV) control, and activity of AF from mock- or *Pto*DC3000*ΔhQ*-infiltrated plants, was subtracted as background. Error bars represent mean ± SE of N=3 paired biological replicates, which are distinguished by colour. Statistical significance was calculated by repeated-measures one-way ANOVA with Šidák correction. *, P<0.05.

Next, we confirmed that the reduction in *Nb*RD21 activity after mixing with AF from *Pto*DC3000*ΔhQ*-infected plants is due to inhibition, not degradation, of *Nb*RD21. We isolated and pooled AF from *rd21* mutant (*4#1-6*) plants infiltrated with 10^6 CFU/mL *Pto*DC3000*ΔhQ* or a mock (water) treatment at 2 days-post infiltration. We used *rd21* mutant plants to prevent the upregulation of endogenous *NbRD21* in response to infection. The pooled AF samples were incubated for 30 minutes with AF isolated from *rd21* plants transiently expressing *NbRD21* at 4 days-post infiltration with N=3 biological replicates. Half of each incubated sample was used to monitor cysteine protease activity with the fluorescent substrate zLR-AMC. Cysteine protease activity was significantly reduced after incubation with AF from infected plants compared to mock-infiltrated plants (**Figure 6.4A**; ratio paired *t*-test, P=0.0163), confirming that *Nb*RD21 is inhibited.

Meanwhile, the remaining half of each incubated sample was boiled for five minutes at 95ºC, and proteins were separated by SDS-PAGE. We detected intermediate and mature

*Nb*RD21 protein using the anti-triticain-α antibody, which targets the wheat ortholog of *NbRD21* (GenBank AB267407; Gorokhovets et al., 2017; **Figure 6.4B**). We quantified the combined intensity of both *Nb*RD21 isoforms. There was no significant difference in *Nb*RD21 protein accumulation when *Nb*RD21 samples were mixed with AF from *N. benthamiana* infected with *Pto*DC3000*ΔhQ* compared to AF from mock-infiltrated plants (**Figure 6.4C**, ratio paired *t*-test, P=0.2694), suggesting the reduction in *Nb*RD21 activity is not due to protein degradation. In further support of *Nb*RD21 inhibition, relative accumulation of iRD21 compared to mature *Nb*RD21 (mRD21) increased from 1.15X to 2.39X after mixing with AF from infected plants, although this was not significant (*t*-test, P=0.105). Since maturation of *Nb*RD21 is autocatalytic (Gu et al., 2012), this is indicative of inhibition.

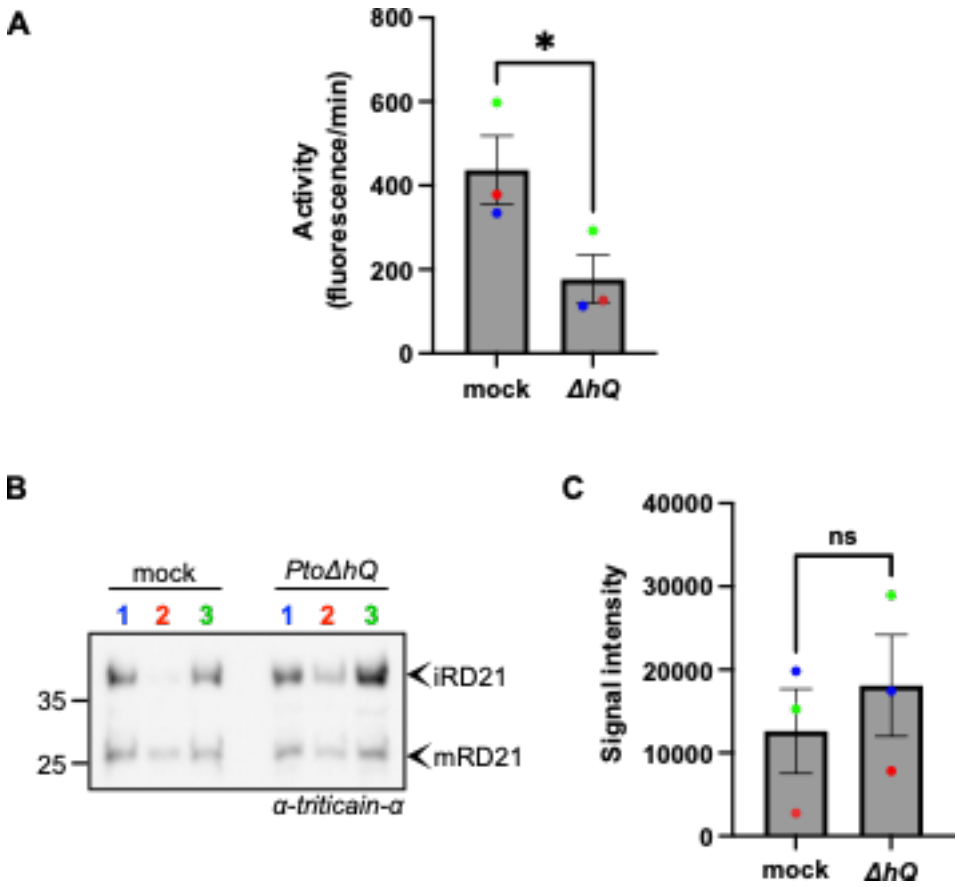


Figure 6.4: Reduction in cysteine protease activity is not due to degradation of *Nb*RD21.
A: Significant reduction in *Nb*RD21 activity in the presence of apoplastic fluid (AF) from *Pto*DC3000*ΔhQ*-infected plants. AF from *rd21* mutant (*4#1-6*) plants transiently co-expressing *NbRD21* with the silencing inhibitor P19 was isolated at 4 dpi and mixed with AF pooled at 2 dpi from *N. benthamiana* infected with 10^6 CFU/mL *Pto*DC3000*ΔhQ* or a water (mock) control. After 30 minutes preincubation, samples were mixed with 40 µM Z-Leu-Arg-AMC and fluorescence at 380ex/460em was measured in a plate reader. Cysteine protease activity of AF from plants transiently expressing an empty-vector (EV) control, and AF from mock- or *Pto*DC3000*ΔhQ*-infiltrated plants, was subtracted as background. Error bars represent mean ± SE of N=3 paired biological replicates, which are distinguished by colour. Statistical significance was calculated by ratio paired *t*-test. *, P<0.05.
B: *Nb*RD21 protein levels are unchanged by AF from *Pto*DC3000*ΔhQ*-infected plants. Mixed AF samples (**A**) were separated by SDS-PAGE and visualised by western blotting with α-triticain-α.
C: Quantification of signal intensities. Signal intensities of both *Nb*RD21 isoforms (indicated with arrowheads (**B**)) were quantified using Fiji and combined into single values. Error bars represent mean ± SE of N=3 paired biological replicates, which are distinguished by colour. Statistical significance was calculated by ratio paired *t*-test. Ns, not significant.

6.3.3 *in vitro* production of *Nb*RD21 inhibitor

Whilst we detected significant and robust inhibition of *Nb*RD21 by AF from infected plants, the source of this inhibition is unclear. Infection with *Pto*DC3000*ΔhQ* triggers a plant stress response that alters the apoplastic environment in a way that might be unfavourable to

protease activity (Qi et al., 2017; Wang et al., 2019b). To discount *Nb*RD21 inhibition being caused by the plant stress response, we tested methods of *in vitro* inhibitor production. First, we grew *Pto*DC3000*ΔhQ* in M9-fructose media, which induces the T3SS via *hrpL* (O'Malley and Anderson, 2021). Bacteria grown overnight in M9-fructose media at OD_{600} = 1 were centrifuged and the supernatant, containing putative secreted inhibitors, was passed through a 0.22 µM pore syringe filter to remove bacteria. The supernatant samples were mixed with AF from plants transiently expressing *NbRD21*. M9-fructose media without bacteria was used as a negative control. After 30 minutes incubation, we monitored cleavage of the fluorescent substrate zLR-AMC in a plate reader. We detected no reduction in *Nb*RD21 activity after mixing AF with bacterial supernatant (**Figure 6.5A**, ratio paired *t*-test, P=0.4677), suggesting *Pto*DC3000*ΔhQ* grown in M9-fructose media does not secrete an *Nb*RD21 inhibitor.

Next, we isolated the supernatant of bacteria grown in mannitol-glutamate (MG) media, which has a lower salt content than M9 and promotes both coronatine biosynthesis and induction of the T3SS (Park et al., 2010). We tested if supernatant isolated from bacteria grown in MG media could inhibit *Nb*RD21 processing of zLR-AMC. There was a subtle but significant reduction in *Nb*RD21 activity (17%) when AF was mixed with bacterial supernatant isolated from MG media compared to the negative control (MG media without bacteria) (**Figure 5B**; ratio paired *t*-test, P=0.005). This indicates that *Pto*DC3000*ΔhQ* grown in MG media secretes an inhibitor of *Nb*RD21.

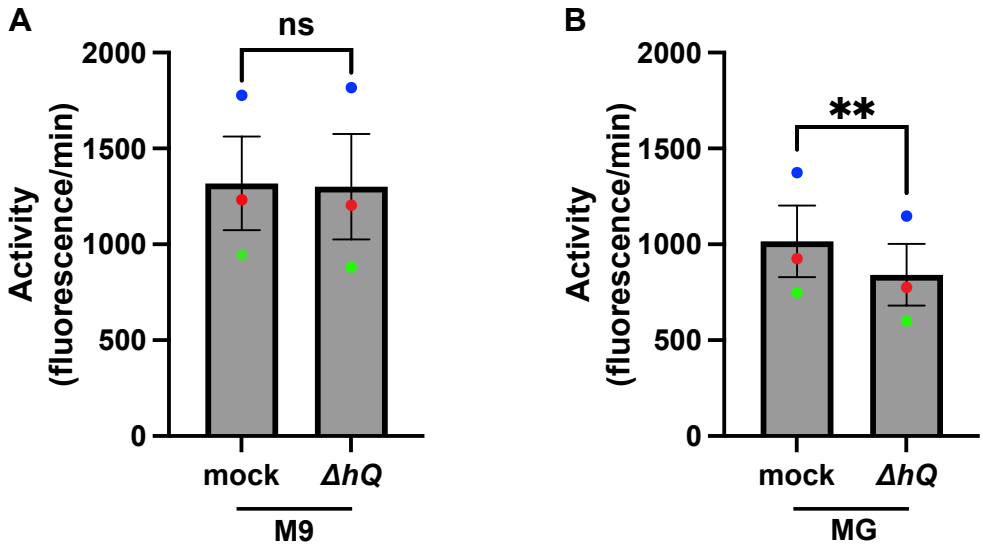


Figure 6.5: *Pto*DC3000*ΔhQ* grown in MG media, but not M9, can inhibit *Nb*RD21. Apoplastic fluid isolated from wildtype *N. benthamiana* transiently co-expressing *NbRD21* with the silencing inhibitor P19 was isolated at 4 dpi and mixed with the supernatant of *Pto*DC3000*ΔhQ* cultures grown overnight at OD_{600} = 1 in M9-fructose media (**A**) or mannitol-glutamate (MG) media (**B**). Mock samples containing only media were used as controls. After 30 minutes incubation, samples were mixed with 40 µM Z-Leu-Arg-AMC and fluorescence at 380ex/460em was measured in a plate reader. Error bars represent mean ± SE of N=3 paired biological replicates, which are distinguished by colour. Statistical significance was calculated by ratio paired *t*-test. Ns, not significant; **, P<0.01.

Finally, we tested the inhibitory activity of supernatant from *Pto*DC3000*ΔhQ* grown in Luria-Bertani (LB) broth, a peptide-rich media that suppresses *hrp* expression (Rico and Preston, 2008). To reduce the variation in activity between biological replicates caused by varying levels of transient *NbRD21* expression, we pooled the AF from several plants transiently expressing *NbRD21* into a single sample. Instead, independent isolations of bacterial supernatant were used as biological replicates.

We used the fluorescent substrate zLR-AMC to compare *Nb*RD21 inhibition by the supernatant of *Pto*DC3000*ΔhQ* grown in MG media to LB broth. We found that LB broth increases *Nb*RD21 activity compared to MG media, even in the presence of putative inhibitors (**Figure 6.6**). The salt content of LB broth is 50X higher than that of MG media, which could induce *Nb*RD21 activity (Lam et al., 2011; Mohamed Ahmed et al., 2010). Importantly, *Nb*RD21 activity was reduced by 16% after mixing with bacterial supernatant in both LB broth and MG media, but the inhibition of *Nb*RD21 activity by bacterial

supernatant in LB broth was more significant (**Figure 6.6**; one-way ANOVA with Dunnett correction; MG, P=0.0421; LB, P=0.0008). This indicates that out of the tested media, LB broth is optimal for *Nb*RD21 inhibitor production.

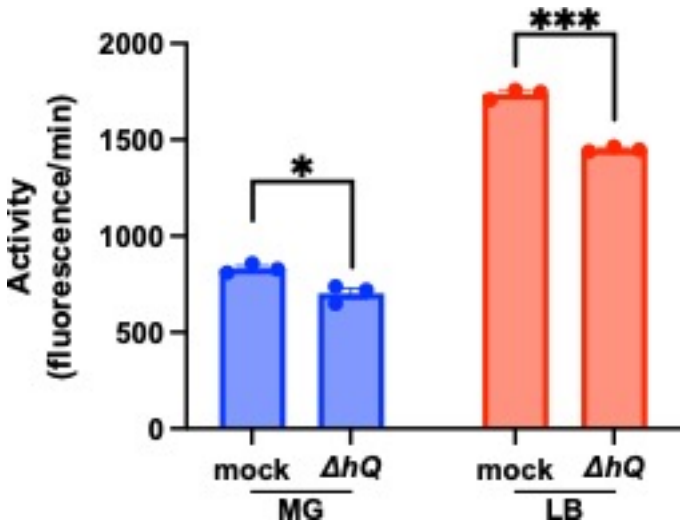


Figure 6.6: LB broth induces greater *Nb*RD21 inhibitor production than MG media. Apoplastic fluid (AF) isolated from *N. benthamiana* transiently co-expressing *NbRD21* with the silencing inhibitor P19 was isolated at 4 dpi and pooled. The AF was mixed with the supernatant of *Pto*DC3000*ΔhQ* grown overnight at OD_{600} = 1 in mannitol-glutamate (MG) media or Luria-Bertani (LB) broth. Mock samples containing MG or LB-only were used as controls. After 30 minutes preincubation, samples were mixed with 40 µM Z-Leu-Arg-AMC and fluorescence at 380ex/460em was measured in a plate reader. Cysteine protease activity of AF from plants transiently expressing an empty-vector control, and activity of samples containing putative inhibitors, was subtracted as background. Error bars represent mean ± SE of N=3 biological replicates. Statistical significance was calculated by one-way ANOVA followed by post-hoc comparison using the Dunnett test. *, P<0.05; ***, P<0.001.

6.3.4 Optimising the protocol for detecting *Nb*RD21 inhibition

We optimised our protocol to detect maximum *Nb*RD21 inhibition. First, we tested the effect of substrate concentration on *Nb*RD21 inhibition. We expected to detect increased inhibition with lower substrate concentrations due to reduced competition in binding to *Nb*RD21. The supernatant of *Pto*DC3000*ΔhQ* grown in MG media was mixed with AF from plants transiently expressing *NbRD21*. After incubation, we monitored the processing of five different concentrations of zLR-AMC. The 80 µM zLR-AMC stock was diluted 10X, 5X, 3X, 2X and 1X to give final concentrations of 4, 8, 13.3, 20 and 40 µM after mixing with *Nb*RD21

samples. The optimal concentration of fluorescent substrate was 40 μM (**Figure 6.7**), which suggests that a minimum threshold of zLR-AMC is required to monitor *Nb*RD21 inhibition.

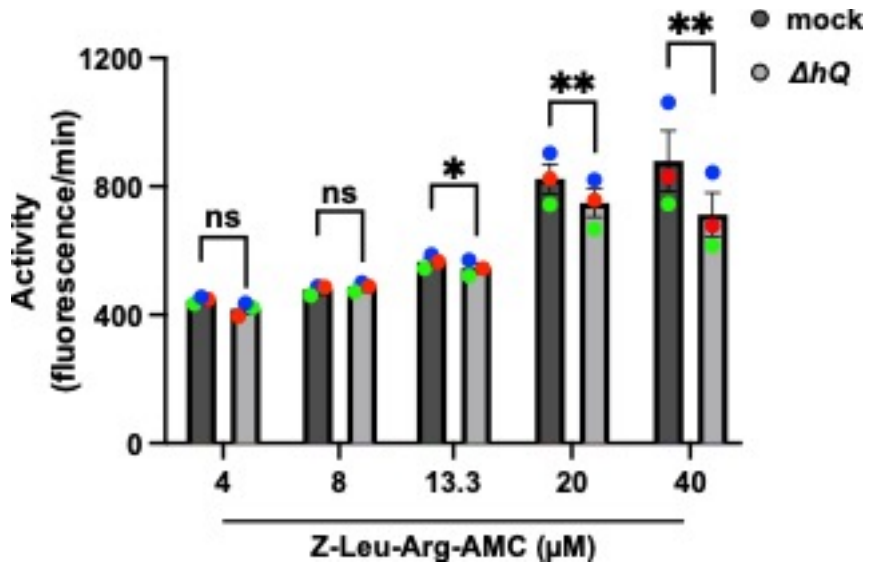


Figure 6.7: Optimising cysteine protease substrate concentration. Apoplastic fluid isolated from plants transiently co-expressing *NbRD21* with the silencing inhibitor P19 was isolated at 4 dpi and mixed with the supernatant of *Pto*DC3000*ΔhQ* grown overnight at OD_{600} = 1 in mannitol-glutamate (MG) media. After 30 minutes incubation, samples were mixed with five different concentrations of Z-Leu-Arg-AMC (μM) and fluorescence at 380ex/460em was measured in a plate reader. Error bars represent mean ± SE of N=3 paired biological replicates, which are distinguished by colour. Statistical significance was calculated by ratio-paired *t*-tests. Ns, not significant; *, P<0.05; **, P<0.01.

Second, we increased the frequency of fluorescence measurements from 20 second intervals to a final frequency interval of 15 minutes. The benefits of this were twofold. Increasing the measurement interval decreases the likelihood of fluorophore photobleaching or quenching, both of which reduce fluorescence intensity (Picciolo and Kaplan, 1984). In addition, by monitoring fluorescence over a longer time period we could observe how *Nb*RD21 activity changes over time. Rather than direct inhibition, reduced *Nb*RD21 activity in our assays could be explained by interaction with a bacterial substrate that competes with zLR-AMC for the active site of *Nb*RD21. In this scenario, *Nb*RD21 activity should eventually return to mock-treated levels once the available substrate is depleted. However, we found that the activity of *Nb*RD21 mixed with samples containing

putative inhibitors does not recover to mock-treated levels, even after several hours (**Figure 6.8**). This provides support for irreversible inhibition of *Nb*RD21. Future experiments should confirm the inhibition is irreversible by determining if elimination of excess inhibitor, by gel filtration for example, restores *Nb*RD21 activity.

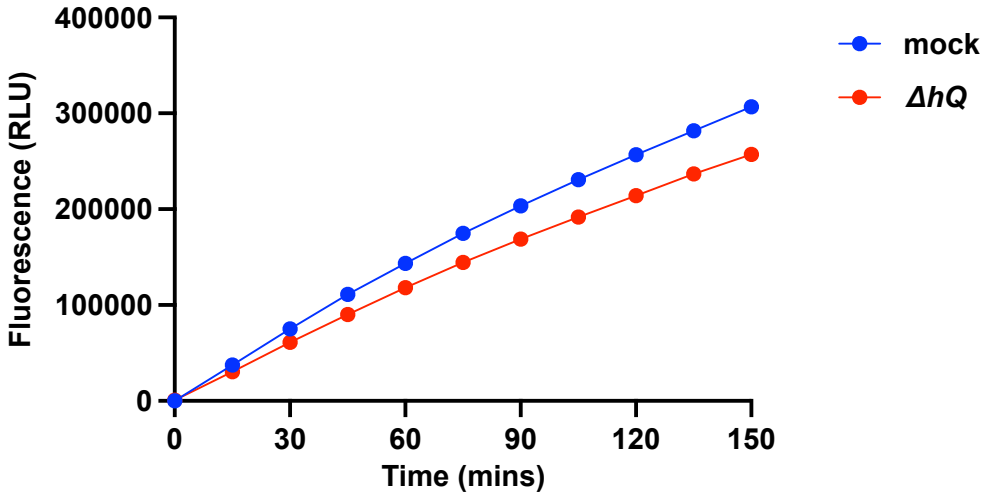


Figure 6.8: Time-course of *Nb*RD21 activity. Apoplastic fluid (AF) isolated from wildtype *N. benthamiana* transiently co-expressing *NbRD21* with the silencing inhibitor P19 was isolated at 4 dpi and pooled. The AF was mixed with the supernatant of *Pto*DC3000*ΔhQ* grown overnight at OD_{600} = 1 in Luria-Bertani (LB) broth. Mock samples containing LB-only were used as controls. After 30 minutes incubation, samples were mixed with 40 μM Z-Leu-Arg-AMC and fluorescence at 380ex/460em was measured in a plate reader in 15-minute intervals for 2.5 hours. Cysteine protease activity of AF from plants transiently expressing an empty-vector control, and samples containing putative inhibitors, was subtracted as background. Error bars (hidden beneath symbols) represent mean ± SE of N=3 biological replicates.

6.3.5 Characterisation of the inhibitor

We began to determine the biochemical characteristics of the *Nb*RD21 inhibitor. First, we separated the supernatant of *Pto*DC3000*ΔhQ* grown in LB broth into >3 and <3 kDa fractions by centrifugation through an Amicon Ultra-15 3 kDa filter. We tested the ability of each fraction to inhibit processing of zLR-AMC by *Nb*RD21 (**Figure 6.9**). As a positive control, we confirmed that the unfiltered supernatant of *Pto*DC3000*ΔhQ* grown in LB broth significantly reduced *Nb*RD21 activity compared to unfiltered LB broth without bacteria (one-way ANOVA with Dunnett correction, P=0.0036). *Nb*RD21 activity was reduced by

14% after mixing with the >3 kDa protein-rich fraction (P=0.0137). Interestingly, *Nb*RD21 activity was also reduced by 61% after mixing with the <3 kDa peptide and metabolite-rich fraction (P<0.0001). Inhibition of *Nb*RD21 activity by both fractions suggests there could be two biochemically distinct inhibitors secreted by *Pto*DC3000*ΔhQ*.

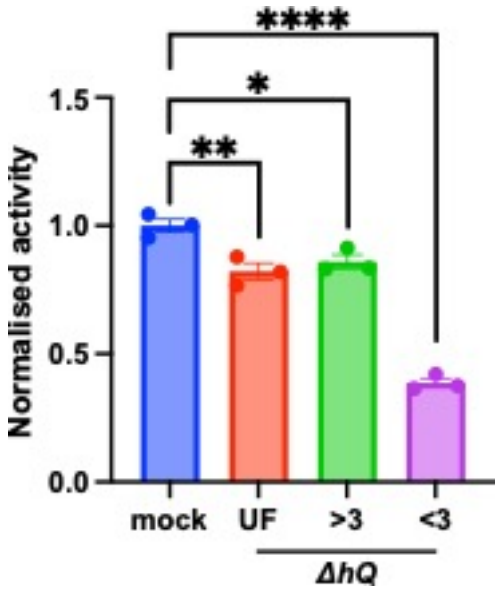


Figure 6.9: *Nb*RD21 is inhibited by distinct molecular weight fractions of *Pto*DC3000*ΔhQ* supernatant. The supernatant of *Pto*DC3000*ΔhQ* grown overnight at OD_{600} = 1 in Luria-Bertani (LB) broth was centrifuged using an Amicon Ultra-15 3 kDa filter at 4°C for 30 minutes. The supernatant (>3; kDa), flow-through (<3; kDa) and unfiltered (UF) fractions were mixed with apoplastic fluid (AF) isolated at 4 dpi and pooled from *N. benthamiana* transiently co-expressing *NbRD21* with the silencing inhibitor P19. Mock samples containing LB-only were used as controls. After 30 minutes incubation, samples were mixed with 40 µM Z-Leu-Arg-AMC and fluorescence at 380ex/460em was measured in a plate reader. Cysteine protease activity of AF from plants transiently expressing an empty-vector (EV) control, and samples containing putative inhibitors, were subtracted as background. Activity was normalised to that of the mock control. Error bars represent mean ± SE of N=3 biological replicates. Statistical significance was calculated by one-way ANOVA followed by post-hoc comparison using the Dunnett test. *, P<0.05; **, P<0.01; ****, P<0.0001.

To determine the heat-resistance of the inhibitor, AF isolated at 2 days-post infiltration from plants infected with 10^6 CFU/mL *Pto*DC3000*ΔhQ* was boiled at 95°C for five minutes and mixed with AF from plants transiently expressing *NbRD21*. Cleavage of the fluorescent substrate zLR-AMC was monitored in a plate reader (**Figure 6.10**). Unboiled AF from infected or mock (water)-infiltrated plants were used as positive and negative controls, respectively. On average, *Nb*RD21 activity was reduced by 44% after treatment with

unboiled AF from *Pto*DC3000*ΔhQ*-infected plants compared to mock treatment, although this was not quite significant (repeated-measures one-way ANOVA with Dunnett correction, P=0.0516). Nonetheless, the reduction in *Nb*RD21 activity was abolished when AF from infected plants was boiled prior to mixing (P=0.128). The detected heat-sensitivity combined with inhibitory activity of the >3 kDa fraction indicates the presence of a proteinaceous inhibitor.

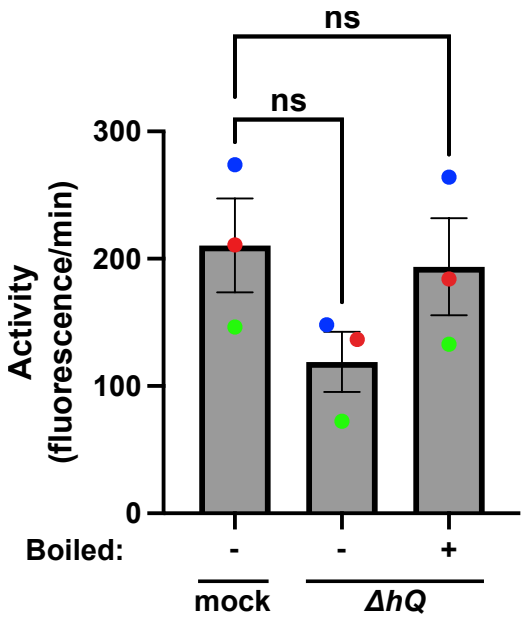


Figure 6.10: *Nb*RD21 inhibitor is probably temperature sensitive. Apoplastic fluid (AF) from *N. benthamiana* infected with 10^6 CFU/mL *Pto*DC3000*ΔhQ* or a mock (water) control was isolated at 2 dpi and pooled. An infected sample was boiled at 95°C for five minutes, samples were centrifuged, and the supernatant was collected. Samples were mixed with AF isolated at 4 dpi from *N. benthamiana* transiently co-expressing *NbRD21* with the silencing inhibitor P19. After 30 minutes incubation, samples were mixed with 40 µM Z-Leu-Arg-AMC and fluorescence at 380ex/460em was measured in a plate reader. Cysteine protease activity of AF from plants transiently expressing an empty-vector control, and samples containing putative inhibitors, was subtracted as background. Error bars represent mean ± SE of N=3 paired biological replicates, which are distinguished by colour. Statistical significance was calculated by repeated-measures one-way ANOVA followed by post-hoc comparison using the Dunnett test. Ns, not significant.

6.3.6 *Nb*RD21 inhibitor is not cip1

A previous study discovered that *Pto*DC3000 secretes Cip1 to inhibit C14, the tomato ortholog of *NbRD21* (Shindo et al., 2016). We tested whether *Pto*DC3000 lacking *Cip1*

could still inhibit *Nb*RD21. We incubated the supernatant from wildtype and *cip1* mutant (Shindo et al., 2016) *Pto*DC3000 grown in LB broth with AF from plants transiently expressing *NbRD21* and monitored processing of zLR-AMC (**Figure 6.11**). *Nb*RD21 activity was reduced by 16% in the absence of *Cip1*, similar to the wildtype control (one-way ANOVA with Dunnett correction, P<0.0001). This suggests that Cip1 is not the *Nb*RD21 inhibitor.

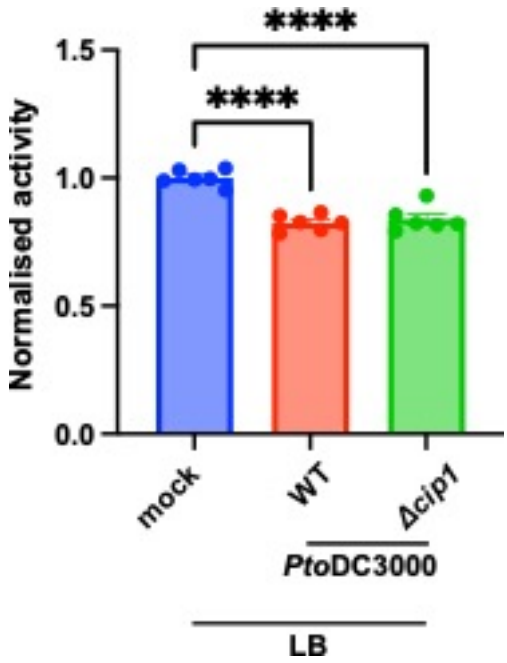


Figure 6.11: *Nb*RD21 inhibitor is still produced by *cip1* mutant *Pto*DC3000. Apoplastic fluid (AF) isolated from wildtype *N. benthamiana* transiently co-expressing *NbRD21* with the silencing inhibitor P19 was isolated at 4 dpi and pooled. The AF was mixed with the supernatant of wildtype and *cip1* mutant (*Δcip1b*; Shindo et al., 2016) *Pto*DC3000 grown overnight at OD_{600} = 1 in Luria-Bertani (LB) broth. Mock samples containing LB-only were used as controls. After 30 minutes incubation, samples were mixed with 40 µM Z-Leu-Arg-AMC and fluorescence at 380ex/460em was measured in a plate reader. Cysteine protease activity of AF from plants transiently expressing an empty-vector control, and samples containing putative inhibitors, were subtracted as background. Activity was normalised to that of the mock control. Error bars represent mean ± SE of N=6 biological replicates. Statistical significance was calculated by one-way ANOVA followed by post-hoc comparison using the Dunnett test. ****, P<0.0001.

6.3.7 Determining the breadth of *Nb*RD21 inhibition

To determine if *Nb*RD21 inhibitor production is specific to *Pto*DC3000, we tested if other *P. syringae* strains could also inhibit *Nb*RD21. First, we tested whether supernatant from *P. syringae* pv. *syringae* B728a (*Psy*B728a) and *P. syringae* pv. *tabaci* 6605 (*Pta*6605) cultures could inhibit *Nb*RD21 processing of zLR-AMC. *Pto*DC3000*ΔhQ* was included as a positive control. When bacteria were grown in MG media, none of the collected supernatants could significantly inhibit *Nb*RD21 activity (**Supplementary Figure 6.1**). In contrast, when bacteria were grown in LB broth there was a significant reduction in *Nb*RD21 activity of 18% and 19% after mixing with supernatant from *Psy*B728a and *Pta*6605, respectively (**Figure 6.12**; one-way ANOVA with Dunnett correction, $P<0.0001$). This suggests that *Psy*B728a and *Pta*6605 also produce an inhibitor of *Nb*RD21 when cultured in LB broth.

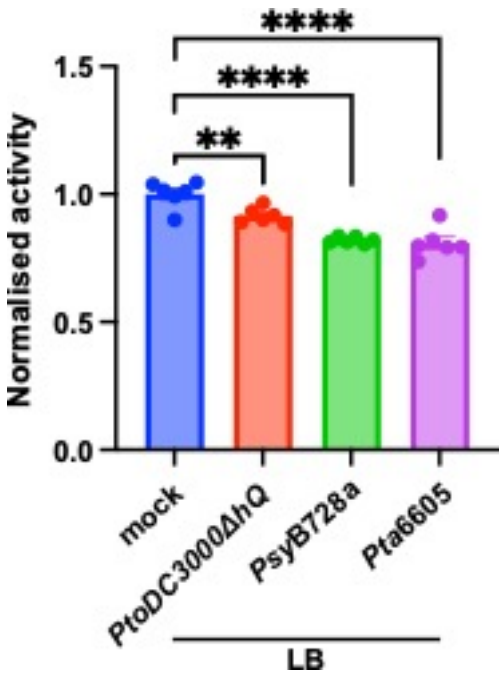


Figure 6.12: *Psy*B728a and *Pta*6605 also produce an *Nb*RD21 inhibitor
Apoplastic fluid (AF) isolated from wildtype *N. benthamiana* transiently co-expressing *NbRD21* with the silencing inhibitor P19 was isolated at 4 dpi and pooled. The AF was mixed with the supernatant of *Pto*DC3000*ΔhQ*, *Psy*B728a and *Pta*6605 grown overnight at OD_{600} = 1 in Luria-Bertani (LB) broth. Mock samples containing LB-only were used as controls. After 30 minutes incubation, samples were mixed with 40 µM Z-Leu-Arg-AMC and fluorescence at 380ex/460em was measured in a plate reader. Cysteine protease activity of AF from plants transiently expressing an empty-vector control, and samples containing putative inhibitors, were subtracted as background. Activity was normalised to that of the mock control. Error bars represent mean ± SE of N=6 biological replicates. Statistical significance was calculated by one-way ANOVA followed by post-hoc comparison using the Dunnett test. **, P<0.01; ****, P<0.0001.

Next, we tested whether 21 additional strains of *P. syringae* could inhibit *Nb*RD21. We also included *P. syringae* pv. *maculicola* ES4326, which was recently *renamed Pseudomonas cannabina* pv. *alisalensis* (Sakata et al., 2021). We isolated and filtered supernatant from bacteria grown in MG media or LB broth. Bacteria were divided into four experimental groups with *Pto*DC3000*ΔhQ* included as a positive control each time. Putative inhibitor samples were mixed with AF from plants transiently expressing *NbRD21* and we measured processing of zLR-AMC in a plate reader. When strains were grown in MG media, we only detected significant inhibition of *Nb*RD21 activity by *P. syringae* pv. *tomato* T1 (**Supplementary Figure 6.2**; repeated-measures one-way ANOVA with Dunnett correction, P=0.0405). In contrast, every *P. syringae* strain grown in LB broth significantly reduced *Nb*RD21 activity by 6-30% relative to the LB-only control (**Figure 6.13**). This

suggests that growth in LB broth induces production of an *Nb*RD21 inhibitor that is ubiquitous to *P. syringae*.

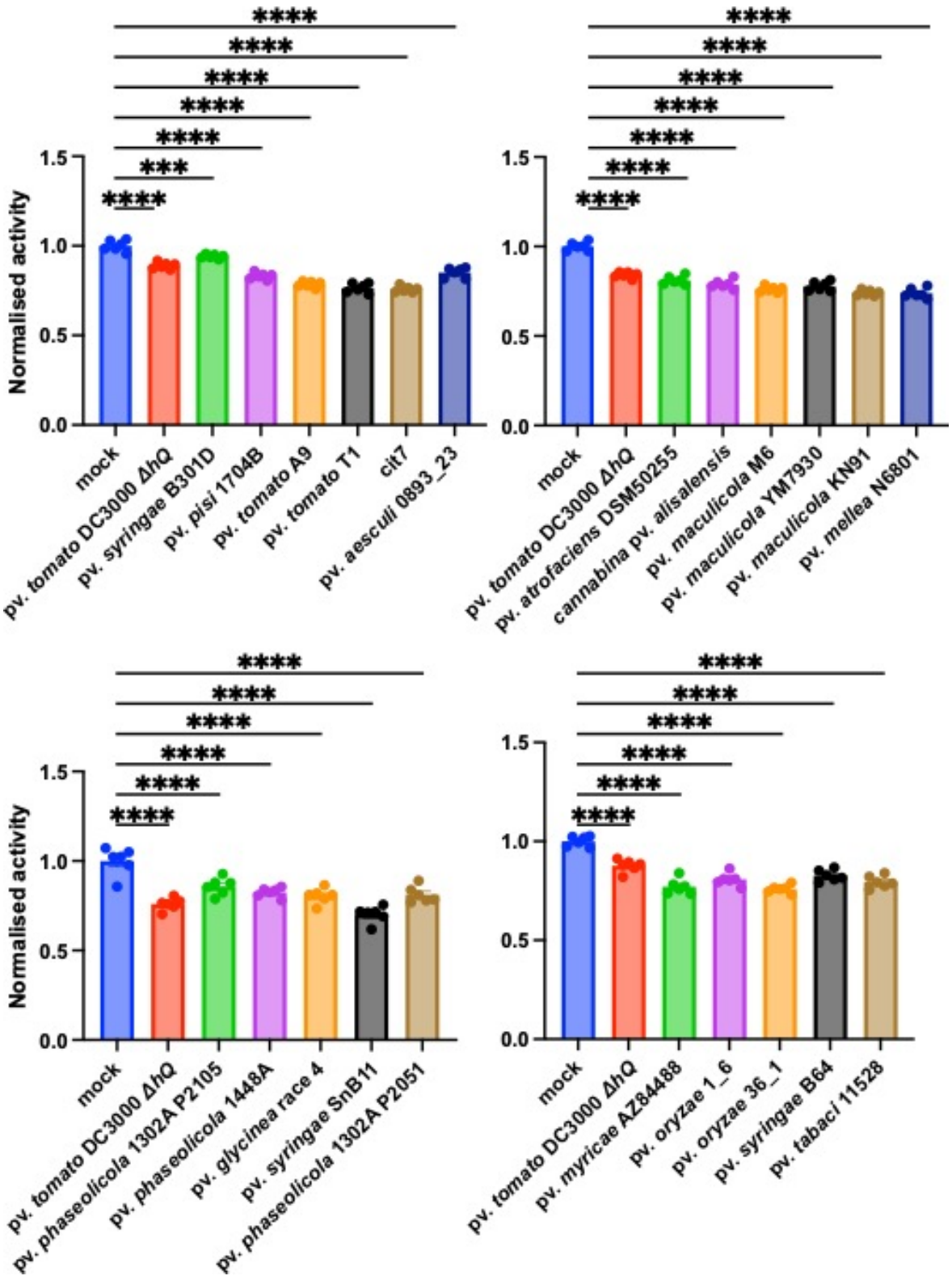


Figure 6.13: Screen of *Nb*RD21 inhibition by *Pseudomonas* strains grown in LB broth. Apoplastic fluid (AF) isolated from wildtype *N. benthamiana* transiently co-expressing *NbRD21* with the silencing inhibitor P19 was isolated at 4 dpi and pooled. The AF was mixed with the supernatant of 22 *Pseudomonas* strains grown overnight at OD_{600} = 1 in Luria-Bertani (LB) broth. Untreated LB broth (mock) and PtoDC3000*ΔhQ* supernatant were used as negative and positive controls, respectively. After 30 minutes incubation, samples were mixed with 40 µM Z-Leu-Arg-AMC and fluorescence at 380ex/460em was measured in a plate reader. Cysteine protease activity of AF from plants transiently expressing an empty-vector control, and samples containing putative inhibitors,

were subtracted as background. Activity was normalised to that of the mock control. Error bars represent mean ± SE of N=6 biological replicates. Statistical significance was calculated by one-way ANOVA followed by post-hoc comparison using the Dunnett test. ***, P<0.001; ****, P<0.0001.

6.3.8 *Nb*RD21 inhibition by multiple species of bacteria

The ubiquitous inhibition of *Nb*RD21 activity by the supernatant of bacteria grown in LB broth warranted further investigation. It is possible that *Nb*RD21 inhibition is an artefact of changes in LB broth upon bacterial growth which are detrimental to *Nb*RD21 activity, rather than the existence of a specific inhibitor. We searched for a bacterial species that could not inhibit *Nb*RD21 to use as a negative control.

We grew *Agrobacterium tumefaciens* GV3101 and *Escherichia coli* DH10β in LB broth overnight at OD_{600} = 1 with N=6 biological replicates. *Pto*DC3000*ΔhQ* was used as a positive control. Cultures were centrifuged and the collected supernatant was filtered and mixed with a pooled AF sample isolated from plants transiently expressing *NbRD21*. After 30 minutes incubation, we monitored *Nb*RD21 activity using the fluorescent substrate zLR-AMC. We found that supernatant from both *A. tumefaciens* (one-way ANOVA with Dunnett correction, P=0.0002) and *E. coli* (P<0.0001) was able to significantly reduce *Nb*RD21 activity compared to a mock (LB) control (**Figure 6.14A**). Therefore, this experiment does not rule out *Nb*RD21 inhibition being due to changes in media composition (such as pH, oxidation, salt levels) upon bacterial growth.

To test this, we separated the supernatant from *A. tumefaciens* grown in LB broth into >3 and <3 kDa fractions by centrifugation through an Amicon Ultra-15 3 kDa filter. If the reduction in *Nb*RD21 activity was due to a change in environmental composition rather than a bona fide inhibitor, then only the <3 kDa fraction would inhibit *Nb*RD21. Both the >3 kDa (one-way ANOVA with Dunnett correction, P=0.002) and <3 kDa (P<0.0001) fractions

significantly reduced *Nb*RD21 activity (**Figure 6.14B**). Inhibition by the former fraction is evidence for a ubiquitous, proteinaceous inhibitor rather than an artefact of bacterial growth.

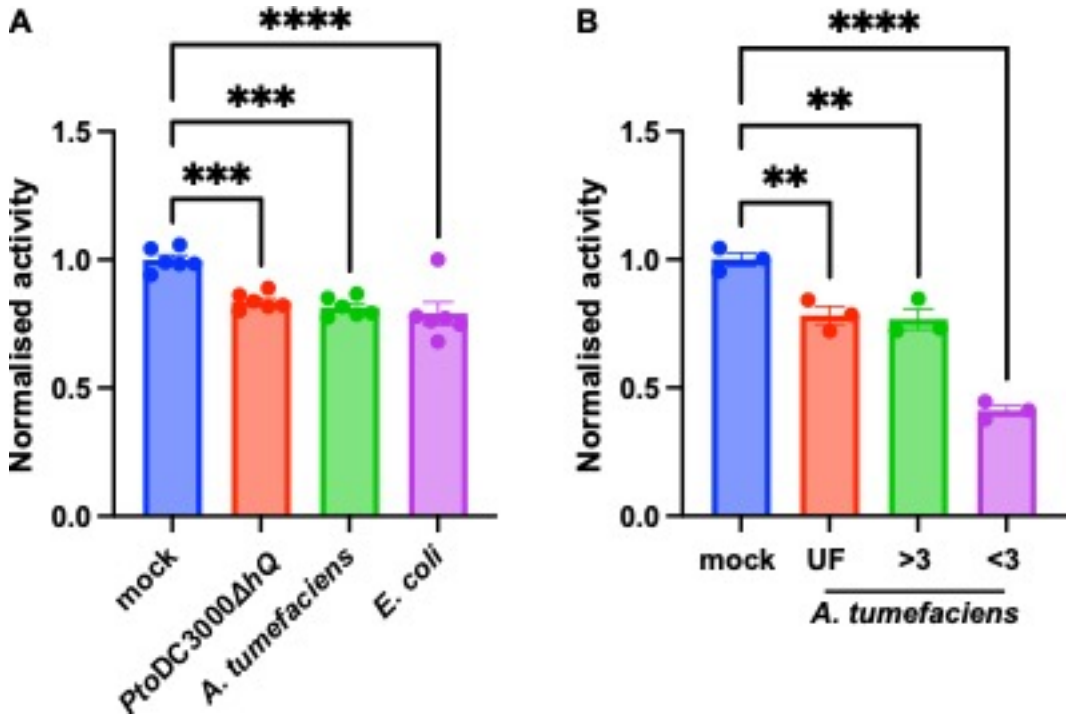


Figure 6.14: Culture supernatants from unrelated bacterial species inhibit *Nb*RD21 activity.
A: *A. tumefaciens* and *E. coli* culture supernatant inhibits *Nb*RD21. Apoplastic fluid (AF) isolated from plants transiently co-expressing *NbRD21* with the silencing inhibitor P19 was isolated at 4 dpi and pooled. The AF was mixed with the supernatant of *A. tumefaciens and E. coli* grown overnight at OD_{600} = 1 in Luria-Bertani (LB) broth. Untreated LB broth (mock) and PtoDC3000*ΔhQ* supernatant were used as negative and positive controls, respectively. After 30 minutes incubation, samples were mixed with 40 µM Z-Leu-Arg-AMC and fluorescence at 380ex/460em was measured in a plate reader. Cysteine protease activity of AF from plants transiently expressing an empty-vector control, and samples containing putative inhibitors, were subtracted as background. Activity was normalised to that of the mock control. Error bars represent mean ± SE of N=6 biological replicates. Statistical significance was calculated by one-way ANOVA followed by post-hoc comparison using the Dunnett test. ***, P<0.001; ****, P<0.0001.
B: *Nb*RD21 is inhibited by distinct molecular weight fractions of *A. tumefaciens* supernatant. The supernatant of *A. tumefaciens* grown overnight at OD_{600} = 1 in Luria-Bertani (LB) broth was centrifuged using an Amicon Ultra-15 3 kDa filter at 4°C for 30 minutes. The supernatant (>3; kDa), flow-through (<3; kDa) and unfiltered (UF) fractions were mixed with apoplastic fluid (AF) isolated at 4 dpi and pooled from plants transiently co-expressing *NbRD21* with the silencing inhibitor P19. Mock samples containing untreated LB broth were used as controls. After 30 minutes incubation, samples were mixed with 40 µM Z-Leu-Arg-AMC and fluorescence at 380ex/460em was measured in a plate reader. Cysteine protease activity of AF from plants transiently expressing an empty-vector control, and samples containing putative inhibitors, were subtracted as background. Activity was normalised to that of the mock control. Error bars represent mean ± SE of N=3 biological replicates. Statistical significance was calculated by one-way ANOVA followed by post-hoc comparison using the Dunnett test. **, P<0.01; ****, P<0.0001.

6.4 Discussion

In this chapter, we used two distinct methods to confirm that *Nb*RD21 is inhibited by *Pto*DC3000*ΔhQ*. We developed and optimised a high-throughput assay for detecting *Nb*RD21 inhibition in a plate reader using the fluorescent cysteine protease substrate zLR-AMC and used this to determine the size and heat-sensitivity of the inhibitor. Finally, we found evidence that the *Nb*RD21 inhibitor is not Cip1 and is produced by multiple bacterial species.

Convolution ABPP can detect *Nb*RD21 inhibition

We used the fluorescent TK009 probe to monitor *Nb*RD21 inhibition by convolution ABPP. We detected a significant reduction in *Nb*RD21 signal intensity when samples were mixed prior to labelling compared to mixing labelled samples (**Figure 6.1**). However, there are limitations to inhibitor identification by convolution ABPP. First, convolution ABPP is a time-consuming method requiring a three-hour probe incubation step and subsequent separation by SDS-PAGE. Sample size is also limited by the size of the acrylamide gel. Both factors make the approach relatively low throughput. Furthermore, using software to estimate intensity of fluorescent signals is inherently subjective and may be confounded by multiple proteins accumulating at the same molecular weight.

Generating a rapid assay for detecting *Nb*RD21 inhibition

Considering these limitations, we developed a higher-throughput method for detecting *Nb*RD21 inhibition. We used the fluorescent cysteine protease substrate zLR-AMC to monitor the activity of *Nb*RD21 mixed with AF or supernatant containing putative inhibitors. Our first challenge was to identify and discount cysteine protease activity that was not caused by transiently expressed *Nb*RD21. We subtracted fluorescence caused by bacteria

and other plant cysteine proteases as background, although effects of this correction were minimal since the activity of *Nb*RD21 samples was 50X higher than that of EV samples (**Figure 6.3**). This indicates that most cysteine protease activity is attributable to transiently expressed *NbRD21*. We obtained the same result when we mixed *Nb*RD21 samples with supernatant from bacteria grown in LB broth (**Supplementary Figure 6.3**). Due to this, AF from plants transiently expressing *NbRD21* was always diluted 2-5 fold before incubation with putative inhibitors, to ensure fluorescent signals were within the signal detection limits of the plate reader. On average, *Nb*RD21 activity was reduced by 57% after mixing with AF from plants infected with *Pto*DC3000*ΔhQ* compared to AF from mock-infiltrated plants (**Figure 6.3**). We determined that this reduction in activity is due to inhibition, rather than degradation of *Nb*RD21, because *Nb*RD21 protein levels are unchanged (**Figure 6.4**). Importantly, we used *rd21* mutants because endogenous *Nb*RD21 is likely to be upregulated by infection (Kaschani et al., 2010). This ensured that western blotting only detected accumulation of transiently expressed *Nb*RD21.

Clarifying the source of *Nb*RD21 inhibition

We needed to clarify that the inhibition was derived from a bacterial inhibitor rather than a plant response to infection. For example, cysteine proteases are susceptible to oxidation which is detrimental to their activity (Lalmanach et al., 2020; Petushkova and Zamyatnin, 2020). Free oxidative species generated in the apoplast by plants in response to pathogen invasion could inhibit *Nb*RD21. The initial rapid oxidative burst upon pathogen recognition takes place long before mixing of samples in our experiments, but there are secondary sources of oxidation produced later (Qi et al., 2017). Polyamines are small aliphatic, hygroscopic amines that are produced by the host in response to pathogen invasion (Wang et al., 2019b). Terminal catabolism of polyamines generates hydrogen peroxide, which could oxidise *Nb*RD21. Alternatively, pathogenesis-related proteins such as apoplastic peroxidases are induced upon infection and catalyse the production of reactive oxygen

species which could inhibit *Nb*RD21 (Farvardin et al., 2020). We tried to prevent oxidation by measuring *Nb*RD21 activity in the presence of the reducing agent dithiothreitol (DTT). However, experiments should be repeated using tris(2-carboxyethyl)phosphine (TCEP), which is a more powerful and stable reducing agent than DTT (Getz et al., 1999). In addition, the original ABPP-MS experiments on which this thesis is based (Sueldo et al., 2023) could be repeated by monitoring apoplastic hydrolase dynamics upon treatment with purified PAMPs, rather than bacterial infection. This would clarify if the inhibition is due to a plant immune response or direct suppression by the pathogen. Nonetheless, we performed subsequent experiments using supernatant from bacteria grown *in vitro* to discount the possibility of plant-derived inhibition.

We found that the supernatant of bacteria grown in M9-fructose media was unable to inhibit *Nb*RD21 activity, whilst MG media facilitated subtle but significant *Nb*RD21 inhibition (**Figure 6.5**). The most significant inhibition was detected when bacteria were grown in LB broth (**Figure 6.6**). Many gram-negative bacteria utilise the T3SS to shuttle effector proteins into host cells (Deng et al., 2017). Minimal medias such as M9 and MG are good activators of the T3SS because they mimic apoplastic conditions that activate *hrp* expression such as low pH, the presence of simple sugars including fructose, and the absence of sources of complex carbon or nitrogen (Mole et al., 2007, Sanguankiattichai, 2021). Conversely, these properties are absent in LB broth, suggesting that inhibitor delivery is independent of the T3SS and production may require peptides or other compounds such as iron found in rich growth media (Bronstein et al., 2008). Future experiments should confirm this by testing if *hrp* mutants lacking T3SS structural or regulatory genes can still inhibit *Nb*RD21.

Biochemical characterisation suggests the *Nb*RD21 inhibitor is proteinaceous

We began to determine the biochemical properties of the *Nb*RD21 inhibitor. We found that *Nb*RD21 could be inhibited by two distinct molecular weight fractions (>3 and <3 kDa,

Figure 6.9). Further, we found that boiling AF from plants infected with *Pto*DC3000*ΔhQ* abolished *Nb*RD21 inhibition, suggesting that the inhibitor is heat-sensitive (**Figure 6.10**). Inhibitory activity of the >3 kDa fraction, together with the finding of heat-sensitivity, is indicative that that the inhibitor might be proteinaceous. Future experiments should confirm this by testing if the precipitate of chloroform-methanol extraction can inhibit *Nb*RD21, or inhibition is abolished by the addition of proteinase K to samples containing the putative inhibitor (Ebeling et al., 1974), Ultimately, protein identity must be confirmed by mass-spectrometry.

The inhibitory activity of the <3 kDa fraction is puzzling and can be explained by multiple scenarios. First, there may be two distinct inhibitors of different molecular weights produced by *Pto*DC3000*ΔhQ*. The small inhibitor is more likely to be a small protein or peptide than a metabolite due to heat-sensitivity (**Figure 6.10**). Second, there may only be a single <3 kDa inhibitor, and inhibition from the >3 kDa fraction is a result of incomplete filtration. Finally, inhibition from the <3 kDa fraction could be explained by changes to the properties of the media upon bacterial growth, rather than production of an inhibitor. Bacteria dynamically alter the composition of their environment as they grow, including the pH and sugar content, which could influence *Nb*RD21 activity (Smith et al., 2018). Nonetheless, the heat-sensitivity of *Nb*RD21 inhibition supports the existence of a bona fide inhibitor, although this experiment should be repeated using minimal media as an inhibitor source rather than AF from infected plants, to clarify that this heat-sensitive inhibitor is not plant-derived.

Many more properties of the *Nb*RD21 inhibitor await clarification. For instance, methanol-chloroform precipitation can be used to determine if the inhibitor is hydrophilic or hydrophobic by detecting inhibitory activity from the methanol or chloroform fractions, respectively. If the inhibitor is basic it will bind to cation-exchange resin, and finally the pH

stability of the inhibitor can be determined by incubating supernatants containing putative inhibitors with acids or bases and testing if they can still inhibit *Nb*RD21.

Determining the novelty and breadth of the *Nb*RD21 inhibitor

We tested whether the secreted *Pto*DC3000 effector Cip1, inhibitor of tomato C14, is also the *Nb*RD21 inhibitor. We detected a significant reduction in *Nb*RD21 activity even when *Cip1* was absent from *Pto*DC3000, which implies our identified inhibitor is not Cip1 (**Figure 6.11**, **Supplementary Figure 6.4**). Furthermore, Cip1 is predicted to be a lipoprotein anchored to the bacterial cell membrane (pseudomonas.com genome database; PSPTO4211), and hence should not be present in our tested supernatant samples, which were filtered to remove bacteria. Finally, Cip1 cannot be responsible for the <3 kDa inhibitory activity, since the protein accumulates at 16 kDa (Shindo et al., 2016).

Next, we tested if production of the *Nb*RD21 inhibitor was specific to *Pto*DC3000, or ubiquitous to *P. syringae* strains. When bacteria were grown in MG media, we could not detect inhibition of *Nb*RD21 activity (**Supplementary Figure 6.1-6.2**). This could be due to high variability between samples, or the multiple comparisons correction could have prevented detection of robust inhibition, given the large number of comparisons made in each experiment (Rothman, 1990). Furthermore, the absence of inhibition from the positive control suggests poor inhibitor production in MG media. However, we found that the supernatant isolated from *Psy*B728a, *Pta*6605 and 22 additional *Pseudomonas* strains grown in LB broth significantly reduced *Nb*RD21 activity compared to a mock (LB) control (**Figure 6.12**-**13**).

The ubiquitous inhibition of *Nb*RD21 activity led us to test other species of bacteria, both to clarify the breadth of inhibitor production and identify a negative control to verify our results. The supernatant of both *A. tumefaciens* and *E. coli* grown in LB broth significantly inhibited

*Nb*RD21 activity (**Figure 6.14A**). This could indicate that the detected *Nb*RD21 inhibition is an artefact of changes in LB broth composition during bacterial growth, rather than production of a specific, ubiquitous *Nb*RD21 inhibitor. To exclude this possibility, future experiments should test additional species of bacteria to identify a negative control that cannot inhibit *Nb*RD21. Alternatively, if an unrelated cysteine protease is also inhibited by bacterial supernatants, then the reduction in activity is likely due to changes in environmental composition rather than specific inhibition. Regardless, we found that *Nb*RD21 is inhibited by a >3 kDa fraction from *A. tumefaciens* culture supernatant. This indicates the presence of an inhibitor rather than simply a media composition change (**Figure 6.14B**). Still, future work should exclude the possibility that the reduced fluorescence is caused by *Nb*RD21 interacting with bacterial substrates, rather than inhibitors. For instance, the overnight bacterial cultures that we used to isolate putative inhibitors are likely to contain dead and lysed bacterial cells, which could release potential protein substrates for plant proteases such *Nb*RD21.

Future steps to identify the *Nb*RD21 inhibitor

Insights into inhibitor production can be gained using mutants lacking key virulence factor biosynthesis genes. To confirm that *Nb*RD21 inhibitor production is independent of the T3SS or the GacS/GacA regulatory system, inhibition assays should include bacteria lacking *hrcC*, *gacS* and *gacA* (Guo et al., 2009; Heeb and Haas, 2001). Interestingly, *P. syringae* strains containing *avrD* deliver syringolide elicitors to host cells independently of the T3SS (Okinaka et al., 2002). Syringolide recognition by the soybean receptor Rpg4 triggers the hypersensitive response mediated by its interaction with the soybean allergen P34, which is an inactive cysteine protease (Okinaka et al., 2002), making syringolide a good candidate *Nb*RD21 inhibitor. The *avrD* gene is present in several *P. syringae* strains including pv. *glycinea* and pv. *tomato* T1 and there is even evidence for horizontal transfer of *avrD* genes to other bacterial species (Almeida et al., 2009; Hanekamp et al., 1997).

However, *avrD* genes are absent from pv. *tomato* DC3000, so syringolide cannot be the inhibitor (Hulin et al., 2018).

The toxin coronatine is synthesised by *Pto*DC3000 independently of the T3SS using both polyketide synthesis and non-ribosomal peptide synthase pathways and performs a variety of virulence functions, including mediating stomatal opening (Geng et al., 2014). Coronatine can inhibit the activity of proteases including chymopapain (Bender et al., 1999; Palmer and Bender, 1995). In fact, drought-induced resistance to *Pto*DC3000 is mediated by *At*RD21A and bacterial growth is significantly increased in a coronatine-defective mutant *Pst*-DB29 in the absence of *AtRD21A* (Liu et al., 2020). The importance of coronatine in *Nb*RD21 inhibition could be tested using coronatine-defective mutants such as *Pst*-DB29 (Elizabeth and Bender, 2007). Furthermore, mutants defective in polyketide and non-ribosomal peptide biosynthesis pathways could determine if these pathways regulate *Nb*RD21 inhibitor biosynthesis, similar to other small virulence factors (Bender et al., 1999).

To ultimately identify the inhibitor biosynthesis genes, a forward genetic screen could be applied, as was done previously to identify genes responsible for production of the BGAL1 inhibitor (Sanguankiattichai, 2021). Briefly, a *Pto*DC3000 mutant library generated using random transposon insertion mutagenesis could be screened to identify inhibitors of *Nb*RD21 in a 384-well plate format using the fluorescent substrate zLR-AMC. Alternatively, *Nb*RD21 inhibition can be monitored using a polarisation screen with a fluorescent cysteine protease ABPP probe (FluoPol-ABPP; Bachovchin et al., 2009). If a mutant no longer inhibits *Nb*RD21, then a transposon must have been inserted into a gene involved in inhibitor biosynthesis or regulation. Transposon insertion sites can be identified by sequencing the products of inverse PCR (Ochman et al., 1988). Candidate biosynthesis genes should be verified with genomic expression data during infection. If the *Nb*RD21 inhibitor is indeed conserved across multiple *P. syringae* strains (and even bacterial species), then we would expect these strains to all carry the inhibitor biosynthesis genes.

If the inhibitor is a metabolite, then the ultimate goal is to purify the inhibitor and elucidate its structure. Purification of a metabolite would involve fractionation according to biochemical characteristics, followed by high-performance liquid chromatography (HPLC) (Graham, 1991). For instance, the BGAL1 inhibitor galactosyrin was enriched by coupling cation exchange resin with hydrophilic interaction liquid chromatography (HILIC) HPLC (Sanguankiattichai, 2021). Conversely, proteinaceous inhibitors can be identified using yeast two-hybrid or coimmunoprecipitation followed by mass-spectrometry, with *Nb*RD21 as bait (Brückner et al., 2009; Lin and Lai, 2017). For example, yeast two-hybrid screening using the *Ralstonia solanacearum* effector PopP2 as bait identified an interaction with Arabidopsis RD19 (Bernoux et al., 2008). Furthermore, coimmunoprecipitation was previously coupled to mass-spectrometry to identify *N. benthamiana* proteins interacting with the *Phytophthora infestans* effector AvrBlb2 (Bozkurt et al., 2011) and the plant nucleotide-binding leucine-rich repeat Rx (Sacco et al., 2007).

Finally, it would be interesting to uncover the effect that NbRD21 inhibition has on the activity and degradation of receptor-like kinases (RLKs) such as *Nb*FERONIA and *Nb*BAM1. We previously found that these RLKs accumulate in *rd21* plants (**Figure 5.13**; **Figure 5.17**). It would be prudent to test if these results are replicated upon *P. syringae* infection.

6.5 Conclusion

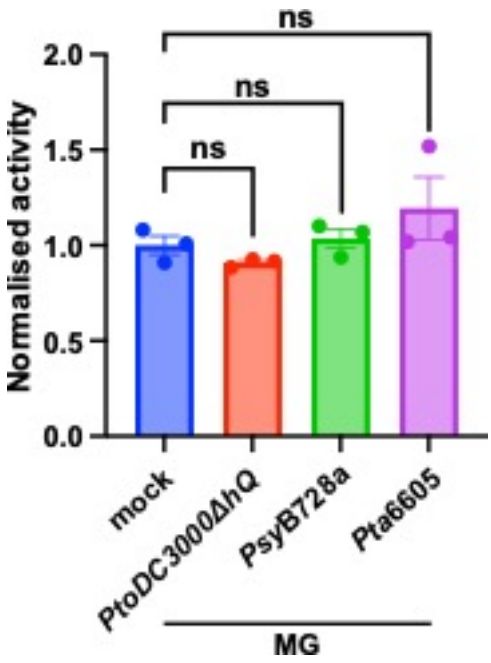
In this chapter, we confirmed that *Nb*RD21 activity is suppressed by an inhibitor produced both *in vivo* and *in vitro*. This inhibitor is novel, heat-sensitive, and inhibition is detected in two distinct molecular weight fractions. Our data suggests that a combination of both changes to growth media composition upon bacterial growth, and a bona fide secreted

inhibitor not restricted to *P. syringae*, are responsible for the observed reduction in *Nb*RD21 activity.

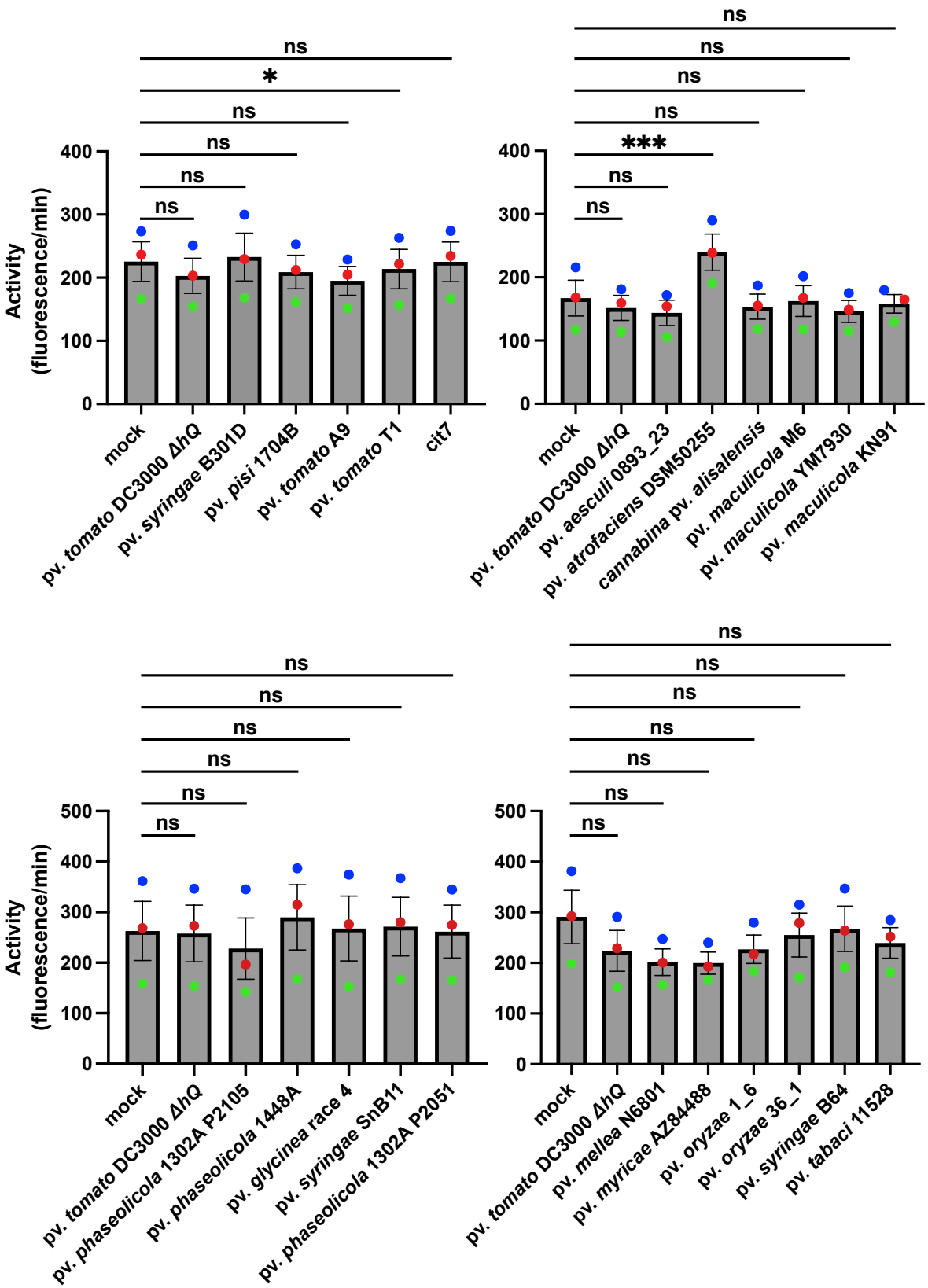
6.6 Contributions

The α-triticain-α antibody was donated by Andrey Zamyatnin, Sechenov First Moscow State Medical University.

6.7 Supplementary Figures

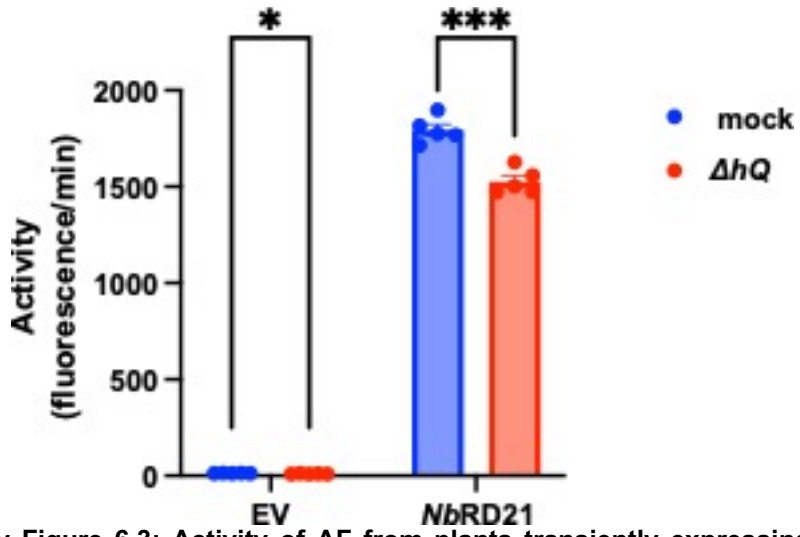


Supplementary Figure 6.1: *Psy*B728a and *Pta*6605 grown in MG media do not inhibit *Nb*RD21 Apoplastic fluid (AF) isolated from wildtype plants transiently co-expressing *NbRD21* with the silencing inhibitor P19 was isolated at 4 dpi and pooled. The AF was mixed with the supernatant of *Pto*DC3000*ΔhQ*, *Psy*B728a and *Pta*6605 cultures grown overnight at OD_{600} = 1 in mannitol-glutamate (MG) media with N=3 biological replicates. Mock samples containing MG-only were used as controls. After 30 minutes incubation, samples were mixed with 40 μM Z-Leu-Arg-AMC and fluorescence at 380ex/460em was measured in a plate reader. Cysteine protease activity of AF from plants transiently expressing an empty-vector control, and samples containing putative inhibitors, were subtracted as background. Activity was normalised to that of the mock control. Error bars represent mean ± SE of N=3 biological replicates. Statistical significance was calculated by one-way ANOVA followed by post-hoc comparison using the Dunnett test. Ns, not significant.

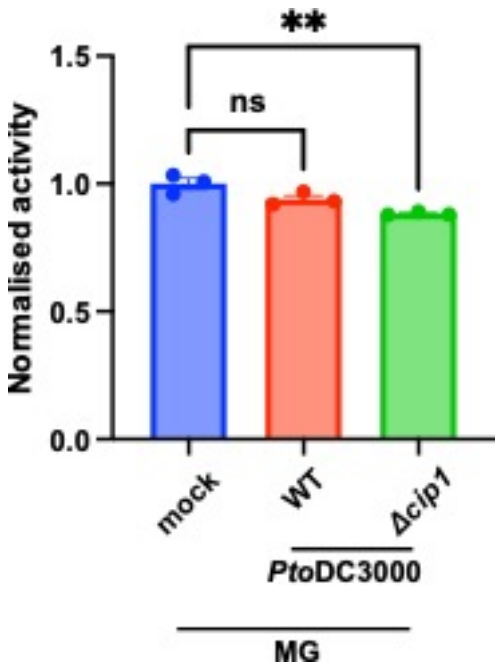


Supplementary Figure 6.2: Screen of *Nb*RD21 inhibition by *Pseudomonas* strains grown in MG media. Apoplastic fluid isolated from plants transiently co-expressing *NbRD21* with the silencing inhibitor P19 was isolated at 4 dpi with N=3 biological replicates and mixed with the supernatant of 22 *Pseudomonas* strains grown overnight at OD_{600} = 1 in mannitol-glutamate (MG) media in four experimental groups. Untreated MG media (mock) and *Pto*DC3000*ΔhQ* supernatant were used as negative and positive controls, respectively. After 30 minutes incubation, samples were mixed with 40 µM Z-Leu-Arg-AMC and fluorescence at 380ex/460em was measured in a plate reader. Cysteine

protease activity of AF from plants transiently expressing an empty-vector control, and samples containing putative inhibitors, were subtracted as background. Error bars represent mean ± SE of N=3 paired biological replicates, which are distinguished by colour. Statistical significance was calculated by repeated-measures one-way ANOVA followed by post-hoc comparison using the Dunnett test. Ns, not significant; *, P<0.05; ***, P<0.001.



Supplementary Figure 6.3: Activity of AF from plants transiently expressing *NbRD21* is a proxy for *Nb*RD21 activity. Apoplastic fluid (AF) isolated from wildtype *N. benthamiana* transiently co-expressing *NbRD21* or an empty-vector (EV) control with the silencing inhibitor P19 was isolated at 4 dpi and pooled. The AF was mixed with the supernatant of *Pto*DC3000*ΔhQ* grown overnight at OD_{600} = 1 in Luria-Bertani (LB) broth with N=6 biological replicates. Mock samples containing LB-only were used as controls. After 30 minutes incubation, samples were mixed with 40 μM Z-Leu-Arg-AMC and fluorescence at 380ex/460em was measured in a plate reader. Cysteine protease activity of samples containing putative inhibitors was subtracted as background. Error bars represent mean ± SE of N=6 biological replicates. Statistical significance was calculated by one-way ANOVA followed by post-hoc comparison using the Dunnett test. *, P<0.05; ***, P<0.001.



Supplementary Figure 6.4: *Nb*RD21 inhibitor is still produced by *cip1* mutant *Pto*DC3000 grown in MG media. Apoplastic fluid (AF) isolated from plants transiently co-expressing *NbRD21* with the silencing inhibitor P19 was isolated at 4 dpi and pooled. The AF was mixed with the supernatant of wildtype and *cip1* (*Δcip1b*; Shindo et al., 2016) mutant *Pto*DC3000 grown overnight at OD_{600} = 1 in mannitol-glutamate (MG) media with N=3 biological replicates. Mock samples containing MG-only were used as controls. After 30 minutes incubation, samples were mixed with 40 µM Z-Leu-Arg-AMC and fluorescence at 380ex/460em was measured in a plate reader. Cysteine protease activity of AF from plants transiently expressing an empty-vector control, and samples containing putative inhibitors, were subtracted as background. Activity was normalised to that of the mock control. Error bars represent mean ± SE of N=3 biological replicates. Statistical significance was calculated by one-way ANOVA followed by post-hoc comparison using the Dunnett test. Ns, not significant; **, P<0.01.

6.8 Methods

Plant growth conditions – *N. benthamiana* was grown in a growth chamber at room temperature with a 16-hour light cycle and 60% humidity and watered on alternating days.

Bacterial strains – bacterial strains used in this chapter are summarised in Table **6.1**.

Table 6.1: Bacterial strains used in this chapter.

Name	Description	Reference
P. syringae pv. *tomato* DC3000	Wildtype	Buell et al., 2003
P. syringae pv. *tomato* DC3000ΔhQ	*P. syringae* pv. *tomato* DC3000 lacking the *hopQ1-1* effector	Wei et al., 2007
P. syringae pv. *tomato* DC3000Δcip1b	*P. syringae* pv. *tomato* DC3000 with a non-polar mutation in *cip1*	Shindo et al., 2016
P. syringae pv. *syringae* B728a	Wildtype	Feil et al., 2005
P. syringae pv. *tabaci* 6605	Wildtype	Matsui et al., 2021
P. syringae pv. *syringae* B301D	Wildtype	Dudnik and Dudler., 2014
P. syringae pv. *pisi* 1704B	Wildtype	Baltrus et al., 2011
P. syringae pv. *tomato* A9	Wildtype	Thapa and Coaker, 2016
P. syringae pv. *tomato* T1	Wildtype	Almeida et al., 2009
P. syringae cit7	Wildtype	Baltrus et al., 2011
P. syringae pv. *aesculi* 0893_23	Wildtype	Ma et al., 2007
P. syringae pv. *atrofaciens* DSM50255	Wildtype	Ranković et al., 2023
P. syringae pv. *maculicola* ES4326	Wildtype	Stavrinides and Guttman., 2004
P. syringae pv. *maculicola* M6	Wildtype	Debener et al., 1991
P. syringae pv. *maculicola* YM7930	Wildtype	Guttman et al., 2006
P. syringae pv. *maculicola* KN91	Wildtype	Shinohara, 2014
P. syringae pv. *phaseolicola* 1302A P2105	Wildtype	Taylor et al., 1996
P. syringae pv. *phaseolicola* 1448A	Wildtype	Joardar et al., 2005
P. syringae pv. *glycinea* race 4	Wildtype	Kobayashi et al., 1989
P. syringae SnB11	Wildtype	Fones et al., 2016
P. syringae pv. *phaseolicola* 1302A P2051	Wildtype	Taylor et al., 1996
P. syringae pv. *mellea* N6801	Wildtype	Shinohara, 2014
P. syringae pv. *myricae* AZ84488	Wildtype	Shinohara, 2014
P. syringae pv. *oryzae* 1_6	Wildtype	Baltrus and Clark, 2020
P. syringae pv. *oryzae* 36_1	Wildtype	Kuwata, 1985
P. syringae pv. *syringae* B64	Wildtype	Dudnik and Dudler, 2013
P. syringae pv. *tabaci* 11528	Wildtype	Studholme et al., 2009
A. tumefaciens GV3101	Derivative of *A. tumefaciens* C58 carrying pMP90 plasmid	Koncz and Schell., 1986
E. coli DH10B	Chemically competent *E. coli*	Thermo Fisher Scientific EC0113

Molecular cloning – constructs used in this chapter are summarised in **Table 6.2**. Method for cloning pPB034 is described in **Chapter 3.8**.

Table 6.2: Constructs used in this chapter

Name	Description	Reference
P19	Binary 35S::P19	Van der Hoorn et al., 2003
pJK001c	Binary empty vector (EV)	Paulus et al., 2020
pPB034	Binary 35S::*Nb*RD21	This work

Agroinfiltration – performed as described in **Chapter 3.8**.

Apoplastic fluid (AF) isolation – see **Chapter 3.8**.

Bacterial growth medias – recipes are as follows:

- Luria-Bertani (LB) broth: 10 g/L tryptone, 5 g/L yeast extract, 10 g/L NaCl
- Mannitol-glutamate (MG) medium (Bronstein et al., 2008): 10 g/L mannitol, 2 g/L L-glutamic acid, 0.5 g/L KH_2PO_4, 0.2 g/L NaCl, 0.2 g/L $MgSO_4.7H_2O$, pH 7.
- M9 medium: 6 g/L Na_2HPO_4, 3 g/L KH_2PO_4, 0.5 g/L NaCl, 1 g/L NH_4Cl, 0.1 mM $CaCl_2$, 2 mM $MgSO_4$, 22 mM sugar fructose, pH 7

Isolation of material containing putative inhibitors – For *in vivo* inhibitor production, *Pto*DC3000*ΔhQ* cultures were grown for 24 hours in LB broth at 28°C and inoculated into 4-week-old *N. benthamiana* leaves at 10^6 CFU/mL. *N. benthamiana* infiltrated with milliQ water was used as a mock treatment. Two days later, AF from infected and mock-treated leaves was isolated, pooled, and passed through a 0.22 µM pore syringe filter (Merck-Millipore, SLGP033RS). For *in vitro* inhibitor production, bacteria were grown in LB broth for 24 hours at 28°C (*P. syringae*, no antibiotic; *A. tumefaciens*, kanamycin 50 µg/mL and gentamicin 10 µg/mL) or 8 hours at 37°C (*E. coli*, kanamycin 50 µg/mL). Cultures were

centrifuged at 3,500 *g* for 10 minutes at room temperature, washed with milliQ water and resuspended in M9-fructose, mannitol-glutamate media or LB broth at OD_{600} = 1. After incubation at 28°C (*P. syringae*, *A. tumefaciens*) or 37°C (*E. coli*) overnight, cultures were centrifuged at 3,500 *g* for 10 minutes at room temperature. Culture supernatants were extracted and passed through a 0.22 µM pore syringe filter. Samples were used immediately or flash-frozen in liquid nitrogen and stored at -20°C.

Convolution ABPP – Apoplastic fluid was collected from *N. benthamiana* leaves transiently expressing *NbRD21* and the silencing inhibitor P19 at 4 days post infiltration with N=3 biological replicates. The supernatant of *Pto*DC3000*ΔhQ* grown in mannitol-glutamate media was collected as above. Active cysteine proteases were labelled using 2 µM TK009 (Sueldo et al., 2023) as described previously (**Chapter 3.8**). Two additional sample groups were created. To create the 'mix-label' sample, 107.5 µL AF from *N. benthamiana* leaves transiently expressing *NbRD21* with the silencing inhibitor P19 was mixed with 107.5 µL bacterial supernatant. Samples were mixed thoroughly and incubated at room temperature for 30 minutes before labelling with 2 µM TK009. After 3 hours incubation with the probe, the reaction was stopped by precipitation in 4x ice-cold acetone followed by resuspension in 4x gel loading buffer (200 mM Tris-HCl pH 6.8, 400 mM dithiotreitol, 8% SDS, 40% glycerol, 0.04% bromophenol blue) and heating at 90°C for 5 minutes. To create the 'label-mix' sample, 5 µL of labelled AF samples was mixed with 5 µL labelled bacterial supernatant immediately before loading onto acrylamide gels. Proteins were separated by SDS-PAGE and visualised using a Typhoon scanner with Cy5 filter. Intensity of fluorescent signals was quantified using Fiji (Schindelin et al., 2012).

zLR-AMC inhibition assay – Apoplastic fluid from 4-week-old *N. benthamiana* leaves transiently expressing *NbRD21* or empty-vector (EV) with the silencing inhibitor P19 was isolated at 4 days post infiltration. *Nb*RD21 samples were diluted 2-5X in milliQ water, depending on transient expression levels, to prevent fluorescence exceeding the detection

limits of the plate reader (values were corrected during analysis). Samples were mixed with 50 µL putative inhibitor sample or a mock control (apoplastic fluid from water-infiltrated plants, or growth media without bacteria) and incubated for 30 minutes at room temperature. Cysteine protease activity was measured using the fluorogenic substrate Z-Leu-Arg-7-amino-4-methylcoumarin (zLR-AMC, R&D Systems). 10 µL mixed proteome was mixed with 4-40 µM zLR-AMC in a black 96-well plate in the presence of 2.5 mM DTT and 31.25 mM sodium acetate pH 5 at a final reaction volume of 100 µL. Fluorescence at 380 nm excitation / 460 nm emission was recorded in a plate reader (Tecan Infinite M200) at 0.3-15 minute intervals for up to 3 hours. Activity attributable to cysteine proteases, both plant and bacterial, other than transiently expressed *NbRD21* was subtracted as background. Activity was calculated by change in fluorescence over time. When biological replicates were independent apoplastic fluid isolations from plants transiently expressing *NbRD21*, P-values were determined by ratio-paired *t*-tests or repeated-measures one-way ANOVA. When biological replicates were independent isolations of putative inhibitor, P-values were determined by one-way ANOVA. Where appropriate, P-values were corrected for multiple comparisons by Šidák or Dunnett correction.

Western blot – Western blotting was performed as previously described (**Chapter 4.8**). Briefly, after 30 minutes incubation, 40 µL of mixed samples (AF from plants transiently expressing *NbRD21* mixed with putative inhibitor samples) was aliquoted into clean 1.5 mL Eppendorf tubes. Proteins were precipitated with ice-cold acetone and samples were boiled at 90°C for 5 minutes. Proteins were separated by SDS-PAGE and transferred to a PVDF membrane. After blocking in 5% milk with PBS-T, the membrane was incubated overnight in α-triticain-α (3:10,000, Andrey Zamyatnin) at room temperature. The next day, the membrane was washed and incubated in α-Rabbit HRP (GE Healthcare NA934V, 1:1000) in 5% milk in PBS-T for one hour at room temperature. Clarity Western ECL substrate (Bio-Rad) was used for signal detection and signal intensity was quantified using Fiji (Schindelin et al., 2012).

Chapter 7: General discussion

This thesis focused on uncovering the role of suppressed hydrolases during *Pseudomonas syringae* infection. We identified *Nb*PR3, a glycosyl hydrolase with a potential function in bacterial elicitor release, despite its annotation as an endochitinase. We also identified *Nb*RD21, a papain-like cysteine protease that appears to have an effector-triggered immunity (ETI)-dependent function in immunity. We uncovered a role for *Nb*RD21 in receptor-like kinase (RLK) processing and began to characterise a bacterial inhibitor that suppresses *Nb*RD21 activity.

7.1 A novel method to detect plant immune hydrolases

In **Chapter 3**, we utilised a novel technique to identify plant immune hydrolases through their suppression. By coupling ABPP to mass-spectrometry (MS), the activity of 171 hydrolases in the *Nicotiana benthamiana* apoplast was simultaneously monitored during infection with *P. syringae* (Sueldo et al., 2023). The activity of 60 of these hydrolases was suppressed upon bacterial infection compared to a mock treatment, suggesting their involvement in the immune response. We transiently expressed six of the sixty suppressed hydrolases in *N. benthamiana* and tested their role in immunity using 'agromonas' assays. We identified positive roles for *Nb*PR3 and *Nb*RD21, a success rate of 33%. This suggests that, of the remaining 53 hydrolases (excluding the previously identified ß-galactosidase BGAL1), immune functions for approximately 18 more could await discovery. This method of immune hydrolase discovery is unique because other methods only monitor single hydrolase-inhibitor interactions. For example, coimmunoprecipitation performed on tomato apoplastic fluid containing FLAG-tagged Kazal-like inhibitor EPI1 identified an interaction with P69 subtilases (Tian et al., 2004), and yeast two-hybrid using type III effector PopP2 as bait uncovered its interaction with *At*RD19 (Bernoux et al., 2008). This thesis provides

evidence that ABPP-MS is a more efficient and rapid method of detecting many potential immune hydrolases simultaneously.

However, the suppression of apoplastic hydrolases should be addressed with caution. Even if a hydrolase is suppressed upon infection, this is not necessarily achieved through direct inhibition. Suppression can also be achieved through the absence of cofactors (da Fonseca-Pereira et al., 2023), allostery (Byun et al., 2020) or post-translational modifications (Kokkinidis et al., 2020). Even if suppression is achieved through competitive inhibition, the inhibitor is not necessarily pathogen derived. For example, if the hydrolase negatively regulates immunity, then its activity may be suppressed by an endogenous inhibitor upon infection to initiate the defence response. For example, *Arabidopsis thaliana* (Arabidopsis) RPM1-interacting protein 4 (RIN4) negatively regulates PAMP-triggered immunity and is phosphorylated upon pathogen invasion to derepress the defence response (Ray et al., 2019). Positive and negative regulators of defence were distinguished by 'agromonas' assays in **Chapter 3**, but the remaining 53 hydrolases await identification. For example, the significant increase in susceptibility to *P. syringae* pv. *tomato* DC3000*ΔhQ* upon transient expression of *NbFla1* suggests it could be a negative regulator of immunity, although we were unable to confirm expression (**Figure 3.5**). Alternatively, suppression may reflect changes to apoplastic conditions upon bacterial growth that are unfavourable to hydrolase activity (Kesten et al., 2019; O'Leary et al., 2016; Tahir et al., 2019). Untangling direct and indirect hydrolase inhibition was a recurring theme throughout the thesis, also impeding characterisation of the *Nb*RD21 inhibitor in **Chapter 6**. This highlights the need for careful interpretation of results and the requirement of the appropriate controls when monitoring hydrolase inhibition.

Characterisation of the role of the remaining suppressed hydrolases in immunity is a clear next step. Alternative methods of monitoring pathogen growth could increase the efficiency of hydrolase characterisation. Bioluminescent *P. syringae* strains expressing the *lux* operon

have recently been generated and could rapidly and objectively monitor bacterial viability as an alternative to the 'agromonas' assays used here (Soldan et al., 2021). In addition, bioinformatic analysis of suppressed hydrolases could be used to identify those most likely to perform immune functions, in order to concentrate time and resources. For example, immune hydrolases are likely to be induced upon infection, show evidence of positive selection imposed by pathogen inhibitors, and contain immune-associated GO-term domains (**Chapter 2**; Godson and van der Hoorn, 2021).

7.2 The challenges of identifying biological substrates

In **Chapters 4** and **5**, we attempted to characterise the biological functions of *Nb*PR3 and *Nb*RD21. In **Chapter 4**, we showed that *Nb*PR3 is not a functioning endochitinase, but does require catalytic activity to perform its immune function. We identified a *Nicotiana*-specific glutamate to glutamine substitution at the catalytic general base that is essential for bacterial defence. It would be interesting to determine if other *Nicotiana* PR3s containing this substitution (**Figure 4.6**) similarly confer bacterial resistance. We were unable to identify a substrate for *Nb*PR3 and future work must focus on optimising and performing the glycan array to determine *Nb*PR3 glycan affinity. Still, we did uncover a potential role for *Nb*PR3 in elicitor release because AF from plants transiently expressing *Nb*PR3 triggered an elevated oxidative burst response to *P. syringae* (**Figure 4.16**). Oxidative burst assays using *N. benthamiana* mutants lacking key elicitor pattern-recognition receptors should be used in combination with results from the glycan array to identify the *Nb*PR3 substrate. Nonetheless, in this chapter we identified two important considerations for future work: 1) the need to optimise transient protein expression. Transformation efficiency can differ greatly between individual plants or even leaves of the same plant, increasing variation between replicates and obscuring immune phenotypes (**Figure 4.16**). 2) the benefit of gene silencing or knockout in deciphering immune functions. As a pathogenesis-

related (PR) protein, endogenous *Nb*PR3 levels are induced by infection (**Figure 4.2**). When coupled with poor transient expression in agroinfiltrated plants, there is often negligible difference in *Nb*PR3 accumulation between *NbPR3*-expressing plants and controls. Due to this, immune phenotypes can be obscured. For instance, BGAL1 expression only increases the oxidative burst in a *bgal1* background (**Figure 4.16**; Buscaill et al., 2019).

In **Chapter 5**, we studied the function of *Nb*RD21. We showed that *Nb*RD21 requires catalytic activity to confer bacterial resistance. We used both transiently expressed *NbRD21* and two independent *rd21* mutant lines to test hypotheses for the immune function of *Nb*RD21. We found no evidence that *Nb*RD21 directly reduces bacterial growth, induces PR protein accumulation, confers resistance to *Phytophthora infestans* or promotes release of a bacterial elicitor. However, we used MS to compare the proteomes of wildtype and *rd21* plants and identified a role for *Nb*RD21 in RLK processing. However, this experiment was performed using material from unchallenged plants. In future, this experiment should be repeated using infected or stressed plant material to determine if this is also the mechanism by which *Nb*RD21 mediates bacterial immunity.

The precise substrates of *Nb*RD21 in both infected and unchallenged conditions await discovery. To this end, alternative proteomic methods could be used to maximise identification of differential protein groups in *rd21* mutant plants and identify the specific substrates of *Nb*RD21 (Thomas, 2020). High-Efficiency Undecanal-based N-Termini EnRichment (HUNTER) could be used to compare the N-terminomes of wildtype and *rd21* plants (Weng et al., 2019). In this technique, protein amines from proteomes with differential protease accumulation are blocked with amine-reactive agents. Trypsin digest generates new non-N-terminal peptides that are attached to hydrophobic hexadecanal. This allows their retention on a liquid chromatography column, whilst N-terminal peptides pass through and are analysed by mass-spectrometry (Weng et al., 2019). This technique could be

combined with an investigation of the cleavage site preference of *Nb*RD21 using Proteomic Identification of protease Cleavage Sites (PICS; Biniossek et al., 2016). In PICS, proteomes are digested with trypsin and differentially incubated with the candidate protease. The cleavage products are then labelled and analysed by mass-spectrometry to determine the protease's cleavage site motif preference. Proteins identified by HUNTER that contain the preferred cleavage site motif of *Nb*RD21 identified using PICS are strong candidates to be the direct substrates of *Nb*RD21.

Both the glycan array and the above proteomics techniques are likely to uncover multiple potential substrates. Identifying which of these are biologically relevant represents a future challenge. For example, *Nb*PR3 may bind to substrates in the glycan array that are not naturally produced by either *N. benthamiana* or *P. syringae*. Furthermore, it is still unclear whether the putative elicitor released by *Nb*PR3 is pathogen-derived (microbe-associated molecular pattern) or host-derived (damage-associated molecular pattern). Positive hits from the glycan array will therefore need to be carefully checked against the extracellular glycomes of both organisms. For *Nb*RD21, substrate identification could be hindered by redundancy between hydrolases. Multiple hydrolases may cleave the same substrate, preventing the detection of differential cleavage profiles between wildtype and *rd21* plants. This could explain the subtle disease phenotype we observed in *rd21* mutants, despite their strong biochemical phenotype (**Figure 5.7-5.8**). Similarities in cleavage specificity have been described for some proteases, such as VPEs and subtilases (Paulus et al., 2020; Vorster et al., 2019). Potential redundancy between hydrolases can be inferred by proteomics data. Several proteases are significantly upregulated in *rd21* plants, suggesting they could act redundantly with *Nb*RD21, and their expression is induced as a compensatory mechanism. Still, if a redundant hydrolase is activated by suppression of an endogenous inhibitor rather than induced expression then it may be undetected by proteomics techniques. Furthermore, it is not always possible to predict redundancy because cleavage may be dependent on substrate conformation rather than specific target

sequence (Thomas, 2020). In addition, catalytic activity prediction programmes are not infallible – look no further than *Nb*PR3 for evidence of this. Ultimately, advances in cleavage redundancy prediction tools and detailed analyses of individual hydrolases, such as those described in this thesis, will pave the way towards a better understanding of hydrolase activities.

7.3 The importance of hydrolase localisation and regulation

An important theme throughout this thesis is the importance of regulating hydrolase activity, both at the activity level and the localisation level. This regulation can be both pathogen and plant derived.

7.3.1 Pathogen-derived regulators

Both *Nb*PR3 and *Nb*RD21 are suppressed at the activity level upon infection. This suppression could be caused by a bacterial inhibitor since both are required for host resistance. Future identification of a potential *Nb*PR3 inhibitor is dependent on establishment of an assay to monitor *Nb*PR3 activity. Advances in inhibitor discovery should also capitalise on the rapidly developing field of machine learning. Programmes such as Alphafold can be used to predict interactions between secreted *P. syringae* proteins and structural models of hydrolases, which could guide inhibitor identification (Tsuchiya et al., 2022).

In **Chapter 6** we began to uncover the bacterial inhibitor of *Nb*RD21. The high activity of PLCPs along with the availability of fluorescent probes and substrates make it relatively easy to monitor their inhibition (Petushkova et al., 2022). Indeed, inhibition of *Nb*RD21 orthologs has already been described (Clark et al., 2018; Kaschani et al., 2010; Shindo et

al., 2016). We highlighted the difficulty of untangling pathogen-derived inhibition from host inhibition, both direct and indirect. Because of this, we isolated putative inhibitors from bacteria grown *in vitro* to exclude the possibility of monitoring host-derived inhibition. We found evidence that the *Nb*RD21 inhibitor is not cip1, is heat-sensitive and >3 kDa. However, many questions regarding the nature of the inhibitor remain unanswered, including the secretion system utilised by *P. syringae* to deliver the inhibitor, the genes required for inhibitor production and regulation, and further biochemical characterisation. It would also be interesting to uncover the evolution of the inhibitor, if the inhibitor is indeed secreted by several bacterial species.

Pathogen-derived effectors that mediate hydrolase re-localisation have been explored for other immune proteases and are discussed in a published review (**Chapter 2**). Whether *P. syringae* secretes effectors that mediate re-localisation of *Nb*PR3 and *Nb*RD21 as an infection strategy is a potential avenue of future research.

7.3.2 Plant-derived regulators

As a PR protein, *Nb*PR3 is induced upon infection as part of the plant stress response and is secreted into the apoplast (**Figure 4.2**). *Nb*PR3 appears to have a strict substrate specificity which likely limits the outcomes of its hydrolytic activity (**Figure 4.9**). Therefore, regulation of *Nb*PR3 activity is likely focused on its timely expression, rather than controlled suppression.

Orthologs of *Nb*RD21 are induced upon infection (Avrova et al., 1999; Clark et al., 2018) and potential activation of *Nb*RD21 by VPEs has been discussed previously (Thomas, 2020). *Nb*RD21 is a highly active protease (**Figure 5.7**) with many potential substrates (**Figure 5.13**). Therefore, in contrast to *Nb*PR3 we expect that controlled suppression of *Nb*RD21 activity plays a more critical role in its regulation. Orthologs of *Nb*RD21 are

inhibited by the endogenous regulators PDI5 (Andème Ondzighi et al., 2008), Serpin1 (Lampl et al., 2013) and WSCP (Rustgi et al., 2017). Suppression of *Nb*RD21 by an endogenous regulator is evidenced by the significantly reduced accumulation of a cystatin in *rd21* plants (**Figure 5.13**), suggesting it is no longer required to regulate *Nb*RD21 (Martinez and Diaz, 2008).

*Nb*PR3 and *Nb*RD21 are both secreted into the *N. benthamiana* apoplast. However, the localisation of *Nb*RD21 orthologs (Bozkurt et al., 2011; Gu et al., 2012; Shindo et al., 2016) as well as the labelling of *Nb*RD21 in total leaf extract (**Figure 5.7**) suggest that *Nb*RD21 also accumulates within the cell. The dynamic localisation of *Nb*RD21 is likely an important factor contributing to its regulation. *Nb*RD21 is a highly active protease and may have a relatively low substrate specificity. Indeed, the 45 proteins accumulating significantly more in *rd21* plants could be substrates of *Nb*RD21 (**Figure 5.13**) and Arabidopsis RD21 rapidly degrades rubisco after treatment with SDS (Gu et al., 2012). It is likely that *Nb*RD21 function is therefore partially determined by substrate availability based on controlled localisation, rather than substrate specificity. Indeed, the cysteine protease inhibitor PDI5 colocalises with *At*RD21A and inhibits its activity during trafficking to the vacuoles before the initiation of programmed cell death (Andème Ondzighi et al., 2008). We propose that an important trigger for *Nb*RD21 relocalisation is infection with avirulent bacteria, which causes fusion of the vacuole with the plasma membrane and the putative release of *Nb*RD21 into the apoplast (Hatsugai et al., 2009). This exposes *Nb*RD21 to a new substrate pool, enabling the protease to suppress bacterial growth. Several other proteases have dual localisation in the vacuole and apoplast, suggesting that this could be a common mechanism of ETI-dependent immunity waiting to be uncovered. For example, the PLCPs ALP, CathB and RD19 have been detected in the apoplast of *N. benthamiana* (**Chapter 3**, Gilroy et al., 2007, Grosse-Holz et al., 2018) and vacuoles of Arabidopsis (Bernoux et al., 2008; Carter et al., 2004), suggesting they may also have dual localisation. Indeed, if this was a general

mechanism for plant immune proteases, it would explain the subtle susceptibility phenotype of the *rd21* plants.

It remains to be determined whether the role of *Nb*RD21 in RLK processing is distinct from its role in resistance to avirulent bacteria. We found evidence that *Nb*RD21 is involved in the processing of both immune and developmental RLKs, but it is unclear whether processing takes place inside or outside the cell. The putative vacuolar location of *Nb*RD21 under both unchallenged conditions and infection with virulent bacteria, combined with the accumulation of potential intracellular substrates such as vacuolar-sorting receptors in *rd21* plants, suggests that *Nb*RD21 performs an intracellular RLK processing function that is distinct from its apoplastic immune function. On the other hand, *Nb*RD21 released into the apoplast upon bacteria-induced membrane fusion could interact with RLKs at the plasma membrane, linking ETI to receptor-mediated endocytosis. The dynamic re-localisation of proteases can make identifying the location of hydrolase function a challenge. For instance, tomato phytaspase is secreted into the apoplast and reimported into the cell upon cell death (Chichkova et al., 2010) and the cotton subtilase *Gb*SBT1 relocates from the apoplast to the cytosol upon infection with *Verticillium dahliae* (Duan et al., 2016). Furthermore, vacuolar fusion with the plasma membrane during ETI often blurs the distinction between cellular compartments. Proteomics data using apoplastic fluid isolated from *rd21* plants along with localisation studies using fluorescent-tagged *Nb*RD21 will ultimately clarify the distinct functions of *Nb*RD21 in different cellular compartments.

7.4 Overall conclusions and future perspectives

Our current knowledge of plant immunity only begins to scratch the surface of this complex and multi-layered response. The application of this understanding to the development of resistant crops necessitates uncovering immune hydrolase functions at the molecular level.

In this thesis, we investigated the results of a previous experiment that simultaneously monitored the activity of 171 hydrolases in the *N. benthamiana* apoplast upon *P. syringae* infection. We identified *Nb*PR3, a glycosyl hydrolase that lacks endochitinase activity but has gained a function in bacterial resistance, underpinned by a substitution in its catalytic general base. Future work should determine if other *Nicotiana* PR3 proteins also confer bacterial resistance and clarify the role of *Nb*PR3 in elicitor release.

This thesis also identified the PLCP *Nb*RD21 as having an ETI-dependent function in bacterial resistance. Future efforts should determine if this represents a general mechanism of resistance to avirulent pathogens, or if this is unique to *Nb*RD21. Indeed, *Nb*RD21 is clearly an active and abundant protease with a striking effect on the plant proteome. Our proteomics data identified 54 proteins that are directly or indirectly affected by the absence of *Nb*RD21. We demonstrated a role for *Nb*RD21 in RLK processing, but additional targets await further discovery. Finally, we began characterisation of the *Nb*RD21 inhibitor. Biochemical characterisation, evolution of inhibitor production and identification of genes underpinning inhibitor biosynthesis represent exciting avenues of future research.

Bibliography

1. Ahuja, I., Kissen, R., Bones, A.M. 2012. Phytoalexins in defense against pathogens. Trends in Plant Science **17**, 73–90. https://doi.org/10.1016/j.tplants.2011.11.002

2. Alam MM, Nakamura H, Ichikawa H, Miyao A, Hirochika H, Kobayashi K, Yamaoka N, Nishiguchi M. 2014. Response of an aspartic protease gene *Os*AP77 to fungal, bacterial and viral infections in rice. Rice **7**, 9.

3. Alfano, J.R., Collmer, A. 2004. Type III secretion system effector proteins: double agents in bacterial disease and plant defense. Annual Review of Phytopathology **42**, 385–414. https://doi.org/10.1146/annurev.phyto.42.040103.110731

4. Ali, K., Li, W., Qin, Y., Wang, S., Feng, L., Wei, Q., Bai, Q., Zheng, B., Li, G., Ren, H., Wu, G. 2022. Kinase Function of Brassinosteroid Receptor Specified by Two Allosterically Regulated Subdomains. Frontiers in Plant Science **12**.

5. Ali, S., Ganai, B.A., Kamili, A.N., Bhat, A.A., Mir, Z.A., Bhat, J.A., Tyagi, A., Islam, S.T., Mushtaq, M., Yadav, P., Rawat, S., Grover, A. 2018. Pathogenesis-related proteins and peptides as promising tools for engineering plants with multiple stress tolerance. Microbiological Research **212–213**, 29–37. https://doi.org/10.1016/j.micres.2018.04.008

6. Ali, Y.B., Verger, R., Abousalham, A. 2012. Lipases or esterases: does it really matter? Toward a new bio-physico-chemical classification. Methods in Molecular Biology Clifton NJ **861**, 31–51. https://doi.org/10.1007/978-1-61779-600-5_2

7. Almeida, N.F., Yan, S., Lindeberg, M., Studholme, D.J., Schneider, D.J., Condon, B., Liu, H., Viana, C.J., Warren, A., Evans, C., Kemen, E., Maclean, D., Angot, A., Martin, G.B., Jones, J.D., Collmer, A., Setubal, J.C., Vinatzer, B.A. 2009. A draft genome sequence of *Pseudomonas syringae* pv. *tomato* T1 reveals a type III effector repertoire significantly divergent from that of *Pseudomonas syringae* pv. *tomato* DC3000. Molecular Plant-Microbe Interactions MPMI **22**, 52–62. https://doi.org/10.1094/MPMI-22-1-0052

8. Anand, A., Uppalapati, S.R., Ryu, C.-M., Allen, S.N., Kang, L., Tang, Y., Mysore, K.S. 2008. Salicylic Acid and Systemic Acquired Resistance Play a Role in Attenuating Crown Gall Disease Caused by *Agrobacterium tumefaciens*. Plant Physiology **146**, 323–324. https://doi.org/10.1104/pp.107.111302

9. Andème Ondzighi, C., Christopher, D.A., Cho, E.J., Chang, S.-C., Staehelin, L.A. 2008. Arabidopsis Protein Disulfide Isomerase-5 Inhibits Cysteine Proteases during Trafficking to Vacuoles before Programmed Cell Death of the Endothelium in Developing Seeds. Plant Cell **20**, 2205–2220. https://doi.org/10.1105/tpc.108.058339

10. Andersen, M.D., Jensen, A., Robertus, J.D., Leah, R., Skriver, K. 1997. Heterologous expression and characterization of wild-type and mutant forms of a 26 kDa endochitinase from barley (*Hordeum vulgare L.*). Biochemistry Journal **322**, 815–822.

11. Araki, T., Torikata, T. 1995. Structural Classification of Plant Chitinases : Two Subclasses in Class I and Class II Chitinases. Bioscience, Biotechnology and Biochemistry **59**, 336–338. https://doi.org/10.1271/bbb.59.336

12. Armenteros, J.J.A., Salvatore, M., Emanuelsson, O., Winther, O., von Heijne, G., Elofsson, A., Nielsen, H. 2019. Detecting sequence signals in targeting peptides using deep learning. Life Science Alliance **2**. 10.26508/lsa.201900429

13. Armenteros, J.J.A, Tsirigos, K.D., Sønderby, C.K., Petersen, T.N., Winther, O., Brunak, S., Von Heijne, G., Nielsen, H. 2019. SignalP 5.0 improves signal peptide predictions using deep neural networks. Nature Biotechnology **37**, 420–423.

14. Arnold, D.L., Preston, G.M. 2019. *Pseudomonas syringae*: enterprising epiphyte and stealthy parasite. Microbiology **165**, 251–253. https://doi.org/10.1099/mic.0.000715

15. Arrebola, E., Cazorla, F.M., Perez-García, A., de Vicente, A. 2011. Chemical and Metabolic Aspects of Antimetabolite Toxins Produced by *Pseudomonas syringae* Pathovars. Toxins **3**, 1089–1110. https://doi.org/10.3390/toxins3091089

16. Avrova AO, Stewart HE, De Jong WD, Heilbronn J, Lyon GD, Birch PR. 1999. A cysteine protease gene is expressed early in resistant potato interactions with *Phytophthora infestans*. Molecular Plant-Microbe Interactions **12**, 1114–1119.
17. Avrova AO, Taleb N, Rokka VM, Heilbronn J, Campbell E, Hein I, Gilroy EM, Cardle L, Bradshaw JE, Stewart HE, Fakim YJ, Loake G, Birch PRJ. 2004. Potato oxysterol binding protein and cathepsin B are rapidly up-regulated in independent defence pathways that distinguish *R* gene-mediated and field resistances to Phy*tophthora infestans*. Molecular Plant Pathology **5**, 45–56.
18. Azarkan M, Dibiani R, Baulard C, Baeyens-Volant D. 2006. Effects of mechanical wounding on *Carica papaya* cysteine endopeptidases accumulation and activity. International Journal of Biological Macromolecules **38**, 216–224.
19. Bacete, L., Mélida, H., Miedes, E., Molina, A. 2018. Plant cell wall-mediated immunity: cell wall changes trigger disease resistance responses. Plant Journal **93**, 614–636. https://doi.org/10.1111/tpj.13807
20. Bachovchin, D.A., Brown, S.J., Rosen, H., Cravatt, B.F. 2009. Identification of selective inhibitors of uncharacterized enzymes by high-throughput screening with fluorescent activity-based probes. Nature Biotechnology **27**, 387–394. https://doi.org/10.1038/nbt.1531
21. Bae, S., Park, J., Kim, J.-S. 2014. Cas-OFFinder: a fast and versatile algorithm that searches for potential off-target sites of Cas9 RNA-guided endonucleases. Bioinformatics Oxford Academic **30**, 1473–1475. https://doi.org/10.1093/bioinformatics/btu048
22. Balakireva AV, Zamyatnin AA. 2018. Indispensable role of proteases in plant innate immunity. International Journal of Molecular Sciences **19**, 629.
23. Balakireva AV, Zamyatnin AA. 2019. Cutting out the gaps between proteases and programmed cell death. Frontiers in Plant Science **10**, 704.
24. Baltrus, DA., Clark, M. 2020. Complete Genome Sequence of *Pseudomonas coronafaciens* pv. *oryzae* 1_6. Microbiology Resource Announcements **9**. https://doi.org/10.1128/MRA.01564-19
25. Baltrus, DA., Nishimura, MT., Romanchuk, A., Chang, JH., Shahid Mukhtar, M., Cherkis, K., Roach, J., Grant, SR., Jones, CD., Dangl, JL. 2011. Dynamic Evolution of Pathogenicity Revealed by Sequencing and Comparative Genomics of 19 *Pseudomonas syringae* Isolates. PLOS Pathogens **7**, e1002132.
26. Bao, Y., Howell, S.H. 2017. The Unfolded Protein Response Supports Plant Development and Defense as well as Responses to Abiotic Stress. Frontiers in Plant Science **8**, 344.
27. Bateman, A., Bennett, H.P.J. 2009. The granulin gene family: from cancer to dementia. BioEssays **31**, 1245–1254. https://doi.org/10.1002/bies.200900086
28. Beintema, J.J. 1994. Structural features of plant chitinases and chitin-binding proteins. FEBS Letters **350**, 159–163. https://doi.org/10.1016/0014-5793(94)00753-5
29. Beloshistov RE, Dreizler K, Galiullina RA, Tuzhikov AI, Serebryakova MV, Reichardt S, Shaw J, Taliansky ME, Pfannstiel J, Chichkova NV, Stintzi A, Schaller A, Vartapetian AB. 2018. Phytaspase-mediated precursor processing and maturation of the wound hormone systemin. New Phytologist **218**, 1167–1178.
30. Bendahmane, A., Kanyuka, K., Baulcombe, D.C. 1999. The Rx Gene from Potato Controls Separate Virus Resistance and Cell Death Responses. Plant Cell **11**, 781–791. https://doi.org/10.2307/3870814
31. Bender, C.L., Alarcón-Chaidez, F., Gross, D.C. 1999. *Pseudomonas syringae* Phytotoxins: Mode of Action, Regulation, and Biosynthesis by Peptide and Polyketide Synthetases. Microbiology and Molecular Biology Reviews **63**, 266–292.
32. Bender, C.L., Scholz-Schroeder, B.K. 2004. New Insights Into the Biosynthesis, Mode of Action, and Regulation of Syringomycin, syringopeptin, and Coronatine, in: Virulence and Gene Regulation. Ramos, J.-L. Springer US, Boston, MA, pp. 125–158. https://doi.org/10.1007/978-1-4419-9084-6_4
33. Berardini, T.Z., Reiser, L., Li, D., Mezheritsky, Y., Muller, R., Strait, E., Huala, E. 2015. The arabidopsis information resource: Making and mining the “gold standard”

annotated reference plant genome. genesis **53**, 474–485. https://doi.org/10.1002/dvg.22877
34. Bernoux, M., Timmers, T., Jauneau, A., Brière, C., de Wit, P.J.G.M., Marco, Y., Deslandes, L. 2008. RD19, an Arabidopsis cysteine protease required for RRS1-R-mediated resistance, is relocalized to the nucleus by the *Ralstonia solanacearum* PopP2 effector. Plant Cell **20**, 2252–2264. https://doi.org/10.1105/tpc.108.058685
35. Bethke, G., Grundman, R.E., Sreekanta, S., Truman, W., Katagiri, F., Glazebrook, J. 2014. Arabidopsis PECTIN METHYLESTERASEs Contribute to Immunity against *Pseudomonas syringae*. Plant Physiology **164**, 1093–1107. https://doi.org/10.1104/pp.113.227637
36. Biniossek, M.L., Niemer, M., Maksimchuk, K., Mayer, B., Fuchs, J., Huesgen, P.F., McCafferty, D.G., Turk, B., Fritz, G., Mayer, J., Haecker, G., Mach, L., Schilling, O. 2016. Identification of Protease Specificity by Combining Proteome-Derived Peptide Libraries and Quantitative Proteomics. Molecular & Cellular Proteomics MCP **15**, 2515–2524. https://doi.org/10.1074/mcp.O115.056671
37. Bishop, J.G., Dean, A.M., Mitchell-Olds, T. 2000. Rapid evolution in plant chitinases: Molecular targets of selection in plant-pathogen coevolution. Proceedings of the National Academy of Sciences U. S. A. **97**, 5322–5327.
38. Bishop, J.G., Ripoll, D.R., Bashir, S., Damasceno, C.M.B., Seeds, J.D., Rose, J.K.C. 2005. Selection on Glycine β-1,3-Endoglucanase Genes Differentially Inhibited by a Phytophthora Glucanase Inhibitor Protein. Genetics **169**, 1009–1019. https://doi.org/10.1534/genetics.103.025098
39. Blixt, O., Head, S., Mondala, T., Scanlan, C., Huflejt, M.E., Alvarez, R., Bryan, M.C., Fazio, F., Calarese, D., Stevens, J., Razi, N., Stevens, D.J., Skehel, J.J., van Die, I., Burton, D.R., Wilson, I.A., Cummings, R., Bovin, N., Wong, C.-H., Paulson, J.C. 2004. Printed covalent glycan array for ligand profiling of diverse glycan binding proteins. Proceedings of the National Academy of Sciences U. S. A. **101**, 17033–17038. https://doi.org/10.1073/pnas.0407902101
40. Bornhorst, J.A., Falke, J.J. 2000. Purification of Proteins Using Polyhistidine Affinity Tags. Methods in Enzymology **326**, 245–254.
41. Bozkurt, T.O., Schornack, S., Win, J., Shindo, T., Ilyas, M., Oliva, R., Cano, L.M., Jones, A.M.E., Huitema, E., Hoorn, R.A.L. van der, Kamoun, S. 2011. *Phytophthora infestans* effector AVRblb2 prevents secretion of a plant immune protease at the haustorial interface. Proceedings of the National Academy of Sciences **108**, 20832–20837. https://doi.org/10.1073/pnas.1112708109
42. Breen, S., Solomon, P.S., Bedon, F., Vincent, D. 2015. Surveying the potential of secreted antimicrobial peptides to enhance plant disease resistance. Frontiers in Plant Science **6**, 900. https://doi.org/10.3389/fpls.2015.00900
43. Breitenbach HH, Wenig M, Wittek F, Jordá L, Maldonado-Alconada AM, Sarioglu H, Colby T, Knappe C, Bichlmeier M, Pabst E, Mackey D, Parker JE, Vlot AC. 2014. Contrasting roles of the apoplastic aspartyl protease APOPLASTIC, ENHANCED DISEASE SUSCEPTIBILITY-DEPENDENT and LEGUME LECTIN-LIKE PROTEIN in Arabidopsis systemic acquired resistance. Plant Physiology **165**, 791–809.
44. Broderick, S.R., Jones, M.L. 2014. An Optimized Protocol to Increase Virus-Induced Gene Silencing Efficiency and Minimize Viral Symptoms in Petunia. Plant Molecular Biology Reporter **32**, 219–233. https://doi.org/10.1007/s11105-013-0647-3
45. Bronstein, P.A., Filiatrault, M.J., Myers, C.R., Rutzke, M., Schneider, D.J., Cartinhour, S.W. 2008. Global transcriptional responses of *Pseudomonas syringae* DC3000 to changes in iron bioavailability in vitro. BMC Microbiology **8**, 209. https://doi.org/10.1186/1471-2180-8-209
46. Brückner, A., Polge, C., Lentze, N., Auerbach, D., Schlattner, U. 2009. Yeast Two-Hybrid, a Powerful Tool for Systems Biology. International Journal of Molecular Sciences **10**, 2763–2788. https://doi.org/10.3390/ijms10062763
47. Brunner, F., Stintzi, A., Fritig, B., Legrand, M. 1998. Substrate specificities of tobacco chitinases. Plant Journal **14**, 225–234. https://doi.org/10.1046/j.1365-313X.1998.00112.x

48. Buell CR., Vinita J., Lindeberg M., Selengut J., Paulsen IT., Gwinn ML., Dodson RJ., Deboy RT, Durkin AS., Kolonay JF., Madupu R., Daugherty S., Brinkac L., Beanan MJ., Haft DH., Nelson WC., Davidsen T., Zafar N., Zhou L.,Liu J.,Yuan Q., Khouri H., Fedorova N., Tran B., Russel D., Berry K., Utterback T., Van Aken SE., Feldblyum TV., D'Ascenzo M., Deng WL., Ramos AR., Alfano JR., Cartinhour S., Chatterjee AK., Delaney TP., Lazarowitz SG., Martin GB., Schneider DJ., Tang X., Bender CL., White O., Fraser CM., Collmer A. 2003. The complete genome sequence of the Arabidopsis and tomato pathogen *Pseudomonas syringae* pv. *tomato* DC3000. Proceedings of the National Academy of Sciences U. S. A **100**, 10181-10186.
49. Buscaill, P., Chandrasekar, B., Sanguankiattichai, N., Kourelis, J., Kaschani, F., Thomas, E.L., Morimoto, K., Kaiser, M., Preston, G.M., Ichinose, Y., van der Hoorn, R.A.L. 2019. Glycosidase and glycan polymorphism control hydrolytic release of immunogenic flagellin peptides. Science **364**. https://doi.org/10.1126/science.aav0748
50. Buscaill, P., Rivas, S. 2014. Transcriptional control of plant defence responses. Current Opinion in Plant Biology, SI: Biotic interactions **20**, 35–46. https://doi.org/10.1016/j.pbi.2014.04.004
51. Buscaill, P., Sanguankiattichai, N., Lee, Y.J., Kourelis, J., Preston, G., van der Hoorn, R.A.L. 2021. Agromonas: a rapid disease assay for *Pseudomonas syringae* growth in agroinfiltrated leaves. Plant Journal **105**, 831–840. https://doi.org/10.1111/tpj.15056
52. Buscaill, P., van der Hoorn, R.A.L. 2021. Defeated by the nines: nine extracellular strategies to avoid microbe-associated molecular patterns recognition in plants. Plant Cell. https://doi.org/10.1093/plcell/koab109
53. Büttner, D. 2016. Behind the lines–actions of bacterial type III effector proteins in plant cells. FEMS Microbiology Reviews **40**, 894–937. https://doi.org/10.1093/femsre/fuw026
54. Byun, JA., VanSchouwen, B., Akimoto, M., Melacini, G. 2020. Allosteric inhibition explained through conformational ensembles sampling distinct "mixed" states. Computational and Structural Biotechnology Journal **18**, 3803-3818. https://doi.org/10.1016/j.csbj.2020.10.026
55. Camejo, D., Guzmán-Cedeño, Á., Moreno, A. 2016. Reactive oxygen species, essential molecules, during plant–pathogen interactions. Plant Physiology and Biochemistry **103**, 10–23. https://doi.org/10.1016/j.plaphy.2016.02.035
56. Cantarel, B.L., Coutinho, P.M., Rancurel, C., Bernard, T., Lombard, V., Henrissat, B. 2009. The Carbohydrate-Active EnZymes database (CAZy): an expert resource for Glycogenomics. Nucleic Acids Research **37**, D233–D238. https://doi.org/10.1093/nar/gkn663
57. Carter, C., Pan, S., Zouhar, J., Avila, E.L., Girke, T., Raikhel, N.V. 2004. The Vegetative Vacuole Proteome of *Arabidopsis thaliana* Reveals Predicted and Unexpected Proteins. Plant Cell **16**, 3285–3303. https://doi.org/10.1105/tpc.104.027078
58. Casamitjana-Martínez E, Hofhuis HF, Xu J, Liu CM, Heidstra R, Scheres B. 2003. Root-Specific CLE19 Overexpression and the sol1/2 Suppressors Implicate a CLV-like Pathway in the Control of Arabidopsis Root Meristem Maintenance. Current Biology **13**, 1435-1441.
59. Chandrasekar, B., Colby, T., Emon, A.E.K., Jiang, J., Hong, T.N., Villamor, J.G., Harzen, A., Overkleeft, H.S., van der Hoorn, R.A.L. 2014. Broad-range Glycosidase Activity Profiling. Molecular & Cellular Proteomics **13**, 2787–2800. https://doi.org/10.1074/mcp.O114.041616
60. Chandrasekar, B., Hong, T.N., van der Hoorn, R.A.L. 2017. Inhibitor Discovery by Convolution ABPP, in: Overkleeft, H.S., Florea, B.I. (Eds.), Activity-Based Proteomics: Methods and Protocols, Methods in Molecular Biology. Springer New York, New York, NY, pp. 47–56. https://doi.org/10.1007/978-1-4939-6439-0_4
61. Chichkova NV, Kim SH, Titova ES, Kalkum M, Morozov VS, Rubtsov YP, Kalinina NO, Taliansky ME, Vartapetian AB. 2004. A plant caspase-like protease activated during the hypersensitive response. The Plant Cell **16**, 157–171.
62. Chichkova, N.V., Shaw, J., Galiullina, R.A., Drury, G.E., Tuzhikov, A.I., Kim, S.H., Kalkum, M., Hong, T.B., Gorshkova, E.N., Torrance, L., Vartapetian, A.B., Taliansky,

M. 2010. Phytaspase, a relocalisable cell death promoting plant protease with caspase specificity. EMBO Journal **29**, 1149–1161. https://doi.org/10.1038/emboj.2010.1
63. Chinnapun D, Tian M, Day B, Churngchow N. 2009. Inhibition of a *Hevea brasiliensis* protease by a Kazal-like serine protease inhibitor from *Phytophthora palmivora*. Physiological and Molecular Plant Pathology **74**, 27–33.
64. Christensen AB, Cho BH, Næsby M, Gregersen PL, Brandt J, Madriz-Ordeñana K, Collinge DB, Thordal-Christensen H. 2002. The molecular characterization of two barley proteins establishes the novel PR-17 family of pathogenesis-related proteins. Molecular Plant Pathology **3**, 135–144.
65. Clark, K., Franco, J.Y., Schwizer, S., Pang, Z., Hawara, E., Liebrand, T.W.H., Pagliaccia, D., Zeng, L., Gurung, F.B., Wang, P., Shi, J., Wang, Y., Ancona, V., van der Hoorn, R.A.L., Wang, N., Coaker, G., Ma, W. 2018. An effector from the Huanglongbing-associated pathogen targets citrus proteases. Nature Communications **9**. https://doi.org/10.1038/s41467-018-04140-9
66. Claus, L.A.N., Savatin, D.V., Russinova, E. 2018. The crossroads of receptor-mediated signaling and endocytosis in plants. Journal of Integrated Plant Biology **60**, 827–840. https://doi.org/10.1111/jipb.12672
67. Coculo, D., Del Corpo, D., Ozáez Martínez, M., Vera, P., Piro, G., De Caroli, M., Lionetti, V. 2023. Arabidopsis subtilases promote defense-related pectin methylesterase activity and robust immune responses to botrytis infection. Plant Physiology and Biochemistry **201**. https://doi.org/10.1016/j.plaphy.2023.107865
68. Coffeen, W.C., Wolpert, T.J. 2004. Purification and Characterization of Serine Proteases That Exhibit Caspase-Like Activity and Are Associated with Programmed Cell Death in *Avena sativa*. Plant Cell **16**, 857–873. https://doi.org/10.1105/tpc.017947
69. Collmer, A., Badel, J.L., Charkowski, A.O., Deng, W.-L., Fouts, D.E., Ramos, A.R., Rehm, A.H., Anderson, D.M., Schneewind, O., van Dijk, K., Alfano, J.R. 2000. *Pseudomonas syringae Hrp* type III secretion system and effector proteins. Proceedings of the National Academy of Sciences **97**, 8770–8777. https://doi.org/10.1073/pnas.97.16.8770
70. Cox, J., Neuhauser, N., Michalski, A., Scheltema, R.A., Olsen, J.V., Mann, M. 2011. Andromeda: A Peptide Search Engine Integrated into the MaxQuant Environment. Journal of Proteome Research **10**, 1794–1805. https://doi.org/10.1021/pr101065j
71. Cui, F., Wu, S., Sun, W., Coaker, G., Kunkel, B., He, P., Shan, L. 2013. The *Pseudomonas syringae* Type III Effector AvrRpt2 Promotes Pathogen Virulence via Stimulating Arabidopsis Auxin/Indole Acetic Acid Protein Turnover. Plant Physiology **162**, 1018–1029. https://doi.org/10.1104/pp.113.219659
72. Cui, H., Tsuda, K., Parker, J.E. 2015. Effector-triggered immunity: from pathogen perception to robust defense. Annual Review of Plant Biology **66**, 487–511. https://doi.org/10.1146/annurev-arplant-050213-040012
73. Cunnac, S., Lindeberg, M., Collmer, A. 2009. *Pseudomonas syringae* type III secretion system effectors: repertoires in search of functions. Current Opinion in Microbiology **12**, 53–60. https://doi.org/10.1016/j.mib.2008.12.003
74. da Fonseca-Pereira, P., Monteiro-Batista, RDC., Araújo, WL., Nunes-Nesi, A. 2023. Harnessing enzyme cofactors and plant metabolism: an essential partnership. The Plant Journal https://doi.org/10.1111/tpj.16167
75. Dahiya, N., Tewari, R., Hoondal, G.S. 2006. Biotechnological aspects of chitinolytic enzymes: a review. Applied Microbiology and Biotechnology **71**, 773–782. https://doi.org/10.1007/s00253-005-0183-7
76. Davies, G., Henrissat, B. 1995. Structures and mechanisms of glycosyl hydrolases. Structure **3**, 853–859. https://doi.org/10.1016/S0969-2126(01)00220-9
77. Davies, L.J., Zhang, L., Elling, A.A. 2015. The *Arabidopsis thaliana* papain-like cysteine protease RD21 interacts with a root-knot nematode effector protein. Nematology **17**, 655–666. https://doi.org/10.1163/15685411-00002897
78. Davis, K.M., Nakamura, S., Weiser, J.N. 2011. Nod2 sensing of lysozyme-digested peptidoglycan promotes macrophage recruitment and clearance of *S. pneumoniae*

colonization in mice. Journal of Clinical Investigation **121**, 3666–3676. https://doi.org/10.1172/JCI57761
79. Debener , T., Lehnackers, H., Arnold, M., Dangl, JL. 1991. Identification and molecular mapping of a single *Arabidopsis thaliana* locus determining resistance to a phytopathogenic *Pseudomonas syringae* isolate. The Plant Journal **1**, 289-302.
80. DebRoy, S., Thilmony, R., Kwack, Y.-B., Nomura, K., He, S.Y. 2004. A family of conserved bacterial effectors inhibits salicylic acid-mediated basal immunity and promotes disease necrosis in plants. Proceedings of the National Academy of Sciences U. S. A. **101**, 9927–9932. https://doi.org/10.1073/pnas.0401601101
81. Delaunois, B., Jeandet, P., Clément, C., Baillieul, F., Dorey, S., Cordelier, S. 2014. Uncovering plant-pathogen crosstalk through apoplastic proteomic studies. Frontiers in Plant Science **5**.
82. Del Corpo, D., Fullone, M.R., Miele, R., Lafond, M., Pontiggia, D., Grisel, S., Kieffer-Jaquinod, S., Giardina, T., Bellincampi, D., Lionetti, V. 2020. *At*PME17 is a functional *Arabidopsis thaliana* pectin methylesterase regulated by its PRO region that triggers PME activity in the resistance to *Botrytis cinerea*. Molecular Plant Pathology **21**, 1620–1633. https://doi.org/10.1111/mpp.13002
83. Demain, A.L., Vaishnav, P. 2009. Production of recombinant proteins by microbes and higher organisms. Biotechnology Advances **3**, 297-306. https://doi.org/10.1016/j.biotechadv.2009.01.008
84. Deng, W., Marshall, N.C., Rowland, J.L., McCoy, J.M., Worrall, L.J., Santos, A.S., Strynadka, N.C.J., Finlay, B.B. 2017. Assembly, structure, function and regulation of type III secretion systems. Nature Reviews Microbiology **15**, 323–337. https://doi.org/10.1038/nrmicro.2017.20
85. Deng, X., Liang, H., Chen, K., He, C., Lan, L., Tang, X. 2014. Molecular mechanisms of two-component system RhpRS regulating type III secretion system in *Pseudomonas syringae*. Nucleic Acids Research 42, 11472–11486. https://doi.org/10.1093/nar/gku865
86. de Torres Zabala, M., Littlejohn, G., Jayaraman, S., Studholme, D., Bailey, T., Lawson, T., Tillich, M., Licht, D., Bölter, B., Delfino, L., Truman, W., Mansfield, J., Smirnoff, N., Grant, M. 2015. Chloroplasts play a central role in plant defence and are targeted by pathogen effectors. Nature Plants **1**, 1–10. https://doi.org/10.1038/nplants.2015.74
87. Dillon, M.M., Almeida, R.N.D., Laflamme, B., Martel, A., Weir, B.S., Desveaux, D., Guttman, D.S. 2019. Molecular Evolution of *Pseudomonas syringae* Type III Secreted Effector Proteins. Frontiers in Plant Science **10**.
88. Ding, L.-N., Li, M., Wang, W.-J., Cao, J., Wang, Z., Zhu, K.-M., Yang, Y.-H., Li, Y.-L., Tan, X.-L. 2019. Advances in plant GDSL lipases: from sequences to functional mechanisms. Acta Physioligiae Plantarum **41**, 151. https://doi.org/10.1007/s11738-019-2944-4
89. Dixon MS, Golstein C, Thomas CM, Van der Biezen EA, Jones JDG. 2000. Genetic complexity of pathogen perception by plants: The example of Rcr3, a tomato gene required specifically by Cf-2. Proceeding of the National Academy of Sciences, USA **97**, 8807–8814.
90. Dodds, P.N., Rathjen, J.P. 2010. Plant immunity: towards an integrated view of plant–pathogen interactions. Nature Reviews Genetics **11**, 539–548. https://doi.org/10.1038/nrg2812
91. Doehlemann, G., Hemetsberger, C. 2013. Apoplastic immunity and its suppression by filamentous plant pathogens. New Phytologist **198**, 1001–1016. https://doi.org/10.1111/nph.12277
92. Dommes, A.B., Gross, T., Herbert, D.B., Kivivirta, K.I., Becker, A. 2019. Virus-induced gene silencing: empowering genetics in non-model organisms. Journal of Experimental Botany **70**, 757–770. https://doi.org/10.1093/jxb/ery411
93. Dong S, Stam R, Cano LM, Song J, Sklenar J, Yoshida K, Bozkurt TO, Oliva R, Liu Z, Tian M, Win J, Banfield MJ, Jones AME, Van der Hoorn RAL, Kamoun S. 2014. Effector specialization in a lineage of the Irish potato famine pathogen. Science **343**, 552–555.

94. Duan, X., Zhang, Z., Wang, J., Zuo, K. 2016. Characterization of a Novel Cotton Subtilase Gene *Gb*SBT1 in Response to Extracellular Stimulations and Its Role in *Verticillium* Resistance. PLOS ONE **11**. https://doi.org/10.1371/journal.pone.0153988
95. Dudnik, A., Dudler, R. 2014. Genome and Transcriptome Sequences of *Pseudomonas syringae* pv. *syringae* B301D-R. Genome Announcements **2**.
96. Dudnik, A., Dudler, R. 2013. Non contiguous-finished genome sequence of *Pseudomonas syringae* pathovar *syringae* strain B64 isolated from wheat. Standards in Genomic Sciences **8**, 420-429. 10.4056/sigs.3997732.
97. Ebeling, W., Hennrich, N., Klockow, M., Metz, H., Orth, H.D., Lang, H. 1974. Proteinase K from Tritirachium album Limber. European Journal of Biochemistry **47**, 91–97. https://doi.org/10.1111/j.1432-1033.1974.tb03671.x
98. Ekchaweng K, Evangelisti E, Schornack S, Tian M, Churngchow N. 2017. The plant defense and pathogen counterdefense mediated by *Hevea brasiliensis* serine protease HbSPA and *Phytophthora palmivora* extracellular protease inhibitor *Pp*EPI10. PLoS One **12**, e0175795.
99. El-Brolosy, M.A., Stainier, D.Y.R. 2017. Genetic compensation: A phenomenon in search of mechanisms. PLoS Genetics **13**. doi: 10.1371/journal.pgen.1006780.
100. Elizabeth, S.V., Bender, C.L. 2007. The phytotoxin coronatine from *Pseudomonas syringae* pv. *tomato* DC3000 functions as a virulence factor and influences defence pathways in edible brassicas. Molecular Plant Pathology **8**, 83–92. https://doi.org/10.1111/j.1364-3703.2006.00372.x
101. El Moussaoui A, Nijs M, Paul C, Wintjens R, Vincentelli J, Azarkan M, Looze Y. 2001. Revisiting the enzymes stored in the laticifers of *Carica papaya* in the context of their possible participation in the plant defence mechanism. Cellular and Molecular Life Sciences **58**, 556–570.
102. Engler, C., Kandzia, R., Marillonnet, S. 2008. A One Pot, One Step, Precision Cloning Method with High Throughput Capability. PLOS ONE **3**, e3647. https://doi.org/10.1371/journal.pone.0003647
103. Engler, C., Youles, M., Gruetzner, R., Ehnert, T.-M., Werner, S., Jones, J.D.G., Patron, N.J., Marillonnet, S. 2014. A Golden Gate Modular Cloning Toolbox for Plants. ACS Synthetic Biology **3**, 839–843. https://doi.org/10.1021/sb4001504
104. Fan, P., Aguilar, E., Bradai, M., Xue, H., Wang, H., Rosas-Diaz, T., Tang, W., Wolf, S., Zhang, H., Xu, L., Lozano-Durán, R. 2021. The receptor-like kinases BAM1 and BAM2 are required for root xylem patterning. Proceedings of the National Academy of Sciences U. S. A. **118**, e2022547118. https://doi.org/10.1073/pnas.2022547118
105. Fares MA. 2015. The origins of mutational robustness. Trends in Genetics **31**, 373-381.
106. Farvardin, A., González-Hernández, A.I., Llorens, E., García-Agustín, P., Scalschi, L., Vicedo, B. 2020. The Apoplast: A Key Player in Plant Survival. Antioxidants **9**, 604. https://doi.org/10.3390/antiox9070604
107. Feil, H., Feil, W.S., Chain, P., Larimer, F., DiBartolo, G., Copeland, A., Lykidis, A., Trong, S., Nolan, M., Goltsman, E., Thiel, J., Malfatti, S., Loper, J.E., Lapidus, A., Detter, J.C., Land, M., Richardson, P.M., Kyrpides, N.C., Ivanova, N., Lindow, S.E. 2005. Comparison of the complete genome sequences of *Pseudomonas syringae* pv. *syringae* B728a and pv. *tomato* DC3000. Proceedings of the National Academy of Sciences U. S. A. **102**, 11064–11069. https://doi.org/10.1073/pnas.0504930102
108. Fernández MB, Daleo GR, Guevara MG. 2015. Isolation and characterization of a *Solanum tuberosum* subtilisin-like protein with caspase-3 activity (*St*SBTc-3). Plant Physiology and Biochemistry **86**, 137–146.
109. Fernández MB, Daleo GR, Guevara MG. 2012. DEVDase activity is induced in potato leaves during *Phytophthora infestans* infection. Plant Physiology and Biochemistry **61**, 197–203.
110. Fescemyer, H.W., Sandoya, G.V., Gill, T.A., Ozkan, S., Marden, J.H., Luthe, D.S. 2013. Maize toxin degrades peritrophic matrix proteins and stimulates compensatory

transcriptome responses in fall armyworm midgut. Insect Biochemistry and Molecular Biology **43**, 280–291. https://doi.org/10.1016/j.ibmb.2012.12.008
111. Figueiredo A, Monteiro F, Sebastiana M. 2014. Subtilisin-like proteases in plant–pathogen recognition and immune priming: a perspective. Frontiers in Plant Science **5**, 739.
112. Finn, R.D., Bateman, A., Clements, J., Coggill, P., Eberhardt, R.Y., Eddy, S.R., Heger, A., Hetherington, K., Holm, L., Mistry, J., Sonnhammer, E.L.L., Tate, J., Punta, M. 2014. Pfam: the protein families database. Nucleic Acids Research **42**, D222–D230. https://doi.org/10.1093/nar/gkt1223
113. Flinn BS. 2008. Plant extracellular matrix metalloproteinases. Functional Plant Biology **35**, 1183.
114. Floerl, S., Majcherczyk, A., Possienke, M., Feussner, K., Tappe, H., Gatz, C., Feussner, I., Kües, U., Polle, A. 2012. *Verticillium longisporum* Infection Affects the Leaf Apoplastic Proteome, Metabolome, and Cell Wall Properties in *Arabidopsis thaliana*. PLoS ONE **7**, e31435. https://doi.org/10.1371/journal.pone.0031435
115. Fojan, P., Jonson, P.H., Petersen, M.T.N., Petersen, S.B. 2000. What distinguishes an esterase from a lipase: A novel structural approach. Biochimie, Lipase 2000 **82**, 1033–1041. https://doi.org/10.1016/S0300-9084(00)01188-3
116. Fones, HN., McCurrach, H., Mithani, A., Smith, JAC., Preston, GM. 2016. Local adaptation is associated with zinc tolerance in *Pseudomonas* endophytes of the metal-hyperaccumulator plant *Noccaea caerulescens*. Proceedings of the Royal Society: Biological Sciences **283**. https://doi.org/10.1098/rspb.2016.0648
117. Fouts, D.E., Abramovitch, R.B., Alfano, J.R., Baldo, A.M., Buell, C.R., Cartinhour, S., Chatterjee, A.K., D'Ascenzo, M., Gwinn, M.L., Lazarowitz, S.G., Lin, N.-C., Martin, G.B., Rehm, A.H., Schneider, D.J., van Dijk, K., Tang, X., Collmer, A. 2002. Genomewide identification of *Pseudomonas syringae* pv. *tomato* DC3000 promoters controlled by the HrpL alternative sigma factor. Proceedings of the National Academy of Sciences **99**, 2275–2280. https://doi.org/10.1073/pnas.032514099
118. Fraser, C.M., Rider, L.W., Chapple, C. 2005. An Expression and Bioinformatics Analysis of the Arabidopsis Serine Carboxypeptidase-Like Gene Family. Plant Physiology **138**, 1136–1148. https://doi.org/10.1104/pp.104.057950
119. Gao, M., Wang, X., Wang, D., Xu, F., Ding, X., Zhang, Z., Bi, D., Cheng, Y.T., Chen, S., Li, X., Zhang, Y. 2009. Regulation of cell death and innate immunity by two receptor-like kinases in Arabidopsis. Cell Host Microbe **6**, 34–44. https://doi.org/10.1016/j.chom.2009.05.019
120. Garcia-Casado, G., Collada, C., Allona, I., Casado, R., Pacios, L.F., Aragoncillo, C., Gomez, L. 1998. Site-directed mutagenesis of active site residues in a class I endochitinase from chestnut seeds. Glycobiology **8**, 1021–1028. https://doi.org/10.1093/glycob/8.10.1021
121. Garnham, C.P., Campbell, R.L., Walker, V.K., Davies, P.L. 2011. Novel dimeric β-helical model of an ice nucleation protein with bridged active sites. BMC Structural Biology **11**, 36. https://doi.org/10.1186/1472-6807-11-36
122. Ge Y, Cai YM, Bonneau L, Rotari V, Danon A, McKenzie EA, McLellan H, Mach L, Gallois P. 2016. Inhibition of cathepsin B by caspase-3 inhibitors blocks programmed cell death in Arabidopsis. Cell Death & Differentiation **23**, 1493-1501.
123. Geng, X., Jin, L., Shimada, M., Kim, M.G., Mackey, D. 2014. The phytotoxin coronatine is a multifunctional component of the virulence armament of *Pseudomonas syringae*. Planta **240**, 1149–1165. https://doi.org/10.1007/s00425-014-2151-x
124. Getz, E.B., Xiao, M., Chakrabarty, T., Cooke, R., Selvin, P.R. 1999. A comparison between the sulfhydryl reductants tris(2-carboxyethyl)phosphine and dithiothreitol for use in protein biochemistry. Analytical Biochemistry **273**, 73–80. https://doi.org/10.1006/abio.1999.4203
125. Gibson, DG., Young, L., Chuang, RY., Venter, JC., Hutchison, CA., Smith, HO. 2009. Enzymatic assembly of DNA molecules up to several hundred kilobases. Nature Methods **6**, 343-345. https://doi.org/10.1038/nmeth.1318

126. Gilroy, E.M., Hein, I., van der Hoorn, R., Boevink, P.C., Venter, E., McLellan, H., Kaffarnik, F., Hrubikova, K., Shaw, J., Holeva, M., López, E.C., Borras-Hidalgo, O., Pritchard, L., Loake, G.J., Lacomme, C., Birch, P.R.J. 2007. Involvement of cathepsin B in the plant disease resistance hypersensitive response. The Plant Journal for Cell and Molecular Biology **52**, 1–13. https://doi.org/10.1111/j.1365-313X.2007.03226.x
127. Girard, L., Höfte, M., Mot, R.D. 2020. Lipopeptide families at the interface between pathogenic and beneficial *Pseudomonas*-plant interactions. Critical Reviews in Microbiology **46**, 397–419. https://doi.org/10.1080/1040841X.2020.1794790
128. Godson, A., van der Hoorn, R.A.L. 2021. The front line of defence: a meta-analysis of apoplastic proteases in plant immunity. Journal of Experimental Botany **72**, 3381–3394. https://doi.org/10.1093/jxb/eraa602
129. Golldack, D., Vera, P., Dietz, K.-J. 2003. Expression of subtilisin-like serine proteases in *Arabidopsis thaliana* is cell-specific and responds to jasmonic acid and heavy metals with developmental differences. Physiologia Plantarum **118**, 64–73. https://doi.org/10.1034/j.1399-3054.2003.00087.x
130. Goodin, M.M., Zaitlin, D., Naidu, R.A., Lommel, S.A. 2008. *Nicotiana benthamiana*: Its History and Future as a Model for Plant–Pathogen Interactions. Molecular Plant-Microbe Interactions **21**, 1015–1026. https://doi.org/10.1094/MPMI-21-8-1015
131. Görlach J, Volrath S, Knauf-Beiter G, Hengy G, Beckhove U, Kogel KH, Oostendorp M, Staub T, Ward E, Kessmann H, Ryals J. 1996. Benzothiadiazole, a novel class of inducers of systemic acquired resistance, activates gene expression and disease resistance in wheat. The Plant Cell **8**, 629–643.
132. Gorokhovets, N.V., Makarov, V.A., Petushkova, A.I., Prokopets, O.S., Rubtsov, M.A., Savvateeva, L.V., Zernii, E.Yu., Zamyatnin, A.A. 2017. Rational Design of Recombinant Papain-Like Cysteine Protease: Optimal Domain Structure and Expression Conditions for Wheat-Derived Enzyme Triticain-α. International Journal of Molecular Sciences **18**, 1395. https://doi.org/10.3390/ijms18071395
133. Goulet, Charles, Goulet, Catherine, Goulet, M.-C., Michaud, D. 2010. 2-DE proteome maps for the leaf apoplast of *Nicotiana benthamiana*. PROTEOMICS **10**, 2536–2544. https://doi.org/10.1002/pmic.200900382
134. Graham, T.L. 1991. A rapid, high resolution high performance liquid chromatography profiling procedure for plant and microbial aromatic secondary metabolites. Plant Physiology **95**, 584–593. https://doi.org/10.1104/pp.95.2.584
135. Granell A, Bellés JM, Conejero V. 1987. Induction of pathogenesis-related proteins in tomato by citrus exocortis viroid, silver ion and ethephon. Physiological and Molecular Plant Pathology **31**, 83–90.
136. Greenbaum, D., Medzihradszky, K.F., Burlingame, A., Bogyo, M. 2000. Epoxide electrophiles as activity-dependent cysteine protease profiling and discovery tools. Chemistry & Biology **7**, 569–581. https://doi.org/10.1016/s1074-5521(00)00014-4
137. Grosse-Holz, F., Kelly, S., Blaskowski, S., Kaschani, F., Kaiser, M., van der Hoorn, R.A.L. 2018. The transcriptome, extracellular proteome and active secretome of agroinfiltrated *Nicotiana benthamiana* uncover a large, diverse protease repertoire. Plant Biotechnology Journal **16**, 1068–1084. https://doi.org/10.1111/pbi.12852
138. Grover, A. 2012. Plant Chitinases: Genetic Diversity and Physiological Roles. Critical Reviews in Plant Sciences **31**, 57–73. https://doi.org/10.1080/07352689.2011.616043
139. Gu, C., Shabab, M., Strasser, R., Wolters, P.J., Shindo, T., Niemer, M., Kaschani, F., Mach, L., van der Hoorn, R.A.L. 2012. Post-Translational Regulation and Trafficking of the Granulin-Containing Protease RD21 of *Arabidopsis thaliana*. PLOS ONE **7**, e32422. https://doi.org/10.1371/journal.pone.0032422
140. Guan, Y., Ramalingam, S., Nagegowda, D., Taylor, P.W.J., Chye, M.-L. 2008. *Brassica juncea* chitinase *Bj*CHI1 inhibits growth of fungal phytopathogens and agglutinates Gram-negative bacteria. Journal of Experimental Botany **59**, 3475–3484. https://doi.org/10.1093/jxb/ern197
141. Guerra-Guimarães LL, Tenente RER, Pinheiro CC, Chaves II, Silva MDC, Cardoso FF, Planchon SS, De Barros DRD, Renaut JJ, Ricardo CPC. 2015. Proteomic analysis

of apoplastic fluid of *Coffea arabica* leaves highlights novel biomarkers for resistance against *Hemileia vastatrix*. Frontiers in Plant Science **6**, 478.
142. Guevara MG, Daleo GR, Oliva CR. 2001. Purification and characterization of an aspartic protease from potato leaves. Physiologia Plantarum **112**, 321–326.
143. Guevara MG, Oliva CR, Huarte M, Daleo GR. 2002. An Aspartic protease with antimicrobial activity is induced after infection and wounding in intercellular fluids of potato tubers. European Journal of Plant Pathology **108**, 131–137.
144. Guevara MG, Oliva CR, Machinandiarena M, Daleo GR. 1999. Purification and properties of an aspartic protease from potato tuber that is inhibited by a basic chitinase. Physiologia Plantarum **106**, 164–169.
145. Guevara MG, Veríssimo P, Pires E, Faro C, Daleo GR. 2004. Potato aspartic proteases: induction, antimicrobial activity and substrate specificity. Journal of Plant Pathology **86**, 233–238.
146. Gumtow R, Wu D, Uchida J, Tian M. 2018. A *Phytophthora palmivora* extracellular cystatin-like protease inhibitor targets papain to contribute to virulence on papaya. Molecular Plant-Microbe Interactions **31**, 363–373.
147. Guo B, Wang H, Yang B, Jiang W, Jing M, Li H, Xia Y, Xu Y, Hu Q, Wang F, Yu F, Wang Y, Ye W, Dong S, Xing W, Wang Y. 2019. *Phytophthora sojae* Effector PsAvh240 inhibits host aspartic protease secretion to promote infection. Molecular Plant **12**, 552–564.
148. Guo, M., Tian, F., Wamboldt, Y., Alfano, J.R. 2009. The Majority of the Type III Effector Inventory of *Pseudomonas syringae* pv. *tomato* DC3000 Can Suppress Plant Immunity. Molecular Plant-Microbe Interactions MPMI **22**, 1069–1080. https://doi.org/10.1094/MPMI-22-9-1069
149. Guttman, DS., Gropp, SJ., Morgan, RL., Wang, PW. 2006. Diversifying Selection Drives the Evolution of the Type III Secretion System Pilus of *Pseudomonas syringae*. Molecular Biology and Evolution **23**, 2342-2354. https://doi.org/10.1093/molbev/msl103
150. Hamilton, J.M.U., Simpson, D.J., Hyman, S.C., Ndimba, B.K., Slabas, A.R. 2003. Ara12 subtilisin-like protease from *Arabidopsis thaliana*: purification, substrate specificity and tissue localization. Biochemical Journal **370**, 57–67. https://doi.org/10.1042/BJ20021125
151. Han, L.-B., Li, Y.-B., Wang, F.-X., Wang, W.-Y., Liu, J., Wu, J.-H., Zhong, N.-Q., Wu, S.-J., Jiao, G.-L., Wang, H.-Y., Xia, G.-X. 2019. The Cotton Apoplastic Protein CRR1 Stabilizes Chitinase 28 to Facilitate Defense against the Fungal Pathogen *Verticillium dahliae*. Plant Cell **31**, 520–536. https://doi.org/10.1105/tpc.18.00390
152. Hanekamp, T., Kobayashi, D., Hayes, S., Stayton, M.M. 1997. Avirulence gene D of *Pseudomonas syringae* pv. *tomato* may have undergone horizontal gene transfer. FEBS Letters **415**, 40–44. https://doi.org/10.1016/S0014-5793(97)01089-2
153. Harrak H, Azelmat S, Baker EN, Tabaeizadeh Z. 2001. Isolation and characterization of a gene encoding a drought-induced cysteine protease in tomato (*Lycopersicon esculentum*). Genome **44**, 368–374.
154. Hartl, M., Merker, H., Schmidt, D.D., Baldwin, I.T. 2008. Optimized virus-induced gene silencing in *Solanum nigrum* reveals the defensive function of leucine aminopeptidase against herbivores and the shortcomings of empty vector controls. New Phytologist **179**, 356–365. https://doi.org/10.1111/j.1469-8137.2008.02479.x
155. Hatsugai, N., Iwasaki, S., Tamura, K., Kondo, M., Fuji, K., Ogasawara, K., Nishimura, M., Hara-Nishimura, I. 2009. A novel membrane fusion-mediated plant immunity against bacterial pathogens. Genes & Development **23**, 2496–2506. https://doi.org/10.1101/gad.1825209
156. Hayashida, K., Bartlett, A.H., Chen, Y., Park, P.W. 2010. Molecular and Cellular Mechanisms of Ectodomain Shedding. The Anatomical Record Hoboken NJ 2007 **293**, 925–937. https://doi.org/10.1002/ar.20757
157. Heeb, S., Haas, D. 2001. Regulatory Roles of the GacS/GacA Two-Component System in Plant-Associated and Other Gram-Negative Bacteria. Molecular Plant-Microbe Interactions **14**, 1351–1363. https://doi.org/10.1094/MPMI.2001.14.12.1351
158. Hodge, A., Gooday, G.W., Alexander, I.J. 1996. Inhibition of chitinolytic activities

from tree species and associated fungi. Phytochemistry **41**, 77–84. https://doi.org/10.1016/0031-9422(95)00571-4
159. Hollis, T., Honda, Y., Fukamizo, T., Marcotte, E., Day, P.J., Robertus, J.D. 1997. Kinetic Analysis of Barley Chitinase. Archives of Biochemistry and Biophysics **344**, 335–342. https://doi.org/10.1006/abbi.1997.0225
160. Hörger AC, Van der Hoorn RAL. 2013. The structural basis of specific protease–inhibitor interactions at the plant–pathogen interface. Current Opinion in Structural Biology **23**, 842–850.
161. Hou S, Liu Z, Shen H, Wu D. 2019. Damage-associated molecular pattern-triggered immunity in plants. Frontiers in Plant Science **10**, 646.
162. Howden, A.J.M., Rico, A., Mentlak, T., Miguet, L., Preston, G.M. 2009. *Pseudomonas syringae* pv. *syringae* B728a hydrolyses indole-3-acetonitrile to the plant hormone indole-3-acetic acid. Molecular Plant Pathology **10**, 857-865. https://doi.org/10.1111/j.1364-3703.2009.00595.x
163. Huang, W.R.H., Schol, C., Villanueva, S.L., Heidstra, R., Joosten, M.H.A.J. 2020. Knocking out SOBIR1 in *Nicotiana benthamiana* abolishes functionality of transgenic receptor-like protein Cf-4. Plant Physiology **185**, 290–294. https://doi.org/10.1093/plphys/kiaa047
164. Hulin, M.T., Armitage, A.D., Vicente, J.G., Holub, E.B., Baxter, L., Bates, H.J., Mansfield, J.W., Jackson, R.W., Harrison, R.J. 2018. Comparative genomics of *Pseudomonas syringae* reveals convergent gene gain and loss associated with specialization onto cherry (*Prunus avium*). New Phytologist. **219**, 672–696. https://doi.org/10.1111/nph.15182
165. Hunter, S., Apweiler, R., Attwood, T.K., Bairoch, A., Bateman, A., Binns, D., Bork, P., Das, U., Daugherty, L., Duquenne, L., Finn, R.D., Gough, J., Haft, D., Hulo, N., Kahn, D., Kelly, E., Laugraud, A., Letunic, I., Lonsdale, D., Lopez, R., Madera, M., Maslen, J., McAnulla, C., McDowall, J., Mistry, J., Mitchell, A., Mulder, N., Natale, D., Orengo, C., Quinn, A.F., Selengut, J.D., Sigrist, C.J.A., Thimma, M., Thomas, P.D., Valentin, F., Wilson, D., Wu, C.H., Yeats, C. 2009. InterPro: the integrative protein signature database. Nucleic Acids Research **37**, D211–D215. https://doi.org/10.1093/nar/gkn785
166. Husaini, A.M., Morimoto, K., Chandrasekar, B., Kelly, S., Kaschani, F., Palmero, D., Jiang, J., Kaiser, M., Ahrazem, O., Overkleeft, H.S., van der Hoorn, R.A.L. 2018. Multiplex Fluorescent, Activity-Based Protein Profiling Identifies Active α-Glycosidases and Other Hydrolases in Plants. Plant Physiol. 177, 24–37. https://doi.org/10.1104/pp.18.00250
167. Han, B., Zhou, K., Li, Z., Sun, B., Ni, Q., Meng, X., Pan, G., Li, C., Long, M., Li, T., Zhou, C., Li, W., Zhou, Z. 2016. Characterization of the First Fungal Glycosyl Hydrolase Family 19 Chitinase (NbchiA) from *Nosema bombycis* (Nb). Journal of Eukaryotic Microbiology **63**, 37–45. https://doi.org/10.1111/jeu.12246
168. Ichinose, Y., Taguchi, F., Mukaihara, T. 2013. Pathogenicity and virulence factors of *Pseudomonas syringae*. Journal of General Plant Pathology **79**, 285–296. https://doi.org/10.1007/s10327-013-0452-8
169. Ilyas M, Hörger AC, Bozkurt TO, Van den Burg HA, Kaschani F, Kaiser M, Belhaj K, Smoker M, Joosten MHAJ, Kamoun S, Van der Hoorn RAL. 2015. Functional divergence of two secreted immune proteases of tomato. Current Biology **25**, 2300–2306.
170. Irani, N.G., Di Rubbo, S., Mylle, E., Van den Begin, J., Schneider-Pizoń, J., Hniliková, J., Šíša, M., Buyst, D., Vilarrasa-Blasi, J., Szatmári, A.-M., Van Damme, D., Mishev, K., Codreanu, M.-C., Kohout, L., Strnad, M., Caño-Delgado, A.I., Friml, J., Madder, A., Russinova, E. 2012. Fluorescent castasterone reveals BRI1 signaling from the plasma membrane. Nature Chemical Biology **8**, 583–589. https://doi.org/10.1038/nchembio.958
171. Jashni, M.K., Dols, I.H.M., Iida, Y., Boeren, S., Beenen, H.G., Mehrabi, R., Collemare, J., de Wit, P.J.G.M. 2015a. Synergistic Action of a Metalloprotease and a Serine Protease from *Fusarium oxysporum* f. sp. *lycopersici* Cleaves Chitin-Binding Tomato Chitinases, Reduces Their Antifungal Activity, and Enhances Fungal Virulence. Molecular Plant-Microbe Interactions 28, 996–1008. https://doi.org/10.1094/MPMI-04-15-0074-R

172. Jashni, M.K., Mehrabi, R., Collemare, J., Mesarich, C.H., de Wit, P.J.G.M. 2015b. The battle in the apoplast: further insights into the roles of proteases and their inhibitors in plant–pathogen interactions. Frontiers in Plant Sciences **6**. https://doi.org/10.3389/fpls.2015.00584
173. Joardar, V., Lindeberg, M., Jackson, RW., Selengut, J., Dodson, R., Brinkac, LM., Daugherty, SC., Deboy, R., Durkin, AS., Giglio, MG., Madupu, R., Nelson, WC., Rosovitz, MJ., Sullivan, S., Crabtree, J., Creasy, T., Davidsen, T., Haft, DH., Zafar, N., Zhou, L., Halpin, R., Holley, T., Khouri, H., Feldblyum, T., White, O., Fraser, CM., Chatterjee, AK., Cartinhour, S., Schneider, DJ., Mansfield, J., Collmer, A., Buell, CR. 2005. Whole-genome sequence analysis of *Pseudomonas syringae* pv. *phaseolicola* 1448A reveals divergence among pathovars in genes involved in virulence and transposition. Journal of Bacteriology **187**, 6488-6498. https://doi.org/10.1128/JB.187.18.6488-6498.2005
174. Johnson, M., Zaretskaya, I., Raytselis, Y., Merezhuk, Y., McGinnis, S., Madden, T.L. 2008. NCBI BLAST: a better web interface. Nucleic Acids Research **36**, W5–W9. https://doi.org/10.1093/nar/gkn201
175. Jones, J.D.G., Dangl, J.L. 2006. The plant immune system. Nature **444**, nature05286. https://doi.org/10.1038/nature05286
176. Jones, P., Binns, D., Chang, H.-Y., Fraser, M., Li, W., McAnulla, C., McWilliam, H., Maslen, J., Mitchell, A., Nuka, G., Pesseat, S., Quinn, A.F., Sangrador-Vegas, A., Scheremetjew, M., Yong, S.-Y., Lopez, R., Hunter, S. 2014. InterProScan 5: genome-scale protein function classification. Bioinformatics **30**, 1236–1240. https://doi.org/10.1093/bioinformatics/btu031
177. Jonge, R. de, Esse, H.P. van, Kombrink, A., Shinya, T., Desaki, Y., Bours, R., Krol, S. van der, Shibuya, N., Joosten, M.H.A.J., Thomma, B.P.H.J. 2010. Conserved Fungal LysM Effector Ecp6 Prevents Chitin-Triggered Immunity in Plants. Science **329**, 953–955. https://doi.org/10.1126/science.1190859
178. Jordá L, Coego A, Conejero V, Vera P. 1999. A genomic cluster containing four differentially regulated subtilisin-like processing protease genes is in tomato plants. Journal of Biological Chemistry **274**, 2360–2365.
179. Jordá L, Conejero V, Vera P. 2000. Characterization of *P69E* and *P69F*, two differentially regulated genes encoding new members of the subtilisin-like proteinase family from tomato plants. Plant Physiology **122**, 67-74.
180. Jumper, J., Evans, R., Pritzel, A., Green, T., Figurnov, M., Ronneberger, O., Tunyasuvunakool, K., Bates, R., Žídek, A., Potapenko, A., Bridgland, A., Meyer, C., Kohl, S.A.A., Ballard, A.J., Cowie, A., Romera-Paredes, B., Nikolov, S., Jain, R., Adler, J., Back, T., Petersen, S., Reiman, D., Clancy, E., Zielinski, M., Steinegger, M., Pacholska, M., Berghammer, T., Bodenstein, S., Silver, D., Vinyals, O., Senior, A.W., Kavukcuoglu, K., Kohli, P., Hassabis, D. 2021. Highly accurate protein structure prediction with AlphaFold. Nature **596**, 583-598. https://doi.org/10.1038/s41586-021-03819-2
181. Jutras, P.V., Goulet, M., Lavoie, P., D'Aoust, M., Sainsbury, F., Michaud, D. 2018. Recombinant protein susceptibility to proteolysis in the plant cell secretory pathway is pH-dependent. Plant Biotechnology Journal **16**, 1928–1938. https://doi.org/10.1111/pbi.12928
182. Kämper, J., Kahmann, R., Bölker, M., Ma, L.-J., Brefort, T., Saville, B.J., Banuett, F., Kronstad, J.W., Gold, S.E., Müller, O., Perlin, M.H., Wösten, H.A.B., Vries, R. de, Ruiz-Herrera, J., Reynaga-Peña, C.G., Snetselaar, K., McCann, M., Pérez-Martín, J., Feldbrügge, M., Basse, C.W., Steinberg, G., Ibeas, J.I., Holloman, W., Guzman, P., Farman, M., Stajich, J.E., Sentandreu, R., González-Prieto, J.M., Kennell, J.C., Molina, L., Schirawski, J., Mendoza-Mendoza, A., Greilinger, D., Münch, K., Rössel, N., Scherer, M., Vraneš, M., Ladendorf, O., Vincon, V., Fuchs, U., Sandrock, B., Meng, S., Ho, E.C.H., Cahill, M.J., Boyce, K.J., Klose, J., Klosterman, S.J., Deelstra, H.J., Ortiz-Castellanos, L., Li, W., Sanchez-Alonso, P., Schreier, P.H., Häuser-Hahn, I., Vaupel, M., Koopmann, E., Friedrich, G., Voss, H., Schlüter, T., Margolis, J., Platt, D., Swimmer, C., Gnirke, A., Chen, F., Vysotskaia, V., Mannhaupt, G., Güldener, U.,

Münsterkötter, M., Haase, D., Oesterheld, M., Mewes, H.-W., Mauceli, E.W., DeCaprio, D., Wade, C.M., Butler, J., Young, S., Jaffe, D.B., Calvo, S., Nusbaum, C., Galagan, J., Birren, B.W. 2006. Insights from the genome of the biotrophic fungal plant pathogen *Ustilago maydis*. Nature **444**, 97–101. https://doi.org/10.1038/nature05248
183. Karki, H.S., Halterman, D.A. 2021. *Phytophthora infestans* (Late blight) Infection Assay in a Detached Leaf of Potato. Bio-Protocol Journal **11**, e3926. https://doi.org/10.21769/BioProtoc.3926
184. Kaschani, F., Shabab, M., Bozkurt, T., Shindo, T., Schornack, S., Gu, C., Ilyas, M., Win, J., Kamoun, S., van der Hoorn, R.A.L. 2010. An effector-targeted protease contributes to defense against *Phytophthora infestans* and is under diversifying selection in natural hosts. Plant Physiology **154**, 1794–1804. https://doi.org/10.1104/pp.110.158030
185. Kaschani, F., Van der Hoorn, R.A. 2011. A model of the C14-EPIC complex indicates hotspots for a protease-inhibitor arms race in the oomycete-potato interaction. Plant Signaling & Behavior **6**, 109–112. https://doi.org/10.4161/psb.6.1.14190
186. Kawase, T., Yokokawa, S., Saito, A., Fujii, T., Nikaidou, N., Miyashita, K., Watanabe, T. 2006. Comparison of Enzymatic and Antifungal Properties between Family 18 and 19 Chitinases from *S. coelicolor* A3(2). Bioscience, Biotechnology and Biochemistry **70**, 988–998. https://doi.org/10.1271/bbb.70.988
187. Keppler, L.D., Baker, C.J., Atkinson, M.M. 1989. Active oxygen production during a bacteria-induced hypersensitive reaction in tobacco suspension cells. Phytopathology USA.
188. Kesten, C., Gámez-Arjona, F.M., Menna, A., Scholl, S., Dora, S., Huerta, A.I., Huang, H.-Y., Tintor, N., Kinoshita, T., Rep, M., Krebs, M., Schumacher, K., Sánchez-Rodríguez, C. 2019. Pathogen-induced pH changes regulate the growth-defense balance in plants. EMBO Journal **38**, e101822. https://doi.org/10.15252/embj.2019101822
189. Khan, M., Seto, D., Subramaniam, R., Desveaux, D. 2018. Oh, the places they'll go! A survey of phytopathogen effectors and their host targets. Plant Journal **93**, 651–663. https://doi.org/10.1111/tpj.13780
190. Kim, B.H., Kim, S.Y., Nam, K.H. 2013. Assessing the Diverse Functions of BAK1 and Its Homologs in Arabidopsis, beyond BR Signaling and PTI Responses. Molecules and Cells **35**, 7–16. https://doi.org/10.1007/s10059-013-2255-3
191. Kim, H.G., Kwon, S.J., Jang, Y.J., Chung, J.H., Nam, M.H., Park, O.K. 2014. GDSL lipase 1 regulates ethylene signaling and ethylene-associated systemic immunity in Arabidopsis. FEBS Letters **588**, 1652–1658. https://doi.org/10.1016/j.febslet.2014.02.062
192. Kobayashi, DY., Tamaki, SJ., Keen, NT. 1989. Cloned avirulence genes from the tomato pathogen *Pseudomonas syringae* pv. *tomato* confer cultivar specificity on soybean. Proceedings of the National Academy of Sciences USA **86**, 157-161. 10.1073/pnas.86.1.157
193. Kobayashi, D.Y., Tamaki, S.J., Keen, N.T. 1990. Molecular characterization of avirulence gene D from *Pseudomonas syringae* pv. *tomato*. Molecular Plant-Microbe Interactions **3**, 94–102. https://doi.org/10.1094/mpmi-3-094
194. Koizumi, M., Yamaguchi-Shinozaki, K., Tsuji, H., Shinozaki, K. 1993. Structure and expression of two genes that encode distinct drought-inducible cysteine proteinases in *Arabidopsis thaliana*. Gene **129**, 175–182. https://doi.org/10.1016/0378-1119(93)90266-6
195. Kokkinidis, M., Glykos, NM., Fadouloglou, VE. 2020. Catalytic activity regulation through post-translational modification: the expanding universe of protein diversity. Advances in Protein Chemistry and Structural Biology **122**, 97-125. https://doi.org/10.1016/bs.apcsb.2020.05.001
196. Koncz C., Schell., J. 1986. The promoter of T_L-DNA gene *5* controls the tissue-specific expression of chimaeric genes carried by a novel type of *Agrobacterium* binary vector. Molecular Genetics and Genomics **204**, 383-396.
197. Konno K, Hirayama C, Nakamura M, Tateishi K, Tamura Y, Hattori M, Kohno K. 2004. Papain protects papaya trees from herbivorous insects: role of cysteine proteases in latex. The Plant Journal **37**, 370–378.
198. Körner, E., von Dahl, C.C., Bonaventure, G., Baldwin, I.T. 2009. Pectin

methylesterase *Na*PME1 contributes to the emission of methanol during insect herbivory and to the elicitation of defence responses in *Nicotiana attenuata*. Journal of Experimental Botany **60**, 2631–2640. https://doi.org/10.1093/jxb/erp106
199. Kourelis, J., van der Hoorn, R.A.L. 2018. Defended to the Nines: 25 Years of Resistance Gene Cloning Identifies Nine Mechanisms for R Protein Function. Plant Cell **30**, 285–299. https://doi.org/10.1105/tpc.17.00579
200. Kourelis, J., Kaschani, F., Grosse-Holz, F.M., Homma, F., Kaiser, M., van der Hoorn, R.A.L. 2019. A homology-guided, genome-based proteome for improved proteomics in the alloploid *Nicotiana benthamiana*. BMC Genomics **20**, 722. https://doi.org/10.1186/s12864-019-6058-6
201. Kovács J, Poór P, Szepesi Á, Tari I. 2016. Salicylic acid induced cysteine protease activity during programmed cell death in tomato plants. Biologia Futura **67**, 148–158.
202. Krüger J, Thomas CM, Golstein C, Dixon MS, Smoker M, Tang S, Mulder L, Jones JDG. 2002. A tomato cysteine protease required for Cf-2-dependent disease resistance and suppression of autonecrosis. Science **296**, 744–747.
203. Kutschera, A., Dawid, C., Gisch, N., Schmid, C., Raasch, L., Gerster, T., Schäffer, M., Smakowska-Luzan, E., Belkhadir, Y., Vlot, A.C., Chandler, C.E., Schellenberger, R., Schwudke, D., Ernst, R.K., Dorey, S., Hückelhoven, R., Hofmann, T., Ranf, S. 2019. Bacterial medium-chain 3-hydroxy fatty acid metabolites trigger immunity in Arabidopsis plants. Science **364**, 178–181. https://doi.org/10.1126/science.aau1279
204. Kuwata, H. 1985. *Pseudomonas syringae* pv. *oryzae* pv. nov., Causal Agent of Bacterial Halo Blight of Rice. Japanese Journal of Phytopathology **51**, 212-218. https://doi.org/10.3186/jjphytopath.51.212
205. Kvitko, B.H., Park, D.H., Velásquez, A.C., Wei, C.-F., Russell, A.B., Martin, G.B., Schneider, D.J., Collmer, A. 2009. Deletions in the Repertoire of *Pseudomonas syringae* pv. *tomato* DC3000 Type III Secretion Effector Genes Reveal Functional Overlap among Effectors. PLoS Pathogens **5**, e1000388. https://doi.org/10.1371/journal.ppat.1000388
206. Lalmanach, G., Saidi, A., Bigot, P., Chazeirat, T., Lecaille, F., Wartenberg, M. 2020. Regulation of the Proteolytic Activity of Cysteine Cathepsins by Oxidants. International Journal of Molecular Sciences **21**, 1944. https://doi.org/10.3390/ijms21061944
207. Lam, S.Y., Yeung, R.C.Y., Yu, T.-H., Sze, K.-H., Wong, K.-B. 2011. A Rigidifying Salt-Bridge Favors the Activity of Thermophilic Enzyme at High Temperatures at the Expense of Low-Temperature Activity. PLOS Biology **9**, e1001027. https://doi.org/10.1371/journal.pbio.1001027
208. Lamb, C., Dixon, R.A. 1997. The Oxidative Burst In Plant Disease Resistance. Annual Review of Plant Physiology and Plant Molecular Biology **48**, 251–275. https://doi.org/10.1146/annurev.arplant.48.1.251
209. Lampl, N., Alkan, N., Davydov, O., Fluhr, R. 2013. Set-point control of RD21 protease activity by *At*Serpin1 controls cell death in Arabidopsis. Plant Journal **74**, 498–510. https://doi.org/10.1111/tpj.12141
210. Lavergne, F., Richard, C., Saudreau, M., Venisse, J.-S., Fumanal, B., Goupil, P. 2017. Effect of acibenzolar-S-methyl phototransformation on its elicitation activity in tobacco cells. Plant Physiology and Biochemistry **118**, 370–376. https://doi.org/10.1016/j.plaphy.2017.07.008
211. Lee, D.S., Kim, B.K., Kwon, S.J., Jin, H.C., Park, O.K. 2009. Arabidopsis GDSL lipase 2 plays a role in pathogen defense via negative regulation of auxin signaling. Biochemical and Biophysical Research Communications **379**, 1038–1042. https://doi.org/10.1016/j.bbrc.2009.01.006
212. Lee, H.-J., Park, O.K. 2019. Lipases associated with plant defense against pathogens. Plant Science **279**, 51–58. https://doi.org/10.1016/j.plantsci.2018.07.003
213. Lee, S., Yang, D.S., Uppalapati, S.R., Sumner, L.W., Mysore, K.S. 2013. Suppression of plant defense responses by extracellular metabolites from *Pseudomonas syringae* pv. *tabaci* in *Nicotiana benthamiana*. BMC Plant Biology **13**, 65. https://doi.org/10.1186/1471-2229-13-65

214. Lee, Y.C., Yang, D. 2002. Determination of lysozyme activities in a microplate format. Analytical Biochemistry **310**, 223–224. https://doi.org/10.1016/s0003-2697(02)00320-2
215. Lemoine, F., Correia, D., Lefort, V., Doppelt-Azeroual, O., Mareuil, F., Cohen-Boulakia, S., Gascuel, O. 2019. NGPhylogeny.fr: new generation phylogenetic services for non-specialists. Nucleic Acids Research **47**, W260–W265. https://doi.org/10.1093/nar/gkz303
216. Letunic, I., Bork, P. 2016. Interactive tree of life (iTOL) v3: an online tool for the display and annotation of phylogenetic and other trees. Nucleic Acids Research **44**, W242–W245. https://doi.org/10.1093/nar/gkw290
217. Li C, Song X, Li G, Wang P. 2009. Midgut cysteine protease-inhibiting activity in *Trichoplusia ni* protects the peritrophic membrane from degradation by plant cysteine proteases. Insect Biochemistry and Molecular Biology **39**, 726–734.
218. Li D, Zhang H, Song Q, Wang L, Liu S, Hong Y, Huang L, Song F. 2015. Tomato Sl3-MMP, a member of the Matrix metalloproteinase family, is required for disease resistance against *Botrytis cinerea* and *Pseudomonas syringae* pv. *tomato* DC3000. BMC Plant Biology **15**, 143.
219. Li J, Lease KA, Tax FE, Walker JC. 2001. BRS1, a serine carboxypeptidase, regulates BRI1 signaling in *Arabidopsis thaliana*. Proceedings of the National Academy of Sciences USA **98**, 5916-5921.
220. Li, W., Yadeta, K.A., Elmore, J.M., Coaker, G. 2013. The *Pseudomonas syringae* effector HopQ1 promotes bacterial virulence and interacts with tomato 14-3-3 proteins in a phosphorylation-dependent manner. Plant Physiology **161**, 2062-2074. 10.1104/pp.112.211748
221. Liao, H., Tang, R., Zhang, X., Luan, S., Yu, F. 2017. FERONIA Receptor Kinase at the Crossroads of Hormone Signaling and Stress Responses. Plant and Cell Physiology **58**, 1143–1150. https://doi.org/10.1093/pcp/pcx048
222. Libantová, J., Kämäräinen, T., Moravcíková, J., Matusíková, I., Salaj, J. 2009. Detection of chitinolytic enzymes with different substrate specificity in tissues of intact sundew (*Drosera rotundifolia L.*): chitinases in sundew tissues. Molecular Biology Reports **36**, 851–856. https://doi.org/10.1007/s11033-008-9254-z
223. Lin, J.-S., Lai, E.-M. 2017. Protein-Protein Interactions: Co-Immunoprecipitation. Methods in Molecular Biology Clifton NJ **1615**, 211–219. https://doi.org/10.1007/978-1-4939-7033-9_17
224. Lionetti, V., Raiola, A., Camardella, L., Giovane, A., Obel, N., Pauly, M., Favaron, F., Cervone, F., Bellincampi, D. 2007. Overexpression of Pectin Methylesterase Inhibitors in Arabidopsis Restricts Fungal Infection by *Botrytis cinerea*. Plant Physiology **143**, 1871–1880. https://doi.org/10.1104/pp.106.090803
225. Liu H, Wang X, Zhang H, Yang Y, Ge X, Song F. 2008. A rice serine carboxypeptidase-like gene *Os*BISCPL1 is involved in regulation of defense responses against biotic and oxidative stress. Gene **420**, 57–65.
226. Liu, P.-L., Du, L., Huang, Y., Gao, S.-M., Yu, M. 2017. Origin and diversification of leucine-rich repeat receptor-like protein kinase (LRR-RLK) genes in plants. BMC Evolutionary Biology **17**, 47. https://doi.org/10.1186/s12862-017-0891-5
227. Liu, X., Grabherr, H.M., Willmann, R., Kolb, D., Brunner, F., Bertsche, U., Kühner, D., Franz-Wachtel, M., Amin, B., Felix, G., Ongena, M., Nürnberger, T., Gust, A.A. 2014. Host-induced bacterial cell wall decomposition mediates pattern-triggered immunity in Arabidopsis. eLife **3**. https://doi.org/10.7554/eLife.01990
228. Liu Y, Dammann C, Bhattacharyya MK. 2001. The matrix metalloproteinase gene *Gm*MMP2 is activated in response to pathogenic infections in soybean. Plant Physiology **127**, 1788–1797.
229. Liu, Y., Patricelli, M.P., Cravatt, B.F. 1999. Activity-based protein profiling: the serine hydrolases. Proceedings of the National Academy of Sciences U. S. A. **96**, 14694–14699. https://doi.org/10.1073/pnas.96.26.14694

230. Liu, Y., Schiff, M., Marathe, R., Dinesh-Kumar, S.P. 2002. Tobacco Rar1, EDS1 and NPR1/NIM1 like genes are required for N-mediated resistance to tobacco mosaic virus. Plant Journal **30**, 415–429. https://doi.org/10.1046/j.1365-313X.2002.01297.x
231. Liu, Y., Wang, K., Cheng, Q., Kong, D., Zhang, X., Wang, Z., Wang, Q., Qi, X., Yan, J., Chu, J., Ling, H., Li, Q., Miao, J., Zhao, B. 2020. Cysteine protease RD21A regulated by E3 ligase SINAT4 is required for drought-induced resistance to *Pseudomonas syringae* in Arabidopsis. Journal of Experimental Botany https://doi.org/10.1093/jxb/eraa255
232. Lopez L, Camas A, Shivaji R, Ankala A, Williams P, Luthe D. 2007. Mir1-CP, a novel defense cysteine protease accumulates in maize vascular tissues in response to herbivory. Planta **226**, 517–527.
233. Louis J, Basu S, Varsani S, Castano-Duque L, Jiang V, Williams WP, Felton GW, Luthe DS. 2015. Ethylene contributes to maize insect resistance1-mediated maize defense against the phloem sap-sucking corn leaf aphid. Plant Physiology **169**, 313–324.
234. Lozano-Torres, J.L., Wilbers, R.H.P., Gawronski, P., Boshoven, J.C., Finkers-Tomczak, A., Cordewener, J.H.G., America, A.H.P., Overmars, H.A., Van 't Klooster, J.W., Baranowski, L., Sobczak, M., Ilyas, M., van der Hoorn, R.A.L., Schots, A., de Wit, P.J.G.M., Bakker, J., Goverse, A., Smant, G. 2012. Dual disease resistance mediated by the immune receptor Cf-2 in tomato requires a common virulence target of a fungus and a nematode. Proceedings of the National Academy of Sciences U. S. A. **109**, 10119–10124. https://doi.org/10.1073/pnas.1202867109
235. Lu, R., Martin-Hernandez, A.M., Peart, J.R., Malcuit, I., Baulcombe, D.C. 2003. Virus-induced gene silencing in plants. Methods San Diego Calif **30**, 296–303. https://doi.org/10.1016/s1046-2023(03)00037-9
236. Ma, X., Zhu, Q., Chen, Y., Liu, Y.-G. 2016. CRISPR/Cas9 Platforms for Genome Editing in Plants: Developments and Applications. Molecular Plant **9**, 961–974. https://doi.org/10.1016/j.molp.2016.04.009
237. Ma, Z., Smith, JJ., Zhao, Y., Jackson, RW., Arnold, DL., Murillo, J., Sundin, GW. 2007. Phylogenetic Analysis of the pPT23A Plasmid Family of *Pseudomonas syringae*. Applied and Environmental Microbiology **73**, 1287-1295.
238. Macho, A.P. 2016. Subversion of plant cellular functions by bacterial type-III effectors: beyond suppression of immunity. New Phytologist **210**, 51–57. https://doi.org/10.1111/nph.13605
239. Maidment JM, Moore D, Murphy GP, Murphy G, Clark IM. 1999. Matrix Metalloproteinase Homologues from *Arabidopsis thaliana* - Expression and activity. Journal of Biological Chemistry **274**, 34706-34710.
240. Mamaeva, A., Lyapina, I., Knyazev, A., Golub, N., Mollaev, T., Chudinova, E., Elansky, S., Babenko, V.V., Veselovsky, V.A., Klimina, K.M., Gribova, T., Kharlampieva, D., Lazarev, V., Fesenko, I. 2023. RALF peptides modulate immune response in the moss *Physcomitrium patens*. Frontiers in Plant Science **14**. https://doi.org/10.3389/fpls.2023.1077301
241. Mandal MK, Fischer R, Schillberg S, Schiermeyer A. 2010. Biochemical properties of the matrix metalloproteinase *Nt*MMP1 from *Nicotiana tabacum* cv. BY-2 suspension cells. Planta **232**, 899-910.
242. Marino G, Funk C. 2012. Matrix metalloproteinases in plants: a brief overview. Physiologia Plantarum **145**, 196–202.
243. Marino G, Huesgen PF, Eckhard U, Overall CM, Schröder WP, Funk C. 2014. Family-wide characterization of matrix metalloproteinases from *Arabidopsis thaliana* reveals their distinct proteolytic activity and cleavage site specificity. Biochemical Journal **457**, 335-346.
244. Martinez, M., Diaz, I. 2008. The origin and evolution of plant cystatins and their target cysteine proteinases indicate a complex functional relationship. BMC Evolutionary Biology **8**, 198. https://doi.org/10.1186/1471-2148-8-198
245. Martínez-Caballero, S., Cano-Sánchez, P., Mares-Mejía, I., Díaz-Sánchez, A.G., Macías-Rubalcava, M.L., Hermoso, J.A., Rodríguez-Romero, A. 2014. Comparative study of two GH19 chitinase-like proteins from *Hevea brasiliensis,* one exhibiting a novel

carbohydrate-binding domain. FEBS Journal **281**, 4535–4554. https://doi.org/10.1111/febs.12962
246. Martínez-González, A.P., Ardila, H.D., Martínez-Peralta, S.T., Melgarejo-Muñoz, L.M., Castillejo-Sánchez, M.A., Jorrín-Novo, J.V. 2018. What proteomic analysis of the apoplast tells us about plant–pathogen interactions. Plant Pathology **67**, 1647–1668. https://doi.org/10.1111/ppa.12893
247. Masachis, S., Segorbe, D., Turrà, D., Leon-Ruiz, M., Fürst, U., El Ghalid, M., Leonard, G., López-Berges, M.S., Richards, T.A., Felix, G., Di Pietro, A. 2016. A fungal pathogen secretes plant alkalinizing peptides to increase infection. Nature Microbiology **1**, 16043. https://doi.org/10.1038/nmicrobiol.2016.43
248. Matika, D.E.F., Loake, G.J. 2014. Redox Regulation in Plant Immune Function. Antioxidants & Redox Signaling **21**, 1373-1388. doi: 10.1089/ars.2013.5679
249. Matsui, H., Nishimura T., Asai, S., Masuda, S., Shirasu, K., Yamamoto, M., Noutoshi, Y., Toyoda, K., Ichinosea, Y. 2021. Complete Genome Sequence of *Pseudomonas amygdali* pv. *tabaci* Strain 6605, a Causal Agent of Tobacco Wildfire Disease. Microbiology Resource Announcements **28**.
250. McClerklin, S.A., Lee, S.G., Harper, C.P., Nwumeh, R., Jez, J.M., Kunkel, B.N. 2018. Indole-3-acetaldehyde dehydrogenase-dependent auxin synthesis contributes to virulence of *Pseudomonas syringae* strain DC3000. PLOS Pathogens **14**, e1006811. https://doi.org/10.1371/journal.ppat.1006811
251. McLellan, H., Gilroy, E.M., Yun, B.-W., Birch, P.R.J., Loake, G.J. 2009. Functional redundancy in the Arabidopsis Cathepsin B gene family contributes to basal defence, the hypersensitive response and senescence. New Phytologist **183**, 408–418. https://doi.org/10.1111/j.1469-8137.2009.02865.x
252. Mendieta JR, Pagano MR, Muñoz FF, Daleo GR, Guevara MG. 2006. Antimicrobial activity of potato aspartic proteases (*St*APs) involves membrane permeabilization. Microbiology **152**, 2039–2047.
253. Meng, X., Zhang, S. 2013. MAPK cascades in plant disease resistance signaling. Annual Review of Phytopathology **51**, 245-266. https://doi.org/10.1146/annurev-phyto-082712-102314
254. Meyer M, Huttenlocher F, Cedzich A, Procopio S, Stroeder J, Pau-Roblot C, Lequart-Pillon M, Pelloux J, Stintzi A, Schaller A. 2016a. The subtilisin-like protease SBT3 contributes to insect resistance in tomato. Journal of Experimental Botany **67**, 4325–4338.
255. Meyer M, Leptihn S, Welz M, Schaller A. 2016b. Functional characterization of propeptides in plant subtilases as intramolecular chaperones and inhibitors of the mature protease. Journal of Biological Chemistry **9**, 19449-19461.
256. Minic, Z. 2007. Physiological roles of plant glycoside hydrolases. Planta **227**, 723. https://doi.org/10.1007/s00425-007-0668-y
257. Misas-Villamil, J.C., Kolodziejek, I., Crabill, E., Kaschani, F., Niessen, S., Shindo, T., Kaiser, M., Alfano, J.R., van der Hoorn, R.A.L. 2013. *Pseudomonas syringae* pv. *syringae* Uses Proteasome Inhibitor Syringolin A to Colonize from Wound Infection Sites. PLOS Pathogens **9**, e1003281. https://doi.org/10.1371/journal.ppat.1003281
258. Misas-Villamil JC, Mueller AN, Demir F, Meyer U, Ökmen B, Hüynck JS, Breuer M, Dauben H, Win J, Huesgen P, Doehlemann G. 2019. A fungal substrate mimicking molecule suppresses plant immunity via an inter-kingdom conserved motif. Nature Communications **10**, 1576.
259. Misas-Villamil, J.C., van der Hoorn, R.A. 2008. Enzyme–inhibitor interactions at the plant–pathogen interface. Current Opinion in Plant Biology, Biotic Interactions **11**, 380–388. https://doi.org/10.1016/j.pbi.2008.04.007
260. Misas-Villamil JC, Van der Hoorn RAL, Doehlemann G. 2016. Papain-like cysteine proteases as hubs in plant immunity. New Phytologist **212**, 902–907.
261. Modrzejewski, D., Hartung, F., Lehnert, H., Sprink, T., Kohl, C., Keilwagen, J., Wilhelm, R. 2020. Which Factors Affect the Occurrence of Off-Target Effects Caused by

the Use of CRISPR/Cas: A Systematic Review in Plants. Frontiers in Plant Science **11**, 574959. https://doi.org/10.3389/fpls.2020.574959
262. Mohamed Ahmed, I.A., Babiker, E.E., Mori, N. 2010. pH stability and influence of salts on activity of a milk-clotting enzyme from Solanum dubium seeds and its enzymatic action on bovine caseins. LWT - Food Sciience and Technology **43**, 759–764. https://doi.org/10.1016/j.lwt.2009.12.011
263. Mohan S, Ma PWK, Pechan T, Bassford ER, Williams WP, Luthe DS. 2006. Degradation of the *S. frugiperda* peritrophic matrix by an inducible maize cysteine protease. Journal of Insect Physiology **52**, 21–28.
264. Mole, B.M., Baltrus, D.A., Dangl, J.L., Grant, S.R. 2007. Global virulence regulation networks in phytopathogenic bacteria. Trends in Microbiology **15**, 363–371. https://doi.org/10.1016/j.tim.2007.06.005
265. Morel, J.-B., Dangl, J.L. 1997. The hypersensitive response and the induction of cell death in plants. Cell Death & Differentiation **4**, 671–683. https://doi.org/10.1038/sj.cdd.4400309
266. Morimoto, K., van der Hoorn, R.A.L. 2016. The Increasing Impact of Activity-Based Protein Profiling in Plant Science. Plant and Cell Physiology **57**, 446–461. https://doi.org/10.1093/pcp/pcw003
267. Mucyn, T.S., Yourstone, S., Lind, A.L., Biswas, S., Nishimura, M.T., Baltrus, D.A., Cumbie, J.S., Chang, J.H., Jones, C.D., Dangl, J.L., Grant, S.R. 2014. Variable Suites of Non-effector Genes Are Co-regulated in the Type III Secretion Virulence Regulon across the *Pseudomonas syringae* Phylogeny. PLOS Pathogens **10**, e1003807. https://doi.org/10.1371/journal.ppat.1003807
268. Mueller AN, Ziemann S, Treitschke S, Aßmann D, Doehlemann G. 2013. Compatibility in the *Ustilago maydis*–maize interaction requires inhibition of host cysteine proteases by the fungal effector Pit2. PLoS Pathogens **9**, e1003177.
269. Mugford ST, Milkowski C. 2012. Chapter Fourteen - Serine carboxypeptidase-like acyltransferases from plants, in: Hopwood DA (Ed.), Methods in Enzymology, Natural Product Biosynthesis by Microorganisms and Plants, Part B. Academic Press, pp. 279–297.
270. Muñoz FF, Mendieta JR, Pagano MR, Paggi RA, Daleo GR, Guevara MG. 2010. The swaposin-like domain of potato aspartic protease (StAsp-PSI) exerts antimicrobial activity on plant and human pathogens. Peptides **31**, 777–785.
271. Nash, J.A., Ballard, T.N.S., Weaver, T.E., Akinbi, H.T. 2006. The Peptidoglycan-Degrading Property of Lysozyme Is Not Required for Bactericidal Activity In Vivo. The Journal of Immunology **177**, 519–526. https://doi.org/10.4049/jimmunol.177.1.519
272. Naumann, T.A., Wicklow, D.T., Kendra, D.F. 2009. Maize seed chitinase is modified by a protein secreted by Bipolaris zeicola. Physiological and Molecular Plant Pathology **74**, 134–141. https://doi.org/10.1016/j.pmpp.2009.10.004
273. Niño MC, Kang KK, Cho YG. 2020. Genome-wide transcriptional response of papain-like cysteine protease-mediated resistance against *Xanthomonas oryzae* pv. *oryzae* in rice. Plant Cell Reports **39**, 457–472.
274. Ochman, H., Gerber, AS., Hartl, DL. 1988. Genetic Applications of an Inverse Polymerase Chain Reaction. Genetics **120**, 621-623. 10.1093/genetics/120.3.621.
275. Okinaka, Y., Yang, C.-H., Herman, E., Kinney, A., Keen, N.T. 2002. The P34 Syringolide Elicitor Receptor Interacts with a Soybean Photorespiration Enzyme, NADH-Dependent Hydroxypyruvate Reductase. Molecular Plant-Microbe Interactions **15**, 1213–1218. https://doi.org/10.1094/MPMI.2002.15.12.1213
276. Okushima Y, Koizumi N, Kusano T, Sano H. 2000. Secreted proteins of tobacco cultured BY2 cells: identification of a new member of pathogenesis-related proteins. Plant Molecular Biology **42**, 479–488.
277. O'Leary, B.M., Neale, H.C., Geilfus, C., Jackson, R.W., Arnold, D.L., Preston, G.M. 2016. Early changes in apoplast composition associated with defence and disease in interactions between *Phaseolus vulgaris* and the halo blight pathogen *Pseudomonas*

syringae Pv. *phaseolicola*. Plant, Cell & Environment **39**, 2172–2184. https://doi.org/10.1111/pce.12770
278. Olvera-Carrillo, Y., Van Bel, M., Van Hautegem, T., Fendrych, M., Huysmans, M., Simaskova, M., van Durme, M., Buscaill, P., Rivas, S., S. Coll, N., Coppens, F., Maere, S., Nowack, M.K. 2015. A Conserved Core of Programmed Cell Death Indicator Genes Discriminates Developmentally and Environmentally Induced Programmed Cell Death in Plants. Plant Physiology **169**, 2684–2699. https://doi.org/10.1104/pp.15.00769
279. O'Malley, M.R., Anderson, J.C. 2021. Regulation of the *Pseudomonas syringae* Type III Secretion System by Host Environment Signals. Microorganisms **9**, 1227. https://doi.org/10.3390/microorganisms9061227
280. Ormancey, M., Thuleau, P., van der Hoorn, R.A.L., Grat, S., Testard, A., Kamal, K.Y., Boudsocq, M., Cotelle, V., Mazars, C. 2019. Sphingolipid-induced cell death in Arabidopsis is negatively regulated by the papain-like cysteine protease RD21. Plant Science **280**, 12–17. https://doi.org/10.1016/j.plantsci.2018.10.028
281. Paireder, M., Mehofer, U., Tholen, S., Porodko, A., Schähs, P., Maresch, D., Biniossek, M.L., van der Hoorn, R.A.L., Lenarcic, B., Novinec, M., Schilling, O., Mach, L. 2016. The death enzyme CP14 is a unique papain-like cysteine proteinase with a pronounced S2 subsite selectivity. Archives of Biochemistry & Biophysics **603**, 110–117. https://doi.org/10.1016/j.abb.2016.05.017
282. Palmer, D.A., Bender, C.L. 1995. Utrastructure of tomato leaf tissue treated with the pseudomonad phytotoxin coronatine and comparison with methyl jasmonate. Molecular Plant-Microbe Interactions USA **8**, 683-692.
283. Park, C.-J., Ronald, P.C. 2012. Cleavage and nuclear localization of the rice XA21 immune receptor. Natire Communications **3**, 920. https://doi.org/10.1038/ncomms1932
284. Park, D.H., Mirabella, R., Bronstein, P.A., Preston, G.M., Haring, M.A., Lim, C.K., Collmer, A., Schuurink, R.C. 2010. Mutations in γ-aminobutyric acid (GABA) transaminase genes in plants or *Pseudomonas syringae* reduce bacterial virulence. Plant Journal **64**, 318–330. https://doi.org/10.1111/j.1365-313X.2010.04327.x
285. Passarinho, P.A., de Vries, S.C. 2002. Arabidopsis Chitinases: a Genomic Survey. The Arabidopsis Book - American Society of Plant Biologists **1**. https://doi.org/10.1199/tab.0023
286. Paulus, J.K., Kourelis, J., Ramasubramanian, S., Homma, F., Godson, A., Hörger, A.C., Hong, T.N., Krahn, D., Carballo, L.O., Wang, S., Win, J., Smoker, M., Kamoun, S., Dong, S., van der Hoorn, R.A.L. 2020. Extracellular proteolytic cascade in tomato activates immune protease Rcr3. Proceedings of the National Academy of Sciences **117**, 17409–17417. https://doi.org/10.1073/pnas.1921101117
287. Pechan T, Cohen A, Williams WP, Luthe DS. 2002. Insect feeding mobilizes a unique plant defense protease that disrupts the peritrophic matrix of caterpillars. Proceedings of the National Academic of Sciences USA **99**, 13319–13323.
288. Pechan T, Ye L, Chang Y, Mitra A, Lin L, Davis FM, Williams WP, Luthe DS. 2000. A unique 33-kD cysteine proteinase accumulates in response to larval feeding in maize genotypes resistant to fall armyworm and other Lepidoptera. The Plant Cell **12**, 1031–1040.
289. Pel, M.J.C., van Dijken, A.J.H., Bardoel, B.W., Seidl, M.F., van der Ent, S., van Strijp, J.A.G., Pieterse, C.M.J. 2014. *Pseudomonas syringae* evades host immunity by degrading flagellin monomers with alkaline protease AprA. Molecular Plant-Microbe Interactions **27**, 603–610. https://doi.org/10.1094/MPMI-02-14-0032-R
290. Perrot, T., Pauly, M., Ramírez, V. 2022. Emerging Roles of β-Glucanases in Plant Development and Adaptative Responses. Plants **11**, 1119. https://doi.org/10.3390/plants11091119
291. Petushkova, A.I., Savvateeva, L.V., Zamyatnin, A.A. 2022. Structure determinants defining the specificity of papain-like cysteine proteases. Computational and Structural Biotechnology Journal **20**, 6552–6569. https://doi.org/10.1016/j.csbj.2022.11.040
292. Petushkova, A.I., Zamyatnin, A.A. 2020. Redox-Mediated Post-Translational Modifications of Proteolytic Enzymes and Their Role in Protease Functioning. Biomolecules **10**, 650. https://doi.org/10.3390/biom10040650

293. Petutschnig, E.K., Stolze, M., Lipka, U., Kopischke, M., Horlacher, J., Valerius, O., Rozhon, W., Gust, A.A., Kemmerling, B., Poppenberger, B., Braus, G.H., Nürnberger, T., Lipka, V. 2014. A novel Arabidopsis CHITIN ELICITOR RECEPTOR KINASE 1 (CERK1) mutant with enhanced pathogen-induced cell death and altered receptor processing. New Phytologist **204**, 955–967. https://doi.org/10.1111/nph.12920
294. Pfeilmeier, S., Caly, D.L., Malone, J.G. 2016. Bacterial pathogenesis of plants: future challenges from a microbial perspective. Molecular Plant Pathology **17**, 1298–1313. https://doi.org/10.1111/mpp.12427
295. Picciolo, G.L., Kaplan, D.S. 1984. Reduction of Fading of Fluorescent Reaction Product for Microphotometric Quantitation, in: Laskin, A.I. (Ed.), Advances in Applied Microbiology. Academic Press, pp. 197–234. https://doi.org/10.1016/S0065-2164(08)70056-X
296. Planas-Marquès M, Bernardo-Faura M, Paulus J, Kaschani F, Kaiser M, Valls M, Van der Hoorn RAL, Coll NS. 2018. Protease activities triggered by *Ralstonia solanacearum* infection in susceptible and tolerant tomato lines. Molecular and Cellular Proteomics **17**, 1112–1125.
297. Pogorelko, G.V., Juvale, P.S., Rutter, W.B., Hütten, M., Maier, T.R., Hewezi, T., Paulus, J., Hoorn, R.A. van der, Grundler, F.M., Siddique, S., Lionetti, V., Zabotina, O.A., Baum, T.J. 2019. Re-targeting of a plant defense protease by a cyst nematode effector. Plant Journal **98**, 1000–1014. https://doi.org/10.1111/tpj.14295
298. Preston, G.M. 2000. *Pseudomonas syringae* pv. *tomato*: the right pathogen, of the right plant, at the right time. Molecular Plant Pathology **1**, 263–275. https://doi.org/10.1046/j.1364-3703.2000.00036.x
299. Porodko A, Cirnski A, Petrov D, Raab T, Paireder M, Mayer B, Maresch D, Nika L, Biniossek ML, Gallois P, Schilling O, Oostenbrink C, Novinec M, Mach L. 2018. The two cathepsin B-like proteases of *Arabidopsis thaliana* are closely related enzymes with discrete endopeptidase and carboxydipeptidase activities. Biological Chemistry **399**, 1223-1235.
300. Prasad BD, Creissen G, Lamb C, Chattoo BB. 2009. Overexpression of rice (*Oryza sativa* L.) *Os*CDR1 leads to constitutive activation of defense responses in rice and Arabidopsis. Molecular Plant-Microbe Interactions **22**, 1635–1644.
301. Qi, J., Wang, J., Gong, Z., Zhou, J.-M. 2017. Apoplastic ROS signaling in plant immunity. Current Opinion in Plant Biology **38**, 92–100. https://doi.org/10.1016/j.pbi.2017.04.022
302. Ramírez, V., López, A., Mauch-Mani, B., Gil, M.J., Vera, P. 2013. An Extracellular Subtilase Switch for Immune Priming in Arabidopsis. PLOS Pathogens **9**, e1003445. https://doi.org/10.1371/journal.ppat.1003445
303. Ranf, S., Gisch, N., Schäffer, M., Illig, T., Westphal, L., Knirel, Y.A., Sánchez-Carballo, P.M., Zähringer, U., Hückelhoven, R., Lee, J., Scheel, D. 2015. A lectin S-domain receptor kinase mediates lipopolysaccharide sensing in *Arabidopsis thaliana*. Nature Immunology **16**, 426–433. https://doi.org/10.1038/ni.3124
304. Ranković, T., Nikolić, I., Berić, T., Popović, T., Lozo, J., Medić, O., Stanković, S. 2023. Genome Analysis of Two *Pseudomonas syringae* pv. *aptata* Strains with Different Virulence Capacity Isolated from Sugar Beet: Features of Successful Pathogenicity in the Phyllosphere Microbiome. Microbiology Spectrum https://doi.org/10.1128/spectrum.03598-22
305. Rawlings ND, Barrett AJ, Bateman A. 2011. Asparagine peptide lyases. Journal of Biological Chemistry **286**, 38321–38328.
306. Rawlings ND, Morton FR, Kok CY, Kong J, Barrett AJ. 2008. MEROPS: the peptidase database. Nucleic Acids Research **36**, D320–D325.
307. Ray, S.K., Macoy, D.M., Kim, W.-Y., Lee, S.Y., Kim, M.G. 2019. Role of RIN4 in Regulating PAMP-Triggered Immunity and Effector-Triggered Immunity: Current Status and Future Perspectives. Molecules and Cells **42**, 503–511. https://doi.org/10.14348/molcells.2019.2433

308. Redman, J., Whitcraft, J., Johnson, C., Arias, J. 2002. Abiotic and biotic stress differentially stimulate as-1 element activity in Arabidopsis. Plant Cell Reports **21**, 180–185. https://doi.org/10.1007/s00299-002-0472-x
309. Reichardt, S., Repper, D., Tuzhikov, A.I., Galiullina, R.A., Planas-Marquès, M., Chichkova, N.V., Vartapetian, A.B., Stintzi, A., Schaller, A. 2018. The tomato subtilase family includes several cell death-related proteinases with caspase specificity. Scientific Reports **8**, 1–14. https://doi.org/10.
310. Richau, K.H., Kaschani, F., Verdoes, M., Pansuriya, T.C., Niessen, S., Stuber, K., Colby, T., Overkleeft, H.S., Bogyo, M., Van der Hoorn, R.A.L. 2012. Subclassification and Biochemical Analysis of Plant Papain-Like Cysteine Proteases Displays Subfamily-Specific Characteristics. Plant Physiology **158**, 1583–1599. https://doi.org/10.1104/pp.112.194001
311. Rico, A., Preston, G.M. 2008. *Pseudomonas syringae* pv. *tomato* DC3000 uses constitutive and apoplast-induced nutrient assimilation pathways to catabolize nutrients that are abundant in the tomato apoplast. Molecular Plant-Microbe Interactions **21**, 269–282. https://doi.org/10.1094/MPMI-21-2-0269
312. Rooney, H.C.E., Klooster, J.W. van't, van der Hoorn, R.A.L., Joosten, M.H.A.J., Jones, J.D.G., de Wit, P.J.G.M. 2005. *Cladosporium* Avr2 Inhibits Tomato Rcr3 Protease Required for Cf-2-Dependent Disease Resistance. Science **308**, 1783–1786. https://doi.org/10.1126/science.1111404
313. Rose, J.K.C., Ham, K.-S., Darvill, A.G., Albersheim, P. 2002. Molecular Cloning and Characterization of Glucanase Inhibitor Proteins. Plant Cell **14**, 1329–1345. https://doi.org/10.1105/tpc.002253
314. Rothman, K.J. 1990. No adjustments are needed for multiple comparisons. Epidemiology Cambridge Mass **1**, 43–46.
315. Rustgi, S., Boex-Fontvieille, E., Reinbothe, C., Wettstein, D. von, Reinbothe, S. 2017. Serpin1 and WSCP differentially regulate the activity of the cysteine protease RD21 during plant development in *Arabidopsis thaliana*. Proceedings of the National Academy of Sciences **114**, 2212–2217. https://doi.org/10.1073/pnas.1621496114
316 Ryan CA. 2000. The systemin signaling pathway: differential activation of plant defensive genes. Biochimica et Biophysica Acta (BBA) – Protein Structure and Molecular Enzymology **1477**, 112-121.
317. Sacco, M.A., Mansoor, S., Moffett, P. 2007. A RanGAP protein physically interacts with the NB-LRR protein Rx, and is required for Rx-mediated viral resistance. Plant Journal **52**, 82–93. https://doi.org/10.1111/j.1365-313X.2007.03213.x
318. Saijo, Y., Loo, E.P., Yasuda, S. 2018. Pattern recognition receptors and signaling in plant–microbe interactions. Plant Journal **93**, 592–613. https://doi.org/10.1111/tpj.13808
319. Sakata, N., Ishiga, T., Masuo, S., Hashimoto, Y., Ishiga, Y. 2021. Coronatine Contributes to *Pseudomonas cannabina* pv. *alisalensis* Virulence by Overcoming Both Stomatal and Apoplastic Defenses in Dicot and Monocot Plants. Molecular Plant-Microbe Interactions **34**, 746-757. doi: 10.1094/MPMI-09-20-0261-R.
320. Sánchez-Rangel, D., Sánchez-Nieto, S., Plasencia, J. 2012. Fumonisin B1, a toxin produced by *Fusarium verticillioides*, modulates maize β-1,3-glucanase activities involved in defense response. Planta **235**, 965–978. https://doi.org/10.1007/s00425-011-1555-0
321. Sanguankiattichai, N. 2021. Investigating the production of an inhibitor of plant β-galactosidase by the plant pathogen *Pseudomonas syringae*. PhD thesis, University of Oxford.
322. Saur, I.M.L., Kadota, Y., Sklenar, J., Holton, N.J., Smakowska, E., Belkhadir, Y., Zipfel, C., Rathjen, J.P. 2016. *Nb*CSPR underlies age-dependent immune responses to bacterial cold shock protein in *Nicotiana benthamiana*. Proceedings of the National Academy of Sciences U. S. A. **113**, 3389–3394. https://doi.org/10.1073/pnas.1511847113
323. Savatin DV, Gramegna G, Modesti V, Cervone F. 2014. Wounding in the plant tissue: the defense of a dangerous passage. Frontiers in Plant Sciences **5**, 470.

324. Schaller A, Ryan CA. 1996. Molecular cloning of a tomato leaf cDNA encoding an aspartic protease, a systemic wound response protein. Plant Molecular Biology **31**, 1073–1077.
325. Schaller A, Stintzi A, Rivas S, Serrano I, Chichkova NV, Vartapetian AB, Martínez D, Guiamét JJ, Sueldo DJ, Van der Hoorn RAL, Ramírez V, Vera P. 2018. From structure to function – a family portrait of plant subtilases. New Phytologist **218**, 901-915.
326. Schellenberg, B., Ramel, C., Dudler, R. 2010. *Pseudomonas syringae* Virulence Factor Syringolin A Counteracts Stomatal Immunity by Proteasome Inhibition. Molecular Plant-Microbe Interactions **23**, 1287–1293. https://doi.org/10.1094/MPMI-04-10-0094
327. Scheltinga, A.C.T. van, Kalk, K.H., Beintema, J.J., Dijkstra, B.W. 1994. Crystal structures of hevamine, a plant defence protein with chitinase and lysozyme activity, and its complex with an inhibitor. Structure **2**, 1181–1189. https://doi.org/10.1016/S0969-2126(94)00120-0
328. Schiermeyer A, Hartenstein H, Mandal MK, Otte B, Wahner V, Schillberg S. 2009. A membrane-bound matrix-metalloproteinase from *Nicotiana tabacum* cv. BY-2 is induced by bacterial pathogens. BMC Plant Biology **9**, 83.
329. Schindelin, J., Arganda-Carreras, I., Frise, E., Kaynig, V., Longair, M., Pietzsch, T., Preibisch, S., Rueden, C., Saalfeld, S., Schmid, B., Tinevez, J.-Y., White, D.J., Hartenstein, V., Eliceiri, K., Tomancak, P., Cardona, A. 2012. Fiji: an open-source platform for biological-image analysis. Nature Methods **9**, 676–682. https://doi.org/10.1038/nmeth.2019
330. Schultink, A., Qi, T., Lee, A., Steinbrenner, A.D., Staskawicz, B. 2017. Roq1 mediates recognition of the *Xanthomonas* and *Pseudomonas* effector proteins XopQ and HopQ1. The Plant Journal for Cell and Molecular Biology **92**, 787–795. https://doi.org/10.1111/tpj.13715
331. Schuster, M., Paulus, J.K., Kourelis, J., van der Hoorn, R.A.L. 2022. Purification of His-Tagged Proteases from the Apoplast of Agroinfiltrated *Nicotiana benthamiana* (*N. benthamiana*), in: Klemenčič, M., Stael, S., Huesgen, P.F. (Eds.), Plant Proteases and Plant Cell Death: Methods and Protocols, Methods in Molecular Biology. Springer US, New York, NY, pp. 53–66. https://doi.org/10.1007/978-1-0716-2079-3_5
332. Schweizer P, Pokorny J, Abderhalden O, Dudler R. 1999. A transient assay system for the functional assessment of defense-related genes in wheat. Molecular Plant-Microbe Interactions **12**, 647–654.
333. Sela-Buurlage, M.B., Ponstein, A.S., Bres-Vloemans, S.A., Melchers, L.S., Van Den Elzen, PJM., Cornelissen, BJC. 1993. Only Specific Tobacco (*Nicotiana tabacum*) Chitinases and [beta]-1,3-Glucanases Exhibit Antifungal Activity. Plant Physiology **101**, 857–863.
334. Sénéchal F, Graff L, Surcouf O, Marcelo P, Rayon C, Bouton S, Mareck A, Mouille G, Stintzi A, Höfte H, Lerouge P, Schaller A, Pelloux J. 2014. Arabidopsis PECTIN METHYLESTERASE17 is co-expressed with and processed by SBT3.5, a subtilisin-like serine protease. Annals of Botany **114**, 1161–1175.
335. Senthil-Kumar, M., Mysore, K.S. 2014. Tobacco rattle virus–based virus-induced gene silencing in *Nicotiana benthamiana*. Nature Protocols **9**, 1549–1562. https://doi.org/10.1038/nprot.2014.092
336. Shabab M, Shindo T, Gu C, Kaschani F, Pansuriya T, Chintha R, Harzen A, Colby T, Kamoun S, Van der Hoorn RAL. 2008. Fungal effector protein AVR2 targets diversifying defense-related Cys proteases of tomato. The Plant Cell **20**, 1169–1183.
337. Shang-Guan, K., Wang, M., Htwe, N.M.P.S., Li, P., Li, Y., Qi, F., Zhang, D., Cao, M., Kim, C., Weng, H., Cen, H., Black, I.M., Azadi, P., Carlson, R.W., Stacey, G., Liang, Y. 2018. Lipopolysaccharides Trigger Two Successive Bursts of Reactive Oxygen Species at Distinct Cellular Locations. Plant Physiology **176**, 2543–2556. https://doi.org/10.1104/pp.17.01637
338. Shapiguzov, A., Vainonen, J., Wrzaczek, M., Kangasjärvi, J. 2012. ROS-talk – how the apoplast, the chloroplast, and the nucleus get the message through. Frontiers in Plant Science **3**.

339. Shen, G., Sun, W., Chen, Z., Shi, L., Hong, J., Shi, J. 2022. Plant GDSL Esterases/Lipases: Evolutionary, Physiological and Molecular Functions in Plant Development. Plants **11**, 468. https://doi.org/10.3390/plants11040468
340. Shi, G., Hao, M., Tian, B., Cao, G., Wei, F., Xie, Z. 2021. A Methodological Advance of Tobacco Rattle Virus-Induced Gene Silencing for Functional Genomics in Plants. Frontiers in Plant Science **12**, 671091. https://doi.org/10.3389/fpls.2021.671091
341. Shindo T, Kaschani F, Yang F, Kovács J, Tian F, Kourelis J, Hong TN, Colby T, Shabab M, Chawla R, Kumari S, Ilyas M, Hörger AC, Alfano JR, Van der Hoorn RAL. 2016. Screen of non-annotated small secreted proteins of *Pseudomonas syringae* reveals a virulence factor that inhibits tomato immune proteases. PLoS Pathogens **12**, e1005874.
342. Shindo, T., Misas-Villamil, J.C., Hörger, A.C., Song, J., van der Hoorn, R.A.L. 2012. A Role in Immunity for Arabidopsis Cysteine Protease RD21, the Ortholog of the Tomato Immune Protease C14. PLoS ONE **7**. https://doi.org/10.1371/journal.pone.0029317
342. Shinohara, H. 2014. Bactericide susceptibility of plant pathogenic bacteria. MAFF Microorganism Genetic Resources Manual **36**, 1-15
344. Shrawat, A.K., Lörz, H. 2006. Agrobacterium-mediated transformation of cereals: a promising approach crossing barriers. Plant Biotechnology Journal **4**, 575–603. https://doi.org/10.1111/j.1467-7652.2006.00209.x
345. Sievers, F., Wilm, A., Dineen, D., Gibson, T.J., Karplus, K., Li, W., Lopez, R., McWilliam, H., Remmert, M., Söding, J., Thompson, J.D., Higgins, D.G. 2011. Fast, scalable generation of high-quality protein multiple sequence alignments using Clustal Omega. Molecular Systems Biology **7**, 539. https://doi.org/10.1038/msb.2011.75
346. Sijwali, P.S., Shenai, B.R., Gut, J., Singh, A., Rosenthal, P.J. 2001. Expression and characterization of the *Plasmodium falciparum* haemoglobinase falcipain-3. Biochemical Journal **360**, 481–489.
347. Silby, M.W., Winstanley, C., Godfrey, S.A.C., Levy, S.B., Jackson, R.W. 2011. *Pseudomonas* genomes: diverse and adaptable. FEMS Microbiology Reviews **35**, 652–680. https://doi.org/10.1111/j.1574-6976.2011.00269.x
348. Simões I, Faro C. 2004. Structure and function of plant aspartic proteinases. European Journal of Biochemistry **271**, 2067–2075.
349. Simões I, Faro R, Bur D, Faro C. 2007. Characterization of recombinant CDR1, an Arabidopsis aspartic proteinase involved in disease resistance. Journal of Biological Chemistry **282**, 31358–31365.
350. Smith, A., Kaczmar, A., Bamford, R.A., Smith, C., Frustaci, S., Kovacs-Simon, A., O'Neill, P., Moore, K., Paszkiewicz, K., Titball, R.W., Pagliara, S. 2018. The Culture Environment Influences Both Gene Regulation and Phenotypic Heterogeneity in *Escherichia coli*. Frontiers in Microbiology **9**.
351. Soldan, R., Sanguankiattichai, N., Bach-Pages, M., Bervoets, I., Huang, W.E., Preston, G.M. 2021. From macro to micro: a combined bioluminescence-fluorescence approach to monitor bacterial localization. Environmental Microbiology **23**, 2070–2085. https://doi.org/10.1111/1462-2920.15296
352. Song J, Win J, Tian M, Schornack S, Kaschani F, Ilyas M, Van der Hoorn RAL, Kamoun S. 2009. Apoplastic effectors secreted by two unrelated eukaryotic plant pathogens target the tomato defense protease Rcr3. Proceedings of the National Academy of Sciences, USA **106**, 1654–1659.
353. Sperschneider J, Dodds PN, Singh KB, Taylor JM. 2018. ApoplastP: prediction of effectors and plant proteins in the apoplast using machine learning. New Phytologist **217**, 1764–1778.
354. Sprague-Piercy, M.A., Bierma, J.C., Crosby, M.G., Carpenter, B.P., Takahashi, G.R., Paulino, J., Hung, I., Zhang, R., Kelly, J.E., Kozlyuk, N., Chen, X., Butts, C.T., Rachel W. Martin, R.W. 2020. The Droserasin 1 PSI: A Membrane-Interacting Antimicrobial Peptide from the Carnivorous Plant *Drosera capensis*. Biomolecules **10**, https://doi.org/10.3390/biom10071069

355. Spriestersbach, A., Kubicek, J., Schäfer, F., Block, H., Maertens, B. 2015. Chapter One - Purification of His-Tagged Proteins, in: Lorsch, J.R. (Ed.), Methods in Enzymology, Laboratory Methods in Enzymology: Protein Part D. Academic Press, pp. 1–15. https://doi.org/10.1016/bs.mie.2014.11.003
356. Sreedharan, A., Penaloza-Vazquez, A., Kunkel, B.N., Bender, C.L. 2006. CorR regulates multiple components of virulence in *Pseudomonas syringae* pv. *tomato* DC3000. Molecular Plant-Microbe Interactions **19**, 768–779. https://doi.org/10.1094/MPMI-19-0768
357. Stavrinides, J., Guttman, DS. 2004. Nucleotide Sequence and Evolution of the Five-Plasmid Complement of the Phytopathogen *Pseudomonas syringae* pv. *maculicola* ES4326. Journal of Bacteriology **186**, 5101-5115. https://doi.org/10.1128/JB.186.15.5101-5115.2004
358. Studholme, DJ., Gimenez Ibanez, S., MacLean, D., Dangl, JL., Chang, JH., Rathjen, JP. 2009. A draft genome sequence and functional screen reveals the repertoire of type III secreted proteins of *Pseudomonas syringae* pathovar *tabaci* 11528. BMC Genomics **10**. 10.1186/1471-2164-10-395
359. Suarez, V., Staehelin, C., Arango, R., Holtorf, H., Hofsteenge, J., Meins, F. 2001. Substrate specificity and antifungal activity of recombinant tobacco class I chitinases. Plant Molecular Biology **45**, 609–618. https://doi.org/10.1023/A:1010619421524
360. Subroto, T., Sufiati, S., Beintema, J.J. 1999. Papaya (*Carica papaya*) Lysozyme Is a Member of the Family 19 (Basic, Class II) Chitinases. Journal of Molecular Evolution **49**, 819–821. https://doi.org/10.1007/PL00000075
361. Sueldo D, Ahmed A, Misas-Villamil J, Colby T, Tameling W, Joosten MHAJ, Van der Hoorn RAL. 2014. Dynamic hydrolase activities precede hypersensitive tissue collapse in tomato seedlings. New Phytologist **203**, 913–925.
362. Sueldo, D.J., Godson, A., Kaschani, F., Krahn, D., Kessenbrock, T., Buscaill, P., Schofield, C.J., Kaiser, M., van der Hoorn, R.A.L. 2023. Activity-based proteomics uncovers suppressed hydrolases and a neo-functionalised antibacterial enzyme at the plant–pathogen interface. New Phytologist https://doi.org/10.1111/nph.18857
363. Sun, Yue, Wang, Yan, Zhang, X., Chen, Z., Xia, Y., Wang, L., Sun, Yujing, Zhang, M., Xiao, Y., Han, Z., Wang, Yuanchao, Chai, J. 2022. Plant receptor-like protein activation by a microbial glycoside hydrolase. Nature **610**, 335–342. https://doi.org/10.1038/s41586-022-05214-x
364. Tahir, J., Rashid, M., Afzal, A.J. 2019. Post-translational modifications in effectors and plant proteins involved in host–pathogen conflicts. Plant Pathology **68**, 628–644. https://doi.org/10.1111/ppa.12983
365. Tanaka K. 2009. The proteasome: overview of structure and functions. Proceedings of the Japan Academy Series B Physical and Biological Sciences **85**, 12–36.
366. Tang, C.M., Chye, M.-L., Ramalingam, S., Ouyang, S.-W., Zhao, K.-J., Ubhayasekera, W., Mowbray, S.L. 2004. Functional analyses of the chitin-binding domains and the catalytic domain of *Brassica juncea* chitinase *Bj*CHI1. Plant Molecular Biology **56**, 285–298. https://doi.org/10.1007/s11103-004-3382-1
367. Tang, Y., Liu, Q., Liu, Y., Zhang, L., Ding, W. 2017. Overexpression of *Nt*PR-Q Up-Regulates Multiple Defense-Related Genes in *Nicotiana tabacum* and Enhances Plant Resistance to *Ralstonia solanacearum*. Frontiers in Plant Science **8**. https://doi.org/10.3389/fpls.2017.01963
368. Taylor, JD., Teverson, DM., Allen, DJ., Pastor-Corrales, MA. 1996. Identification and origin of races of *Pseudomonas syringae* pv. *phaseolicola* from Africa and other bean growing areas. Plant Pathology **45**, 469-478. https://doi.org/10.1046/j.1365-3059.1996.d01-147.x
369. Thapa, SP., Coaker, G. 2016. Genome Sequences of Two *Pseudomonas syringae* pv. *tomato* Race 1 Strains, Isolated from Tomato Fields in California. Genome Announcements **4**, e01671-15. 10.1128/genomeA.01671-15
370. Thomas, E. 2020. Protein processing in *Nicotiana benthamiana* by Vacuolar Processing Enzymes and other proteases. PhD thesis, University of Oxford.

371. Thomas EL, Van der Hoorn RAL. 2018. Ten prominent host proteases in plant-pathogen interactions. International Journal of Molecular Sciences **19**, 639.
372. Tian, M., Benedetti, B., Kamoun, S. 2005. A Second Kazal-Like Protease Inhibitor from *Phytophthora infestans* Inhibits and Interacts with the Apoplastic Pathogenesis-Related Protease P69B of Tomato. Plant Physiology **138**, 1785–1793. https://doi.org/10.1104/pp.105.061226
373. Tian, M., Huitema, E., Cunha, L. da, Torto-Alalibo, T., Kamoun, S. 2004. A Kazal-like Extracellular Serine Protease Inhibitor from *Phytophthora infestans* Targets the Tomato Pathogenesis-related Protease P69B. Journal of Biological Chemistry **279**, 26370–26377. https://doi.org/10.1074/jbc.M400941200
374. Tian M, Win J, Song J, Van der Hoorn RAL, Van der Knaap E, Kamoun S. 2007. A *Phytophthora infestans* cystatin-like protein targets a novel tomato papain-like apoplastic protease. Plant Physiology **143**, 364–377.
375. Tian, S., Wang, X., Li, P., Wang, H., Ji, H., Xie, J., Qiu, Q., Shen, D., Dong, H. 2016. Plant Aquaporin *At*PIP14 Links Apoplastic H_2O_2 Induction to Disease Immunity Pathways. Plant Physiology **171**, 1635–1650. https://doi.org/10.1104/pp.15.01237
376. Tornero P, Mayda E, Gómez MD, Cañas L, Conejero V, Vera P. 1996. Characterization of LRP, a leucine-rich repeat (LRR) protein from tomato plants that is processed during pathogenesis. The Plant Journal **10**, 315–330.
377. Tornero P, Conejero V, Vera P. 1997. Identification of a new pathogen-induced member of the subtilisin-like processing protease family from plants. Journal of Biological Chemistry **272**, 14412–14419.
378. Torres, M.A., Jones, J.D.G., Dangl, J.L. 2006. Reactive Oxygen Species Signaling in Response to Pathogens. Plant Physiology **141**, 373–378. https://doi.org/10.1104/pp.106.079467
379. Tsuchiya, Y., Yamamori, Y., Tomii, K. 2022. Protein–protein interaction prediction methods: from docking-based to AI-based approaches. Biophysical Reviews **14**, 1341–1348. https://doi.org/10.1007/s12551-022-01032-7
380. Tyanova, S., Temu, T., Sinitcyn, P., Carlson, A., Hein, M.Y., Geiger, T., Mann, M., Cox, J. 2016. The Perseus computational platform for comprehensive analysis of (prote)omics data. Nature Methods **13**, 731–740. https://doi.org/10.1038/nmeth.3901
381. Tyler, L., Bragg, J.N., Wu, J., Yang, X., Tuskan, G.A., Vogel, J.P. 2010. Annotation and comparative analysis of the glycoside hydrolase genes in *Brachypodium distachyon*. BMC Genomics **11**, 600. https://doi.org/10.1186/1471-2164-11-600
382. Ubhayasekera, W., Rawat, R., Ho, S.W.T., Wiweger, M., Von Arnold, S., Chye, M.-L., Mowbray, S.L. 2009. The first crystal structures of a family 19 class IV chitinase: the enzyme from Norway spruce. Plant Molecular Biology **71**, 277–289. https://doi.org/10.1007/s11103-009-9523-9
383. Uemura, T., Hachisu, M., Desaki, Y., Ito, A., Hoshino, R., Sano, Y., Nozawa, A., Mujiono, K., Galis, I., Yoshida, A., Nemoto, K., Miura, S., Nishiyama, M., Nishiyama, C., Horito, S., Sawasaki, T., Arimura, G. 2020. Soy and Arabidopsis receptor-like kinases respond to polysaccharide signals from *Spodoptera* species and mediate herbivore resistance. Communications Biology **3**, 1–11. https://doi.org/10.1038/s42003-020-0959-4
384. The UniProt Consortium, 2017. UniProt: the universal protein knowledgebase. Nucleic Acids Res. **45**, D158–D169. https://doi.org/10.1093/nar/gkw1099
385. van der Hoorn RAL. 2008. Plant proteases: from phenotypes to molecular mechanisms. Annual Review of Plant Biology **59**, 191–223.
386. van der Hoorn RAL, Colby T, Nickel S, Richau K, Schmidt J, Kaiser M. 2011. Mining the active proteome of *Arabidopsis thaliana*. Frontiers in Plant Science. **2**, 89.
387. van der Hoorn, R.A.L., Leeuwenburgh, M.A., Bogyo, M., Joosten, M.H.A.J., Peck, S.C. 2004. Activity Profiling of Papain-Like Cysteine Proteases in Plants. Plant Physiology **135**, 1170–1178. https://doi.org/10.1104/pp.104.041467
388. van der Hoorn, R.A.L., Rivas, S., Wulff, B.B.H., Jones, J.D.G., Joosten, M.H.A.J. 2003. Rapid migration in gel filtration of the Cf-4 and Cf-9 resistance proteins is an intrinsic property of Cf proteins and not because of their association with high-molecular-weight

proteins. The Plant Journal **35**, 305–315. https://doi.org/10.1046/j.1365-313X.2003.01803.x
389. van der Linde K, Hemetsberger C, Kastner C, Kaschani F, Van der Hoorn RAL, Kumlehn J, Doehlemann G. 2012. A maize cystatin suppresses host immunity by inhibiting apoplastic cysteine proteases. The Plant Cell **24**, 1285–1300.
390. van Esse, H.P., Bolton, M.D., Stergiopoulos, I., de Wit, P.J.G.M., Thomma, B.P.H.J. 2007. The Chitin-Binding Cladosporium fulvum Effector Protein Avr4 Is a Virulence Factor. Molecular Plant-Microbe Interactions **20**, 1092–1101. https://doi.org/10.1094/MPMI-20-9-1092
391. van Loon, L. C., Rep, M., Pieterse, C.M.J. 2006. Significance of Inducible Defense-related Proteins in Infected Plants. Annual Review of Phytopathology **44**, 135–162. https://doi.org/10.1146/annurev.phyto.44.070505.143425
392. Vanneste, J.L. 2017. The Scientific, Economic, and Social Impacts of the New Zealand Outbreak of Bacterial Canker of Kiwifruit (*Pseudomonas syringae* pv. *actinidiae*). Annual Review of Phytopathology **55**, 377–399. https://doi.org/10.1146/annurev-phyto-080516-035530
393. Varsani S, Basu S, Williams WP, Felton GW, Luthe DS, Louis J. 2016. Intraplant communication in maize contributes to defense against insects. Plant Signalling and Behaviour **11**, e1212800
394. Villamor-Sernestrand, JG. 2016. Profiling protein kinases and other ATP-binding proteins in Arabidopsis using acyl-ATP probes. PhD thesis, Universität zu Köln
395. Vinatzer, B.A., Teitzel, G.M., Lee, M.-W., Jelenska, J., Hotton, S., Fairfax, K., Jenrette, J., Greenberg, J.T. 2006. The type III effector repertoire of *Pseudomonas syringae* pv. *syringae* B728a and its role in survival and disease on host and non-host plants. Molecular Microbiology **62**, 26–44. https://doi.org/10.1111/j.1365-2958.2006.05350.x
396. Vollmer, W., Blanot, D., De Pedro, M.A. 2008. Peptidoglycan structure and architecture. FEMS Microbiology Reviews **32**, 149–167. https://doi.org/10.1111/j.1574-6976.2007.00094.x
397. Vorster, B.J., Cullis, C.A., Kunert, K.J. 2019. Plant Vacuolar Processing Enzymes. Frontiers in Plant Science **10**, 479. https://doi.org/10.3389/fpls.2019.00479
398. Wang, H., Guo, B., Yang, B., Li, H., Xu, Y., Zhu, J., Wang, Y., Ye, W., Duan, K., Zheng, X., Wang, Y. 2021. An atypical *Phytophthora sojae* RxLR effector manipulates host vesicle trafficking to promote infection. PLOS Pathogens **17**. https://doi.org/10.1371/journal.ppat.1010104
399. Wang S, Xing R, Wang Y, Shu H, Fu S, Paulus JK, Schuster M, Saunders DGO, Win J, Vleeshouwers V, Zheng X, Van der Hoorn RAL, Kamoun S, Dong S. 2019a. Cleavage of a pathogen apoplastic protein by plant subtilases activates immunity. bioRxiv.12.16.878272.
400. Wang, W., Paschalidis, K., Feng, J.-C., Song, J., Liu, J.-H. 2019b. Polyamine Catabolism in Plants: A Universal Process With Diverse Functions. Frontiers in Plant Science **10**, 561. https://doi.org/10.3389/fpls.2019.00561
401. Wang, Y., Garrido-Oter, R., Wu, J., Winkelmüller, T.M., Agler, M., Colby, T., Nobori, T., Kemen, E., Tsuda, K. 2019c. Site-specific cleavage of bacterial MucD by secreted proteases mediates antibacterial resistance in Arabidopsis. Nature Communications **10**, 1–12. https://doi.org/10.1038/s41467-019-10793-x
402. Wang, Y., Li, J., Hou, S., Wang, X., Li, Y., Ren, D., Chen, S., Tang, X., Zhou, J.-M. 2010. A *Pseudomonas syringae* ADP-Ribosyltransferase Inhibits Arabidopsis Mitogen-Activated Protein Kinase Kinases. Plant Cell **22**, 2033–2044. https://doi.org/10.1105/tpc.110.075697
403. Wang, Yan, Wang, Yuanchao, 2017. Trick or Treat: Microbial Pathogens Evolved Apoplastic Effectors Modulating Plant Susceptibility to Infection. Molecular Plant-Microbe Interactions **31**, 6–12. https://doi.org/10.1094/MPMI-07-17-0177-FI

404. Wang, Yan, Wang, Yuanchao, Wang, Yiming, 2020. Apoplastic Proteases: Powerful Weapons against Pathogen Infection in Plants. Plant Communications **1**, 100085. https://doi.org/10.1016/j.xplc.2020.100085
405. Washington, E.J., Mukhtar, M.S., Finkel, O.M., Wan, L., Banfield, M.J., Kieber, J.J., Dangl, J.L. 2016. *Pseudomonas syringae* type III effector HopAF1 suppresses plant immunity by targeting methionine recycling to block ethylene induction. Proceedings of the National Academy of Sciences **113**, E3577–E3586. https://doi.org/10.1073/pnas.1606322113
406. Watson, J.M., Fusaro, A.F., Wang, M., Waterhouse, P.M. 2005. RNA silencing platforms in plants. FEBS Letters **579**, 5982-5987. https://doi.org/10.1016/j.febslet.2005.08.014
407. Wei, C.-F., Kvitko, B.H., Shimizu, R., Crabill, E., Alfano, J.R., Lin, N.-C., Martin, G.B., Huang, H.-C., Collmer, A. 2007. A *Pseudomonas syringae* pv. *tomato* DC3000 mutant lacking the type III effector HopQ1-1 is able to cause disease in the model plant *Nicotiana benthamiana*. The Plant Journal **51**, 32–46. https://doi.org/10.1111/j.1365-313X.2007.03126.x
408. Wei, H.-L., Chakravarthy, S., Mathieu , J., Helmann, T.C., Stodghill P., Swingle, B., Martin, G.B., Collmer, A. 2015. *Pseudomonas syringae* pv. *tomato* DC3000 Type III Secretion Effector Polymutants Reveal an Interplay between HopAD1 and AvrPtoB. Cell Host Microbe **17**, 752-762. https://doi.org/10.1016/j.chom.2015.05.007
409. Weng, S.S.H., Demir, F., Ergin, E.K., Dirnberger, S., Uzozie, A., Tuscher, D., Nierves, L., Tsui, J., Huesgen, P.F., Lange, P.F. 2019. Sensitive determination of proteolytic proteoforms in limited microscale proteome samples. bioRxiv. https://doi.org/10.1101/566109
410. Wessel, D., Flügge, U.I. 1984. A method for the quantitative recovery of protein in dilute solution in the presence of detergents and lipids. Analytical Biochemistry **138**, 141–143. https://doi.org/10.1016/0003-2697(84)90782-6
411. Whitacre JM. 2012. Biological robustness: paradigms, mechanisms, and systems principles. Frontiers in Genetics **3**, 67.
412. Woollard, A.A., Moore, I. 2008. The functions of Rab GTPases in plant membrane traffic. Current Opinion in Plant Biology, Cell Biology **11**, 610–619. https://doi.org/10.1016/j.pbi.2008.09.010
413. Wu CH, Abd-El-Haliem A, Bozkurt TO, Belhaj K, Terauchi R, Vossen JH, Kamoun S. 2017. NLR network mediates immunity to diverse plant pathogens. Proceedings of the National Academic of Sciences **114**, 8113-8118.
414. Wu, L., Xiao, H., Zhao, L., Cheng, Q. 2022. CRISPR/Cas9-mediated generation of fls2 mutant in *Nicotiana benthamiana* for investigating the flagellin recognition spectrum of diverse FLS2 receptors. Plant Biotechnology Journal **20**, 1853–1855. https://doi.org/10.1111/pbi.13898
415. Xia, Y., Suzuki, H., Borevitz, J., Blount, J., Guo, Z., Patel, K., Dixon, R.A., Lamb, C. 2004. An extracellular aspartic protease functions in Arabidopsis disease resistance signaling. EMBO Journal **23**, 980–988. https://doi.org/10.1038/sj.emboj.7600086
416. Xiang, T., Zong, N., Zou, Y., Wu, Y., Zhang, J., Xing, W., Li, Y., Tang, X., Zhu, L., Chai, J., Zhou, J.-M. 2008. *Pseudomonas syringae* Effector AvrPto Blocks Innate Immunity by Targeting Receptor Kinases. Current Biology **18**, 74–80. https://doi.org/10.1016/j.cub.2007.12.020
417. Xi, Y., Chochois, V., Kroj, T., Cesari, S. 2021. A novel robust and high-throughput method to measure cell death in *Nicotiana benthamiana* leaves by fluorescence imaging. Molecular Plant Pathology **22**, 1688–1696. https://doi.org/10.1111/mpp.13129
418. Xie W, Goodwin PH. 2009. A *PRp27* gene of *Nicotiana benthamiana* contributes to resistance to *Pseudomonas syringae* pv. *tabaci* but not to *Colletotrichum destructivum* or *Colletotrichum orbiculare*. Functional Plant Biology **36**, 351–361.
419. Xin, X.-F., Kvitko, B., He, S.Y. 2018. *Pseudomonas syringae*: what it takes to be a pathogen. Nature Reviews Microbiology **16**, 316–328. https://doi.org/10.1038/nrmicro.2018.17

420. Yamada, K., Fuji, K., Shimada, T., Nishimura, M., Hara-Nishimura, I. 2005. Endosomal proteases facilitate the fusion of endosomes with vacuoles at the final step of the endocytotic pathway. The Plant Journal **41**, 888–898. https://doi.org/10.1111/j.1365-313X.2005.02349.x
421. Yamada, K., Matsushima, R., Nishimura, M., Hara-Nishimura, I. 2001. A Slow Maturation of a Cysteine Protease with a Granulin Domain in the Vacuoles of Senescing Arabidopsis Leaves. Plant Physiology **127**, 1626–1634.
422. Yu, X., Lund, S.P., Scott, R.A., Greenwald, J.W., Records, A.H., Nettleton, D., Lindow, S.E., Gross, D.C., Beattie, G.A. 2013. Transcriptional responses of *Pseudomonas syringae* to growth in epiphytic versus apoplastic leaf sites. Proceedings of the National Academy of Sciences U. S. A. **110**, E425–E434. https://doi.org/10.1073/pnas.1221892110
423. Zhang, G., Meredith, T.C., Kahne, D. 2013. On the Essentiality of Lipopolysaccharide to Gram-Negative Bacteria. Current Opinion in Microbiology **16**, 779–785. https://doi.org/10.1016/j.mib.2013.09.007
424. Zhang, Z., Thomma, B.P.H.J. 2013. Structure-function Aspects of Extracellular Leucine-rich Repeat-containing Cell Surface Receptors in Plants. Journal of Integrative Plant Biology **55**, 1212–1223. https://doi.org/10.1111/jipb.12080
425. Zhao P, Zhang F, Liu D, Imani J, Langen G, Kogel KH. 2017. Matrix metalloproteinases operate redundantly in Arabidopsis immunity against necrotrophic and biotrophic fungal pathogens. PLoS One **12**.
426. Zhao Y, Thilmony R, Bender CL, Schaller A, He SY, Howe GA. 2003. Virulence systems of *Pseudomonas syringae* pv. *tomato* promote bacterial speck disease in tomato by targeting the jasmonate signaling pathway. The Plant Journal **36**, 485–499.
427. Zhao, Y., Wu, G., Shi, H., Tang, D. 2019. RECEPTOR-LIKE KINASE 902 Associates with and Phosphorylates BRASSINOSTEROID-SIGNALING KINASE1 to Regulate Plant Immunity. Molecular Plant **12**, 59–70. https://doi.org/10.1016/j.molp.2018.10.008
428. Ziemann S, Van der Linde K, Lahrmann U, Acar B, Kaschani F, Colby T, Kaiser M, Ding Y, Schmelz E, Huffaker A, Holton N, Zipfel C, Doehlemann G. 2018. An apoplastic peptide activates salicylic acid signalling in maize. Nature Plants **4**, 172–180.
429. Zimmermann, D., Gomez-Barrera, J.A., Pasule, C., Brack-Frick, U.B., Sieferer, E., Nicholson, T.M., Pfannstiel, J., Stintzi, A., Schaller, A. 2016. Cell Death Control by Matrix Metalloproteinases. Plant Physiology **171**, 1456–1469. https://doi.org/10.1104/pp.16.00513
430. Zipfel, C. 2014. Plant pattern-recognition receptors. Trends in Immunology **35**, 345–351. https://doi.org/10.1016/j.it.2014.05.004